

00000140

8003 240 654

TABLE OF CONTENTS

<u>Section</u>		<u>Page</u>
3	<u>REACTOR</u>	3-1
3.1	<u>DESIGN BASES</u>	3-1
3.1.1	PERFORMANCE OBJECTIVES	3-1
3.1.2	LIMITS	3-1
3.1.2.1	<u>Nuclear Limits</u>	3-1
3.1.2.2	<u>Reactivity Control Limits</u>	3-2
3.1.2.3	<u>Thermal and Hydraulic Limits</u>	3-2
3.1.2.4	<u>Mechanical Limits</u>	3-3
3.2	<u>REACTOR DESIGN</u>	3-6
3.2.1	GENERAL SUMMARY	3-6
3.2.2	NUCLEAR DESIGN AND EVALUATION	3-7
3.2.2.1	<u>Nuclear Characteristics of the Design</u>	3-7
3.2.2.2	<u>Nuclear Evaluation</u>	3-20
3.2.3	THERMAL AND HYDRAULIC DESIGN AND EVALUATION	3-32
3.2.3.1	<u>Thermal and Hydraulic Characteristics</u>	3-32
3.2.3.2	<u>Thermal and Hydraulic Evaluation</u>	3-41
3.2.4	MECHANICAL DESIGN LAYOUT	3-68
3.2.4.1	<u>Internal Layout</u>	3-68
3.2.4.2	<u>Fuel Assemblies</u>	3-73
3.2.4.3	<u>Control Rod Drive System</u>	3-86
3.3	<u>TESTS AND INSPECTIONS</u>	3-95
3.3.1	NUCLEAR TESTS AND INSPECTION	3-95
3.3.1.1	<u>Critical Experiments</u>	3-95
3.3.1.2	<u>Zero Power, Approach to Power, and Power Testing</u>	3-95
3.3.2	THERMAL AND HYDRAULIC TESTS AND INSPECTION	3-95

00000141

CONTENTS (Cont'd)

<u>Section</u>		<u>Page</u>
3.3.2.1	<u>Reactor Vessel Flow Distribution and Pressure Drop Test</u>	3-95
3.3.2.2	<u>Fuel Assembly Heat Transfer and Fluid Flow Tests</u>	3-96
3.3.2.3	<u>Preoperational Testing and Postoperational Testing</u>	3-98
3.3.3	FUEL ASSEMBLY, CONTROL ROD ASSEMBLY, AND CONTROL ROD DRIVE MECHANICAL TESTS AND INSPECTION	3-98
3.3.3.1	<u>Prototype Testing</u>	3-98
3.3.3.2	<u>Model Testing</u>	3-98
3.3.3.3	<u>Component and/or Material Testing</u>	3-99
3.3.3.4	<u>Control Rod Drive Tests and Inspection</u>	3-100
3.3.4	INTERNALS TESTS AND INSPECTIONS	3-103
3.4	<u>REFERENCES</u>	3-104

00000142

LIST OF TABLES

<u>Table No.</u>	<u>Title</u>	<u>Page</u>
3-1	Core Design, Thermal, and Hydraulic Data	3-6
3-2	Nuclear Design Data	3-8
3-3	Excess Reactivity Conditions	3-9
3-4	First Cycle Reactivity Control Distribution	3-9
3-5	Shutdown Reactivity Analysis	3-13
3-6	Soluble Boron Levels and Worth	3-14
3-7	Exterior Neutron Levels and Spectra	3-17
3-8	Calculated and Experimental Rod and Rod Assembly Comparison	3-22
3-9	Reference Core Parameters	3-28
3-10	First Mode Threshold Dimensions and Flatness	3-28
3-11	Threshold Ratio and Power Flatness	3-29
3-12	Coefficients of Variation	3-35
3-13	DNB Results - Maximum Design Condition	3-57
3-14	DNB Results - Most Probable Condition	3-58
3-15	Heat Transfer Test Data	3-59
3-16	Comparison of Heat Transfer Test Data	3-50
3-17	Hot Channel Coolant Conditions	3-51
3-18	DNB Ratios in the Fuel Assembly Channels	3-64
3-19	Clad Circumferential Stresses	3-78
3-20	LRD Fuel Swelling Irradiation Program	3-84
3-21	Control Rod Drive Design Data	3-88
3-22	Control Rod Assembly Design Data	3-93
3-23	Axial Power Shaping Rod Assembly Data	3-94

00000143

LIST OF FIGURES

(At rear of Section)

<u>Figure No.</u>	<u>Title</u>
3-1	Boron Concentration versus Core Life
3-2	Axial Peak to Average Power versus Xenon Override Rod Insertion
3-3	Axial Power Profile, Xenon Override Rods 55 Per Cent Inserted
3-4	Moderator Temperature Coefficient versus Boron Concentration
3-5	Moderator Temperature Coefficient versus Moderator Temperature and Various Boron Levels
3-6	Per Cent Initial Power versus Time Following Trip
3-7	Effect of Fuel Temperature (Doppler) on Xenon Oscillations - Beginning of Life
3-8	Effect of Fuel Temperature (Doppler) on Xenon Oscillations - Near End of Life
3-9	Control of Axial Oscillation with Partial Rods
3-10	Population Included in the Statistical Statement Versus DNB Ratio
3-11	Power Shape Reflecting Increased Axial Power Peak for 144-Inch Core
3-12	Distribution of Fuel Rod Peaking
3-13	Possible Fuel Rod DNB's for Maximum Design Conditions - 36,816-Rod Core
3-14	Possible Fuel Rod DNB's for Most Probable Conditions - 36,816-Rod Core
3-15	Distribution of Population Protected, P, and 1-P versus Number Rods for Most Probable Conditions
3-16	DNB Ratios (BAW-168) versus Reactor Power
3-17	Maximum Hot Channel Exit Quality versus Reactor Overpower
3-18	Thermal Conductivity of UO ₂
3-19	Fuel Center Temperature at the Hot Spot versus Linear Power
3-20	Number of Data Points versus ϕ_E/ϕ_C
3-21	Hot Channel Factor versus Per Cent Population Protected

00000144

00000144

00000144

FIGURES (Cont'd)

<u>Figure No.</u>	<u>Title</u>
3-22	Burnout Factor versus Population for Various Confidence Levels
3-23	Rods in Jeopardy versus Power
3-24	Ratio of Experimental to Calculated Burnout Heat Flux
3-25	Ratio of Experimental to Calculated Burnout Heat Flux
3-26	Ratio of Experimental to Calculated Burnout Heat Flux
3-27	Ratio of Experimental to Calculated Burnout Heat Flux
3-28	Ratio of Experimental to Calculated Burnout Heat Flux
3-29	Ratio of Experimental to Calculated Burnout Heat Flux
3-30	Ratio of Experimental to Calculated Burnout Heat Flux
3-31	Ratio of Experimental to Calculated Burnout Heat Flux
3-32	Ratio of Experimental to Calculated Burnout Heat Flux
3-33	Ratio of Experimental to Calculated Burnout Heat Flux
3-34	Ratio of Experimental to Calculated Burnout Heat Flux
3-35	Ratio of Experimental to Calculated Burnout Heat Flux
3-36	Ratio of Experimental to Calculated Burnout Heat Flux
3-37	Ratio of Experimental to Calculated Burnout Heat Flux
3-38	Ratio of Experimental to Calculated Burnout Heat Flux
3-39	Ratio of Experimental to Calculated Burnout Heat Flux
3-40	Maximum Hot Channel Exit Quality versus Reactor Power
3-41	Hottest Design and Nominal Channel Exit Quality versus Reactor Power (without Engineering Hot Channel Factors)
3-42	Flow Regime Map for Unit Cell Channel at 2,120 psig
3-43	Flow Regime Map for Unit Cell Channel
3-44	Flow Regime Map for Corner Channel
3-45	Flow Regime Map for Wall Channel

00000145

FIGURES (Cont'd)

<u>Figure No.</u>	<u>Title</u>	
3-46	Hot Channel DNB Ratio Comparison	
3-47	Reactor Coolant Flow versus Power	
3-48	Thermal Conductivity of 95 Per Cent Dense Sintered UO ₂ Pellets	
3-49	Fuel Center Temperature for Beginning-of-Life Conditions	
3-50	Fuel Center Temperature for End-of-Life Conditions	
3-51	Per Cent Fission Gas Released as a Function of the Average Temperature of the UO ₂ Fuel	
3-52	Axial Local to Average Burnup and Instantaneous Power Comparisons	
3-53	Fission Gas Release for 1.50 and 1.70 Max/Avg Axial Power Shapes	
3-54	Gas Pressure inside the Fuel Clad for Various Axial Burnup and Power Shapes	
3-55	Nominal Fuel Rod Power Peaks and Cell Exit Enthalpy Rise Ratios	
3-56	Maximum Fuel Rod Power Peaks and Cell Exit Enthalpy Rise Ratios	
3-57	Calculated and Design Limit Local Heat Flux versus Enthalpy in the Hot Corner Cell at the Nominal Condition	
3-58	Calculated and Design Limit Local Heat Flux versus Enthalpy in the Hot Corner Cell at the Postulated Worst Condition	
3-59	Reactor Vessel and Internals - General Arrangement	
3-60	Reactor Vessel and Internals - Cross Section	
3-61	Core Flooding Arrangement	
3-61a	Internals Vent Valve	1
3-62	Fuel Assembly	
3-63	Orifice Rod Assembly	
3-64	Control Rod Drive - General Arrangement	
3-65	Control Rod Drive - Vertical Section	
3-66	Control Rod Drive System and Trip Block Diagram	
3-67	(Deleted)	
3-68	(Deleted)	
3-69	Control Rod Assembly	
3-70	Axial Power Shaping Rod Assembly	7

00000146 | 7

3 REACTOR

3.1 DESIGN BASES

The reactor is designed to meet the performance objectives specified in 3.1.1 without exceeding the limits of design and operation specified in 3.1.2.

3.1.1 PERFORMANCE OBJECTIVES

The reactor is designed to operate initially at 2,452 MWt with sufficient design margins to accommodate transient operation and instrument error without damage to the core and without exceeding the pressure at the safety valve settings in the reactor coolant system. The ultimate operating power level of the reactor is expected to be 2,544 MWt, but additional operating information will be required to justify operation at this higher power level. Thus, this section of the report describes only reactor operation at the initial power level.

The fuel rod cladding is designed to maintain its integrity for the anticipated core life. The effects of gas release, fuel dimensional changes, and corrosion- or irradiation-induced changes in the mechanical properties of cladding are considered in the design of fuel assemblies.

Reactivity is controlled by control rod assemblies (CRA's) and chemical poison dissolved in the coolant. Sufficient CRA worth is available to shut the reactor down ($k_{eff} \leq 0.99$) in the hot condition at any time during the life cycle with the most reactive CRA stuck in the fully withdrawn position. Redundant equipment is provided to add soluble poison to the reactor coolant to insure a similar shutdown capability when the reactor coolant is cooled to ambient temperatures.

The reactivity worth of CRA's, and the rate at which reactivity can be added, is limited to insure that credible reactivity accidents cannot cause a transient capable of damaging the reactor coolant system or causing significant fuel failure.

3.1.2 LIMITS

3.1.2.1 Nuclear Limits

The core has been designed to the following nuclear limits:

- a. Fuel has been designed for an average burnup of 28,200 MWD/MTU and for a maximum burnup of 55,000 MWD/MTU.
- b. The power coefficient is negative, and the control system is capable of compensating for reactivity changes resulting from nuclear coefficients, either positive or negative.
- c. Control systems will be available to handle core xenon instabilities should they occur during operation, without jeopardizing the safety conditions of the system.

00000147

- d. The core will have sufficient excess reactivity to produce the design power level and lifetime without exceeding the control capacity or shutdown margin.
- e. Controlled reactivity insertion rates have been limited to 1.1×10^{-4} $\Delta k/k/sec$ for a single regulating CRA group withdrawal, and 7×10^{-6} $\Delta k/k/sec$ for soluble boron removal.
- f. Reactor control and maneuvering procedures will not produce peak-to-average power distributions greater than those listed in Table 3-1. The low worth of CRA groups inserted during power operation limits power peaks to acceptable values.

7

3.1.2.2 Reactivity Control Limits

The control system and the operational procedures will provide adequate control of the core reactivity and power distribution. The following control limits will be met:

- a. Sufficient control will be available to produce a shutdown margin of at least 1% $\Delta k/k$.
- b. The shutdown margin will be maintained with the CRA of highest worth stuck out of the core.
- c. CRA withdrawal limits the reactivity insertion rate to 1.1×10^{-4} $\Delta k/k/sec$ on a single regulating group. Boron dilution is also limited to a reactivity insertion rate of 7×10^{-6} $\Delta k/k/sec$.

7

3.1.2.3 Thermal and Hydraulic Limits

The reactor core is designed to meet the following limiting thermal and hydraulic conditions:

- a. No central melting at the design overpower (114 per cent).
- b. A 99 per cent confidence that at least 99.5 per cent of the fuel rods in the core are in no jeopardy of experiencing a departure from nucleate boiling (DNB) during continuous operation at the design overpower.
- c. Essentially 100 per cent confidence that at least 99.96 per cent of the fuel rods in the core are in no jeopardy of experiencing a DNB during continuous operation at rated power.
- d. The generation of net steam in the hottest core channels is permissible, but steam voids will be low enough to prevent flow instabilities.

The design overpower is the highest credible reactor operating power permitted by the safety system. Normal overpower to trip is significantly less than the design overpower. Core rated power is 2,452 MWt.

00000148

3.1.2.4 Mechanical Limits

3.1.2.4.1 Reactor Internals

The reactor internal components are designed to withstand the stresses resulting from startup; steady state operation with one, two, three, or four reactor coolant pumps running; and shutdown conditions. No damage to the reactor internals will occur as a result of loss of pumping power.

Reactor internals will be fabricated from SA-240 (Type 304) material and will be designed within the allowable stress levels permitted by the ASME Code, Section III, for normal reactor operation and transients. Structural integrity of all core support assembly circumferential welds will be assured by compliance with ASME Code Sections III and IX, radiographic inspection acceptance standards, and welding qualifications.

The core support structure will be designed as a Class I structure, as defined in Appendix 5A of this report, to resist the effects of seismic disturbances. The basic design guide for the seismic analysis will be AEC publication TID-7024, "Nuclear Reactors and Earthquakes".

Lateral deflection and torsional rotation of the lower end of the core support assembly will be limited to prevent excessive movements resulting from seismic disturbance and thus prevent interference with control rod assemblies (CRA's). Core drop in the event of failure of the normal supports will be limited so that the CRA's do not disengage from the fuel assembly guide tubes.

The structural internals will be designed to maintain their functional integrity in the event of a major loss-of-coolant accident as described in 3.2.4.1. The dynamic loading resulting from the pressure oscillations because of a loss-of-coolant accident will not prevent CRA insertion.

Internals vent valves are provided to relieve pressure generated by steaming in the core following a postulated reactor coolant inlet pipe rupture so that the core will remain sufficiently covered with coolant.

3.1.2.4.2 Fuel Assemblies

The fuel assemblies are designed to operate satisfactorily to design burnup and to retain adequate integrity at the end of life to permit safe removal from the core.

The assemblies are designed to operate safely during steady state and transient conditions under the combined effects of flow-induced vibration, cladding strain caused by reactor pressure, fission gas pressure, fuel growth, and differential thermal expansion. The cold-worked Zircaloy-4 cladding is designed to be free-standing. Fuel rods are held in place by mechanical spacer grids that are designed to maintain dimensional control of the fuel rod spacing throughout the design life without impairing cladding integrity. Contact loads are limited to prevent fretting.

The spacer grids are also designed to permit differential thermal expansion of the fuel rods without restraint that would cause distortion of the rods. The fuel assembly upper end fitting and the control rod guide tube in the internals structure are both indexed to the grid plate above the fuel assemblies, thus insuring continuous alignment of the guide channels for the CRA's. The control rod travel is designed so that the rods are always engaged in the fuel assembly

guide tubes, thus insuring that CRA's can always be inserted. The assembly structure is also designed to withstand handling loads, shipping loads, and earthquake loads.

Stress and strain for all anticipated normal and abnormal operating conditions will be limited as follows:

- a. Stresses that are not relieved by small deformations of the material will be prevented from leading to failure by not permitting these stresses to exceed the yield strength of the material nor to exceed levels that would use in excess of 75 per cent of the stress rupture life of the material. An example of this type of stress is the circumferential membrane stress in the clad due to internal or external pressure.
- b. Stresses that are relieved by small deformations of the material, and the single occurrence of which will not make a significant contribution to the possibility of a failure, will be permitted to exceed the yield strength of the material. Where such stresses exceed the material yield strength, strain limits will be set, based on low-cycle fatigue techniques, using no more than 90 per cent of the material fatigue life. Evaluations of cyclic loadings will be based on conservative estimates of the number of cycles to be experienced. An example of this type of stress is the thermal stress resulting from the thermal gradient across the clad thickness.
- c. Combinations of these two types of stresses, in addition to the individual treatment outlined above, will be evaluated on the low-cycle fatigue basis of Item b. Also, clad plastic strain due to diameter increases resulting from thermal ratcheting and/or creep, including the effects of internal gas pressure and fuel swelling, will be limited to about 1 per cent.
- d. Minimum clad collapse pressure margins will be required as follows:
 - (1) 10 per cent margin over system design pressure, on short time collapse, at end void.
 - (2) End void must not collapse (must be either freestanding or have adequate support) on a long time basis.
 - (3) 10 per cent margin over system operating pressure, on short time collapse, at hot spot average temperature through the clad wall.
 - (4) Clad must be freestanding at design pressure on a short time basis at ≈ 725 F hot spot average temperature through the clad wall.

00000150

3.1.2.4.3 Control Rod Assembly (CRA)

The control rod clad is designed to the same criteria as the fuel clad, as applicable. Adequate clearance will be provided between the control rods and the guide tubes, which position them within the fuel assembly, so that control rod overheating will be avoided and unacceptable mechanical interference between the control rod and the guide tube will not occur under any operating condition, including earthquake.

Overstressing of the CRA components during a trip will be prevented by minimizing the shock loads by snubbing and by providing adequate strength.

3.1.2.4.4 Control Rod Drive

Deleted sentence.

The control rod drives provide control rod assembly (CRA) insertion and withdrawal rates consistent with the required reactivity changes for reactor operational load changes. This rate is based on the worths of the various rod groups, which have been established to limit power-peaking flux patterns to design values. The maximum reactivity addition rate is specified to limit the magnitude of a possible nuclear excursion resulting from a control system or operator malfunction. The normal insertion and withdrawal velocity has been established as 30 in./min.

The control rod drives provide a "trip" of the CRA's which results in a rapid shutdown of the reactor for conditions that cannot be handled by the reactor control system. The trip is based on the results of various reactor emergency analyses, including instrument and control delay times and the amount of reactivity that must be inserted before deceleration of the CRA occurs. The maximum travel time for a 2/3 insertion on a trip command of a CRA has been established as 1.4 sec.

The control rod drives can be coupled and uncoupled to their respective CRA's without any withdrawal movement of the CRA's.

All pressure-containing components are designed to meet the requirements of the ASME Code, Section III, Nuclear Vessels, for Class A vessels.

Materials selected for the control rod drive are capable of operating within the specified reactor environment for the life of the mechanism without any deleterious effects. Adequate clearance will be provided between the stationary and moving parts of the control rod drives so that the CRA trip time to full insertion will not be adversely affected by mechanical interference under all operating conditions and seismic disturbances.

Structural integrity and adherence to allowable stress limits of the control rod drive and related parts during a trip will be achieved by establishing a limit on impact loads through snubbing.

00000151

3.2 REACTOR DESIGN

3.2.1 GENERAL SUMMARY

The important core design, thermal, and hydraulic characteristics are tabulated in Table 3-1.

Table 3-1
Core Design, Thermal, and Hydraulic Data

Reactor

Type	Pressurized Water
Rated Heat Output, MWt	2,452
Vessel Coolant Inlet Temperature, F	555
Vessel Coolant Outlet Temperature, F	602.8
Core Outlet Temperature, F	604.3
Operating Pressure, psig	2,185

Core and Fuel Assemblies

Total Number of Fuel Assemblies in Core	177
Number of Fuel Rods per Fuel Assembly	208
Number of Control Rods per Control Rod Assembly	16
Number of Incore Instrumentation Positions per Fuel Assembly	1
Fuel Rod Outside Diameter, in.	0.420
Clad Thickness, in.	0.026
Fuel Rod Pitch, in.	0.558
Fuel Assembly Pitch Spacing, in.	8.587
Unit Cell Metal/Water Ratio	0.80
Clad Material	Zircaloy-4 (cold-worked)

Fuel

Material	UO ₂
Form	Dished-End, Cylindrical Pellets
Diameter, in.	0.362
Active Length, in.	144
Density, % of theoretical	95

Heat Transfer and Fluid Flow at Rated Power

Total Heat Transfer Surface in Core, ft ²	48,578
Average Heat Flux, Btu/hr-ft ²	167,620
Maximum Heat Flux, Btu/hr-ft ²	543,000
Average Power Density in Core, kw/l	79.60
Average Thermal Output, kw/ft of fuel rod	5.4
Maximum Thermal Output, kw/ft of fuel rod	17.49
Maximum Clad Surface Temperature, F	654
Average Core Fuel Temperature, F	1,385
Maximum Fuel Central Temperature at Hot Spot, F	4,160

00000152

Table 3-1 (Cont'd)

Total Reactor Coolant Flow, lb/hr	131.32 x 10 ⁶
Core Flow Area (effective for heat transfer), ft ²	47.75
Core Coolant Average Velocity, fps	15.7
Coolant Outlet Temperature at Hot Channel, F	644.4

Power Distribution

Maximum/Average Power Ratio, radial x local (F _{Δh} nuclear)	1.85
Maximum/Average Power Ratio, axial (F _z nuclear)	1.70
Overall Power Ratio (F _q nuclear)	3.15
Power Generated in Fuel and Cladding, %	97.3

Hot Channel Factors

Power Peaking Factor (F _Q)	1.008
Flow Area Reduction Factor (F _A)	0.992
Local Heat Flux Factor (F _{Q"})	1.013
Hot Spot Maximum/Average Heat Flux Ratio (F _q nuc. and mech.)	3.24

DNE Data

Design Overpower Ratio	1.14
DNE Ratio at Design Overpower (BAW-168)	1.38
DNE Ratio at Rated Power (BAW-168)	1.60

3.2.2 NUCLEAR DESIGN AND EVALUATION

The basic design of the core satisfies the following requirements:

- a. Sufficient excess reactivity is provided to achieve the design power level over the specified fuel cycle.
- b. Sufficient reactivity control is provided to permit safe reactor operation and shutdown at all times during core lifetime.

3.2.2.1 Nuclear Characteristics of the Design

3.2.2.1.1 Excess Reactivity

The nuclear design characteristics are given in Table 3-2. The excess reactivities associated with various core conditions are tabulated in Table 3-3. The core will operate for 410 full power days for the first cycle and will have a 310 full power day equilibrium cycle. Design limits will be held with respect to reactivity control and power distribution. Incore instrumentation will be used to insure proper power peaking levels. Single fuel assembly reactivity information is also included in Table 3-3.

Table 3-2
Nuclear Design Data

Fuel Assembly Volume Fractions

Fuel	0.285
Moderator	0.590
Zircaloy	0.099
Stainless Steel	0.011
Void	<u>2.015</u>

1.000

Total UO₂, metric tons

91.61

Core Dimensions, in.

Equivalent Diameter	128.9
Active Height	144.0

Unit Cell H₂O to U Atomic Ratio (fuel assembly)

Cold	2.97
Hot	2.13

Full Power Lifetime, days

First Cycle	410
Each Succeeding Cycle	310

Fuel Irradiation, MWD/MTU

First Cycle Average	12,460
Succeeding Cycle Average	9,410

Feed Enrichments, w/o U-235

First Cycle	2.29/2.64/2.90 (by zone)
Equilibrium Cycle	2.94(a)

Control Data

Control Rod Material	Cd-In-Ag
Number of Control Rod Assemblies	69
Total Rod Worth ($\Delta k/k$), %	10.0
Control Rod Cladding Material	Type 304 SS

13

(a) Average feed enrichment.

00000154

Table 3-3
Excess Reactivity Conditions

Effective Multiplication - BOL^(a)

Cold, Zero Power	1.302	1
Hot, Zero Power	1.247	
Hot, Rated Power	1.229	
Hot, Equilibrium Xe, Rated Power	1.192	
Hot, Equilibrium Xe and Sm, Rated Power ^(b)	1.158	

Single Fuel Assembly^(c)

Hot	0.77
Cold ^(d)	0.87

- (a) BOL - Beginning-of-Life.
- (b) Includes burnup until equilibrium samarium is reached.
- (c) Based on highest probable enrichment of 3.5 weight per cent.
- (d) A center-to-center assembly pitch of 21 in. is required for this k_{eff} in cold, nonborated water with no xenon or samarium.

The minimum critical mass, with and without xenon and samarium poisoning, may be specified in a variety of forms, i.e., single assembly, multiple assemblies in various geometric arrays, damaged or crushed assemblies, etc. The unit fuel assembly has been investigated for comparative purposes. A single cold, clean assembly containing a maximum probable enrichment of 3.5 wt % is subcritical. Two assemblies side-by-side are supercritical except when both equilibrium xenon and samarium are present. Three assemblies side-by-side are supercritical with both equilibrium xenon and samarium present.

3.2.2.1.2 Reactivity Control Distribution

Control of excess reactivity is shown in Table 3-4.

Table 3-4
First Cycle Reactivity Control Distribution

	<u>% $\Delta k/k$</u>	
1. <u>Controlled by Soluble Boron</u>		
a. Moderator Temperature Deficit (70 to 520 K)	3.4	
b. Equilibrium Xenon and Samarium	2.5	1

Table 3-4 (Cont'd)

	<u>% $\Delta k/k$</u>	
c. Fuel Burnup and Fission Product Buildup	16.0	1
2. <u>Controlled by Inserted Control Rod Assemblies</u>		
a. Transient Xenon (normally inserted)	1.4	
3. <u>Controlled by Movable Control Rod Assemblies</u>		
a. Doppler Deficit (0 to 100% rated power)	1.2	
b. Equilibrium Xenon	1.0	
c. Moderator Temperature Deficit (0 to 15% power at end of life)	0.6	
d. Dilution Control	0.2	
e. Shutdown Margin	<u>1.0</u>	
Total Movable Control Worth Required	4.0	
4. <u>Available Control Rod Assembly Worths</u>		
a. Total CRA Worth	10.0	
b. Stuck Rod Worth (rod of highest reactivity value)	(-) 3.0	
c. Minimum Available CRA Worth	7.0	
d. Minimum Movable CRA Worth Available	5.6	

Explanation of Items Above

1. Soluble Boron

Boron in solution is used to control the following relatively slow-moving reactivity changes.

- a. The moderator deficit in going from ambient to operating temperatures. The value shown is for the maximum change which would occur toward the end of the cycle.
- b. Equilibrium samarium and a part (approximately 1.4% $\Delta k/k$) of the equilibrium xenon.
- c. The excess reactivity required for fuel burnup and fission product buildup throughout cycle life.

00000156

Figure 3-1 shows the typical variation in boron concentration with life for Cycle 1 and the equilibrium cycle.

Control rod assemblies (CRA's) will be used to control the reactivity changes associated with the following:

2. Inserted Control

(DELETED)

Sufficient rod worth remains inserted in the core during normal operation to overcome the peak xenon transient following a power reduction. This override capability facilitates the return to normal operating conditions without extended delays. The presence of these rods in the core during operation does not produce power peaks above the design value, and the shutdown margin of the core is not adversely affected. Axial power peak variation, resulting from partial or full insertion of xenon override rods, is described fully in Figures 3-2 and 3-3. The loss of movable reactivity control due to the insertion of this group produces no shutdown difficulties and is reflected in Table 3-5.

3. Movable Control

- a. Power level changes (Doppler) and regulation.
- b. The portion of the equilibrium xenon not controlled by soluble boron, approximately 1% $\Delta k/k$, is held by movable CRA's.

00000157

- c. Between zero and 15 per cent of full power, reactivity compensation by CRA's may be required as a result of the linear increase of reactor coolant temperature from 520 F to the normal operating value.
- d. Additional reactivity is held by a group of partially inserted CRA's (25 per cent insertion maximum) to allow periodic rather than continuous soluble boron dilution. The CRA's are inserted to the 25 per cent limit as the boron is diluted. Automatic withdrawal of these CRA's during operation is allowed to the 5 per cent insertion limit where the dilution procedure is again initiated and this group of CRA's is reinserted.
- e. A shutdown margin of 1% $\Delta k/k$ to the hot critical condition is also required as part of the reactivity controlled by CRA's.

4. Rod Worth

A total of 4.0% $\Delta k/k^{(a)}$ is required in movable control. Analysis of the 69 CRA's under the reference fuel arrangement predicts a total CRA worth of at least 10.0% $\Delta k/k$. The stuck-out CRA worth was also evaluated at a value no larger than 3.0% $\Delta k/k^{(b)}$. This evaluation included selection of the highest worth CRA under the first CRA-out condition. The minimum available CRA worth of 5.6% $\Delta k/k^{(a)}$ is sufficient to meet movable control requirements.

1

3.2.2.1.3 Reactivity Shutdown Analysis

The ability to shut down the core under both hot and cold conditions is illustrated in Table 3-5. In this tabulation both the first and equilibrium cycles are evaluated at the beginning-of-life (BOL) and the end-of-life (EOL) for shutdown capability.

(a) Does not include transient control. See Table 3-4.

(b) First cycle. See Table 3-4.

00000158

Table 3-5
Shutdown Reactivity Analysis

<u>Reactivity Effects, % $\Delta k/k$</u>	<u>First Cycle</u>		<u>Equilibrium</u>	
	<u>BOL</u>	<u>EOL</u>	<u>BOL</u>	<u>EOL</u>
1. Maximum Shutdown CRA Requirement				
Doppler (100 to 0% Power)	1.2	1.5	1.2	1.5
Equilibrium Xenon	1.0	1.0	1.0	1.0
Moderator Deficit (15 to 0% Power)	<u>0.0</u>	<u>0.8</u>	<u>0.0</u>	<u>0.8</u>
Total	2.2	3.3	2.2	3.3
2. Maximum Available CRA Worth ^(a)	-10.0	-10.0	-10.0	-10.0
Transient Xe Insertion Worth	1.4	1.4	1.4	0.0
Possible Dilution Insertion	0.2	0.2	0.2	0.2
3. Minimum Available CRA Worth				
All CRA's In	-8.4	-8.4	-8.4	-9.8
One CRA Stuck-Out ^(b)	-5.4	-5.4	-5.4	-6.8
4. Minimum Hot Shutdown Margin				
All CRA's In	-6.2	-5.1	-6.2	-6.5
One CRA Stuck-Out	-3.2	-2.1	-3.2	-3.5
5. Hot-to-Cold Reactivity Changes ^(c)				
All CRA's In	+0.0	+6.4	+3.0	+8.0
One CRA Stuck-Out	-0.9	+5.5	+2.1	+7.1
6. Cold Reactivity Condition ^(d)				
All CRA's In	-6.2	+1.3	-3.2	+1.5
One CRA Stuck-Out	-4.1	+3.4	-1.1	+3.6
7. PPM Boron Addition Required for k_{eff} = 0.99 (cold)				
All CRA's In	0	170	0	190
One CRA Stuck-Out	0	330	0	350

(a) Total worth of 69 CRA's.

(b) CRA of highest reactivity value.

(c) Includes changes in CRA worth, moderator deficit, and equilibrium Xe held by soluble boron.

(d) No boron addition.

00000159

Examination of Table 3-5 for Minimum Hot Shutdown Margin (Item 4) shows that, with the highest worth CRA stuck out, the core can be maintained in a subcritical condition. Normal conditions indicate a minimum hot shutdown margin of $5.1\% \Delta k/k$ at end-of-life.

| 1

Under conditions where a cooldown to reactor building ambient temperature is required, concentrated soluble boron will be added to the reactor coolant to produce a shutdown margin of a least $1\% \Delta k/k$. The reactivity changes that take place between the hot zero power to cold conditions are tabulated, and the corresponding increases in soluble boron are listed. Beginning-of-life boron levels for several core conditions are listed in Table 3-6 along with boron worth values. Additional soluble boron could be added for situations involving more than a single stuck CRA. The conditions shown with no CRA's illustrate the highest requirements.

Table 3-6
Soluble Boron Levels and Worth

<u>Core Conditions</u>	<u>BOL Boron Levels, ppm</u>
1. Cold, $k_{eff} = 0.99$	
No CRA's In	1,820
All CRA's In	1,290
One Stuck CRA	1,450
2. Hot, Zero Power, $k_{eff} = 0.99$	
No CRA's In	2,080
All CRA's In	1,080
One Stuck CRA	1,380
3. Hot, Rated Power	
No CRA's In	1,860
4. Hot, Equilibrium Xe and Sm, Rated Power	
No CRA's In	1,360

| 1

<u>Core Condition</u>	<u>Boron Worth, ($\% \Delta k/k$)/ppm</u>
Hot	1/100
Cold	1/75

00000140
00000160

3.2.2.1.4 Reactivity Coefficients

Reactivity coefficients form the basis for analog studies involving normal and abnormal reactor operating conditions. These coefficients have been investigated as part of the analysis of this core and are described below as to function and overall range of values.

a. Doppler Coefficient

The Doppler coefficient reflects the change in reactivity as a function of fuel temperature. A rise in fuel temperature results in an increase in the effective absorption cross section of the fuel (the Doppler broadening of the resonance peaks) and a corresponding reduction in neutron production. The range for the Doppler coefficient under operating conditions is expected to be -1.1×10^{-5} to $-1.7 \times 10^{-5} \Delta k/k/F$.

b. Moderator Void Coefficient

The moderator void coefficient relates the change in neutron multiplication to the presence of voids in the moderator. Cores controlled by appreciable amounts of soluble boron may exhibit a small positive coefficient for very small void levels (several per cent void), while higher void levels produce increasingly negative coefficients. The expected range for the void coefficient is $+1.0 \times 10^{-4}$ to $-3.0 \times 10^{-3} \Delta k/k/\%$ void.

c. Moderator Pressure Coefficient

The moderator pressure coefficient relates the change in moderator density, resulting from a reactor coolant pressure change, to the corresponding effect on neutron production. This coefficient is opposite in sign and considerably smaller when compared to the moderator temperature coefficient. A typical range of pressure coefficients over a life cycle would be -1×10^{-6} to $+3 \times 10^{-6} \Delta k/k/psi$.

d. Moderator Temperature Coefficient

The moderator temperature coefficient relates a change in neutron multiplication to the change in reactor coolant temperature. Reactors using soluble boron as a reactivity control have fewer negative moderator temperature coefficients than do cores controlled solely by movable or fixed CRA's. The major temperature effect on the coolant is a change in density. An increasing coolant temperature produces a decrease in water density and an equal percentage reduction in boron concentration. The concentration change results in a positive reactivity component by reducing the absorption in the coolant. The magnitude of this component is proportional to the total reactivity held by soluble boron.

The moderator temperature coefficient has been parameterized for the reference core in terms of boron concentration and reactor coolant temperature. The results of the study are shown in Figures 3-4 and

00000161

~~00000160~~

3-5. Figure 3-4 shows the coefficient variation for ambient and operating temperatures as a function of soluble boron concentration. The operating value ranges from approximately $+1.0 \times 10^{-4}$ at the beginning of the first cycle to $-3.0 \times 10^{-4} \Delta k/k/F$ at the end of the equilibrium cycle. Figure 3-5 shows the moderator temperature coefficient as a function of temperature for various poison concentrations for the first cycle. The coefficients of the equilibrium cycle will be more negative than those of the first cycle since the boron concentration levels are considerably lower.

The positive temperature coefficient during the initial portion of each cycle will not constitute an operational problem. The Doppler deficit represents a much larger reactivity effect in the negative direction and, together with the CRA system response, will provide adequate control.

e. pH Coefficient

Currently, there is no definite correlation to predict pH reactivity effects between various operating reactors, pH effects versus reactor operating time at power, and changes in effects with various clad, temperature, and water chemistry. Yankee (Rowe, Mass.), Saxton, and Con Edison Indian Point Station No. 1 have experienced reactivity changes at the time of pH changes, but there is no clear-cut evidence that pH is the direct influencing variable without considering other items such as clad materials, fuel assembly crud deposition, system average temperature, and prior system water chemistry.

Saxton experiments have indicated a pH reactivity effect of 0.16 per cent reactivity per pH unit change with and without local boiling in the core. Operating reactor data and the results of applying Saxton observations to the reference reactor are as follows:

- (1) The proposed system pH will vary from a cold measured value of approximately 5.5 to a hot calculated value of 7.8 with 1,400 ppm boron and 3 ppm KOH in solution at the beginning of life. Lifetime bleed dilution to 20 ppm boron will reduce pH by approximately 0.8 pH units to a hot calculated pH value of 7.0.
- (2) Considering the maximum system makeup rate of 70 gpm, the corresponding changes in pH are 0.071 pH units per hour for boron dilution and 0.231 pH units per hour for KOH dilution. Applying pH worth values of 0.16% $\Delta k/k$ per pH unit, as observed at Saxton, insertion rates are $3.16 \times 10^{-6} \Delta k/k$ sec and $1.03 \times 10^{-5} \Delta k/k$ sec, respectively. These insertion rates correspond to 1.03 per cent power/hour and 3.4 per cent power/hour, respectively, which are easily compensated by the operator or the automatic control system.

00000162

3.2.2.1.5 Reactivity Insertion Rates

Figure 7-7 displays the integrated rod worth of three overlapping rod banks as a function of distance withdrawn. The indicated groups are those used in the core during power operation. Using approximately 1.2% $\Delta k/k$ CRA groups and a 30 in./min drive speed in conjunction with the reactivity response given in Figure 7-7 yields a maximum reactivity insertion rate of 1.1×10^{-4} ($\Delta k/k$)/sec. The maximum reactivity insertion rate for soluble boron removal is 7×10^{-6} ($\Delta k/k$)/second.

| 7
| 7

3.2.2.1.6 Neutron Flux Distribution and Spectrum

Figure 3-6 displays the beginning-of-life power decay curves for the two least effective CRA worths as outlined in Table 3-5, Item No. 3. The power decay is initiated by the trip release of the CRA's with a 300 msec delay from initiation to start of CRA motion. The time required for 2/3 rod insertion is 1.4 sec.

3.2.2.1.7 Neutron Flux Distribution and Spectrum

The neutron flux levels at the core edge and the pressure vessel wall are given in Table 3-7.

Table 3-7
Exterior Neutron Levels and Spectra

Flux Group		Neutron Flux Levels, n/cm ² /sec ^(a)	
		Core Edge (x 10 ¹³)	Interior Wall of Pressure Vessel (x 10 ¹⁰)
1	0.821 Mev to 10 Mev	6.0	3.4
2	1.230 Kev to 0.821 Mev	9.0	7.5
3	0.414 ev to 1.230 Kev	6.2	5.7
4	Less than 0.414 ev	7.1	2.1

(a) These values include the maximum axial peak-to-average power ratio of 1.7.

The calculations were performed using The Babcock & Wilcox Company's LIFE code (BAW-293, Section 3.6.3) to generate input data for the transport code, TOPIC.⁽¹⁾ A 4-group edit is obtained from the LIFE output which includes diffusion coefficients, absorption, removal, and fission cross sections, and the zeroth and first moments of the scattering cross section. TOPIC is an S_n code designed to solve the 1-dimensional transport equation in cylindrical coordinates for up to six groups of neutrons. For the radial and azimuthal variables, a linear approximation to the transport

00000163

equation is used; for the polar angle, Gauss quadrature is used. Scattering functions are represented by a Legendre series. The azimuthal angle can be partitioned into 4 to 10 intervals on the half-space between 0 and π . The number of mesh points in the radial direction is restricted by the number of these intervals. For the core exterior flux calculations, four intervals on the azimuthal were used. This allows the maximum number of mesh points (240) in the "r" direction to describe the shield complex. An option is available to use either equal intervals on the azimuthal angle or equal intervals on the cosine of the angle. Equal intervals on the cosine were chosen since this provides more detail in the forward direction of the flux (toward the vessel). Five Gauss quadrature points were used on the cosine of the polar angle in the half-space between 0 and π .

Results from the above method of calculation have been compared with thermal flux measurements through an array of iron and water slabs in the LIDO pool reactor.⁽²⁾ Although this is not a direct comparison with fast neutron measurements, it does provide a degree of confidence in the method since the magnitude of the thermal flux in shield regions is governed by fast neutron penetration.

Results of the comparison showed that fluxes predicted by the LIFE-TOPIC calculation were lower, in general, by about a factor of 2. Results of the fast flux calculations are, consequently, increased by a factor of 2 to predict the nvt in the reactor vessel.

The following conservatisms were also incorporated in the calculations:

- a. Neutron fluxes outside the core are based on a maximum power density of 41 watts/cc at the outer edge of the core rather than an estimated average of 28 watts/cc over life, resulting in a safety margin of about 45 per cent.
- b. A maximum axial power peaking factor of 1.7 was used. This is about 30 per cent greater than the 1.3 expected over life.

Uncertainties in the calculations include the following:

1. The use of only four neutron groups to describe the neutron energy spectrum.
2. Use of the LIFE code to generate the 4-group cross sections. In the LIFE program, the 4-group data in all regions are computed from a fission spectrum rather than a leakage spectrum.
3. Having only four intervals, i.e., $n = 4$ in the S_n calculation, to describe the angular segmentation of the flux.

It is expected that the combination of 1 and 2 above will conservatively predict a high fast neutron flux at the vessel wall because it underestimates the effectiveness of the thermal shield in reducing the fast flux. In penetration through water, the average energy of the neutrons in the group above 1 Mev increases above that of a fission spectrum, i.e., the spectrum in this group hardens. For neutrons above 1 Mev, the nonelastic

00000164

cross section of iron increases rapidly with energy. Therefore, the assumption of a fission spectrum to compute cross sections in the thermal shield, and the use of a few-group model to cover the neutron energy spectrum, would underestimate the neutron energy loss in the thermal shield and the subsequent attenuation by the water between the vessel and thermal shield. The results from 34-group P3MG1⁽³⁾ calculations show that reduction of the flux above 1 Mev by the thermal shield is about a factor of 4 greater than that computed from the 4-group calculations.

The effect of 3 above is expected to underestimate the flux at the vessel wall. In calculations at ORNL using the S_n technique, a comparison between an S_4 and an S_{12} calculation was made in penetration through hydrogen. The results for a variety of energies over a penetration range of 140 cm showed the S_4 calculation to be lower than the S_{12} by about a factor of 2 at maximum. Good agreement was obtained between the S_{12} and moments method calculations.

The above uncertainties indicate that the calculation technique should overestimate the fast flux at the reactor vessel wall. However, the comparison with thermal flux data indicates a possible underestimate. Until a better comparison with data can be made, we have assumed that the underestimate is correct and accordingly have increased the flux calculations by a factor of 2 to predict the nvt in the reactor vessel.

The reactor utilizes a larger water gap and thinner thermal shield between the core and the reactor vessel wall when compared to currently licensed plants. The effect of this steel-water configuration on (a) the neutron irradiation, and (b) the thermal stresses in the reactor vessel wall, were evaluated as follows:

a. Neutron Irradiation

Calculations were performed in connection with the reactor vessel design to determine the relative effects of varying the baffle and thermal shield thicknesses on the neutron flux (> 1 Mev) at the vessel wall. These calculations were performed with the P1 option of the P3MG1 code⁽³⁾ using 34 fast neutron groups. The results showed that the neutron flux level at the vessel wall is dependent, for the most part, on the total metal and water thickness between the core and the vessel. However, there was some variation in fluxes depending upon the particular configuration of steel-water laminations. Also, the gain in neutron attenuation by replacing water with steel diminishes somewhat with increasing steel thickness.

In general however, the results showed that for total steel thicknesses in the range of 3 to 6 in., 1 in. of steel in place of 1 in. of water would reduce the neutron flux above 1 Mev by about 30 per cent. In pure water the calculations showed that the neutron flux would be reduced, on the average, by a factor of 6 in 6 in. of water.

Based on the above analysis a comparison has been made of the neutron attenuation in this reactor vessel with those in San Onofre, Turkey Point 3 and 4, Indian Point 2, and Ginna. The total distance between this core and the reactor vessel is 21 in. This provides from 1.5 to as much as 5.75 in. more distance between the core and the

00000165

vessel than in the other reactors. For neutrons above 1 Mev it was found that this additional distance would provide additional attenuation ranging from a factor of 1.1 to 5 times greater than that in the other PWR's considered.

b. Thermal Stresses

The gamma heating in the reactor vessel is produced by primary gammas from the core and by secondary gammas originating in the core liner, barrel, thermal shield, and the vessel itself. In this reactor design the major portion of the heat is generated by gamma rays from the core and by secondary gamma rays from the core liner and barrel.

Since the gammas from each of these sources must penetrate the thermal shield to reach the vessel, the vessel heating rate is dependent on the thermal shield thickness.

For designs which employ thicker thermal shields, or in which internals are to be exposed to higher neutron fluxes, gamma rays originating in the thermal shield or in the vessel itself may govern the vessel heating rates. Since gamma rays from these sources would have to penetrate only portions or none of the thermal shield to reach the vessel, the vessel heating in such cases would be less dependent on thermal shield thickness than in this reactor design.

A comparison was made between the gamma attenuation provided by the water and metal in this reactor vessel and that in other PWR's by assuming that, in each design, the vessel heating was dependent on the gamma ray attenuation provided by the thermal shield. This approach would be conservative since, as noted above for some designs, gamma sources other than those attenuated by the thermal shield may contribute appreciably to the vessel heating. The results of the comparison showed that the difference in gamma attenuation between this reactor and other PWR's ranged from negligible difference to a factor of 5.3 less for this reactor design.

The maximum steady-state stress resulting from gamma heating in the vessel has been calculated to be 3,190 psi (tension). This is a relatively low value, and no problems are anticipated from thermal stresses in the reactor vessel wall.

3.2.2.2 Nuclear Evaluation

Analytical models and the application of these models are discussed in this section. Core instabilities associated with xenon oscillation are also mentioned, with threshold data evaluated under reference conditions.

3.2.2.2.1 Analytical Models

Reactor design calculations are made with a large number of computer codes. The choice of which code set or sets to use depends on which phase of the design is being analyzed. A list of codes used in core analysis with a brief discussion follows in 3.2.2.2.2.

a. Reactivity Calculations

Calculation of the reactivity of a pressurized water reactor core is performed in one, two, or three dimensions. The geometric choice depends on the type of calculations to be made. In a clean type of calculation where there are no strong localized absorbers of a type differing from the rest of the lattice, 1-dimensional analysis is satisfactory. This type of problem is handled quite well by the B&W 1-dimensional depletion package code LIFE. LIFE is a composite of MUFT (Ref. 4), KATE (Ref. 5), RIP, WANDA (Ref. 6), and a depletion routine. Normally the MUFT portion is used with 34 energy groups, an exact treatment of hydrogen, the Greuling-Goertzel approximation for elements of mass less than 10, and Fermi age for all heavier elements. The KATE portion normally uses a Wigner-Wilkins spectrum. In WANDA, 4 energy groups are utilized. Disadvantage factors for input to the thermal group are calculated with the THERMOS (Ref. 7) code. This code set has been shown to give reliable results for a reactivity calculation of this type. Recent check calculations on critical experiments have a standard deviation of less than 0.5% $\Delta k/k$.

A 1-dimensional analysis of a geometric arrangement, where there are localized strong absorbers such as CRA's, requires a preliminary 2-dimensional analysis. The required properties of the 1-dimensional system are then matched to the 2-dimensional analysis. In this manner, it is possible to analyze the simpler 1-dimensional system in a depletion survey problem with only a small loss in accuracy.

The 1-dimensional calculations are used as preliminary guides for the more detailed 2-dimensional analysis that follows. Values of reactivity coefficients, fuel cycle enrichments, lifetimes, and soluble poison concentrations can be found to improve the initial conditions specified for 2-dimensional analysis.

Two-dimensional reactivity calculations are done with either the PDQ (Ref. 8) or TURBO (Ref. 9) diffusion and/or depletion codes. These codes have mesh limitations on the size of configuration which can be shown explicitly and are often studied with quarter core symmetry. Symmetry is desirable in the design and as such in generality occurs. The geometric description includes the fuel assembly and as much detail as is possible, i.e., usually each unit in the fuel assembly. Analysis of this type permits detailed power distribution studies as well as reactivity analysis. The power distribution in a large PWR core which has zone loading cannot be predicted reliably with 1-dimensional calculations. This is particularly true when local power peaking as a function of power history is of interest. It is necessary to study this type of problem with at least a 2-dimensional code, and in some cases 3-dimensional calculations are necessary.

Use of the 2-dimensional programs requires the generation of group constants as a function of material composition, power history, and geometry. For regions where diffusion theory is valid, MUFT and KATE with THERMOS disadvantage factors are used to generate epithermal and thermal coefficients. This would apply at a distance of a

few mean paths from boundaries or discontinuities in the fuel rod lattice. Discontinuities refer to fuel assembly can, water channels, instrumentation ports, and CRA guide tubes. The interfaces between regions of different enrichment are considered to be boundaries as well as the outer limit of the core.

To generate coefficients for regions where diffusion theory is inappropriate several methods are utilized. The arrangement of structural material, water channels, and adjacent fuel rod rows can be represented well in slab geometry. This problem is analyzed by P3MG (Ref. 3) which is effective in slab geometry. The coefficients so generated are utilized in the epithermal energy range. Coefficients for the thermal energy range are generated by a slab THERMOS calculation. The regions adjacent to an interface of material of different enrichment are also well represented with the P3MG code.

The arrangement of instrumentation ports and control rod guide tubes lends itself to cylindrical geometry. DTF-IV (Ref. 10) is quite effective in the analysis of this arrangement. Input to DTF-IV is from GAM (Ref. 11) and THERMOS or KATE. Iteration is required between the codes. The flux shape is calculated by DTF-IV and cross sections by the others. The outer boundary of the core where there is a transition from fuel to reflector and baffle is also represented by the DTF-IV code. The 3-dimensional analysis is accomplished by extending the techniques of 2-dimensional representation.

b. Control Rod Analysis

B&W has developed a procedure for analyzing the reactivity worth of small Ag-In-Cd rods in fuel lattices. Verification of this procedure was made by the comparative analysis of 14 critical experiments with varying rod and rod assembly configurations.^(13,14) Critical lattice geometries were similar to those of the reference core design. Boron concentration ranged from 1,000 to 1,500 ppm. The Ag-In-Cd rods were arranged in various geometrical configurations which bracket the reference design. Water holes, simulating withdrawn rods, were included as part of the lattice study. The resulting comparison of the analytical and experimental worths are shown in Table 3-8. Details of the critical configurations are given in References 13 and 14.

Table 3-8
Calculated and Experimental Rod and Rod Assembly Comparison

Core No.	Assemblies per Core	Ag-In-Cd Rods per Assembly	H ₂ O Holes per Core	Rod Assembly - Calculated Worth, % $\Delta k/k$	Rod Assembly - Experimental Worth, % $\Delta k/k$
5-B	4	4	252	2.00	1.98
4-F	4	9	0	3.38	3.34
5-C	2	12	276	2.38	2.35
4-D	1	16	0	1.43	1.42
5-D	2	16	284	2.80	2.82
4-E	1	20	0	1.54	1.52
5-E	2	20	292	3.05	3.01

The mean error in calculating these configurations is shown to be less than 1 per cent. Comparison of the power shape associated with the 16-rod reference assemblies showed good similarity. Point-to-average power had a maximum variation of less than 2 per cent with experimental data.

The analytical method used for this analysis is based on straight diffusion theory. Thermal coefficients for a control rod are obtained from THERMOS by flux-weighting. Epithermal coefficients for the upper energy groups are generated by the B&W LIFE program. The resulting coefficients are used in the 2-dimensional code PDQ to obtain the required eigenvalues.

GAKER and LIBPM are used to prepare data for THERMOS. GAKER generates scattering cross sections for hydrogen by the Nelkin technique. LIBPM uses the Brown and St. John free gas model for generating the remaining scattering cross sections.

THERMOS is used in two steps. First, the critical fuel cell is analyzed to obtain a velocity-weighted disadvantage factor. This is used in the homogenization of fuel cells and gives a first order correction for spatial and spectral variation. The ratio of flux in the moderator to flux in the fuel was analyzed to within 2 per cent of experimental values using the velocity-weighting technique. The second step is to use THERMOS in a calculation where the Ag-In-Cd rod is surrounded by fuel. This is used to generate the flux-weighted control rod cell coefficients as a function of boron concentration. As a check on the validity of the THERMOS approach, extrapolation distances were compared to those given by the Spinks method.⁽¹⁵⁾ The agreement was within 2.2 per cent for a set of cases wherein the number densities of Ag-In-Cd were varied in a range up to 250 per cent. All other coefficients are generated by LIFE in much the same manner as with THERMOS. The data are used in a 2-dimensional PDQ layout where each fuel rod cell is shown separately.

c. Determination of Reactivity Coefficients

This type of calculation is different from the reactivity analysis only in application, i.e., a series of reactivity calculations being required. Coefficients are determined for moderator temperature, voiding, and pressure, and for fuel temperature. These are calculated from small perturbations in the required parameter over the range of possible values of the parameter.

The moderator temperature coefficient is determined as a function of soluble poison concentration and moderator temperature, and fuel temperature or Doppler coefficient as a function of fuel temperature. The coefficient for voiding is calculated by varying the moderator concentration or per cent void.

3.2.2.2.2 Codes for Reactor Calculations

This section contains a brief description of codes mentioned in the preceding sections.

00000169

- THERMOS (Ref. 7) - This code solves the integral form of the Boltzmann Transport Equation for the neutron spectrum as a function of position. A diagonalized connection to the isotropic transfer matrix has been incorporated allowing a degree of anisotropic scattering.
- MUFT (Ref. 4) - This program solves the P_1 or B_1 multigroup equation for the first two Legendre coefficients of the directional neutron flux, and for the isotropic and anisotropic components of the slowing down densities due to a cosine-shaped neutron source. Coefficients are generated with MUFT for the epithermal energy range.
- KATE (Ref. 5) - The code solves the Wigner-Wilkins differential equation for a homogeneous medium moderated by chemically unbound hydrogen atoms in thermal equilibrium. Coefficients for the thermal energy range are generated by KATE.
- RIP - This program averages cross sections over an arbitrary group structure, calculates resonance integrals for a set of resolved peaks, and computes L-factors for input to MUFT, PLMG, and P3MG.
- WANDA (Ref. 6) - This code provides numerical solutions of the 1-dimensional few-group neutron diffusion equations.
- LIFE - This is a 1-dimensional depletion package code which is a combination of MUFT, KATE, RIP, and WANDA. The combination mechanizes the procedures for using the codes separately.
- GAM (Ref. 11) - This code is a multigroup coefficient generation program that solves the P_1 equations and includes anisotropic scattering. Inelastic scattering and resonance parameters are also treated by GAM.
- P3MG (Ref. 3) - The code solves the multienergy transport equation in various geometries. The code is primarily used for epithermal coefficient generations.
- DTF (Ref. 10) - This code solves the multigroup, 1-dimensional Boltzmann transport equation by the method of discrete ordinates. DTF allows multigroup anisotropic scattering as well as up and down scattering.
- PDQ (Ref. 8) - This program solves the 2-dimensional neutron diffusion-depletion problem with up to five groups. It has a flexible representation of time-dependent cross sections by means of fit options.
- TURBO (Ref. 9) - This code is similar in application to the PDQ depletion program. It, however, lacks the great flexibility of the PDQ fit options.
- CANDLE (Ref. 9) - This code is similar to TURBO, but solves the diffusion equations in one dimension.

TNT (Ref. 9) - This code is similar in application to TURBO, but is a 3-dimensional code extended from DRACO.

3.2.2.2.3 Xenon Stability Analysis

Initial studies of the reference core, where realistic fuel temperatures are generated by thermal-nuclear iteration, indicate no instability at any time during the life cycle. These results are encouraging, but until more detailed analyses are completed, it will be assumed that axial xenon oscillations are possible. Azimuthal oscillations are unlikely, and radial oscillations will not occur.

Since the size, flux level, and power coefficient of current PWR designs are conducive to xenon oscillations, an extensive investigation must be completed before the stability of a core can be ascertained. An adequate solution can be found by first using analytical techniques in the manner of Randall and St. John to predict problematic areas, and then by analyzing these with diffusion theory programs that are coupled with heat transfer equations.

The results of the stability analysis of the reference core are presented below, followed by the methods section containing the details of the threshold and diffusion theory calculations employed. The closing section outlines an overall approach to the solution of the stability problem in regard to additional detailed calculative programs as well as a method for the correction of unbalanced power distributions.

a. Summary of Results

(1) Threshold Analysis

In the threshold analysis axial, azimuthal, and radial oscillations were investigated for beginning-of-life, flattened, and slightly dished power distributions.⁽¹⁷⁾ The results are as follows:

- (a) For a fixed dimension, the tendency toward spatial xenon oscillation is increased as the flux increases.
- (b) For a fixed flux, the tendency toward spatial oscillation is increased as the dimension of the core increases.
- (c) The large size of current PWR designs permits an adequate xenon description using 1-group theory.
- (d) Flattened power distributions are more unstable than normal beginning-of-life distributions. Dished power distributions are even worse.
- (e) In a modal analysis of the reference core, modal coupling can be ignored. In addition, the core is not large enough to permit second-harmonic instability.

00000171

- (f) A large, negative power coefficient tends to dampen oscillations. If this coefficient is sufficiently large, oscillations cannot occur regardless of core size or flux level. Current PWR designs have a substantial negative power coefficient.
- (g) The critical diameter for azimuthal oscillations is larger than the critical height for axial oscillations.
- (h) The reference core design is not large enough to excite radial oscillations.
- (i) Examination of the diameter, height, and power coefficient for this reference design indicates that oscillations should not occur at the beginning of life with unflattened power distributions. However, there exists a finite probability of oscillations at some later time, since core depletion tends to flatten the power distribution.
- (j) The period of oscillation (25 to 30 hours) is long enough to permit easy control of the oscillations.
- (k) The modal analysis of this core toward the end of the initial cycle (with about 80 per cent flatness) showed that axial oscillations are possible, azimuthal oscillations are unlikely, and radial oscillations will not occur.

(2) Depletion Analysis

Diffusion-depletion calculations coupled with heat transfer equations were employed to investigate further the axial stability of the core since the analytical study indicated that this was the most probable mode of oscillation. The results follow:

- (a) Axial instability did not occur at any time during the initial cycle. An average fuel temperature of 1,400 F was maintained during the cycle.
- (b) The threshold for axial instability near the end of the initial cycle was found to coincide with a core average fuel temperature of 900 F.

Diffusion theory was also used to examine the problem of controlling the system with rods if the stabilizing power Doppler was not present. The following was concluded:

- (a) Partial control rods are quite adequate in controlling axial oscillations. These rods have 3-ft-long poison sections which are moved up and down about the midplane of the core to offset oscillatory power shifts.

00000172

- (b) Detailed power profiles will be available to the reactor operator as output from the instrumentation. The large period of the oscillation will allow partial rod movement such that axial power peaks are held well within allowable limits.

b. Methods

(1) Threshold Analysis

The method used in the threshold analysis is an extension of the 1-group treatment including power coefficient introduced by Randall and St. John. One- and 2-group treatments have been compared, and the conclusion drawn is that a 1-group model is satisfactory for large cores. For all three geometries, data were generated as a function of:

- (a) Core size.
- (b) Flux level.
- (c) Degree of flatness in the power distribution.
- (d) Power coefficient.
- (e) Reactivity held by saturation xenon.

In addition, slightly dished power distributions were investigated to show that any dishing resulting from high depletion is not sufficient to require correction to data based on replacing the dished segment with a flat power distribution.

The effect of modal coupling has been examined and shown to be of no consequence for cores similar to the reference reactor design. Values of the critical dimension varied no more than 1 to 2.8 per cent for the same core with and without modal coupling. The lower value was computed with a zero power coefficient and was not conservative without modal coupling. The higher value was computed with the reference power coefficient and was conservative without modal coupling.

Table 3-9 summarizes those parameters for the reference core which affect the xenon stability threshold. The parameters were calculated at two substantially different times in core life. Reference physical dimensions are also shown for comparison purposes in the following discussion.

Table 3-10 shows the threshold dimensions for first mode instability as a function of flux flattening. The percentage of flattening is defined as 100 per cent times the ratio of the flattened power distribution to the total physical dimension under consideration. The parameters of Table 3-9 at two full power days were used since they are virtually the same as those at 150 days but are more conservative. Axial depletion studies

show that power distributions are flattened by 0, 63, and 73 per cent at 2, 150, and 354 full power days, respectively. A maximum flatness of approximately 80 per cent may be expected for long core life.

An examination of the data in Table 3-10 shows that--with the maximum flatness--axial oscillations are possible, azimuthal oscillations are unlikely, and radial oscillations will not occur.

Threshold dimensions for second mode oscillations were 50 per cent larger in magnitude than those shown in Table 3-10 for the first mode. Oscillations in the second mode will not occur in the reference core.

Table 3-9
Reference Core Parameters

	<u>Two Full (Rated) Power Days</u>	<u>150 Full (Rated) Power Days</u>
M^2 , cm^2	57.0	57.0
$\bar{\phi}_{th}$, $\text{n/cm}^2\text{-sec}$	3.9×10^{13}	3.8×10^{13}
a_x (reactivity held by saturation xenon), $\Delta k/k$	0.034	0.033
Doppler Coefficient, $\Delta k/k/F$	-1.1×10^{-5}	-1.1×10^{-5}
Moderator Temperature Coefficient	Positive but Small	Negative
a_T (power coeff.), $\Delta k/k/\text{unit flux}$	$\approx -2.2 \times 10^{-16}$	$\approx -2.3 \times 10^{-16}$
Equivalent Dimensions, ft		
Height		12.00
Diameter		10.74
Radius		5.37

Table 3-10
First Mode Threshold Dimensions and Flatness

<u>Threshold Dimensions, ft</u>	<u>Flatness, %</u>		
	<u>0</u>	<u>50</u>	<u>80</u>
Threshold height (axial oscillations)	18.5	14.1	11.8
Threshold diameter (azimuthal oscillation)	20.4	16.5	14.0
Threshold radius (radial oscillation)	16.8	16.7	14.5

Table 3-11 shows the values of H/D versus power flatness for equal likelihood of axial, azimuthal, and radial first harmonic oscillations, i.e., if the core is just at the axial threshold for axial oscillations, it can also be expected that there will be azimuthal and radial oscillations provided the value of H/D in Table 3-11 is satisfied. H/D for this reference reactor is 1.12.

Table 3-11
Threshold Ratio and Power Flatness

Ratio	Flatness, %				
	0	20	50	80	100
H/D (axial versus azimuthal)	0.91	0.87	0.86	0.86	0.85
H/D (axial versus radial)	0.55	0.49	0.42	0.41	0.41

The modal methods used to examine the xenon oscillation problem made use of core-averaged quantities such as flux, power coefficient, and reactivity held by saturation xenon. In addition, flux distributions were limited to

- (a) Geometric distributions.
- (b) Partially or totally flat.
- (c) Slightly dished.

The power distribution during early life is such that no xenon instabilities will occur. The power flattening effect of fuel burnup with time renders the core more susceptible to xenon oscillations.

(2) Depletion Analysis

Core-averaged quantities were used in the analytical analysis. For a more comprehensive investigation, it is desirable to study xenon oscillations with diffusion-depletion programs including heat transfer. Such calculations, which include the important local temperature effects, allow the designer to look for xenon oscillations under actual operating conditions. For these reasons, the B&W LIFE depletion program was modified to include axial heat transfer. The equations and iteration scheme are outlined below:

- (a) The average fluid temperature for each axial core region is computed from a previously known power density distribution as follows:

00000175

$$\Delta T_i = (T_{out} - T_{in})_i = C \int_{Z_{in}}^{Z_{out}} PD(Z) dz \quad (A)$$

where

ΔT_i = temperature change in region "i"

PD (Z) = power density in Z direction

Z_{in}, Z_{out} = region "i" boundaries

and

$$C = \frac{\Delta T_{core}}{\int_0^H PD(Z) dz} \quad (B)$$

where H = active fuel height.

Equation (A) is solved to T_{out} of region "i". Since T_{in} is known from core inlet conditions, the average fluid temperature is defined as follows:

$$\bar{T}_{fluid_i} = \frac{T_{out} + T_{in}}{2} \quad (C)$$

- (b) The newly computed region-averaged fluid temperatures are used to compute new fluid densities. These fluid densities are then used to adjust the number densities for water and soluble poison. Local or bulk boiling is not permitted.
- (c) The average fuel temperature for each axial core region is then computed from the average fluid temperatures and power densities:

$$\bar{T}_{fuel_i} = K \bar{PD}_i + \bar{T}_{fluid_i} \quad (D)$$

where \bar{PD}_i = coverage power density of region "i" and K is defined by

$$K = \frac{\bar{T}_{fuel} - \bar{T}_{fluid\ core}}{\bar{PD}_{core}} \quad (E)$$

- (d) After the new fluid temperatures, moderator densities, and fuel temperatures are obtained, these quantities are used as new LIFE input to obtain a new power distribution until either a convergence criterion is met or a specified number of iterations is made.

00000176

This analysis used an exact solution in that the spectrum was recalculated for each zone (11 axial zones described the reactor) for each iteration at every time step. This included the effects of the moderator coefficient.

This LIFE package was used to determine the effects of the uncertainty in the power Doppler on the stability of the core. The uncertainty in the Doppler was more than compensated with a reduction in fuel temperature of 500 degrees. The reference core was analyzed with core average fuel temperatures of 1,400 F and 900 F. Figure 3-7 compares the cyclic response of these two cases following the 3-ft insertion and removal (after two hours) of a 1.2% $\Delta k/k$ rod bank near the beginning of life. These studies were made at beginning-of-life boron levels of approximately 1,900 ppm. This level is approximately 200 ppm above the predicted beginning-of-life level, and consequently reflects a more positive moderator temperature coefficient than would be expected. Case 1 on Figure 3-7 depicts the behavior of the core if the heat transfer equations were not included in the calculation. Figure 3-8 shows the effect of fuel temperature toward the end of life. It is easily verified that the 900 F fuel temperature case approached the threshold condition for axial oscillation in this core. On the basis of the information presented, it can be said that for a realistic fuel temperature this core does not exhibit axial instability at any time during the initial cycle. | 1

The 1-D model was used to determine a method of controlling the core without taking into account the stabilizing effect of the power Doppler. Normally, this would produce a divergent oscillation as shown in Figure 3-9. A study was completed wherein a 1% $\Delta k/k$ rod bank with a 3-ft-long section of regular control rod material was successfully maneuvered to control the core after a perturbation of the power shape at a point about 3/4 of the way through Cycle 1. The controlled results are also shown in Figure 3-9. The minimum rod motion was one foot, and the time step employed was 4.8 hours. More precise rod movement over shorter time periods would produce a much smoother power ratio curve. This control mechanism appears quite adequate.

c. Conclusions

Instability in the radial or azimuthal mode is not expected since the diffusion theory study showed that the core is stable throughout lifetime and the L/D ratio is 1.1. The results are encouraging, but until additional analyses are completed, it will be assumed that axial xenon oscillations are possible. Consequently, rod motion will be used to compensate for unbalanced power distribution as indicated by the instrumentation.

Work is underway to provide a 2-dimensional depletion program which allows nuclear-thermal iterations. A detailed quantitative analysis of core stability and control procedures, employing either partial or normal control rods, is to be undertaken with the new program.

00000177

3.2.3 THERMAL AND HYDRAULIC DESIGN AND EVALUATION

3.2.3.1 Thermal and Hydraulic Characteristics

3.2.3.1.1 Fuel Assembly Heat Transfer Design

a. Design Criteria

The criterion for heat transfer design is to be safely below Departure from Nucleate Boiling (DNB) at the design overpower (114 per cent of rated power). A detailed description of the analysis is given in 3.2.3.2.2, Statistical Core Design Technique.

The input information for the statistical core design technique and for the evaluation of individual hot channels consists of the following:

- (1) Heat transfer critical heat flux equations and data correlations.
- (2) Nuclear power factors.
- (3) Engineering hot channel factors.
- (4) Core flow distribution hot channel factors.
- (5) Maximum reactor overpower.

These inputs have been derived from test data, physical measurements, and calculations as outlined below.

b. Heat Transfer Equation and Data Correlation

The heat transfer relationship used to predict limiting heat transfer conditions is presented in BAW-168.⁽¹⁸⁾ The equation is as follows:

$$q'' = (1.83 - 0.000415 P) \times 90,000$$

$$\left[\frac{G}{240} \left(\frac{S}{L} \right) \right]^{0.3987 + 0.001036 \Delta T_{esc} - 1.027 \times 10^{-6} (\Delta T_{esc})^2}$$

where

q'' = critical heat flux as predicted by the best fit form, Btu/hr-ft²

P = core operating pressure, psia

G = channel mass velocity, lb/hr-ft²

S = channel equivalent diameter, ft

L = length up the channel to the point of interest, ft

ΔT_{esc} = inlet subcooling ($T_{sat} - T_{inlet}$), F

T_{sat} = coolant saturation temperature corresponding to P , F

This equation was derived from experimental heat transfer data. An analysis of heat transfer data for this and other relationships is described in detail in 3.2.3.2.3, Correlation of Heat Transfer Data.

Individual channels are analyzed to determine a DNB ratio, i.e., the ratio of the heat flux at which a DNB is predicted to occur to the heat flux in the channel being investigated. This DNB ratio is related to the data correlation as in Figure 3-10. A confidence and population value is associated with every DNB ratio as described in the Statistical Core Design Technique. The plot of DNB versus P shown is for a confidence of 99 per cent.

The DNB and population relationships shown are also the values associated with the single hot channel analysis for the hottest unit cell where a 1.38 DNB ratio corresponds to a 99 per cent confidence that at least 94.5 per cent of the population of all such hot channels are in no jeopardy of experiencing a DNB. This statement is a corollary to the total core statistical statement given in 3.1.2.3, Thermal and Hydraulic Limits. The criterion for evaluating the thermal design margin for individual channels or the total core is the confidence-population relationship. The DNB ratios required to meet the basic criteria or limits are a function of the experimental data and heat transfer correlation used, and vary with the quantity and quality of data.

c. Nuclear Power Factors

The heated surfaces in every flow channel in the core are examined for heat flux limits. The heat input to the fuel rods comprising a coolant channel is determined from a nuclear analysis of the core and fuel assemblies. The results of this analysis are as follows:

- (1) The nominal nuclear peaking factors for the worst time in core life are

$$F\Delta h = 1.79$$

$$Fz = 1.70$$

$$Fq = 3.04$$

- (2) The design nuclear peaking factors for the worst time in core life are

$$F\Delta h = 1.85$$

$$Fz = 1.70$$

$$Fq = 3.15$$

00000179

where

$F\Delta h = \text{max/avg; total power ratio (radial x local nuclear)}$

$Fz = \text{max/avg axial power ratio (nuclear)}$

$Fq = F\Delta h \times Fz \text{ (nuclear total)}$

The nominal values are the maximum calculated values. The design values are obtained by increasing the maximum calculated total power ratio, $F\Delta h$, from 1.79 to 1.85 to obtain a more conservative design.

The axial nuclear factor, Fz , is illustrated in Figure 3-11. The distribution of power expressed as P/\bar{P} is shown for two conditions of reactor operation. The first condition is an inlet peak with a max/avg value of 1.70 resulting from partial insertion of a CRA group for transient control following a power level change. This condition results in the maximum local heat flux and maximum linear heat rate. The second power shape is a symmetrical cosine which is indicative of the power distribution with xenon override rods withdrawn. The flux peak max/avg value is 1.50 in the center of the active core. Both of these flux shapes have been evaluated for thermal DNB limitations. The limiting condition is the 1.5 cosine power distribution. The inlet peak shape has a larger maximum value. However, the position of the 1.5 cosine peak farther up the channel results in a less favorable flux to enthalpy relationship. This effect has been demonstrated in DNB tests of nonuniform flux shapes.⁽¹⁹⁾ The 1.5 cosine axial shape has been used to determine individual channel DNB limits and make the associated statistical analysis.

The nuclear factor for total radial x local rod power, $F\Delta h$, is calculated for each rod in the core. A distribution curve of the fraction of the core fuel rods operating above various peaking factors is shown in Figure 3-12. Line B shows the distribution of the maximum calculated values of $F\Delta h$ for nominal conditions with a maximum value of 1.79. The distribution of peaking factors for the design condition is obtained by increasing the maximum calculated value for all rods in the core by the ratio of 1.85/1.79 or 1.033 to provide conservative results. Determination of the peaking distribution for the design condition in this manner has the effect of increasing reactor power by about 3 per cent. This assumption is conservative since the distribution with a maximum peak $F\Delta h$ of 1.85 will follow a line similar to Line C where the average power of all rods in the core is represented by an $F\Delta h$ of 1.0. The actual shape of the distribution curve is dependent upon statistical peaking relationships, CRA positions, moderator conditions, and operating history. The shape of the distribution curve will be more accurately described during the detailed core design.

00000180

d. Engineering Hot Channel Factors

Power peaking factors obtained from the nuclear analysis are based on mechanically-perfect fuel assemblies. Engineering hot channel factors are used to describe variations in fuel loading, fuel and clad dimensions, and flow channel geometry from perfect physical quantities and dimensions.

The application of hot channel factors is described in detail in 3.2.3.2.2, Statistical Core Design Technique. The factors are determined statistically from fuel assembly as-built or specified data where F_Q is a heat input factor, $F_{Q''}$ is a local heat flux factor at a hot spot, and F_A is a flow area reduction factor describing the variation in coolant channel flow area. Several subfactors are combined statistically to obtain the final values for F_Q , $F_{Q''}$, and F_A . These subfactors are shown in Table 3-12. The factor, the coefficient of variation, the standard deviation, and the mean value are tabulated.

Table 3-12
Coefficients of Variation

<u>CV No.</u>	<u>Description</u>	<u>σ</u>	<u>\bar{x}</u>	<u>CV</u>
1	Flow Area	0.00075	0.17625	0.00426
2	Local Rod Diameter	0.000485	0.420	0.00116
3	Average Rod Diameter (Die-drawn, local and average same)	0.000485	0.420	0.00116
4	Local Fuel Loading			0.00687
	Subdensity	0.00647	0.95	0.00681
	Subfuel area (Diameter effect)	0.000092	0.1029	0.00089
5	Average Fuel Loading			0.00370
	Subdensity	0.00324	0.95	0.00341
	Sublength	0.16181	144	0.00112
	Subfuel area (Diameter effect)	0.000092	0.1029	0.00089
6	Local Enrichment	0.00323	2.24	0.00144
7	Average Enrichment	0.00323	2.24	0.00144
CV	Coefficient of Variation	σ/\bar{x}		
σ	Standard Deviation of Variable			
\bar{x}	Mean Value of Variable			

(Enrichment values are for worst case normal assay batch; maximum variation occurs for minimum enrichment.)

00000181

e. Core Flow Distribution Hot Channel Factors

The physical arrangement of the reactor vessel internals and nozzles results in a nonuniform distribution of coolant flow to the various fuel assemblies. Reactor internal structures above and below the active core are designed to minimize unfavorable flow distribution. A 1/6 scale model test of the reactor and internals is being performed to demonstrate the adequacy of the internal arrangements. The final variations in flow will be determined when the tests are completed. Interim factors for flow distribution effects have been calculated from test data on reactor vessel models for previous pressurized water reactor designs.

A flow distribution factor is determined for each fuel assembly location in the core. The factor is expressed as the ratio of fuel assembly flow to average fuel assembly flow. The finite values of the ratio may be greater or less than 1.0 depending upon the position of the assembly being evaluated. The flow in the central fuel assemblies is in general larger than the flow in the outermost assemblies due to the inherent flow characteristics of the reactor vessel.

The flow distribution factor is related to a particular fuel assembly location and the quantity of heat being produced in the assembly. A flow-to-power comparison is made for all of the fuel assemblies. The worst condition in the hottest fuel assembly is determined by applying model test isothermal flow distribution data and heat input effects at power as outlined in 3.2.3.2.4i. Two assumptions for flow distribution have been made in the thermal analysis of the core as follows:

- (1) For the maximum design condition and for the analysis of the hottest channel, all fuel assemblies receive minimum flow for the worst condition, regardless of assembly power or location.
- (2) For the most probable design conditions predicted flow factors have been assigned for each fuel assembly consistent with location and power. The flow factor assumed for the maximum design condition is conservative. Application of vessel flow test data and individual assembly flow factors in the detailed core design will result in improved statistical statements for the maximum design condition.

f. Maximum Reactor Design Overpower

Core performance is assessed at the maximum design overpower. The selection of the design overpower is based on an analysis of the reactor protective system as described in Section 7. The reactor trip point is 107.5 per cent rated power, and the maximum overpower, which is 114 per cent, will not be exceeded under any conditions.

g. Maximum Design Conditions Analysis Summary

The Statistical Core Design Technique described in 3.2.3.2.2 was used to analyze the reactor at the maximum design conditions described previously. The total number of fuel rods in the core that have a

00000182

possibility of reaching DNB is shown in Figure 3-13 for 100 to 118 per cent overpower. Point A on Line 1 is the maximum design point for 114 per cent power with the design $F\Delta h$ nuclear of 1.85. Line 2 was calculated using the maximum calculated value for $F\Delta h$ nuclear of 1.79 to show the margin between maximum calculated and design conditions. It is anticipated that detailed core nuclear analyses will permit a lowering of the maximum design value for $F\Delta h$.

The number of fuel rods that may possibly reach a DNB at the maximum design condition with an $F\Delta h$ of 1.85 and at 114 per cent overpower, represented by point A on Figure 3-13, forms the basis for this statistical statement:

There is a 99 per cent confidence that at least 99.5 per cent of the fuel rods in the core are in no jeopardy of experiencing a departure from nucleate boiling (DNB) during continuous operation at the design overpower of 114 per cent.

Statistical results for the maximum design condition calculation shown by Figure 3-13 may be summarized as follows in Table 3-13.

Table 3-13
DNB Results - Maximum Design Condition
 (99 per cent Confidence Level)

<u>Point</u>	<u>Power,</u> <u>% of 2,452 Mwt</u>	<u>$F\Delta h$</u>	<u>Possible</u> <u>DNB's</u>	<u>Population</u> <u>Protected, %</u>
A	114	1.85	184	99.50
B	114	1.79	100	99.73
C	100	1.85	17	99.95
D	100	1.79	10	99.98
E	118	1.79	184	99.50

h. Most Probable Design Condition Analysis Summary

The previous maximum design calculation indicates the total number of rods that are in jeopardy when it is conservatively assumed that every rod in the core has the mechanical and heat transfer characteristics of a hot channel as described in 3.2.3.2.2. For example, all channels are analyzed with F_A (flow area factor) less than 1.0, F_Q (heat input factor) greater than 1.0, and with minimum fuel assembly flow. It is physically impossible for all channels to have hot channel characteristics. A more realistic indication of the number of fuel rods in jeopardy may be obtained by the application of the statistical heat transfer data to average rod power and mechanical conditions.

An analysis for the most probable conditions has been made based on the average conditions described in 3.2.3.2.2. The results of this

analysis are shown in Figure 3-14. The analysis may be summarized as follows in Table 3-14.

Table 3-14
DNB Results - Most Probable Condition

<u>Point</u>	<u>Power, % of 2,452 MWt</u>	<u>FΔh</u>	<u>Possible DNB's</u>	<u>Population Protected, %</u>
F	100	1.79	2	99.994
G	114	1.79	32	99.913
H	118	1.79	70	99.815

The analysis was made from Point F at 100 per cent power to Point H at 118 per cent power to show the sensitivity of the analysis with power. The worst condition expected is indicated by Point G at 114 per cent power where it is shown that there is a small possibility that 32 fuel rods may be subject to a departure from nucleate boiling (DNB). This result forms the basis for the following statistical statement for the most probable design conditions:

There is at least a 99 per cent confidence that at least 99.9 per cent of the rods in the core are in no jeopardy of experiencing a DNB, even with continuous operation at the design over-power of 114 per cent.

1. Distribution of the Fraction of Fuel Rods Protected

The distribution of the fraction (P) of fuel rods that have been shown statistically to be in no jeopardy of a DNB has been calculated for the maximum design and most probable design conditions. The computer programs used provide an output of (N) number of rods and (P) fraction of rods that will not experience a DNB grouped for ranges of (P). The results for the most probable design condition are shown in Figure 3-15.

The population protected, (P), and the population in jeopardy, (1-P), are both plotted. The integral of (1-P) and the number of fuel rods gives the number of rods that are in jeopardy for given conditions as shown in Figures 3-13 and 3-14. The number of rods is obtained from the product of the percentage times the total number of rods being considered (36,816). The two distributions shown in Figure 3-15 are for the most probable condition analysis of Points F and G on Figure 3-14. The lower line of Figure 3-15 shows P and (1-P) at the 100 per cent power condition represented by Point F of Figure 3-14. The upper curve shows P and (1-P) at the 114 per cent power condition represented by Point G of Figure 3-14. The integral of N and (1-P) of the upper curve forms the basis for the statistical statement at the most probable design condition described in paragraph h above.

00000184

j. Hot Channel Performance Summary

The hottest unit cell with all surfaces heated has been examined for hot channel factors, DNB ratios, and quality for a range of reactor powers. The cell has been examined for the maximum value of $F\Delta h$ nuclear of 1.85. The hot channel was assumed to be located in a fuel assembly with 95 per cent of the average fuel assembly flow. The heat generated in the fuel is 97.3 per cent of the total nuclear heat. The remaining 2.7 per cent is assumed to be generated in the coolant as it proceeds up the channel within the core and is reflected as an increase in ΔT of the coolant.

Error bands of 65 psi operating pressure and ± 2 F are reflected in the total core and hot channel thermal margin calculations in the direction producing the lowest DNB ratios or highest qualities.

The DNB ratio versus power is shown in Figure 3-16. The DNB ratio in the hot channel at the maximum overpower of 114 per cent is 1.38 which corresponds to a 99 per cent confidence that at least 94.5 per cent of the fuel channels of this type are in no jeopardy of experiencing a DNB. The engineering hot channel factors corresponding to the above confidence-population relationship are described in 3.2.3.2.2 and listed below:

$$F_Q = 1.008$$

$$F_{Q''} = 1.013$$

$$F_A = 0.992$$

The hot channel exit quality for various powers is shown in Figure 3-17. The combined results may be summarized as follows:

<u>Reactor Power, %</u>	<u>DNB Ratio (BAW-168)</u>	<u>Exit Quality, %</u>
100	1.60	0
107.5 (trip setting)	1.47	2.6
114 (maximum power)	1.38	5.4
149	1.00	23.0

3.2.3.1.2 Fuel and Cladding Thermal Conditions

a. Fuel

A digital computer code is used to calculate the fuel temperature. The program uses uniform volumetric heat generation across the fuel diameter, and external coolant conditions and heat transfer coefficients determined for thermal-hydraulic channel solutions. The fuel thermal conductivity is varied in a radial direction as a function of the temperature variation. Values for fuel conductivity were used as

00000185

shown in Figure 3-18, a plot of fuel conductivity versus temperature. The heat transfer from the fuel to the clad is calculated with a fuel and clad expansion model proportional to temperatures. The temperature drop is calculated using gas conductivity at the beginning-of-life conditions when the gas conductivity is 0.1 Btu-ft/hr-F-ft². The gas conduction model is used in the calculation until the fuel thermal expansion relative to the clad closes the gap to a dimension equivalent to a contact coefficient. The contact coefficient is dependent upon pressure and gas conductivity.

A plot of fuel center temperature versus linear heat rate in kw/ft is shown in Figure 3-19 for beginning-of-life conditions. The linear heat rate at the maximum overpower of 114 per cent is 19.9 kw/ft. The corresponding center fuel temperature shown in Table 1-2 is 4,400 F. The center and average temperatures at 100 per cent power are 4,160 and 1,385 F as shown in Table 3-1.

The peaking factors used in the calculation are

$$F_{\Delta h} = 1.85$$

$$F_z = 1.70$$

$$F_{Q''} = 1.03$$

$$F_q \text{ (nuc. and mech.)} = 3.24$$

A conservative value of 1.03 was assumed for the heat flux peaking factor, $F_{Q''}$. The assigned value corresponds to a 99 per cent confidence and 99.99 per cent population-protected relationship as described in the statistical technique.

b. Clad

The assumptions in the preceding paragraph were applied in the calculation of the clad surface temperature at the maximum overpower. Boiling conditions prevail at the hot spot, and the Jens and Lottes relationship⁽²⁰⁾ for the coolant-to-clad ΔT for boiling was used to determine the clad temperature. The resulting maximum calculated clad temperature is 654 F at a system operating pressure of 2,185 psig.

00000136

3.2.3.2 Thermal and Hydraulic Evaluation

3.2.3.2.1 Introduction

Summary results for the characteristics of the reactor design are presented in 3.2.3.1. The Statistical Core Design Technique employed in the design represents a refinement in the methods for evaluating pressurized water reactors. Corresponding single hot channel DNB data were presented to relate the new method with previous criteria. A comprehensive description of the new technique is included in this section to permit a rapid evaluation of the methods used.

The BAW-168 correlation is a B&W design equation. An extensive review of data available in the field was undertaken to derive the correlation and to determine the confidence, population, and DNB relationships included in this section. A comparison of the BAW-168 correlation with other correlations in use is also included.

A detailed evaluation and sensitivity analysis of the design has been made by examining the hottest channel in the reactor for DNB ratio, quality, and fuel temperatures. BAW-168 DNB ratios have been compared with W-3 DNB ratios to facilitate a comparison of the design with PWR reactor core designs previously reviewed.

3.2.3.2.2 Statistical Core Design Technique

The core thermal design is based on a Statistical Core Design Technique developed by B&W. The technique offers many substantial improvements over older methods, particularly in design approach, reliability of the result, and mathematical treatment of the calculation. The method reflects the performance of the entire core in the resultant power rating and provides insight into the reliability of the calculation. This section discusses the technique in order to provide an understanding of its engineering merit.

The statistical core design technique considers all parameters that affect the safe and reliable operation of the reactor core. By considering each fuel rod the method rates the reactor on the basis of the performance of the entire core. The result then will provide a good measure of the core safety and reliability since the method provides a statistical statement for the total core. This statement also reflects the conservatism or design margin in the calculation.

A reactor safe operating power has always been determined by the ability of the coolant to remove heat from the fuel material. The criterion that best measures this ability is the DNB, which involves the individual parameters of heat flux, coolant temperature rise, and flow area, and their intereffects. The DNB criterion is commonly applied through the use of the departure from nucleate boiling ratio (DNBR). This is the minimum ratio of the DNB heat flux (as computed by the DNB correlation) to the surface heat flux. The ratio is a measure of the margin between the operating power and the power at which a DNB might be expected to occur in that channel. The DNBR varies over the channel length, and it is the minimum value of the ratio in the channel of interest that is used.

00000187

The calculation of DNB heat flux involves the coolant enthalpy rise and coolant flow rate. The coolant enthalpy rise is a function of both the heat input and the flow rate. It is possible to separate these two effects; the statistical hot channel factors required are a heat input factor, F_Q , and a flow area factor, F_A . In addition, a statistical heat flux factor, F_Q'' , is required; the heat flux factor statistically describes the variation in surface heat flux. The DNBR is most limiting when the burnout heat flux is based on minimum flow area (small F_A) and maximum heat input (large F_Q), and when the surface heat flux is large (large F_Q''). The DNB correlation is provided in a best-fit form, i.e., a form that best fits all of the data on which the correlation is based. To afford protection against DNB, the DNB heat flux computed by the best-fit correlation is divided by a DNB factor (B.F.) greater than 1.0 to yield the design DNB surface heat flux. The basic relationship

$$\text{DNBR} = \frac{q_{\text{DNB}}''}{\text{B.F.}} \times f(F_A, F_Q) \times \frac{1}{q_{\text{surface}}'' \times F_Q''}$$

involves as parameters statistical hot channel and DNB factors. The DNB factor (B.F.) above is usually assigned a value of unity when reporting DNB ratios so that the margin at a given condition is shown directly by a DNBR greater than 1.0, i.e., 1.38 in the hot channel.

To find the DNB correlation, selected correlations are compared with DNB data obtained in the B&W burnout loop and with published data. The comparison is facilitated by preparing histograms of the ratio of the experimentally determined DNB heat flux (ϕ_E) to the calculated value of the burnout heat flux (ϕ_C). A typical histogram is shown in Figure 3-20.

A histogram is obtained for each DNB correlation considered. The histograms indicate the ability of the correlations to describe the data. They indicate, qualitatively, the dispersion of the data about the mean value--the smaller the dispersion, the better the correlation. Since thermal and hydraulic data generally are well represented with a Gaussian (normal) distribution (Figure 3-20), mathematical parameters that quantitatively rate the correlation can be easily obtained for the histogram. These same mathematical parameters are the basis for the statistical burnout factor (B.F.).

In analyzing a reactor core, the statistical information required to describe the hot channel subfactors may be obtained from data on the as-built core, from data on similar cores that have been constructed, or from the specified tolerances for the proposed core. Regardless of the source of data, the subfactors can be shown graphically (Figures 3-21 and 3-22).

All the plots have the same characteristic shape whether they are for subfactors, hot channel factors, or burnout factor. The factor increases with either increasing population or confidence. The value used for the statistical hot channel and burnout factor is a function of the percentage of confidence desired in the result, and the portion of all possibilities desired, as well as the amount of data used in determining the statistical factor. A frequently used assumption in statistical analyses is that the data available represent an infinite sample of that data. The implications of this assumption should be noted. For instance, if limited data are available, such an assumption leads

to a somewhat optimistic result. The assumption also implies that more information exists for a given sample than is indicated by the data; it implies 100 per cent confidence in the end result. The B&W calculational procedure does not make this assumption, but rather uses the specified sample size to yield a result that is much more meaningful and statistically rigorous. The influence of the amount of data for instance can be illustrated easily as follows: Consider the heat flux factor which has the form

$$F_{Q''} = 1 + K\sigma_{F_{Q''}}$$

where

$F_{Q''}$ is the statistical hot channel factor for heat flux

K is a statistical multiplying factor

$\sigma_{F_{Q''}}$ is the standard deviation of the heat flux factor, including the effects of all the subfactors

If $\sigma_{F_{Q''}} = 0.05$ for 300 data points, then a K factor of 2.608 is required to protect 99 per cent of the population. The value of the hot channel factor then is

$$F_{Q''} = 1 + (2.608 \times 0.050) = 1.1304$$

and will provide 99 per cent confidence for the calculation. If, instead of using the 300 data points, it is assumed that the data represent an infinite sample, then the K factor for 99 per cent of the population is 2.326. The value of the hot channel factor in this case is

$$F_{Q''} = 1 + (2.326 \times 0.050) = 1.1163$$

which implies 100 per cent confidence in the calculation. The values of the K factor used above are taken from SCR-607.⁽²¹⁾ The same basic techniques can be used to handle any situation involving variable confidence, population, and number of points.

Having established statistical hot channel factors and statistical DNB factors, we can proceed with the calculation in the classical manner. The statistical factors are used to determine the minimum fraction of rods protected, or that are in no jeopardy of experiencing a DNB at each nuclear power peaking factor. Since this fraction is known, the maximum fraction in jeopardy is also known. It should be recognized that every rod in the core has an associative DNB ratio that is substantially greater than 1.0, even at the design overpower, and that theoretically no rod can have a statistical population factor of 100 per cent, no matter how large its DNB ratio.

Since both the fraction of rods in jeopardy at any particular nuclear power peaking factor and the number of rods operating at that peaking factor are known, the total number of rods in jeopardy in the whole core

can be obtained by simple summation. The calculation is made as a function of power, and the plot of rods in jeopardy versus reactor overpower is obtained (Figure 3-23). The summation of the fraction of rods in jeopardy at each peaking factor summed over all peaking factors can be made in a statistically rigorous manner only if the confidence for all populations is identical. If an infinite sample is not assumed, the confidence varies with population. To form this summation then, a conservative assumption is required. B&W's total core model assumes that the confidence for all rods is equal to that for the least-protected rod, i.e., the minimum possible confidence factor is associated with the entire calculation.

The result of the foregoing technique, based on the maximum design conditions (114 per cent power), is this statistical statement:

There is at least a 99 per cent confidence that at least 99.5 per cent of the rods in the core are in no jeopardy of experiencing a DNB, even with continuous operation at the design overpower.

The maximum design conditions are represented by these assumptions:

- a. The maximum design values of $F\Delta h$ (nuclear max/avg total fuel rod heat input) are obtained by increasing the maximum calculated value of $F\Delta h$ by a factor of 1.033 to provide additional design margin.
- b. The maximum value for F_z (nuclear max/avg axial fuel rod heat input) is determined for the limiting transient or steady state condition.
- c. Every coolant channel in the core is assumed to have less than the nominal flow area represented by engineering hot channel area factors, F_A , less than 1.0.
- d. Every channel is assumed to receive the minimum flow associated with core flow maldistribution.
- e. Every fuel rod in the core is assumed to have a heat input greater than the maximum calculated value. This value is represented by engineering hot channel heat input factors, F_Q and $F_{Q''}$, which are greater than 1.0.
- f. Every channel and associated fuel rod has a heat transfer margin above the experimental best-fit limits reflected in DNB ratios greater than 1.0 at maximum overpower conditions.

The statistical core design technique may also be used in a similar manner to evaluate the entire core at the most probable mechanical and nuclear conditions to give an indication of the most probable degree of fuel element jeopardy. The result of the technique based on the most probable design conditions leads to a statistical statement which is a corollary to the maximum design statement:

00000190

0000190

There is at least a 99 per cent confidence that at least 99.9 per cent of the rods in the core are in no jeopardy of experiencing a DNB, even with continuous operation at the design overpower.

The most probable design conditions are assumed to be the same as the maximum design conditions with these exceptions:

- a. Every coolant channel is assumed to have the nominal flow area ($F_A = 1.0$).
- b. Every fuel rod is assumed to have (1) the maximum calculated value of heat input, and (2) F_Q and F_Q'' are assigned values of 1.0.
- c. The flow in each coolant channel is based on core flow and power distributions.
- d. Every fuel rod is assumed to have a nominal value for $F\Delta h$ nuclear.

The full meaning of the maximum and most probable design statements requires additional comment. As to the 0.5 per cent or 0.1 per cent of the rods not included in the statements, statistically, it can be said that no more than 0.5 per cent or 0.1 per cent of the rods will be in jeopardy, and that in general the number in jeopardy will be fewer than 0.5 per cent or 0.1 per cent. The statements do not mean to specify a given number of DNB's, but only acknowledge the possibility that a given number could occur for the conditions assumed.

In summary, the calculational procedure outlined here represents a substantially improved design technique in two ways:

- a. It reflects the performance and safety of the entire core in the resultant power rating by considering the effect of each rod on the power rating.
- b. It provides information on the reliability of the calculation and, therefore, the core through the statistical statement.

3.2.3.2.3 Correlation of Heat Transfer Data

The BAW-168 report (Ref. 18) serves as a reference for the "best-fit" form of the design relationship used by B&W. This heat transfer correlation has been found to be the most satisfactory in the representation of both uniform and nonuniform heat flux test data. The BAW-168 correlation is used by comparing the integrated average heat flux along a fuel rod to a DNB heat flux limit predicted by the correlation. For uniform heat flux the integrated average heat flux is equal to the local heat flux. The comparison is carried out over the entire channel length. The point at which the ratio of the DNB heat flux to the integrated average heat flux is a minimum is selected as the DNB point, and that value of the ratio at that point is the DNB ratio (DNBR) for that channel.

This particular discussion deals with the comparison of DNB data to three particular correlations. The correlations selected were the B&W correlation in the case of BAW-168,⁽¹⁸⁾ a correlation with which the industry is familiar in the case of WAPD-188,⁽²²⁾ and a correlation recently proposed for use in the design of pressurized water reactors in the case of W-3.⁽²³⁾

The data considered for the purpose of these comparisons were taken from the following sources:

- a. WAPD-188 (Ref. 22).
- b. AEEW-R213 (Ref. 24).
- c. Columbia University Data (Ref. 25, 26, and 27).
- d. Argonne National Laboratory Data, ANL (Ref. 28).
- e. The Babcock & Wilcox Company Data, B&W (Ref. 29).
- f. The Babcock & Wilcox Company Euratom Data (Ref. 30).

The comparison of data to the BAW-168 correlation is presented as histograms of the ratio of the experimental DNB heat flux (ϕ_E) to the calculated heat flux (ϕ_C). The data from each source were grouped by pressure and analyzed as a group; batches were then prepared including common pressure groups from all sources. Altogether there are 41 different data groups and batches considered. Histograms for only the BAW-168 correlation are presented to minimize the graphical material. The information required for the generation of histograms of the other two correlations was also prepared.

The comparison of the various correlations to each other is facilitated through the use of tabulations of pertinent statistical parameters. The standard deviation and mean value were obtained from the computed values of (ϕ_E/ϕ_C) for each group or batch. A comparison of standard deviations is somewhat indicative of the ability of the correlation to represent the data.

However, differences in mean values from group to group and correlation to correlation tend to complicate this type comparison. A relatively simple method may be used to compare the correlations for various data; this method uses the coefficient of variation (Ref. 31) which is the ratio of the standard deviation (σ) to the mean \bar{x} . The coefficient of variation may be thought of as the standard deviation given in per cent; it essentially normalizes the various standard deviations to a common mean value of 1.0.

Table 3-15 is a tabulation of the data source, heat flux type, and corresponding histogram numbers. The histograms are shown on Figures 3-24 through 3-39.

00000192

Table 3-15
Heat Transfer Test Data

<u>Source</u>	<u>Heat Flux Type</u>	<u>Histogram Number</u>	<u>Figure Number</u>
WAPD-188	Uniform	1-9	3-24 3-25 3-26
AEEW-R-213	Uniform	10-14	3-26 3-27 3-28
Columbia	Uniform	15-19	3-28 3-29 3-30
ANL	Uniform	20	3-30
B&W	Uniform	21	3-31
B&W-Euratom	Uniform	22-24	3-31 3-32
Combined Data (500-720 psia)	Uniform	25	3-32
Combined Data (1,000 psia)	Uniform	26	3-33
Combined Data (1,500 psia)	Uniform	27	3-34
Combined Data (2,000 psia)	Uniform	28	3-35
Combined Data (1,750-2,750 psia)	Uniform	29	3-36
B&W-Euratom Chopped Cosine	Nonuniform	30-32	3-37
B&W-Euratom and B&W Inlet Peak	Nonuniform	33-35	3-37 3-38
Euratom and B&W Outlet Peak	Nonuniform	36-38	3-38 3-39
Combined Nonuniform (1,000 psia)	Nonuniform	39	3-39
Combined Nonuniform (1,500 psia)	Nonuniform	40	3-39
Combined Nonuniform (2,000 psia)	Nonuniform	41	3-39

00000193

The histograms graphically demonstrate the distribution of (ϕ_E/ϕ_C) for each data group. The Gaussian type distribution of (ϕ_E/ϕ_C) about the mean for the group is apparent in the large data groups. Some data groups are too small to provide meaningful histograms, but they are presented in order to complete this survey.

The data were used as presented in the source for the calculation of (ϕ_E/ϕ_C) ; no points were discarded for any reason. A good correlation should be capable of representing DNB data for a full range of all pertinent parameters. The result of the comparison on this basis is demonstrated in Table 3-15. The data source, pressure, histogram figure number, heat flux type, and number of data points in the group are tabulated. For each of the three correlations the following data are indicated:

$\sigma/\bar{\chi}$ The coefficient of variation based on all available data in the group.

n_R The number of data points rejected using Chauvenet's criterion (Ref. 31). This criterion is statistical in nature and is applied to the values of (ϕ_E/ϕ_C) . Data points that fall outside certain limits with respect to the main body of data are rejected.

$(\sigma/\bar{\chi})'$ The coefficient of variation based on the original data sample less those points rejected by Chauvenet's criterion, i.e., based on $n-n_R$ values of (ϕ_E/ϕ_C) .

It is unfortunate that Chauvenet's criterion must be applied to the values of (ϕ_E/ϕ_C) rather than to the original data, since application to (ϕ_E/ϕ_C) leads to the rejection of points for either of two reasons:

- a. Bad data points.
- b. Inability of the correlation to represent a particular data point.

It is not desirable to reject points for the second reason, and yet one might expect to encounter some bad data. The logical choice then is to present data both ways, i.e., with and without Chauvenet's criterion applied. Of the 41 groups and batches analyzed the following is observed from Table 3-15:

<u>Correlation</u>	<u>Groups and Batches of Data With Smallest $\sigma/\bar{\chi}$ Without Chauvenet's Criterion</u>	<u>Groups and Batches of Data With Smallest $\sigma/\bar{\chi}$ With Chauvenet's Criterion</u>
BAW-168	38	36
WAPD-188	2	3
W-3	1	2

00000194

Chauvenet's criterion rejected the following number of points for each correlation:

	<u>Uniform</u>	<u>Nonuniform</u>	<u>Total</u>
BAW-168 (Groups Only)	32	1	33
BAW-168 (Batches Only)	39	0	39
WAPD-188 (Groups Only)	34	2	36
WAPD-188 (Batches Only)	33	0	33
W-3 (Groups Only)	59	12	71
W-3 (Batches Only)	50	9	59

Several notable peculiarities exist in the tabulation of Table 3-16. The Columbia data 500 psia group contained only five data points; four were rejected by Chauvenet's criterion, leaving one point. A standard deviation cannot be computed for one point; therefore all three values of (σ/\bar{x}) are shown as not available (N.A.). Neither the BAW-168 nor the WAPD-188 predicted any negative DNB heat fluxes; the W-3 predicted 93 negative values for uniform data. The fact that only 59 were rejected for this correlation indicates that the remaining 34 uniform points which were negative (93-59 = 34) were close enough to the body of the data to be considered statistically significant. Table 3-16 may be consolidated somewhat as below by tabulating the number of groups and batches of data having coefficients of variation within a specified interval for each correlation.

<u>(σ/\bar{x})</u> <u>Interval</u>	<u>BAW-168</u>	<u>BAW-168'(a)</u>	<u>WAPD-188</u>	<u>WAPD-188'(a)</u>	<u>W-3</u>	<u>W-3'(a)</u>
Negative	0	0	0	0	2	0
0-0.1	6	8	0	0	0	1
0.1-0.2	24	24	13	13	1	5
0.2-0.3	8	8	7	8	3	1
0.3-0.4	1	0	3	4	1	2
0.4-0.5	1	0	5	7	5	6
0.5-0.6	0	0	6	5	3	4
0.6-0.7	0	0	3	2	1	1
0.7-0.8	0	0	2	1	7	8
0.8-0.9	1	0	0	0	1	5
0.9-1.0	0	0	0	0	1	0
Greater than 1.0	<u>0</u>	<u>0</u>	<u>2</u>	<u>0</u>	<u>16</u>	<u>7</u>
Total	41	40	41	40	41	40

(a) Chauvenet's criterion applied.

00000195

Table 3-16
Comparison of Heat Transfer Test Data

Source	Pressure	Histogram No.	Heat Flux Type	Number of Data Points	BMW-168			WAFD-188			W-3		
					σ/\bar{y}	R	$(\sigma/\bar{y})^2$	σ/\bar{y}	R	$(\sigma/\bar{y})^2$	σ/\bar{y}	R	$(\sigma/\bar{y})^2$
WAFD-188	500	1	Uniform	57	0.22792	0	--	0.74018	0	--	1.6785	2	1.7483
WAFD-188	600	2	Uniform	146	0.24525	1	0.23373	0.74506	5	0.54011	0.89407	3	0.81663
WAFD-188	1000	3	Uniform	164	0.27351	1	0.26755	0.37793	4	0.50000	0.75947	0	--
WAFD-188	1500	4	Uniform	46	0.13590	3	0.10557	0.50489	0	--	0.44994	0	--
WAFD-188	1750	5	Uniform	50	0.076698	0	--	0.18176	0	--	0.34816	0	--
WAFD-188	2000	6	Uniform	371	0.13529	4	0.12480	0.23113	6	0.20482	5.1493	7	0.79051
WAFD-188	2250	7	Uniform	9	0.081572	0	--	0.15613	0	--	0.17494	0	--
WAFD-188	2500	8	Uniform	9	0.081765	0	--	0.16477	0	--	0.23851	1	0.19424
WAFD-188	2750	9	Uniform	9	0.097343	0	--	0.11820	0	--	0.24127	0	--
AEEM-R213	560	10	Uniform	148	0.26674	3	0.23709	0.61784	0	--	2.9296	1	1.4097
AEEM-R213	750	11	Uniform	33	0.18958	0	--	0.50684	2	0.43312	2.3964	3	1.3510
AEEM-R213	1000	12	Uniform	322	0.20439	3	0.19366	0.50941	0	--	6.3726	3	1.4589
AEEM-R213	1200	13	Uniform	18	0.15915	0	--	0.42712	0	--	0.58600	0	--
AEEM-R213	1500	14	Uniform	104	0.12926	2	0.079859	0.28924	1	0.27054	0.26514	15	0.090829
Columbia	500	15	Uniform	5	0.13704	4	N.A.	0.12752	4	N.A.	0.91541	4	N.A.
Columbia	750	16	Uniform	29	0.16308	0	--	0.31437	0	--	0.58437	0	--
Columbia	1000	17	Uniform	261	0.06468	6	0.18678	12.009	6	0.45991	0.45519	0	--
Columbia	1200	18	Non-Uniform	15	0.12211	0	--	0.29242	0	--	0.46815	0	--
Columbia	1500	19	Uniform	80	0.21043	3	0.12241	0.69765	3	0.24029	1.5097	3	0.11183
ANL	2000	20	Uniform	232	0.10271	2	0.092803	0.19348	2	0.17973	3.6745	14	0.52340
BMW	2000	21	Uniform	21	0.058701	0	--	0.13647	1	0.11792	-24.400	3	1.1838
Euroton	1000	22	Uniform	18	0.13	0	--	0.47611	0	--	0.77404	0	--
Euroton	1500	23	Uniform	18	0.096646	0	--	0.30104	0	--	0.47690	0	--
Euroton	2000	24	Uniform	14	0.12106	0	--	0.19650	0	--	1.6369	0	--
Combined	500-720	25	Uniform	418	0.31215	5	0.28780	0.72108	10	0.65124	2.7046	2	1.4052
Combined	1000	26	Uniform	765	0.47694	9	0.24909	17.834	8	0.56791	4.1325	3	0.88632
Combined	1500	27	Uniform	144	0.19631	4	0.14211	0.57512	3	0.31718	1.2237	3	0.31734
Combined	2000	28	Uniform	638	0.14976	4	0.14251	0.24186	8	0.21986	5.2840	21	0.81792
Combined	1750-2750	29	Uniform	695	0.18236	17	0.14913	0.24463	4	0.23227	5.1401	21	0.81268
Euroton	1000	30	Chopped Cosine	14	0.17017	0	--	0.43187	0	--	0.72772	0	--
Euroton	1500	31	Chopped Cosine	13	0.2122	0	--	0.24251	0	--	0.66671	0	--
Euroton	2000	32	Chopped Cosine	13	0.13652	0	--	0.19268	0	--	-5.7922	3	0.16023
BMW & Euroton	1000	33	Inlet Peak	16	0.19273	0	--	0.42785	0	--	0.76580	0	--
BMW & Euroton	1500	34	Inlet Peak	12	0.13427	1	0.10703	0.18121	0	--	0.72969	0	--
BMW & Euroton	2000	35	Inlet Peak	32	0.13755	0	--	0.17637	0	--	4.4474	5	0.81144
BMW & Euroton	1000	36	Outlet Peak	12	0.23023	0	--	0.55011	2	0.14656	0.74323	0	--
BMW & Euroton	1500	37	Outlet Peak	16	0.16799	0	--	0.30113	0	--	0.45609	0	--
BMW & Euroton	2000	38	Outlet Peak	36	0.13481	0	--	0.16799	0	--	1.0478	4	0.10233
Combined	1000	39	Non-Uniform	42	0.20445	0	--	0.49656	0	--	0.71082	0	--
Combined	1500	40	Non-Uniform	41	0.17435	0	--	0.25368	0	--	0.58846	0	--
Combined	2000	41	Non-Uniform	81	0.17046	0	--	0.17621	0	--	9.6963	9	0.46885

00000196

As is seen from the tabulation the column for BAW-168 with Chauvenet's criterion applied indicates a grouping of 0.1 to 0.2, and a maximum value of 0.28780 is noted from Table 3-16. For WAPD-188 the spread is greater with a maximum value of 0.74018. For W-3 the spread is still greater, and a maximum value of 1.7483 is noted. The negative values of DNB heat flux predicted by the W-3 correlation are in part responsible for the large spread in (σ/\bar{x}) .

The ability of the BAW-168 correlation to fit both uniform and nonuniform heat flux data over a wide range of pertinent variables leads us to believe that it is the best DNB correlation available.

3.2.3.2.4 Evaluation of the Thermal and Hydraulic Design

a. Hot Channel Coolant Quality and Void Fraction

An evaluation of the hot channel coolant conditions provides additional confidence in the thermal design. Sufficient coolant flow has been provided to insure low quality and void fractions. The quality in the hot channel versus reactor power is shown in Figure 3-40. The sensitivity of channel outlet quality with pressure and power level is shown by the 2,185 and 2,120 psig system pressure conditions examined. These calculations were made for an $F\Delta h$ of 1.85. Additional calculations for a 10 per cent increase in $F\Delta h$ to 2.035 were made at 114 per cent power. The significant results of both calculations are summarized in Table 3-17. The effects of using a $F\Delta h$ of 1.79 are shown in Figure 3-40.

Table 3-17
Hot Channel Coolant Conditions

<u>Power, %</u>	<u>$F\Delta h$</u>	<u>Exit Quality, %</u>	<u>Exit Void Fraction, %</u>	<u>Operating Pressure, psig</u>
100	1.85	(-)2.4 ^(b)	0.5 ^(a)	2,185
114	1.85	2.8	13.5	2,185
130	1.85	9.4	36.9	2,185
114	2.035	8.7	35.0	2,185
100	1.85	0	3.8 ^(a)	2,120
114	1.85	5.4	25.2	2,120
130	1.85	12.1	45.2	2,120
114	2.035	11.0	43.4	2,120

(a) Subcooled voids.

(b) Negative indication of quality denotes subcooling of 10.2 Btu/lb.

00000197

The conditions of Table 3-17 were determined with all of the hot channel factors applied. Additional calculations were made for unit cell channels without engineering hot channel factors to show the coolant conditions more likely to occur in the reactor core. Values for $F\Delta h$ of 1.79 and 1.85 were examined with and without fuel assembly flow distribution hot channel factors at 2,185 psig as shown on Figure 3-41. These results show that the exit qualities from the hottest cells should in general be considerably lower than the maximum design conditions.

b. Core Void Fraction

The core void fractions were calculated at 100 per cent power for the normal operating pressure of 2,185 psig and for the minimum operating pressure of 2,120 psig. The influence of core fuel assembly flow distribution was checked by determining the total voids for both 100 and 95 per cent total core flow for the two pressure conditions.

The results are as follows:

<u>Flow, %</u>	<u>Pressure, psig</u>	<u>Core Void Fraction, %</u>
100	2,185	0.007
100	2,120	0.033
95	2,185	0.041
95	2,120	0.127

The most conservative condition of 95 per cent flow at 2,120 psig results in no more than 0.13 per cent void volume in the core. Conservative maximum design values for $F\Delta h$ nuclear described by Line A of Figure 3-12 were used to make the calculation.

The void program uses a combination of Bowring's (33) model with Zuber's (34) correlation between void fraction and quality. The Bowring model considers three different regions of forced convection boiling. They are:

(1) Highly Subcooled Boiling

In this region the bubbles adhere to the wall while moving upward through the channel. This region is terminated when the subcooling decreases to a point where the bubbles break through the laminar sublayer and depart from the surface. The highly subcooled region starts when the surface temperature of the fuel reaches the surface temperature predicted by the Jens and Lottes equation. The highly subcooled region ends when

$$T_{\text{sat}} - T_{\text{bulk}} = \frac{n\phi}{V} \quad (\text{A})$$

00000198

where ϕ = local heat flux, Btu/hr-ft²
 $\eta = 1.863 \times 10^5 (14 + 0.0068p)$
 V = velocity of coolant, ft/sec
 p = pressure, psia

The void fraction in this region is computed in the same manner as Maurer, (35) except that the end of the region is determined by Equation (A) rather than by a vapor layer thickness. The nonequilibrium quality at the end of the region is computed from the void fraction as follows:

$$x_d^* = \frac{1}{1 + \frac{P_f}{P_g} \left(\frac{1}{a_d} - 1 \right)} \quad (B)$$

where x_d^* = nonequilibrium quality at end of Region 1
 a_d = void fraction at $T_{sat} - T_{bulk} = \frac{\eta \phi}{V}$
 P_f = liquid component density, lb/ft³
 P_g = vapor component density, lb/ft³

(2) Slightly Subcooled Boiling

In this region the bubbles depart from the wall and are transported along the channel (condensation of the bubbles is neglected). This region transcends to point where the thermodynamic quality is zero. In general, this is the region of major concern in the design of pressurized water reactors.

The nonequilibrium quality in this region is computed from the following formula:

$$x^* = x_d^* + \frac{P_h}{m h_{fg}(1 + \epsilon)} \int_{z_d}^z (\phi - \phi_{SP}) dz \quad (C)$$

where x^* = nonequilibrium quality in Region 2
 h_{fg} = latent heat of vaporization, Btu/lb
 $\frac{1}{1 + \epsilon}$ = fraction of the heat flux above the single phase heat flux that actually goes to producing voids
 ϕ_{SP} = single phase heat flux, Btu/hr-ft²

00000199

\dot{m} = mass flow rate, lb/hr

P_h = heated perimeter, ft

z = channel distance, ft

The void fraction in this region is computed from

$$a = \frac{x^*}{C_o \left[x^* + P_g/P_f (1 - x^*) \right] + \frac{38.3 A_f P_g \left[\frac{\sigma g g_c (P_f - P_g)}{P_f^2} \right]^{1/4}}{\dot{m}}} \quad (D)$$

where

g = acceleration due to gravity, ft/sec²

g_c = constant in Newton's Second Law = $32.17 \frac{\text{lb m ft}}{\text{lb f sec}^2}$

C_o = Zuber's distribution parameter

A_f = flow area, ft²

σ = surface tension

Equation (D) results from rearranging equations found in Reference (34) and assuming bubbly turbulent flow in determining the relative velocity between the vapor and the fluid. Zuber has shown that Equation (D) results in a better prediction of the void fraction than earlier models based on empirical slip ratios.

(3) Bulk Boiling

In this region the bulk temperature is equal to the saturation temperature, and all the energy transferred to the fluid results in net vapor generation. Bulk boiling begins when the thermodynamic (heat balance) quality, x , is greater than the nonequilibrium quality, x^* . The void fraction in this region is computed using Equation (D) with the thermodynamic quality, x , replacing x^* .

c. Coolant Channel Hydraulic Stability

A flow regime map was constructed to evaluate channel hydraulic stability. The transition from bubbly to annular flow at high mass velocities was determined using Bakers's⁽³⁶⁾ correlation, and the transition from bubbly to slug flow which occurs at low mass velocities was determined with Rose's⁽³⁷⁾ correlation. The transition from slug flow to annular flow was determined by Haberstroh's⁽³⁸⁾ correlation. Bergles⁽³⁹⁾ found that these correlations, which were developed from adiabatic data, are adequate for locating flow regime transitions with heat addition, and that they adequately predict the effects of pressure. Figure 3-42 shows the flow regime map on which has been

00000700

plotted a point representing operating conditions in the hot channel at 114 per cent overpower. To aid in assessing the conservatism of the design, an additional point is plotted at 130 per cent overpower. Inspection shows that both points lie well within the bubbly flow regime. Since the bubbly flow regime is hydraulically stable, no flow instabilities should occur. This flow regime map was prepared for the hot unit cell at the maximum design condition characteristics outlined in 3.2.3.1.1.

The confidence in the design is based on both experimental results obtained in multiple rod bundle burnout tests and analytical evaluations. Three additional flow regime maps were constructed for nominal and postulated worst case conditions to show the sensitivity of the analysis with respect to mass flow rate, channel dimensions and mixing intensity in unit, corner, and wall-type cells. The results are shown in Figures 3-43, 3-44, and 3-45. The mass velocity and quality in each type of channel for the two cases are plotted on the figures. The conditions assumed for the nominal and postulated worst case are given in 3.2.3.2.4 j.

Data from the burnout tests performed by B&W on a 9-rod bundle simulating the core geometry are also plotted on the maps. The open data points on the maps represent the exit conditions in the various type channels just previous to the burnout condition for a representative sample of the data points obtained at the design operating pressure of 2,200 psia. In all of the bundle tests the pressure drop, flow rate, and rod temperature traces were steady and did not exhibit any of the characteristics associated with flow instability.

Inspection of these maps shows that the nominal conditions are far removed from unstable flow regimes. The evaluation also shows that under the worst conditions that have been postulated the reactor will be operating in the hydrodynamically stable, bubbly flow regime.

d. Hot Channel DNB Comparisons

DNB ratios for the hottest channel have been determined for the BAW-168 and W-3 correlations. The results are shown in Figure 3-46. DNB ratios for both correlations are shown for the 1.50 axial max/avg symmetrical cosine flux shape from 100 to 150 per cent power. The BAW-168 DNB ratio at the maximum design power of 114 per cent is 1.38; the corresponding W-3 value is 1.72. This compares with the suggested W-3 design value of 1.3. It is interesting to note that the calculated DNB ratio reaches a value of 1.0 at about 150 per cent power with the BAW-168 equation which adequately describes DNB at the high quality condition of 20 per cent. The W-3 calculation is accurate to about 130 per cent power, but because of quality limitations it cannot be used to examine the channel at the 150 per cent power condition.

The sensitivity of DNB ratio with $F\Delta h$ and Fz nuclear was examined from 100 to 114 per cent power. The detailed results are labeled in Figure 3-46. A cosine flux shape with an Fz of 1.80 and an $F\Delta h$ of 1.85 results in a W-3 DNB ratio of 1.45 and a BAW-168 ratio of 1.33. The W-3 value is well above suggested design values, and the BAW-168

00000201

value of 1.33 corresponds to a hot channel confidence of 99 per cent that about 93 per cent of the population is in no jeopardy as shown in the Population-DNB ratio plot in 3.2.3.2.2, Statistical Core Design Technique.

The influence of a change in $F\Delta h$ was determined by analyzing the hot channel for an $F\Delta h$ of 2.035. This value is 14 per cent above the maximum calculated value of 1.79 and 10 per cent above the maximum design value of 1.85. The resulting BAW-168 DNB ratio is 1.22 and the W-3 value is 1.26. Both of these values are well above the correlation best-fit values of 1.0 for the severe conditions assumed.

e. Reactor Flow Effects

Another significant variable to be considered in the evaluation of the design is the total system flow. Conservative values for system and reactor pressure drop have been determined to insure that the required system flow is obtained in the as-built plant. The experimental programs previously outlined in Section 1 will confirm the pressure drop and related pump head requirements. It is anticipated that the as-built reactor flow will exceed the design value and will lead to increased power capability.

An evaluation of reactor core flow and power capability was made by determining the maximum steady state power rating versus flow. The analysis was made by evaluating the hot channel at the overpower conditions while maintaining (a) a DNB ratio of 1.38 (BAW-168), and (b) the statistical core design criteria. The results of the analysis are shown in Figure 3-47. The power shown is the 100 per cent rating, and the limiting condition is 114 per cent of the rated power. An examination of the slope of the curve indicates stable characteristics, and a 1 per cent change in flow changes the power capability by only about 1/2 per cent.

f. Reactor Inlet Temperature Effects

The influence of reactor inlet temperature on power capability at a given flow was evaluated in a similar manner. A variation of 1 F in reactor inlet temperature will result in a power capability change of slightly less than 1/2 per cent

g. Fuel Temperature

A fuel temperature and gas pressure computer code was developed to calculate fuel temperatures, expansion, densification, equiaxed and columnar grain growth, center piping of fuel pellets, fission gas release, and fission gas pressure. Program and data comparisons were made on the basis of the fraction of the fuel diameter within these structural regions:

- (1) Outer limit of equiaxed grain growth - 2,700 F.
- (2) Outer limit of columnar grain growth - 3,200 F.
- (3) Outer limit of molten fuel (UO_2) - 5,000 F.

Data from References 40 through 43 were used to compare calculated and experimental fractions of the rod in grain growth and central melting.

The radial expansion of the fuel pellet is computed from the mean fuel temperature and the average coefficient of linear expansion for the fuel over the temperature range considered. This model combined with the model for calculating the heat transfer coefficient was compared with the model developed by Notley et al⁽⁴⁴⁾ of AECL. The difference in fuel growth for the two calculation models was less than the experimental scatter of data.

The fuel may be divided into as many as 30 radial and 70 axial increments for the analysis. An iterative solution for the temperature distribution is obtained, and the thermal conductivity of the fuel is input as a function of temperature. The relative thermal expansion of the fuel and cladding is taken into account when determining the temperature drop across the gap between the fuel and cladding surfaces. The temperature drop across the gap is a function of width, mean temperature, and gas conductivity. The conductivity of the gas in the gap is determined as a function of burnup and subsequent release of fission product gases. In the event of fuel clad contact, contact coefficients are determined on the basis of methods suggested by Ross and Stoute⁽⁴⁸⁾. The contact coefficient is determined as a function of the mean conductivity of the interface materials, the contact pressure, the mean surface roughness, the material hardness, and the conductivity of the gas in the gap.

The analytical model computes the amount of central void expected whenever the temperature approaches the threshold temperature for fuel migration, and readjusts the density according to the new geometry.

The program uses a polynomial fit relationship for fuel thermal conductivity. Three relationships were used to evaluate the effects of conductivity. A comparison of these conductivity relationships with the reference design CVNA-142⁽⁴⁵⁾ is shown in Figure 3-48. The values suggested in GEAP-4624⁽⁴⁶⁾ and CVNA-246⁽⁴⁷⁾ are very similar up to 3,000 F, and the former values are more conservative above 3,000 F. McGrath⁽⁴⁷⁾ concludes that the CVNA-246 values are lower limits for the high temperature conditions. Fuel center temperatures for all three of the conductivity relationships at the peaking factors given in 3.2.3.1.2 have been calculated to evaluate the margin to central melting at the maximum overpower and to show the sensitivity of the calculation with respect to thermal conductivity. Since the power peaks will be burned off with irradiation, the peaking factors used are conservative at end-of-life.

Results

00000203

The results of the analysis with the methods described above are shown in Figures 3-49 and 3-50 for beginning and end-of-life conditions. The beginning and end-of-life gas conductivity values are 0.1 and 0.01 Btu/hr-ft²-F respectively. The calculated end-of-life center fuel

temperatures are higher than the beginning-of-life values because of the reduction in the conductivity of the gas in the gap. The effect is apparent even though a contact condition prevails. The calculation does not include the effects of fuel swelling due to irradiation. The calculated contact pressures are conservatively lower than those expected at end-of-life conditions in the hottest fuel rods, and the fuel temperatures shown in the above figures are conservatively higher.

The B&W model gives very good results when compared to the results of others in the field as is shown in Figure 3-50. In the linear heat range of most interest, i.e., approximately 20 kw/ft, there is only about 300 F difference between the maximum and minimum values calculated. Also the small differences between the B&W curve and the other curves indicate the relative insensitivity of the results to the shape of the conductivity at the elevated temperatures.

The most conservative assumptions, using GEAP-4624 data with relatively little increase in thermal conductivity above 3,000 F, result in central fuel melting at about 22 kw/ft, which is 2 kw/ft higher than the maximum design value of 19.9 kw/ft at 114 per cent power. Further evaluation of the two figures shows that central fuel melting is predicted to occur between 22 and 26 kw/ft depending on the time-in-life and conductivity assumptions.

The transient analyses at accident and normal conditions have been made using the GEAP-4624 fuel thermal conductivity curve to reflect a conservative value for the maximum average temperature and stored energy in the fuel. Use of this curve results in a higher temperature and therefore a lower Doppler coefficient, since it decreases with temperature. Thus the resultant Doppler effect is also conservative.

h. Fission Gas Release

The fission gas release is based on results reported in GEAP-4596⁽⁴⁹⁾ Additional data from GEAP-4314⁽⁵⁰⁾, AECL-603⁽⁵¹⁾, and CF-60-12-14⁽⁵²⁾ have been compared with the suggested release rate curve. The release rate curve⁽⁴⁹⁾ is representative of the upper limit of release data in the temperature region of most importance. A design release rate of 43 per cent and an internal gas pressure of 3,300 psi are used to determine the fuel clad internal design conditions reported in 3.2.4.2. Fuel Assemblies.

The design values for fission gas release from the fuel and for the maximum clad internal pressure were determined by analyzing various operating conditions and assigning suitable margins for possible increases in local or average burnup in the fuel. Adequate margins are provided without utilizing the initial porosity voids present in the UO₂ fuel. A detailed analysis of the design assumptions for fission gas release, and the relationship of burnup, fuel growth, and initial diametral clearance between the fuel and clad, are summarized in the following paragraphs. An evaluation of the effect of having the fuel pellet internal voids available as gas holders is also included.

(1) Design Assumptions

(a) Fission Gas Release Rates

The fission gas release rate is calculated as a function of fuel temperature at the design overpower of 114 per cent. The procedures for calculating fuel temperatures are discussed in 3.2.3.2.4 g. The fission gas release curve and the supporting data are shown in Figure 3-51. Most of the data is on or below the design release rate curve. A release rate of 51 per cent is used for the portion of the fuel above 3,500 F. The fuel temperatures were calculated using the GEAP-4624 fuel thermal conductivity curve to obtain conservatively high values for fuel temperatures.

(b) Axial Power and Burnup Assumptions

The temperature conditions in the fuel are determined for the most severe axial power peaking expected to occur. Two axial power shapes have been evaluated to determine the maximum release rates. These are 1.50 and 1.70 max/avg shapes as shown in Figure 3-11 and repeated as part of Figure 3-52 of this analysis. The quantity of gas released is found by applying the temperature-related release rates to the quantities of fission gas produced along the length of the hot fuel rod.

The quantity of fission gas produced in a given axial location is obtained from reactor core axial region burnup studies. Three curves showing the axial distribution of burnup as a local to average ratio along the fuel rod are shown in Figure 3-52. Values of 100, 300, and 930 days of operation are shown.

The 930-day, or end-of-life condition, is the condition with the maximum fission gas inventory. The average burnup at the end of life in the hot fuel rod is 38,150 MWD/MTU which has been determined as follows:

Calculated Hot Bundle Average Burnup, MWD/MTU	33,000
Hot Fuel Rod Burnup Factor	1.05
Margin for Calculation Accuracy	1.10
Hot Rod Maximum Average Burnup, MWD/MTU	38,150

The local burnup along the length of the fuel rod is the product of the hot rod maximum average value above the local to average ratio shown in Figure 3-52. The resulting hot rod local maximum burnup for the 930-day, end-of-life condition is about 42,000 MWD/MTU. This is the maximum calculated value. However, local values to 55,000 MWD/MTU have been evaluated to insure adequate local fuel cladding

00000205

strength for possible increases in average or local burnup over the life of the fuel for various fuel management procedures.

(c) Hot Rod Power Assumptions

The maximum hot rod total power occurring at any time in the life of the fuel has been used to calculate the overpower temperature conditions. A hot rod power of 1.85 times the average rod power has been applied. This results in a maximum linear heat rate of 19.9 kw/ft which corresponds to 114 per cent of the maximum linear heat (17.49) shown in Table 3-1. This is a conservative assumption when coupled with the end-of-life fission gas inventory since bundle and individual fuel rod power is expected to decrease with fuel burnup. A study of the power histories of all of the fuel assemblies to equilibrium conditions shows that the powers in the bundles during the last 300 days of operation are not more than 1.3 times the average bundle power. The peak bundle ratio of 1.69 (1.85 ÷ hot rod ratio) will only occur during the first two fuel cycles when the fission gas inventory is less than the maximum value.

(d) Fuel Growth Assumptions

The fuel growth was calculated as a function of burnup as indicated in 3.2.4.2.1. Fuel pellet dimensions in the thermal temperature and gas release models were increased to the end-of-life conditions as determined above.

(e) Gas Conductivity and Contact Heat Transfer Assumptions

The quantity of fission gas released is a function of fuel temperature. The temperatures are influenced by three factors: (a) the conductivity of the fission gas in the gap between the fuel and clad, (b) the diametral clearance between fuel and clad, and (c) the heat transfer conditions when the fuel expands enough to contact the clad.

A gas conductivity of 0.01 Btu/hr-ft²-F based on 43 per cent release of fission gas at the end-of-life condition was used in the analysis. Diametral clearances of 0.0025 to 0.0075 in. reflecting minimum and maximum clearances after fuel growth were analyzed. The contact heat transfer coefficients were calculated as suggested in Reference 48.

(2) Summary of Results

The fission gas release rates were determined in the first evaluation. Rates were found for various cold diametral clearances and axial power peaking and burnup shapes. The results are shown in Figure 3-53. The lowest curve is the expected condition for a 1.70 axial power shape with a 930-day axial burnup distribution as shown in Figure 3-52. The increase in release rate with

diametral clearance results from the fact that the fuel temperature must be raised to higher values before contact with the fuel clad is made. The release rate at the minimum clearance of 0.0025 in. is 19 per cent. This is the condition that produces the maximum clad stress due to fuel growth with irradiation. The assembly of maximum size pellets with minimum internal diameter cladding will produce this condition after fuel growth. In the event a few hot pellets have the maximum diameter and the remainder have the minimum diameter, then the average cold gap would be 0.0035 in. producing a slightly larger release rate. The release rate of 33 per cent for the maximum diametral clearance will not occur with the maximum stress condition due to fuel growth, since the fuel can grow into the clearance.

Two additional cases were examined to check the sensitivity of the calculations to axial power and burnup shapes. The results are shown by the upper two curves in Figure 3-53. The top curve is a plot of the release rates when it is assumed that both the axial power and burnup inventory of fission gas are distributed with a 1.70 max/avg ratio as shown on Figure 3-52. Similar results are shown for the 1.50 max/avg ratio. These curves show the release rates expected are not strongly influenced by the various power and burnup shapes.

The second evaluation shows the resulting internal pressures due to the release of fission product gases. Plots of pressures for the expected 930-day axial burnup distribution and a 1.70 max/avg axial power shape are shown in Figure 3-54. The lower curve is a plot of internal gas pressure with open pores (5 per cent of the fuel volume is available to hold the released gas). The upper data band is for a closed pore condition with all released gas contained outside the fuel pellets in spaces between the expanded dished ends of the pellets, the radial gaps (if any), and the void spaces at the ends of the fuel rods. The band of data shown reflects the effect of fuel densification and grain growth described in 3.2.3.2.4. The upper limit is for an ideal thermal model without grain growth or densification; the lower limits are for the design model. The calculation of the maximum pressure is also relatively insensitive to the axial burnup distribution as shown by the dashed line in Figure 3-54 for a 1.50 maximum to average axial power and burnup shape. (This corresponds to a local burnup peak of 57,000 MWD/MTU.)

The allowable design internal pressure of 3,300 psi is well above the maximum values of internal pressures calculated for open or closed pellet pores, and the maximum internal pressure should only occur with the maximum diametral clearance condition. A modest increase in average fuel burnup can be tolerated within the prescribed internal pressure design limits.

It has been indicated in Reference 44 and in AECL-1598 that the UC_2 fuel is plastic enough to flow under low stresses when the temperature is above 1,800 F. That fraction of the fuel below

this temperature may retain a large portion of the original porosity and act as a fission gas holder. The hottest axial locations producing the highest clad stresses will have little if any fuel below 1,800 F. However, the ends of the fuel rods will have some fuel below this temperature. The approximate fraction of the fuel below 1,800 F at overpower for a 1.70 axial power shape is as follows for various cold diametral clearances.

<u>Clearance,</u> <u>in.</u>	<u>Per Cent of Fuel</u> <u>Below 1,800 F, %</u>
0.0025	40
0.005	20
0.0075	5

The retention of fuel porosity in the low temperature and low burnup regions will result in modest reductions in internal gas pressure.

i. Hot Channel Factors Evaluation

(1) Rod Pitch and Bowing

A flow area reduction factor is determined for the as-built fuel assembly by taking channel flow area measurements and statistically determining an equivalent hot channel flow area reduction factor. A fuel assembly has been measured with the results shown in Table 3-12. In the analytical solution for a channel flow, each channel flow area is reduced over its entire length by the F_A factor shown in Figure 3-21 for 99 per cent confidence. With a 99 per cent confidence and 94.5 per cent population relationship described in 3.2.3.1.1 for the hot channel, the area reduction factor is 0.992. The approximate limit of this factor is obtained by examining the value in Figure 3-21 as the population protected approaches 100 per cent. F_A at 99.99 per cent of the population protected is 0.983. The hot channel value is shown in Table 3-1.

Special attention is given to the influence of water gap variation between fuel assemblies when determining rod powers. Nuclear analyses have been made for the nominal and maximum spacing between adjacent fuel assemblies. The nominal and maximum hot assembly fuel rod powers are shown in Figures 3-55 and 3-56 respectively. The hot channel nuclear power factor ($F_{\Delta h}$ nuclear) of 1.85 shown in 3.2.3.1.1 is based on Figure 3-56 for the maximum water gap between fuel assemblies. The factor of 1.85 is a product of the hot assembly factor of 1.69 times the 1.096 hot rod factor. This power factor is assigned to the hottest fuel rod which is analyzed for burnout under unit cell, wall cell, and corner cell flow conditions.

(2) Fuel Pellet Diameter, Density, and Enrichment Factors

Variations in the pellet size, density, and enrichment are reflected in coefficients of variation numbers 2 through 7 of Table 3-12. These variations have been obtained from the measured or specified tolerances and combined statistically as described in 3.2.3.2.2 to give a power factor on the hot rod. For the hot channel confidence and population conditions, this factor, F_Q , is 1.008 and is applied as a power increase over the full length of the hot fuel rod. The local heat flux factor, $F_{Q''}$, for 99 per cent confidence and 94.5 per cent population is 1.013. These hot channel values are shown in Table 3-1. The corresponding values of F_Q and $F_{Q''}$ with 99.99 per cent population protected are 1.017 and 1.03 respectively. A conservative value of $F_{Q''}$ of 1.03 for 99 per cent confidence and 99.99 per cent population is used for finding the maximum fuel linear heat rates as shown in 3.2.3.1.2.

These factors are used in the direct solution for channel enthalpies and are not expressed as factors on enthalpy rise as is often done. The coefficients of variation will be under continuous review during the final design and development of the fuel assembly.

(3) Flow Distribution Effects

Inlet Plenum Effects

The final inlet plenum effects will be determined from the 1/6 scale model flow test now in progress. The initial runs indicate satisfactory flow distribution. Although the final nuclear analysis and flow test data may show that the hot bundle positions receive average or better flow, it has been assumed that the flow in the hot bundle position is 5 per cent less than average bundle flow under isothermal conditions corresponding to the model flow test conditions. An additional reduction of flow due to hot assembly power is described below.

Redistribution in Adjacent Channels of Dissimilar Coolant Conditions

The hot fuel assembly flow is less than the flow through an average assembly at the same core pressure drop because of the increased pressure drop associated with a higher enthalpy and quality condition. This effect is allowed for by making a direct calculation for the hot assembly flow. The combined effects of upper and lower plenum flow conditions and heat input to the hot assemblies will result in a hot assembly flow of about 85 to 95 per cent of the average assembly flow depending on the final plenum effects and assembly power peaks. The worst combination of effects has been assumed in the initial design, and the hot assembly flow has been calculated to be about 85 per cent of the average assembly flow at 114 per cent overpower. Actual hot assembly flows are calculated rather than applying an equivalent hot channel enthalpy rise factor.

Physical Mixing of Coolant Between Channels

The flow distribution within the hot assembly is calculated with a mixing code that allows an interchange of heat between channels. Mixing coefficients have been determined from multirod mixing tests. The fuel assembly, consisting of a 15 x 15 array of fuel rods, is divided into unit, wall, and corner cells as shown by the heavy lines in Figure 3-55. The mixed enthalpy for every cell is determined simultaneously so that the ratio of cell to average assembly enthalpy rise (Enthalpy Rise Factor) and the corresponding local enthalpy are obtained for each cell. Typical enthalpy rise factors are shown in Figures 3-55 and 3-56 for cells surrounding the hottest fuel rod located in the corner of the assembly. The assumptions used to describe the channels for the peaking and enthalpy rise factors shown are given in Wall and Corner Channels Evaluation, 3.2.3.2.4 j, which follows.

j. Evaluation of the DNB Ratios in the Unit, Wall, and Corner Cells

DNB Results

The DNB ratios in the hot unit cell at the maximum design condition described in 3.2.3.1 are shown in Figure 3-46. The relationships shown are based on the application of single channel heat transfer data in the BAW-168(18) and W-3(23,68) correlations. An additional sensitivity analysis of the assembly has been made utilizing 9-rod assembly heat transfer DNB test data that is more representative of the actual wall and corner cells geometry effects than single channel data.

The sensitivity of the assembly design with respect to variations of mass flow rate (G), channel spacing, mixing intensity, and local peaking on the DNB ratios in the fuel assembly channels has been evaluated by analyzing the nominal conditions and a postulated worst case condition. The summary results are shown below in Table 3-18.

Table 3-18
DNB Ratios in the Fuel Assembly Channels

<u>Nominal Case</u>		
<u>Cell Type</u>	<u>G, lb/hr-ft² x 10⁻⁶</u>	<u>DNBR</u>
Corner	1.59	2.20
Wall	1.90	2.11
Unit	2.52	2.01

<u>Postulated Worst Case</u>		
<u>Cell Type</u>	<u>G, lb/hr-ft² x 10⁻⁶</u>	<u>DNBR</u>
Corner	1.32	1.70
Wall	1.64	1.65
Unit	2.29	1.73

The DNBR's above are ratios of the limiting heat flux to the local flux along the length of the channels. The limiting heat fluxes have been determined from the 9-rod assembly DNB test data.

The DNB ratios in all channels are high enough to insure a confidence-population relationship equal to or better than that outlined in 3.2.3.1.1 for the hot unit cell channel. The postulated worst case conditions are more severe than the required maximum design conditions.

The results of the assembly tests and this evaluation show that the performance of the wall and corner cells is more sensitive to local enthalpy than to the local mass velocities. Although the mass flow rates in the corner and wall cells are lower than in the unit cell, the total flow in these cells is relatively higher than the mass flow rates imply because of the increased space between the outer rods and the perforated can. This results in more favorable power-to-flow ratios than the mass flow rates indicate.

The DNB ratios were obtained by comparing the local heat fluxes and coolant conditions with heat transfer data points from 9-rod fuel assembly heat transfer tests for uniform heat flux with an appropriate correction for a nonuniform axial power shape. Typical results are shown in Figures 3-57 and 3-58 for the nominal and worst case conditions in the corner cell. The line defined by a best fit of the data is shown on each figure as a solid line. A design limit line, shown as dotted, has been determined by lowering the best-fit line to account for the effects of nonuniform flux shapes. The magnitude of the reduction was determined by comparison with the results of the atom nonuniform test data Reference 19 and the results of more recent non-uniform tests conducted by B&W.

The limiting best-fit lines were derived from a 9-rod fuel assembly test section 72 in. long with rod diameter, pitch spacing, and spacer grids of the type to be used in the reference design. A total of 513 data points between 1,000 psi and 2,450 psi has been obtained. One hundred and sixty-two of these points were used for the limiting lines in the PWR pressure and mass flow ranges. The ranges of test variables for the 162 data points used were:

Pressure - 1,800 to 2,450 psi
Mass Flow Rate - 1.0 to 3.5 x 10⁶ lb/hr-ft²
Quality - -5 to +20 per cent

All of the cell conditions of interest in this analysis fall within this range of parameters.

Fuel Rod Power Peaks and Cell Coolant Conditions

The nominal case local-to-average rod powers and the local-to-average exit enthalpy rise ratios are shown in Figure 3-55 for the hot corner, hot wall, and hot unit cells in the hot fuel assembly. Values shown are for nominal water gaps between the hot fuel assembly and adjacent

fuel assemblies with nominal rod-to-wall spacing, with nominal flow to the hot fuel assembly, and with a nominal intensity of turbulence, α (*), equal to 0.03.

Additional tests are being run to determine the maximum values of intensity of turbulence associated with the fuel assembly. The expected value is greater than 0.03 since this value is obtained in smooth tubes, and the spacers and can panel perforations should induce more turbulence.

The postulated worst case local-to-average rod powers and exit enthalpy rise ratios in the hot fuel assembly are shown in Figure 3-56. The factors were determined for this case with twice the nominal water gaps between the hot fuel assembly and adjacent fuel assemblies with minimum rod-to-wall spacing, with minimum flow to the hot fuel assembly, and with a minimum assumed intensity of turbulence, α , equal to 0.01.

In neither the nominal nor the postulated worst case analysis has any credit been taken for the coolant which is flowing in the water gaps between the fuel assemblies and which serves to reduce enthalpies in the peripheral cells of the hot fuel assembly by mixing with the coolant in those cells through the can panel perforations. In both cases, however, the effective roughness of the can panel perforations and its effect on reducing the flow in the peripheral cells of the fuel assembly has been accounted for. The magnitude of the effective roughness was obtained from the results of a series of flow tests performed on a mockup of the outer two rows of fuel rods and the can panels of two adjacent fuel assemblies. The rod-to-wall spacing in the peripheral cells of the fuel assembly has been increased to compensate for the effects of the can panel in reducing the flow in the peripheral cells. The nominal distance from the center of the outside rods to the can panel is 0.324 in. The corresponding postulated worst case dimension was assumed to be 0.310 in.

Fuel Assembly Power and Flow Conditions

The nominal and postulated worst cases were run at 114 per cent reactor power with the nominal and worst $F\Delta h$ factors shown in 3.2.3.1.1 c. The 1.50 modified cosine axial power shape of Figure 3-11 was used to describe the worst axial condition.

(*) The intensity of turbulence, α , is defined as

$$\sqrt{V_t'^2}/V$$

where V_t' is the transverse component of the fluctuating turbulent velocity, and V is the coolant velocity in the axial direction. This method of computing mixing is described by Sandberg, R. O., and Bishop, A. A., CVTR Thermal-Hydraulic Design for 65 MW Gross Fission Power, CVNA-227.

The hot assembly flow under nominal conditions without a flow maldistribution effect is 93 per cent of the average assembly flow, and the reduction in flow is due entirely to heat input effects. The hot assembly flow under the worst postulated conditions is 85 per cent of the average assembly flow and considers the worst combined effects of heat input and flow maldistribution.

Summary

Analysis of all B&W bundle data to date indicates that the B&W method will correlate data with less deviation than previous methods. Indications are that this is also true when considering nonuniform axial power distributions. Additional bundle tests will be conducted with nonuniform axial power distribution to confirm that the use of a power shape correction factor based on single channel and annular specimens is conservative.

Completion of the test programs outlined in this report and evaluation of the experimental data will provide final design correlations and flow relationships that will give complete confidence in the conservatism of the design and the B&W analytical procedures.

It should be noted that the postulated worst case is worse than the hot channel permitted by our specifications. Even with this postulated worst case, the design is still conservative, and there is very little difference in the performance of the various channels. This indicates that the outside cell geometries have been compensated correctly to account for wall effects.

00000213

3.2.4 MECHANICAL DESIGN LAYOUT

3.2.4.1 Internal Layout

Reactor internal components include the upper plenum assembly, the core support assembly (consisting of the core support shield, vent valves, core barrel, lower grid and flow baffle, thermal shield, and surveillance specimen holder tubes), and the incore instrument guide extensions. Figure 3-59 shows the reactor vessel, reactor vessel internals arrangement, and the reactor coolant flow path. Figure 3-60 shows a cross section through the reactor vessel, and Figure 3-61 shows the core flooding arrangement. | 1

Reactor internal components do not include fuel assemblies, control rod assemblies (CRA's), surveillance specimen assemblies, or incore instrumentation. Fuel assemblies are described in 3.2.4.2, control rod assemblies and drives in 3.2.4.3, surveillance specimen assemblies in 4.4.3, and incore instrumentation in 7.3.3.

The reactor internals are designed to support the core, maintain fuel assembly alignment, limit fuel assembly movement, and maintain CRA guide tube alignment between fuel assemblies and control rod drives. They also direct the flow of reactor coolant, provide gamma and neutron shielding, provide guides for incore instrumentation between the reactor vessel lower head and the fuel assemblies, support the surveillance specimen assemblies in the annulus between the thermal shield and the reactor vessel wall, and support the internals vent valves. These vent valves are provided to relieve pressure generated by steaming in the core following an inlet pipe rupture so that the core will remain sufficiently covered with coolant. All reactor internal components can be removed from the reactor vessel to allow inspection of the reactor internals and the reactor vessel internal surface. | 1

A shop fitup and checkout of all internal components in an as-built reactor vessel mockup will insure proper alignment of mating parts before shipment. Dummy fuel assemblies and control rod assemblies will be used to check fuel assembly clearances and CRA free movement.

In anticipation of lateral deflection of the lower end of the core support assembly as a result of horizontal seismic loadings, integral weld-attached, deflection-limiting spacer blocks have been placed on the reactor vessel inside wall. In addition, these blocks limit the rotation of the lower end of the core support assembly which could conceivably result from flow-induced torsional loadings. The blocks allow free vertical movement of the lower end of the internals for thermal expansion throughout all ranges of reactor operating conditions, but in the unlikely event of a flange, circumferential weld, or bolted joint failure the blocks will limit the possible core drop to 1/2 in. or less. The final elevation plane of these blocks will be established near the same elevation as the vessel support skirt attachment to minimize dynamic loading effects on the vessel shell or bottom head. Preliminary calculations indicate the impact loading on the stop blocks for a 1/4 in. core drop would be approximately 5 g's total. Block location and geometry will be evaluated and determined to transfer this loading through the vessel support skirt to the reactor building concrete. A significant reduction in impact loading can be achieved through proper stop block design and detailed analysis. A 1/2 in. core drop will not allow the lower end of the CRA poison rods

to disengage from their respective fuel assembly guide tubes if the CRA's are in the full-out position, since approximately 6-1/2 in. of rod length would remain in the fuel assembly guide tubes. A core drop of 1/2 in. will not result in a significant reactivity change. The core cannot rotate and bind the drive lines because rotation of the core support assembly is prevented by the stop blocks.

The failure of the core support shield and core barrel upper flanges, or related flanges and other circumferential joints, is not considered credible on the basis of the conservative design criteria and large safety factors employed in the internals design. The final internals design will be capable of withstanding various combinations of forces and loadings resulting from the static weight of internals (179,000 lb total), core with control rod drive line (303,000 lb total), dynamic load from trip (10 g's gives 207,000 lb), seismic (0.10 g vertical gives 48,000 lb), coolant flow hydraulic loading (230,000 lb), and other related loadings. The algebraic sum of this simplified loading case is 507,000 lb. This results in a tensile stress of about 700 psi in the core support shield shell, which is approximately 4 per cent of the material yield strength. Final internals component weights, seismic analysis, dynamic loadings from flow-induced vibration, detailed stress analysis with consideration for thermal stress during all transients, and resolution of fabrication details such as shell rolling tolerances and weld joint preparation details will increase the stress levels listed above. As a final design criterion, the core support components will meet the stress requirements of the ASME Code, Section III, during normal operation and transients. The structural integrity of all core support circumferential weld joints in the internals shells will be insured by compliance with the radiographic inspection requirements in the code above. The seismic analysis will include detailed calculations to determine the maximum structural response of the reactor vessel and internals. This analysis will be performed as described in 3.1.2.4.1.

In the event of a major loss-of-coolant accident, such as a 36 in. diameter reactor coolant pipe break near the reactor vessel outlet, the fuel assembly and vessel internals would be subjected to dynamic loadings resulting from an oscillating (approximately sinusoidal) differential pressure across the core. A preliminary analysis of this postulated accident indicates that the fuel assemblies would move upward less than 3/8 in. Some deflection of the internals structures would occur, but internals component failure will not occur. The occurrence of a loss-of-coolant accident and resulting loadings will be evaluated during the detailed design period for the fuel assemblies and related internals structural components.

The deflections and movements described above would not prevent CRA insertion because the control rods are guided by split tubes throughout their travel, and the guide tube to fuel assembly alignment cannot change regardless of related component deflections. CRA trip could conceivably be delayed momentarily as a result of the oscillating pressure differential. However, the CRA travel time to full insertion would remain relatively unaffected as transient pressure oscillations are dampened out in approximately 0.5 sec. On this basis, the CRA travel time to 2/3 insertion on a trip command will be approximately 1.55 sec instead of the specified 1.40 sec. Also,

this possible initial minor delay in trip initiation would not contribute to the severity of the loss-of-coolant accident because at the initiation of CRA trip, the core would be subcritical from voids.

Material for the reactor internals bolting will be subjected to rigid quality control requirements to insure structural integrity. The bolts will be dye-penetrant inspected for surface flaw indications after all fabrication operations have been completed. Torque values will be specified for the final assembly to develop full-bolting capability. All fasteners will be lock-welded to insure assembly integrity.

3.2.4.1.1 Upper Plenum Assembly

The upper plenum assembly is located directly above the reactor core and is removed as a single component before refueling. It consists of upper and center grid assemblies, CRA guide tubes, and a flanged cylinder with openings for reactor coolant outlet flow. The upper grid is a series of parallel flat bars intersecting to form square lattices and is welded to the plenum cylinder top flange. A machined upper end on each CRA guide tube is located and welded to the plenum cover which is attached to the upper grid bars. CRA guide tubes provide CRA guidance and protect the CRA from the effects of coolant cross-flow.

Each CRA guide tube consists of an outer tube housing and sixteen slotted tubes which are properly oriented and brazed to a series of castings. As the tubes are slotted for their full length, the brazement provides continuous guidance for the CRA full stroke travel. Design clearances in the guide tube will accommodate some degree of misalignment between the CRA guide tubes and the fuel assemblies. Final design clearances will be established by tolerance studies and by the results of the Control Rod Drive Line Facility (CRDL) prototype tests. Preliminary test results are described in 3.2.4.3.5.

The center grid assembly consists of parallel flat bars intersecting to form square lattices. The bars are attached to a flange which is bolted to the plenum cylinder lower flange. The center grid assembly locates the lower end of the individual CRA guide tube relative to the upper end of the corresponding fuel assembly.

Locating slots in the upper plenum assembly top flange engage the reactor vessel top flange locating devices to align the upper plenum assembly with the reactor vessel, reactor closure head control rod drive penetrations, and the core support shield. The bottom of the upper plenum assembly is guided and aligned by locating blocks attached to the inside of the core support shield.

3.2.4.1.2 Core Support Assembly

The core support assembly consists of the core support shield, core barrel, lower grid and flow baffle, thermal shield, and surveillance specimen holder tubes.

Static loads from the assembled components and fuel assemblies, and dynamic loads from CRA trip, hydraulic flow, thermal expansion, seismic disturbances, and loss-of-coolant accident considerations, are all carried by the core support assembly.

The core support assembly components are described as follows:

a. Core Support Shield

The core support shield is a large flanged cylinder which mates with the reactor vessel opening. The top flange rests on a circumferential ledge in the reactor vessel top closure flange. The core support shield lower flange is bolted to the core barrel. The cylinder wall has two nozzle openings for reactor coolant outlet flow. Locating blocks on the inside of the cylinder wall near the bottom guide and align the upper plenum chamber relative to the core support shield.

The reactor vessel outlet nozzles are sealed to the mating components of the core support shield by the differential thermal expansion between the carbon steel reactor vessel and the stainless steel core support shield. The nozzle seal surfaces are finished and fitted to a predetermined cold gap providing clearance during core support assembly installation and removal. At reactor operating temperature the mating metal surfaces are in contact to make a seal without exceeding allowable stresses in either the reactor vessel or internals.

b. Core Barrel

The core barrel supports the fuel assemblies and lower grid and flow baffle, and directs the reactor coolant flow through the vessel. The barrel consists of a flanged cylinder, a series of internal horizontal spacers bolted to the cylinder, and a series of vertical plates bolted to the inner surfaces of the horizontal spacers to form an inner wall enclosing the fuel assemblies. Construction of the core barrel will be similar to that of the reactor internals component developed by B&W for the Indian Point Station Unit No. 1.

Coolant flow is downward along the outside of the core barrel cylinder and upward through the fuel assemblies contained in the core barrel. A small portion of the coolant flows upward through the space between the core barrel outer cylinder and the inner plate wall.

Coolant pressure in this space is maintained slightly lower than the core coolant pressure to avoid tension loads on the bolts attaching the plates to the horizontal spacers. The vertical plate inner wall will be carefully fitted together to reduce reactor coolant leakage to an acceptable rate.

The upper flange of the core barrel outer cylinder is bolted to the mating lower flange of the core support shield, and the lower flange is bolted to the mating flange of the lower grid and flow baffle. All bolts will be inspected and installed as

described in 3.2.4.1, and will be lock-welded after final assembly.

c. Lower Grid and Flow Baffle

The lower grid provides alignment and support for the fuel assemblies and aligns the incore instrument guide extensions with the fuel assembly incore instrument tubes. The lower grid consists of two flat plate and bar lattice structures separated by short tubular columns surrounded by a flanged cylinder. The top flange is bolted to the lower flange of the core barrel. The lower grid top flange also positions and supports the thermal shield.

The flow baffle is a dished plate with an external flange which is bolted to the bottom flange of the lower grid. The flow baffle is perforated to distribute the reactor coolant entering the bottom of the core.

d. Thermal Shield

A cylindrical stainless steel thermal shield is installed in the annulus between the core barrel outer cylinder and the reactor vessel inner wall. The thermal shield reduces the neutron and gamma internal heat generation in the reactor vessel wall and thereby reduces the resulting thermal stresses.

The thermal shield is supported on, positioned by, and attached to the lower grid top flange. Also, the thermal shield upper end is positioned by spacers between the thermal shield and the core barrel outer cylinder to minimize the possibility of thermal shield vibration. The thermal shield attachment is designed to prevent fasteners from being loaded in shear. Fasteners are lock-welded after final assembly.

e. Surveillance Specimen Holder Tubes

Surveillance specimen holder tubes are installed on the core support assembly outer wall to contain the surveillance specimen assemblies. The tubes extend from the top flange of the core support shield to the lower end of the thermal shield. The tubes will be rigidly attached to prevent flow-induced vibration. Slip joints at the lower end of the core support shield will allow the shield to be removed from the core support assembly without destructively removing the surveillance specimen holder tubes.

f. Internals Vent Valves

Internals vent valves are installed in the core support shield to prevent a pressure unbalance which might interfere with core cooling following a loss-of-coolant accident. In its natural state and under all normal operating conditions, the vent valve will be closed. In the event of a loss-of-coolant accident in the cold leg of the reactor

1

loop, the valve will open to permit steam generated in the core to flow directly to the leak and will prevent the core from becoming more than 1/2-uncovered after emergency core coolant has been supplied to the reactor vessel. The preliminary design of the internals vent valve is shown in Figure 3-61a. 1

Each valve assembly consists of a hinged disc, valve body with sealing surfaces, split-retaining ring, and fasteners. Each valve assembly is installed into a machined mounting ring, integrally welded in the core support shield wall. The mounting ring contains the necessary features to retain and seal the perimeter of the valve assembly. Also, the mounting ring includes an alignment device to maintain the correct orientation of the valve assembly for hinged-disc operation. Each valve assembly will be remotely handled as a unit for removal or installation. Valve component parts, including the disc, will be of captured-design to minimize the possibility of part loss to the coolant system, and all fasteners will include a positive locking device. The hinged-disc will include an integral arm hook, eye, or other device for remote inspection of disc function.

The preliminary arrangement consists of 14-in. diam check valve assemblies installed in the cylindrical wall of the internals core support shield. The valve centers are coplanar and are 42 in. above the plane of the reactor vessel coolant nozzle centers. In cross section, the valves are spaced around the circumference of the core support shield wall.

The hinge design will consist of a shaft, two valve body journal receptacles, two valve disc journal receptacles, and four flanged shaft journals (bushings). Loose clearances will be used between the shaft and journal inside diameters, and between the journal outside diameters and their receptacles. This feature provides eight loose rotational clearances to minimize any possibility of impairment of disc-free motion in service. In the event that one rotational clearance should bind in service, seven loose rotational clearances would remain to allow unhampered disc-free motion. In the worst case, at least four clearances must bind or seize solid to adversely affect valve disc-free motion.

In addition, the valve disc will contain a self-alignment feature so that the external differential pressure will adjust the disc seal face to the valve body seal face. This feature minimizes the possibility of increased leakage and pressure-induced deflection loadings on the hinge parts in service.

The external side of the disc will be contoured to absorb the impact load of the disc on the reactor vessel inside wall without transmitting excessive impact loads to the hinge parts as a result of a loss-of-coolant accident.

00000219

3.2.4.1.3 Incore Instrument Guide Extensions

The incore instrument guide extensions guide the incore instrument assemblies between the instrument penetrations in the reactor vessel bottom head and the instrument tubes in the fuel assemblies. Sufficient clearance in the instrument guide extensions provides for minor misalignment between the reactor vessel instrument penetrations and the instrument guide extension tubes. A perforated shroud tube, concentric with the instrument guide tube, adds rigidity

00000220

to the assembly and reduces the effect of coolant flow forces. Fifty-two in-core instrument guide extensions are provided. The incore instrument guide extensions are designed so that they will not be affected by the core drop described in 3.2.4.1.

3.2.4.2 Fuel Assemblies

3.2.4.2.1 Description

a. General Description

The fuel for the reactor is sintered pellets of low enrichment uranium dioxide clad in Zircaloy-4 tubing. The clad, fuel pellets, end supports, holddown spring, and end caps form a "Fuel Rod". Two hundred and eight fuel rods are mechanically joined in a 15 x 15 array to form a "Fuel Assembly" (Figure 3-62). The center position in the assembly is reserved for instrumentation. The remaining 16 positions in the array are provided with "Guide Tubes" for use as control rod locations. The complete core has 177 fuel assemblies. All assemblies are identical in mechanical construction, i.e., all are designed to accept the control rod assemblies (CRA). However, only 69 have CRA's to control the reactivity of the core under operating conditions. In the 108 fuel assemblies containing no CRA during a given core cycle, the guide tubes are partially filled at the top by an "Orifice Rod Assembly" (Figure 3-63) in order to minimize bypass coolant flow. These orifice rod assemblies also tend to equalize coolant flow between fuel assemblies with CRA's and those with orifice rod assemblies.

Fuel assembly components, materials, and dimensions are listed below.

<u>Item</u>	<u>Material</u>	<u>Dimensions, in.</u>
Fuel	UO ₂ Sintered Pellets	0.362 diam.
Fuel Clad	Zircaloy-4	0.420 OD x 0.368 ID x 152-7/8 long
Fuel Rod Pitch		0.558
Fuel Assembly Pitch		8.587
Active Fuel Length		1.44
Overall Length		≈165
Control Rod Guide Tube	Zircaloy-4	0.530 OD x 0.015 wall

00000221

<u>Item</u>	<u>Material</u>	<u>Dimensions, in.</u>
Incore Instrument Guide Extension	Zircaloy-4	0.530 OD x 0.075 wall
Spacer Grid	Stainless Steel, Tp-304	Spaced at 21-7/16 in.
Can Panel	Stainless Steel, Tp-304	0.031 thick
End Fitting	Stainless Steel, Tp-304	

b. Fuel

The fuel is in the form of sintered and ground pellets of uranium dioxide. The pellets are dished on each end face to minimize the difference in axial thermal expansion between the fuel and cladding. The density of the fuel is 95 per cent of theoretical.

Average design burnup of the fuel is 28,200 MWD/MTU. Peak burnup is 55,000 MWD/MTU. At the peak burnup, the fuel growth is calculated to be 9-1/2 volume per cent by the method given in Reference 53. This growth is accommodated by pellet porosity, by the radial clearance provided between the pellets and the cladding, and by a small amount of plastic strain in the cladding.

Each fuel column is located, at the bottom, by a thin-wall stainless steel pedestal and is held in place during handling by a spring at the top. The spring allows axial differential thermal expansion between fuel and cladding, and axial fuel growth. The bottom pedestal is also collapsible, thus providing a secondary buffer to prevent excess cladding axial strain.

Fission gas release from the fuel is accommodated by voids within the fuel, by the radial gap between the pellets and cladding, and by void space at the top and bottom ends of the fuel rod.

c. Fuel Assembly Structure

(1) General

The fuel assembly shown in Figure 3-62 is the canned type. Eight spacer grids and four perforated can panels form the basic structure. The panels are welded together at the corners for the entire length. The spacer grids are welded to the panels, and the lower and upper end fittings are welded to the panels to complete the structure. The upper end fitting is not attached until the fuel rods,

guide tubes, and instrumentation tube have been installed. At each spacer grid assembly each fuel rod is supported on four sides by integral leaf-type springs. These springs are designed to provide a radial load on the fuel rod sufficient to restrain it so that flow-induced vibrational amplitudes are minimal. However, to avoid undesirable bowing of the fuel rods, the spring loads are designed small enough to permit the relative axial motion required to accommodate the differential thermal expansion between the Zircaloy fuel rod and the stainless steel structure.

(2) Spacer Grid

These grids are composed of ferrules made of square tubing. The ferrule has a portion of each side formed into spring sections which have hydrodynamically shaped "dimples" that contact the fuel rods. The ferrules are joined together by brazing to form the spacer grids. The grids, which provide the desired pitch spacing between fuel rods, are spot-welded at intervals to the perforated stainless steel can panels.

(3) Lower End Fitting

The lower end fitting is constructed from Type 304 stainless steel members which when joined together form a box structure. Four deep cross members serve as the positioning surfaces for the fuel assembly when it is inserted into the lower core support structure. The assembly includes a grid structure which provides a support base for fuel rods while maintaining a maximum inlet flow area for the coolant.

(4) Upper End Fitting

The upper end fitting is similar to the lower end fitting. It positions the upper end of the fuel assembly and provides coupling between the fuel assembly and the handling equipment. A hollow post, welded in the center of the assembly, is designed to provide a means of uncoupling the CRA-to-drive connection and to retain the orifice rod assembly. In order to identify a fuel assembly under water, a serial number is milled into a flat, chrome-plated surface which is welded to the box frame.

(5) Control Rod Guide Tubes

The Zircaloy guide tubes serve to guide the control rods within the fuel assembly during operation. The tubes are restrained axially by the upper and lower end fittings in the fuel assembly and radially by the spacer grids in the same manner as the fuel rods.

00000223

3.2.4.2.2 Evaluation

a. Fuel Rod Assembly

(1) General

The basis for the design of the fuel rod is discussed in 3.1.2.4. Materials testing and actual operation in reactor service with Zircaloy cladding has demonstrated that Zircaloy-4 material has ample corrosion resistance and sufficient mechanical properties to maintain the integrity and serviceability required for design burnup.

(2) Clad Stress

Stress analysis for cladding is based on several conservative assumptions that make the actual margins of safety greater than calculated. For example, it is assumed that the clad with the thinnest wall and the greatest ovality permitted by the specification is operating in the region of the core where performance requirements are severest. Fission gas release rates, fuel growth, and changes in mechanical properties with irradiation are based on a conservative evaluation of currently available data. Thus, it is unlikely that significant failure of the cladding will result during operation.

The actual clad stresses are considerably below the yield strength. Circumferential stresses due to external pressure, calculated using those combinations of clad dimensions, ovality, and eccentricity that produce the highest stresses, are shown in Table 3-19. The maximum stress of 33,000 psi compression, at the design pressure of 2,500 psi, is the sum of 22,000 psi compressive membrane stress plus 11,000 psi compressive bending stress due to ovality at the clad OD in the expansion void, and at the beginning-of-life. The maximum stress in the heat-producing zone is 32,000 psi at design pressure, 27,000 psi at operating pressure. At this stress, the material may creep sufficiently to allow an increase in ovality until further creep is restrained by support from the fuel. Contact loads on the order of 20 lb/in. of length are sufficient to counteract the bending stress. Creep collapse tests have indicated a long time collapse resistance in excess of the requirement to prevent collapse in the end void. As the fuel rod internal pressure builds up with time, these stresses are reduced.

Late in life, the fuel rod internal pressure exceeds the system pressure, up to a maximum difference of 1,110 psi. The resultant circumferential pressure stress of 9,000 psi is about 1/4 of the yield strength and therefore is not a potential source of short time burst. The possibility of stress-rupture burst has been investigated using finite-difference methods to estimate the long time effects of the increasing pressure on the clad. The predicted pressure-time relationship produces stresses that are less than 1/3 of the stress levels that would produce

stress rupture at the end-of-life. Outpile stress-rupture data were used, but the greater than 3:1 margin on stress is more than enough to account for decreased stress-rupture strength due to irradiation. Clad circumferential stresses are listed in Table 3-19.

The free gas content of the fuel rod is calculated by considering (1) initial helium fill gas, (2) initial water vapor and atmospheric gases adsorbed on the fuel, and (3) fission product gases. The water vapor present initially is expected to dissociate over the life of the fuel and enter into hydrating and oxidizing reactions. The gas remaining at the end-of-life, when the maximum internal pressures exist, consists of the atmospheric gases and helium present initially plus the released fission gases.

The fission gas production is evaluated for a range of neutron fluxes and the fissionable material present over the life of the fuel.⁽⁵⁴⁾ A design value for gas production has been determined as 0.29 atoms of gas per fission.

00000225

Table 3-19
Clad Circumferential Stresses

<u>Operating Condition</u>	<u>Calc. Stress, psi</u>	<u>Yield Stress, psi</u>	<u>Ultimate Tensile Stress, psi</u>
1. <u>BOL^(a) - Operating at Design Pressure</u>			
Total Stress (membrane + bending) Due to 2,500 psig System Design Pressure Minus 100 psig Fuel Rod Internal Pressure			
Average Clad Temperature - Approximately 625 F (expansion void)	-33,000	46,000	
2. <u>EOL - Maximum Overpower</u>			
System Pressure - 2,185 psig			
Fuel Rod Internal Pressure - 3,300 psig			
Average Temperature Through Clad Thickness at Hot Spot - Approximately 725 F			
Pressure Stress Only ^(b) Including 4,000 psi Thermal Stress	9,000 13,000	36,000	38,000
3. <u>EOL - Shutdown</u>			
<u>Immediately After Shutdown</u>			
System Pressure - 2,200 psig			
Fuel Rod Internal Pressure - 1,750 psig			
Average Clad Temperature - Approximately 575 F	-4,000	45,000	48,000

- (a) Cladding is being ordered with 45,000 psi minimum yield strength and 10 per cent minimum elongation, both at 650 F. Minimum room temperature strengths will be approximately 75,000 psi yield strength (0.2 per cent offset) and 85,000 psi ultimate tensile strength.
- (b) Cladding stresses due to fuel swelling are discussed further on another page of 3.2.4.2.2.

Table 3-19 (Cont'd)

<u>Operating Condition</u>	<u>Calc. Stress, psi</u>	<u>Yield Stress, psi</u>	<u>Ultimate Tensile Stress, psi</u>
<u>3 Hours Later</u>			
(50 F/hr Pressurizer Cooldown Rate)			
Fuel Rod Internal Pressure - 1,050 psig			
System Pressure - 680 psig			
Average Clad Temperature - Approx- imately 425 F	3,300	52,000	55,000

The total production of fission gas in the hottest fuel rod assembly is based on the hot rod average burnup of 38,000 MWD/MTU. The corresponding maximum burnup at the hot fuel rod midpoint is 55,000 MWD/MTU.

The fission gas release is based on temperature versus re-lease fraction experimental data.⁽⁴⁹⁾ Fuel temperatures are calculated for small radial and axial increments. The total fission gas release is calculated by integrating the incremental releases.

The maximum release and gas pressure buildups are deter-mined by evaluating the following factors for the most con-servative conditions:

- (a) Gas conductivity at the end-of-life with fission gas present.
- (b) Influence of the pellet-to-clad radial gap and contact heat transfer coefficient on fuel temperature and re-lease rate.
- (c) Unrestrained radial and axial thermal growth of the fuel pellets relative to the clad.
- (d) Hot rod local peaking factors.
- (e) Radial distribution of fission gas production in the fuel pellets.
- (f) Fuel temperatures at reactor design overpower.

The fuel temperatures used to determine fission gas release and internal gas pressure have been calculated at the reactor overpower condition. Fuel temperatures, total free gas volume, fission gas release, and internal gas pressure have been evaluated for a range of initial diametral clearances. This evaluation shows that the highest internal pressure results when the maximum diametral gap is assumed because of the resulting high average fuel temperature. The release rate increases rapidly with an increase in fuel temperature, and unrestrained axial growth reduces the relatively cold gas end plenum volumes. A conservative ideal thermal expansion model is used to calculate fuel temperatures as a function of initial cold diametral clearance. Considerably lower resistance to heat transfer between the fuel and clad is anticipated at the end-of-life due to fuel fracture, swelling, and densification. The resulting maximum fission gas release rate is 43 per cent.

(3) Collapse Margins

Short time collapse tests have demonstrated a clad collapsing pressure in excess of 4,000 psi at expansion void maximum temperature. Collapse pressure margin is approximately 1.7. Extrapolation to hot spot average clad temperature (≈ 725 F) indicates a collapse pressure of 3,500 psi and a margin of 1.4, which also greatly exceeds requirement. Outpile creep collapse tests have demonstrated that the clad meets the long time (creep collapse) requirement.

(4) Fuel Swelling

Fuel rod average and hot spot operating conditions and design parameters at 100 per cent power, pertinent to fuel swelling considerations, are listed below.

	<u>Average</u>	<u>Maximum</u>
Heat Flux, Btu/ft ² -hr	167,620	543,000
Linear Heat Rate, kw/ft	5.4	17.5
Fuel Temperature, F	1,385	4,160
Burnup (MWD/MTU) at Equilibrium	28,200	55,000
	<u>Nominal Values</u>	
Pellet OD, in.	0.362	
Pellet Density, % of Theoretical	95	
Pellet-Clad Diametral Gap at Assy., in.	0.004 - 0.008	
Clad Material	Cold-Worked Zr-4	
Clad Thickness, in.	0.026	

The capability of Zircaloy-clad UO_2 fuel in solid rod form to perform satisfactorily in PWR service has been amply demonstrated through operation of the CVTR and Shippingport cores, and through results of their supplementary development programs, up to approximately 40,000 MWD/MTU.

As outlined below, existing experimental information supports the various individual design parameters and operating conditions up to and perhaps beyond the maximum burnup of 55,000 MWL/MTU, but not in a single experiment. However, the LRD irradiation test program, currently in progress, does combine the items of concern in a single experiment, and the results are expected to be available to contribute to final design confirmation.

- (5) Application of Experimental Data to Design Adequacy of the Clad-Fuel Initial Gap to Accommodate Clad-Fuel Differential Thermal Expansion

Experimental Work

Six rabbit capsules, each containing three Zr-2 clad rods of 5 in. fuel length, were irradiated in the Westinghouse Test Reactor⁽⁴⁵⁾ at power levels up to 24 kw/ft. The 94 per cent theoretical density (T.D.) UO_2 pellets (0.430 OD) had initial clad-fuel diametral gaps of 6, 12, and 25 mils. No dimensional changes were observed. Central melting occurred at 24 kw/ft only in the rods that had the 25 mil initial gap.

Two additional capsules were tested.⁽⁵⁵⁾ The specimens were similar to those described above except for length and initial gap. Initial gaps of 2, 6, and 12 mils were used in each capsule. In the A-2 capsule, three 38-in.-long rods were irradiated to 3,450 MWD/MTU at 19 kw/ft maximum. In the A-4 capsule, four 6-in.-long rods were irradiated to 6,250 MWD/MTU at 22.2 kw/ft maximum. No central melting occurred in any rod, but diameter increases up to 3 mils in the A-2 capsule and up to 1.5 mils in the A-4 capsule were found in the rods with the 2 mil initial gap.

Application

In addition to demonstrating the adequacy of Zircaloy-clad UO_2 pellet rods to operate successfully at the power levels of interest (and without central melting), these experiments demonstrate that the design initial clad fuel gap of 4 to 8 mils is adequate to prevent unacceptable clad diameter increase due to differential thermal expansion between the clad and the fuel. A maximum local diametral increase of less than 0.001 in. is indicated for fuel rods having the minimum initial gap, operating at the maximum overpower condition.

00000229

(6) Adequacy of the Available Voids to Accommodate Differential Expansion of Clad and Fuel, Including the Effects of Fuel Swelling

Experimental Work

Zircaloy-clad, UO₂ pellet-type rods have performed successfully in the Shippingport reactor up to approximately 40,000 MWD/MTU.

Bettis Atomic Power Laboratory⁽⁵³⁾ has irradiated plate-type UO₂ fuel (96-98 per cent T.D.) up to 127,000 MWD/MTU and at fuel center temperatures between 1,300 and 3,800 F. This work indicates fuel swelling rates of 0.16% $\Delta V/10^{20}$ f/cc until fuel internal voids are filled, then 0.7% $\Delta V/10^{20}$ f/cc after internal voids are filled. This point of "breakaway" appears to be independent of temperature over the range studied and dependent on clad restraint and the void volume available for collection of fission products. The additional clad restraint and greater fuel plasticity (from higher fuel temperatures) of rod-type elements tend to reduce these swelling effects by providing greater resistance to radial swelling and lower resistance to longitudinal swelling than was present in the plate-type test specimens.

This is confirmed in part by the work of Frost, Bradbury, and Griffiths of Harwell⁽⁵⁶⁾ in which 1/4 in. diameter UO₂ pellets clad in 0.020 in. stainless steel with a 2 mil diametral gap were irradiated to 53,300 MWD/MTU at a fuel center temperature of 3,180 F without significant dimensional change.

In other testing⁽⁵⁷⁾ 0.150 in. OD, 82-96 per cent T.D. oxide pellets (20 per cent Pu, 80 per cent U) clad with 0.016 in. stainless steel with 6-8 mil diametral gaps have been irradiated to 77,000 MWD/MTU at fuel temperatures high enough to approach central melting without apparent detrimental results. Comparable results were obtained on rods swaged to 75 per cent T.D. and irradiated to 100,000 MWD/MTU.

Application

Based on the BAPL experimental data, swelling of the fuel rods is estimated as outlined below.

Fuel is assumed to swell uniformly in all directions. Clad-pellet differential thermal expansion is calculated to be about 0.004 in. at the maximum linear heat rate, so that all of the minimum initial gap of 0.004 in. is filled up by thermal expansion. If the initial gap exceeds the minimum, the additional gap volume is assumed available to accommodate swelling. This additional void volume may initially tend to be filled by pellet thermal expansion

because of the low contact pressure and resultant low contact coefficient, but as the fuel swells, the contact pressure must increase if the clad is to be stretched. Where fuel cracking tends to fill the radial gap, it is assumed that the crack voids are available to absorb swelling.

The external effect of fuel swelling is assumed to occur at $0.16\% \Delta V/10^{20}$ f/cc until the 5 per cent initial void in the 95 per cent T.D. pellets is filled at about 9×10^{20} f/cc. From that time on, swelling is assumed to take place at $0.7\% \Delta V/10^{20}$ f/cc until the maximum burnup of 13.6×10^{20} f/cc (55,000 MWD/MTU) is reached. Total fuel volume increase is 4-1/2 per cent, which results in a 1-1/2 per cent diameter increase in a rod with the 0.004 in. minimum initial gap. Clad stress is estimated at 22,000 psi, so that the elastic strain is about 0.2 per cent. Net plastic strain is 1.3 per cent. Similar calculations indicate that fuel rods with maximum burnup and the nominal clad-fuel gap (0.006 in. at assembly) will have clad plastic strains of about 0.6 per cent at the end-of-life. Based on outpile data, stress rupture should not be a problem at these strains.

Qualitative information from LSBR⁽⁵⁸⁾ suggests that swelling rates for this design may exceed those indicated by the BAPL data because of the higher fuel temperatures. However, the A.E.R.E. tests⁽⁵⁶⁾ and the General Electric tests⁽⁵⁷⁾ do not support more than a small increase in post-"break-away" swelling rates at temperatures of interest.

Fuel Swelling Studies - LRD Irradiation Program⁽⁵⁹⁾

Dimensional stability of UO_2 under inpile conditions simulating large reactor environments is under investigation. This study is currently being carried out under USAEC Contract AT(30-1)-3269, "Large Closed-Cycle Water Reactor Research and Development Program".

Parameters contributing to swelling are burnup, heat rating, fuel density and grain size, and clad restraint. These are systematically being studied by irradiating a series of capsules containing fuel rods. These experiments were assigned by the AEC to ETR/MTR. Test variables are shown in Table 3-20.

00000231

Table 3-20
LRD Fuel Swelling Irradiation Program

Capsule ^(a) <u>WAPD-49</u>	Enrichment, <u>%</u>	Initial Goal Heat Rating ^(b)		Fuel Density, <u>% T.D.</u>	Burnup, <u>MWD/MIU</u>
		<u>kw/</u> <u>ft</u>	<u>watts/</u> <u>cm</u>		
A	18.7	12	394	94 and 97	38,000
B	18.7	12	394	94 and 97	38,000
C	18.7	12	394	90, 94, and 97	38,000
D	16.0	18	591	90 and 97	47,000
E	13.5	18	591	94 and 97	47,000
F	13.5	18	591	90, 94, and 97	47,000
G	16.0	18	591	90 and 97	47,000
H	17.0	24	788	94 and 97	56,000
I	18.7	24	788	94 and 97	56,000
J	20.0	24	788	94 and 97	56,000
K	20.0	24	788	90 and 94	56,000
L	20.0	24	788	94 and 97	56,000

(a) Four rods/capsule.

(b) Fuel center temperatures vary from 1,570 to 4,110 F.

00000232

Effect of Zircaloy Creep

The effect of Zircaloy creep on the amount of fuel rod growth due to fuel swelling has been investigated. Clad creep has the effect of producing a nearly constant total pressure on the clad ID by permitting the clad diameter to increase as the fuel diameter increases. Based on out-of-pile data, ⁽⁶⁰⁾ 1 per cent creep will result in 10,000 hr (corresponding approximately to the end-of-life diametral swelling rate) from a stress of about 22,000 psi at the ≈ 720 F average temperature through the clad at the hot spot. At the start of this high swelling period (roughly the last 1/3 of the core life), the reactor coolant system pressure would more or less be balanced by the rod internal pressure, so the total pressure to produce the clad stress of 22,000 psi would have to come from the fuel. Contact pressure would be 2,400 psi. At the end-of-life, the rod internal pressure exceeds the system pressure by about 1,100 psi, so the clad-fuel contact pressure would drop to 1,300 psi. Assuming that irradiation produces a 3:1 increase in creep rates, the clad stress for 1 per cent strain in 10,000 hr would drop to about 15,000 psi. Contact pressures would be 1,800 psi at the beginning of the high swelling period, 700 psi at the end-of-life. Since the contact pressure was assumed to be 825 psi in calculating the contact coefficient used to determine the fuel pellet thermal expansion, there is only a short period at the very end-of-life (assuming the 3:1 increase in creep rates due to irradiation) when the pellet is slightly hotter than calculated. The effect of this would be a slight increase in pellet thermal expansion and therefore in clad strain. Considering the improbability that irradiation will actually increase creep rates by 3:1, no change is anticipated.

b. Overall Assembly

(1) Assurance of Control Rod Assembly Free Motion

The 0.058 in. diametral clearance between the control rod guide tube and the control rod is provided to cool the control rod and to insure adequate freedom to insert the control rod. As indicated below, studies have shown that fuel rods will not bow sufficiently to touch the guide tube. Thus, the guide tube will not undergo deformation caused by fuel rod bowing effects. Initial lack of straightness of fuel rod and guide tube, plus other adverse tolerance conditions, conceivably could reduce the 0.083 in. nominal gap between fuel rod and guide tube to a minimum of about 0.045 in., including amplification of bowing due to axial friction loads from the spacer grids. The maximum expected flux gradient of 1.176 across a fuel rod will produce a temperature difference of 12 F, which will result in a thermal bow of less than 0.002 in. Under these conditions,

00000233

for the fuel rod to touch the guide tube, the thermal gradient across the fuel rod diameter would have to be on the order of 300 F.

The effect of a DNB occurring on the side of a fuel rod adjacent to a guide tube would result in a large temperature difference. In this case, however, investigation has shown that the clad temperature would be so high that insufficient strength would be available to generate a force of sufficient magnitude to cause a significant deflection of the guide tube. In addition, the guide tube would experience an opposing gradient that would resist fuel rod bowing, and its internal cooling would maintain temperatures much lower than those in the fuel rod cladding, thus retaining the guide tube strength.

(2) Vibration

The semiempirical expression developed by Burgreen⁽⁶¹⁾ was used to calculate the flow-induced vibratory amplitudes for the fuel assembly and fuel rod. The calculated amplitude is 0.010 in. for the fuel assembly and less than 0.005 in. for the fuel rod. The fuel rod vibratory amplitude correlates with the measured amplitude obtained from a test on a 3 x 3 fuel rod assembly. In order to substantiate what is believed to be a conservatively calculated amplitude for the fuel assembly, a direct measurement will be obtained for a full-size prototype fuel assembly during testing of the assembly in the Control Rod Drive Line Facility (CRDL) at the B&W Research Center, Alliance, Ohio.

(3) Demonstration

In addition to the specific items discussed above, the overall mechanical performance of the fuel assembly and its individual components is being demonstrated in an extensive experimental program in the CRDL.

3.2.4.3 Control Rod Drive System

3.2.4.3.1 Description

The control rod drive system includes drive mechanisms which actuate control rod assemblies and axial power shaping rod assemblies, drive controls, power supplies, position indication, operating panels and indicators, safety devices, enclosures, housings, and mountings. Criteria applicable to drive mechanisms for both control rod assemblies and axial power shaping rod assemblies are given in 3.2.4.3.1.1. Additional requirements for the mechanisms which actuate only control rod assemblies are given in 3.2.4.3.1.2.

3.2.4.3.1.1 General Design Criteria

a. Single Failure

No single failure shall inhibit the protective action of the control rod drive system. The effect of a single failure shall be limited to one control rod drive.

00000234

b. Uncontrolled Withdrawal

No single failure or chain of failures shall cause uncontrolled withdrawal of any control rod assembly (CRA).

c. Equipment Removal

The disconnection of plug-in connectors, modules, and subassemblies from the protective circuits shall be annunciated or shall cause a reactor trip.

d. Position Indication

Continuous position indication, as well as an upper and lower position limit indication, shall be provided for each control rod drive. The accuracy of the position indicators shall be consistent with the tolerance set by reactor safety analysis.

e. System Monitoring

The control rod drive control system shall include provisions for monitoring conditions that are important to safety and reliability. These include rod position deviation and power supply voltage.

f. Drive Speed

The control rod drive control system shall provide for single uniform speed of the mechanism. The drive controls, or mechanism and motor combination, shall have an inherent speed limiting feature. The speed of the mechanism shall be 30 in./min for both insertion and withdrawal. The withdrawal speed shall be limited so as not to exceed 25 per cent overspeed in the event of speed control fault.

g. Mechanical Stops

Each control rod drive shall have positive mechanical stops at both ends of the stroke or travel. The stops shall be capable of receiving the full operating force of the mechanisms without failure.

3.2.4.3.1.2 Additional Design Criteria

The following criteria are applicable only to the mechanisms which actuate control rod assemblies.

a. CRA Positioning

The control rod drives shall provide for controlled withdrawal or insertion of the control rod assemblies (CRA) out of, or into, the reactor core to establish and hold the power level required. The drives are also capable of rapid insertion or trip for emergency reactor conditions.

b. CRA Trip

The trip command shall have priority over all other commands. Trip action shall be positive and nonreversible. Trip circuitry shall provide the final protective action and shall be direct-acting, incur minimum delay, and shall not require external power. Circuit interrupting devices shall not prevent reactor trip. Fuses, where used, shall be provided with blown indicators. Circuit breaker position information shall also be indicated.

c. Group Withdrawal

The control rod drive system allows only two out of three regulating CRA groups to withdraw at any time subject to the conditions described in 7.2.2.1.2.

3.2.4.3.2 Control Rod Drive Mechanisms

The control rod drive mechanisms provide for controlled withdrawal or insertion of the control rod assemblies out of or into the core and are capable of rapid insertion or trip. The drive mechanisms are hermetically sealed, reluctance motor-driven screw units. The CRDM data is listed in Table 3-21.

Table 3-21
Control Rod Drive Mechanism Design Data

<u>Mechanism Function</u>	<u>Shim Safety</u>	<u>Axial Power Shaping</u>
Type	Roller Nut Drive	Roller Nut Drive
Quantity	61	8
Location	Top-mounted	Top-mounted
Direction of Trip	Down	Does not trip
Velocity of Normal Withdrawal and Insertion, in./min.	30	30
Maximum Travel Time for Trip		
2/3 Insertion, s	1.40	Drive has no trip function
Length of Stroke, in.	139	139
Design Pressure, psig	2,500	2,500
Design Temperature, F	650	650
Weight of Mechanism (App.)	940 lb	940 lb

The drive mechanism consists of a motor tube which houses a lead screw and its rotor assembly and a buffer. The end of the motor tube is closed by a cap and vent assembly. A motor stator is placed down over the motor tube pressure vessel, and position indication switches are arranged outside the motor tube extension.

The control rod drive output element is a translating screw shaft which is coupled to the control rod. The screw is driven by an anti-friction nut element which is rotated magnetically by a motor stator located outside the pressure boundary. Current impressed on the stator causes the separable nut halves to engage; a mechanical spring causes them to disengage the screw in the absence of a current. For rapid insertion, the nut separates to release the screw shaft which then falls into the core by gravity. A hydraulic buffer within the upper housing decelerates the falling assembly to a low speed a short distance above its full-in position. The final deceleration is accommodated by the down-stop buffer spring.

This mechanism incorporates proven principles and material combinations and is based on extensive analytical, developmental, design, test, and manufacturing experience obtained over the years for the Shippingport and the Naval Nuclear Program.

The control rod drive is shown in Figures 3-64 and 3-65. Subassemblies of the control rod drive are described as follows:

a. Motor Tube

The motor tube is a three-piece welded assembly designed and manufactured in accordance with the requirements of the ASME Code, Section III, for Class A nuclear pressure vessel. Materials conform to ASTM or ASME, Section II, Material Specifications. All welding shall be performed by personnel qualified under ASME Code, Section IX, Welding Qualifications. The motor tube wall between the rotor assembly and the stator is constructed of magnetic material to present a small air gap to the motor. This region of the motor tube is of low alloy steel clad on the inside diameter with stainless steel or with Inconel. The upper end of the motor tube functions only as a pressurized enclosure for the withdrawn lead screw and is made of stainless steel transition-welded to the upper end of the low alloy steel motor section. The lower end of the low alloy steel tube section is welded to a stainless steel machined forging which is flanged at the face which contacts the vessel control rod nozzle. Double gaskets, which are separated by a ported test annulus, seal the flanged connection between the motor tube and the reactor vessel.

b. Motor

The motor is a synchronous reluctance unit with a slip-on stator. The rotor assembly is described in Paragraph (f). The stator is a 48-slot four-pole arrangement with water cooling coils wound on the outside of its casing. The stator is encapsulated after winding to establish a hermetically sealed unit. It is six phase star-connected for operation in a pulse-stepping mode and advances 15 mechanical degrees per step. The stator assembly is mounted over the motor tube housing as shown in Figure 3-65.

00000237

c. Cap and Vent Valve

The upper end of the motor tube is closed by a cap containing a vapor bleed port and vent valve. The bleed port and vent valve and the cap-to-motor tube closures have double seals. The cap is retained by a bolting ring threaded to the outside of the motor tube. The retaining bolts are made long so as to be elastic enough to provide positive seal preload at any assembly temperature from 20 to 650 F. The minimum preload is equal to the 3750 psig proof pressure force.

d. Actuator

The actuator consists of the translating lead screw, its rotating nut assembly, and the torque taker assembly on the screw. The actuator lead screw travel is 139 inches.

e. Lead Screw

The lead screw has a lead of 0.750 in. The thread is double lead with a single pitch spacing of 0.375 in. Thread lead error is held to 0.0005 in. maximum in any 6 in. for uniform loading with the roller nut assemblies. The thread form is a modified ASME with a flank angle that allows the roller nut to disengage without lifting the screw.

f. Rotor Assembly

The rotor assembly consists of a ball bearing supported rotor tube carrying and limiting the travel of a pair of scissors arms. Each of the two arms carry a pair of ball bearing supported roller (nut) assemblies which are skewed at the lead screw helix angle for engagement with the lead screw. The current in the motor stator (two of a six winding stator) causes the arms that are pivoted in the rotor tube to move radially toward the motor tube wall to the limit provided thereby engaging the four roller nuts with the centrally located lead screw. Also, four separating springs mounted in the scissor arms keep the rollers disengaged when the power is removed from the stator coils. A second radial bearing mounted to the upper end of the rotor tube has its outer race pinned to both scissor arms thereby synchronizing their motion during engagement and disengagement. When a three phase rotating magnetic field is applied to the motor stator, the resulting force produces rotor assembly rotation.

g. Torque Extension Tube and Torque Taker

The torque extension tube is a separate tubular assembly containing a keyway that extends the full length of the lead screw travel. The tube assembly is supported against rotation and in elevation by the upper end of the motor tube extension. The lower end of the tube assembly supports the buffer and is the down stop. A set of indexing serrations mate to prevent rotation and orient the torque extension tube with the motor tube below the cap and vent valve assembly. An integral shoulder at the top of the tube rests against a step in the motor tube inside diameter to provide a vertical support.

The torque taker assembly consists of the position indicator permanent magnet, the buffer piston, and a positioning key. The torque taker key fixed at the top of the lead screw is mated with the torque extension tube keyway to provide both radial and tangential positioning of the lead screw.

h. Buffer

The buffer assembly is capable of decelerating the translating mass from the unpressurized terminal velocity to zero velocity without applying greater than ten times the gravitational force on the control rod. The water buffer consists of a piston fixed to the top end of the screw shaft and a cylinder which is fixed to the lower end of the torque extension tube. Twelve inches above the bottom stop, the piston at the top of the screw enters the cylinder. Guiding is accomplished because the piston and torque key are in a single part, and the cylinder and keyway are in a single mating part. As the piston travels into the cylinder, water is driven into the center of the lead screw through holes in the upper section which produce the damping pressure drop. The number of holes presented to the buffer chamber is reduced as the rod moves into the core, so that the damping coefficient increases as the velocity reduces, thereby providing an approximately uniform deceleration. A large helical buffer spring is used to take the kinetic energy of the drive line at the end of the water buffer stroke. The buffer spring accepts a five-foot per second impact velocity of the drive line and control rod with an instantaneous overtravel of one inch past the normal down stop. The inclusion of this buffer spring permits practical clearances in the water buffer.

i. Lead Screw Guide

The lead screw guide bushing acts as a primary thermal barrier and as a guide for the screw shaft. As a primary thermal barrier, the bushing allows only a small path for free convection of water between the mechanism and the closure head nozzle. Fluid temperature in the mechanism is largely governed by the flow of water up and down through this bushing. The diametral clearance between screw shaft and bushing is large enough to preclude jamming the screw shaft and small enough to hold the free convection to an acceptable value. In order to obtain trip travel times of acceptably small values, it is necessary to provide an auxiliary flow path around the guide bushing. The larger area path is necessary to reduce the pressure differential required to drive water into the mechanism to equal the screw displacement. The auxiliary flow paths are closed for small pressure differentials (several inches of water) by ball check valves which prevent the convection flow but open fully during trip.

00000239

j. Position Indications

Two methods of position indication are provided; one, an absolute position indicator and the other, a relative position indicator. The absolute position transducer consists of a series of magnetically operated reed switches mounted in a tube parallel to the motor tube extension. Each switch is hermetically sealed. Switch contacts close when a permanent magnet mounted on the upper end of the lead screw extension comes in close proximity. As the lead screw (and the control rod assembly) moves, switches operate sequentially producing an analogue voltage proportional to position. The accuracy of the analogue signal is ± 1.4 per cent and produces a readout of approximately ± 2.5 per cent accuracy. Additional reed switches are included in the same tube with the absolute position transducer to provide full withdrawal and insertion signals. The relative position indicator consists of a small pulse-stepping motor driving a potentiometer that generates a signal accuracy of $\pm 0.7\%$ producing a position readout of $\pm 1.7\%$ accuracy.

k. Motor Tube Design Criteria

The motor tube design complies with Section III of the ASME Boiler and Pressure Vessel Code for a Class A vessel. The operating transient cycles, which are considered for the stress analysis of the reactor pressure vessel, are also considered in the motor tube design.

Quality standards relative to material selection, fabrication, and inspection are specified to insure safety function of the housings essential to accident prevention. Materials conform to ASTM or ASME, Section II, Material Specifications. All welding shall be performed by personnel qualified under ASME Code, Section IX, Welding Qualifications. These design and fabrication procedures establish quality assurance of the assemblies to contain the reactor coolant safely at operating temperature and pressure.

In the highly unlikely event that a pressure barrier component or the control rod drive assembly does fail catastrophically, i.e., ruptured completely, the following results would ensue:

1. Control Rod Drive Nozzle

The assembly would be ejected upward as a missile until it was stopped by the missile shield over the reactor. This upward motion would have no adverse effect on adjacent assemblies.

2. Motor Tube

The failure of this component anywhere above the lower flange would result in a missile-like ejection into the missile shielding over the reactor. This upward motion would have no adverse effect on adjacent mechanisms.

3.2.4.3.2.2 Axial Power Shaping Rod Drive

For actuating the partial length control rods which maintain their set position during a reactor-trip of the shim safety drive, the CRDM is modified so that the roller nut assembly will not disengage from the lead screw on a loss of power to the stator. Except for this modification, the shim drives and the axial power shaping rod drives are identical.

(D E L E T E D)

00000241

Paragraph deleted.

7

3.2.4.3.3 Control Rod Drive System Evaluation

a. Design Criteria

The system will be designed, tested, and analyzed for compliance with the design criteria. A preliminary safety analysis of the control rod drive motor control subsystem was conducted to determine failures of logic functions. It was concluded that no single failure in any CRA control would prevent CRA insertion, nor cause inadvertent CRA withdrawal of another CRA or CRA group.

b. Materials Selection

Materials are selected to be compatible with, and operate in, the reactor coolant. Certified mill test reports containing chemical analysis and test data of all materials exposed to the reactor system fluid shall be provided and maintained for the control rod drives. Certificates of compliance for other materials and components shall also be provided.

c. Relation to Design Temperature

All parts of the control rod drive exposed to reactor coolant are designed to operate at 650 F, although it is expected that all parts will operate considerably cooler. Some tests have been completed, and additional tests are planned, to closely determine the operating temperature gradients throughout the drive mechanism during all phases of operation. These tests will also provide an indication of the amount of convection that takes place within the water space of the mechanism.

d. Design Life

The design life of the control rod drive control system is as follows:

00000242

- (1) Structural portions, such as flanges and pressure housings - 40 years.
- (2) Moving parts, such as lead screw and roller nuts - 20 years.
- (3) Electronic control circuitry - 20 years.

3.2.4.3.4 Control Rod Assembly (CRA)

Each control rod assembly is made up of 16 control rods which are coupled to a single Type 304 stainless steel spider (Figure 3-69). Each control rod consists of an absorber section of silver-indium-cadmium poison clad with cold-worked, Type 304 stainless steel tubing and Type 304 stainless steel upper and lower end pieces. The end pieces are welded to the clad to form a water and pressure-tight container for the poison. The control rods are loosely coupled to the spider to permit maximum conformity with the channels provided by the guide tubes. The CRA is inserted through the upper end fitting of the fuel assembly, each control rod being guided by an incore guide tube. Guide tubes are also provided in the upper plenum assembly above the core so that full length guidance of the control rods is provided throughout the stroke. With the reactor assembled, the CRA cannot be withdrawn far enough to cause disengagement of the control rods from the incore guide tubes. Pertinent design data are shown in Table 3-22.

Table 3-22
Control Rod Assembly Design Data

<u>Item</u>	<u>Data</u>
Number of CRA	61
Number of Control Rods per Assembly	16
Outside Diameter of Control Rod, in.	0.440
Cladding Thickness, in.	0.020
Cladding Material	Type 304 SS, Cold-Worked
End Plug Material	Type 304 SS, Annealed
Spider Material	SS Grade CF3M
Poison Material	80% Ag, 15% In, 5% Cd
Female Coupling Material	Type 304 SS, Annealed
Length of Poison Section in.	134
Stroke of Control Rod, in.	139

This type of CRA has been developed under the USAEC Large Reactor Development Program and offers the following significant advantages:

- a. More uniform distribution of absorber throughout the core volume.
- b. Shorter reactor vessel and shorter internals owing to elimination of control rod followers.
- c. Lower reactor building requirements owing to reduction of reactor coolant inventory.
- d. Better core power distribution for a given CRA worth.

3.2.4.3.5 Axial Power Shaping Rod Assembly (APSRA)

Each axial power shaping rod assembly (Figure 3-70) has 16 axial power shaping rods, a stainless steel spider, and a female coupling. The 16 rods are attached to the spider by means of a nut threaded to the upper shank of each rod. After assembly all nuts are lock welded. The axial power shaping rod drive is coupled to the APSRA by a bayonet connection. The female couplings of the APSRA and CRA have slight dimensional differences to ensure that each type of rod can only be coupled to the correct type of drive mechanism.

When the APSRA is inserted into the fuel assembly it is guided by the guide tubes of the fuel assembly. Full length guidance of the APSRA is provided by the control rod guide tube of the upper plenum assembly. At the full out position of the control rod drive stroke, the lower end of the APSRA remains within the fuel assembly guide tube to maintain the continuity of guidance throughout the rod travel length. The APSRA's are designed to permit maximum conformity with the fuel assembly guide tube throughout travel.

Each axial power shaping rod has a section of neutron absorber material. This absorber material is an alloy of silver-indium-cadmium and is clad in cold-worked, stainless steel tubing with stainless steel upper and lower end pieces. The end pieces are welded to the clad to form a water and pressure-tight container for the absorber material. The tubing provides the structural strength of the axial power shaping rods and prevents corrosion of the absorber material. Above the section containing the absorber material is a tubular follower made of cold-worked Zircaloy-4 tubing, with Zircaloy-4 upper and lower end pieces. The end pieces are welded to the tubing and are vented to permit the coolant-moderator to fill the follower. The follower and absorber sections are fitted together, pinned, and lock welded to form a complete axial power shaping rod. Pertinent data on the APSRA is shown in Table 3-23.

Table 3-23
Axial Power Shaping Rod Assembly Data

<u>Item</u>	<u>Data</u>
Number of Axial Power Shaping Rod Assemblies	8
Number of Axial Power Shaping Rods per Assembly	16
Outside Diameter of Axial Power Shaping Rod, in.	0.440
Cladding Thickness, in.	0.021
Cladding Material	Type 304 SS, cold-worked
Clad End Plug Material	Type 304 SS, annealed
Follower Tube Material	Zircaloy-4, cold-worked
Follower End Plug Material	Zircaloy-4, annealed
Absorber Section to Follower Pin Material	Type 304 SS, annealed
Poison Material	80% Ag, 15% In, 5% Cd
Spider Material	SS, Grade CF3M
Female Coupling Material	Type 304 SS, Annealed
Length of Poison Section in.	36
Stroke of Control Rod, in.	139

00000244

These axial power shaping rods are designed to withstand all operating loads including those resulting from hydraulic forces and thermal gradients. The ability of the axial power shaping rod clad to resist collapse due to the system pressure has been demonstrated by an extensive collapse test program on Zircaloy-4 tubing. Internal pressure is not generated within the clad since the Ag-In-Cd alloy does not yield gaseous products under irradiation. Swelling of the absorber material is negligible, and will not cause unacceptable clad strain.

Mechanical interference between axial power shaping rods and the fuel assembly guide tubes can be tolerated, since the mechanical interference between axial power shaping rods and the fuel assembly guide tubes must be expected. The parts involved are flexible and result in very small friction drag loads. Thermal distortions of the rods are small because of the low heat generation and adequate cooling. Consequently, the APSRA's will not encounter significant frictional resistance to their motion in the guide tubes.

00000245

3.3 TESTS AND INSPECTIONS

3.3.1 NUCLEAR TESTS AND INSPECTION

3.3.1.1 Critical Experiments

An experimental program⁽⁶⁵⁻⁶⁷⁾ to verify the relative reactivity worth of the CRA has recently been completed. Detailed testing established the worth of the CRA under various conditions similar to those for the reference core. These parameters include control rod arrangement in a CRA, fuel enrichments, fuel element geometry, CRA materials, and soluble boron concentration in the moderator.

Gross and local power peaking were also studied, and three-dimensional power-peaking data were taken as a function of CRA insertion. Detailed peaking data were also taken between fuel assemblies and around the water holes left by withdrawn CRA's. The experimental data are being analyzed and will become part of the experimental bench mark for the analytical models used in the design.

3.3.1.2 Zero Power, Approach to Power, and Power Testing

Boron worth and CRA worth (including stuck-CRA worth) will be determined by physics tests at the beginning of each core cycle. Recalibration of boron worth and CRA worth is expected to be performed at least once during each core cycle. Calculated values of boron worth and CRA worth will be adjusted to the test values as necessary. The boron worth and CRA worth at a given time in core life will be based on CRA position indication and calculated data as adjusted by experimental data.

The reactor coolant will be analyzed in the laboratory periodically to determine the boron concentration, and the reactivity held in boron will then be calculated from the concentration and the reactivity worth of boron.

The method of maintaining the hot shutdown margin (hence stuck-CRA margin) is related to operational characteristics (load patterns) and to the power-peaking restrictions on CRA patterns at power. The CRA pattern restrictions will insure that sufficient reactivity is always fully withdrawn to provide adequate shutdown with the stuck-CRA margin. Power peaking as related to CRA patterns and shutdown margin will be monitored by reactivity calculations, and interlocks will be provided to prevent CRA patterns that produce excessive power peaking and/or reduction of shutdown margin.

Operation under all power conditions will be monitored by incore instrumentation, and the resulting data will be analyzed and compared with multidimensional calculations in a continuing effort to provide sufficient support for further power escalations.

3.3.2 THERMAL AND HYDRAULIC TESTS AND INSPECTION

3.3.2.1 Reactor Vessel Flow Distribution and Pressure Drop Test

A 1/6-scale model of the reactor vessel and internals will be tested to measure

00000246

- a. The flow distribution to each fuel assembly of the reactor core and to develop, if necessary, devices required to produce the desired flow distribution.
- b. Fluid mixing between the vessel inlet nozzle and the core inlet, and between the inlet and outlet of the core.
- c. The overall pressure drop between the vessel inlet and outlet nozzles, and the pressure drop between various points in the reactor vessel flow circuit.

The reactor vessel, thermal shield, flow baffle, core barrel, and upper plenum assembly are made of clear plastic to allow use of visual flow study techniques. All parts of the model except the core are geometrically similar to those in the prototype reactor. However, the simulated core was designed to maintain dynamic similarity between the model and prototype.

Each of the 177 simulated fuel assemblies contains a calibrated flow nozzle at its inlet and outlet. The test loop is capable of supplying cold water (80 F) to three inlet nozzles and hot water (180 F) to the fourth. Temperature will be measured in the inlet and outlet nozzles of the reactor model and at the inlet and outlet of each of the fuel assemblies. Static pressure taps will be located at suitable points along the flow path through the vessel. This instrumentation will provide the data necessary to accomplish the objectives set forth for the tests.

3.3.2.2 Fuel Assembly Heat Transfer and Fluid Flow Tests

B&W is conducting a continuous research and development program for fuel assembly heat transfer and fluid flow applicable to the design of the reference reactor. Single-channel tubular and annular test sections and multiple rod assemblies have been tested at the B&W Research Center.

The reactor thermal design is based upon burnout heat transfer experiments with (a) multiple rod, heated assemblies with uniform heat flux, and (b) single rod, annular heaters with nonuniform axial heat flux, at design conditions of pressure and mass velocity. These experiments are being extended to test nonuniform multiple rod heater assemblies as described in 1.5.4. The results of these tests will be applied to the final thermal design of the reactor and the specification of operating limits.

3.3.2.2.1 Single-Channel Heat Transfer Tests

A large quantity of uniform flux, single-channel, critical heat flux data has been obtained. References to uniform flux data are given in BAW-168 and 3.2.3.2.3 of this report. The effect on the critical heat flux caused by nonuniform axial power generation in a tubular test section at 2,000 psi pressure was investigated as early as 1961.⁽²⁹⁾ This program was extended to include pressures of 1,000, 1,500, and 2,000 psi and mass velocities up to 2.5×10^6 lb/hr-ft².⁽⁶³⁾ The effect on the critical heat flux caused by differences in the radial and axial power distribution in an annular test section was recently investigated at reactor design conditions.⁽⁶⁴⁾ Data were obtained at pressures of 1,000, 1,500, 2,000, and 2,200 psi and at mass velocities up to 2.5×10^6 lb/hr-ft².

The tubular tests included the following axial heat flux shapes where P/\bar{P} is local to average power:

- a. Uniform Heat Flux $(P/\bar{P}) = 1.000$ constant
- b. Sine Heat Flux $(\Gamma/\bar{P})_{\max} = 1.396$ @ 50% L

00000247

c. Inlet Peak Heat Flux $(P/\bar{P})_{\max} = 1.930 @ 25\% L$

d. Outlet Peak Heat Flux $(P/\bar{P})_{\max} = 1.930 @ 75\% L$

Tests of two additional, nonuniform, 72-in. heated length, tubular tests were undertaken to obtain data for peaking conditions more closely related to the reference design. The additional flux shapes being tested are

a. Inlet Peak Heat Flux $(P/\bar{P})_{\max} = 1.65 @ 28\% L$

b. Outlet Peak Heat Flux $(P/\bar{P})_{\max} = 1.65 @ 72\% L$

These tests, still in progress, will cover approximately the same range of pressure, mass flow, and ΔT as the multiple rod fuel assembly tests.

3.3.2.2.2 Multiple Rod Fuel Assembly Heat Transfer Tests

Critical heat flux data are being obtained from 6-ft-long, 9-rod fuel assemblies in a 3 x 3 square array. A total of 513 data points were obtained covering the following conditions:

$$0 \leq T_S \leq 250$$

$$1,000 \leq P \leq 2,400$$

$$0.2 \times 10^6 \leq G \leq 3.5 \times 10^6$$

where

ΔT_S = inlet subcooling, F

P = pressure, psia

G = mass velocity, lb/hr-ft²

The geometry of this section consisted of nine rods of 0.420 in. diameter on a 0.558 in. square pitch. Analysis of the last data of this set is in process.

3.3.2.2.3 Fuel Assembly Flow Distribution and Pressure Drop Tests

Flow visualization and pressure drop data have been obtained from a 10-times-full-scale model of a single rod in a square flow channel. These data have been used to refine the spacer ferrule designs with respect to mixing turbulence and pressure drop.

Flow distribution in a square 4-rod test assembly has been measured. A salt solution injection technique was used to determine the average flow rates in the simulated reactor assembly corner cells, wall cells, and unit cells. Interchannel mixing was obtained for the same assembly. These data have been used to confirm the flow distribution and mixing relationships employed in the core thermal and hydraulic design. Additional mixing, flow distribution, and

00000248

pressure drop data will be obtained to improve the core power capability. The following fuel assembly geometries will be tested to provide additional data:

- a. A 3 x 3 array identical to that for which critical heat flux data have been obtained to provide additional interchannel mixing data.
- b. A 4 x 6 array divided in half by a perforated plate simulating adjacent fuel assemblies to provide data on mixing between assemblies.
- c. A full scale 15 x 15 rod fuel assembly to provide additional flow distribution, mixing, and pressure drop information applicable to a complete assembly.

1

(DELETED)

3.3.3 FUEL ASSEMBLY, CONTROL ROD ASSEMBLY, AND CONTROL ROD DRIVE MECHANICAL TESTS AND INSPECTION

To demonstrate the mechanical adequacy and safety of the fuel assembly, control rod assembly (CRA), and control rod drive, a number of functional tests have been performed, are in progress, or are in the final stages of preparation.

3.3.3.1 Prototype Testing

A full scale prototype fuel assembly, CRA, and control rod drive is presently being tested in the Control Rod Drive Line (CRDL) Facility located at the B&W Research Center, Alliance, Ohio. This full-size loop is capable of simulating reactor environmental conditions of pressure, temperature, and coolant flow. To verify the mechanical design, operating compatibility, and characteristics of the entire control rod drive fuel assembly system, the drive will be stroked and tripped in excess of expected operating life requirements. A portion of the testing will be performed with maximum misalignment conditions. Equipment is available to record and verify data such as fuel assembly pressure drop, vibration characteristics, hydraulic forces, etc., and to demonstrate control rod drive operation and verify scram times. All prototype components will be examined periodically for signs of material fretting, wear, and vibration/fatigue to insure that the mechanical design of the equipment meets reactor operating requirements. Preliminary test results are given in 3.2.4.3.5.

After the prototype fuel assembly has been tested under simulated reactor operating conditions, it will be installed in the full-size, low pressure loop to verify specific fuel assembly design data. These data include pressure drop, coolant interchannel mixing, and coolant velocity profiles.

3.3.3.2 Model Testing

Many functional improvements have been incorporated in the design of the prototype fuel assembly as a result of model tests run to date. For example, the

spacer grid to fuel rod contact area was fabricated to 10 times reactor size and tested in a loop simulating coolant flow Reynolds numbers of interest. Thus, visually, the shape of the fuel rod support areas was optimized with respect to minimizing the severity of flow vortices. Also, a 9-rod (3 x 3) actual size model was fabricated (using production fuel assembly materials) and tested at 640 F, 2,200 psi, and 13 fps coolant flow. Principal objectives of this test were to evaluate fuel rod cladding to spacer grid contact wear, and/or fretting corrosion resulting from flow-induced vibration. A wide range of contact loads (including small clearances) was present in this specimen. No significant wear or other flow-induced damage was observed after 210 days of loop operation.

3.3.3.3 Component and/or Material Testing

3.3.3.3.1 Fuel Rod Cladding

Extensive short time collapse testing was performed on Zircaloy-4 tube specimens as part of the B&W overall creep-collapse testing program. Initial test specimens were 0.436 in. OD with wall thicknesses of 0.020 in., 0.024 in., and 0.028 in. Ten 8-in.-long specimens of each thickness were individually tested at 680 F at slowly increasing pressure until collapse occurred. Collapse pressures for the 0.020 in. wall thickness specimens ranged from 1,800 to 2,200 psig, the 0.024 in. specimens ranged from 2,800 to 3,200 psig, and the 0.028 in. specimens ranged from 4,500 to 4,900 psig. The material yield strength of these specimens ranged from 65,000 to 72,000 psi at room temperature, and was 35,800 psi at 680 F.

Additional Zircaloy-4 short time collapse specimens were prepared with a material yield stress of 78,000 psi at room temperature and 48,500 psi at 615 F. Fifteen specimens having an OD of 0.410 in. and an ID of 0.365 in. (0.0225 in. nominal wall thickness) were tested at 615 F at increasing pressure until collapse occurred. Collapse pressures ranged from 4,470 to 4,960 psig.

Creep-collapse testing was performed on the 0.436 in. OD specimens. Twelve specimens of 0.024 in. wall thickness and 30 specimens of 0.028 in. wall thickness were tested in a single autoclave at 680 F and 2,050 psig. During this test, two 0.024 in. wall thickness specimens collapsed during the first 30 days and two collapsed between 30 and 60 days. None of the 0.028 in. wall thickness specimens had collapsed after 60 days. Creep-collapse testing was then performed on thirty 0.410 in. OD by 0.365 in. ID (0.0225 in. nominal wall) specimens for 60 days at 615 F and 2,140 psig. None of these specimens collapsed, and there were no significant increases in ovality after 60 days.

Results of the 60-day, creep-collapse testing on the 0.410 in. OD specimens showed no indication of incipient collapse. The 60-day period for creep-collapse testing is used since it exceeds the point of primary creep of the material, yet is sufficiently long to enter the stage when fuel rod pressure begins to build up during reactor operation, i.e., past the point of maximum differential pressure that the clad would be subjected to in the reactor.

In order to help optimize the final clad thickness, additional clad-collapse testing is scheduled for 1967 using specimens fabricated to the reference design fuel clad dimensions, material specifications, and operating conditions.

00000250

3.3.3.3.2 Fuel Assembly Structural Components

The mechanical design of the prototype can panel assembly is the result of an extensive can panel design and structural evaluation program. The full-size, simulated loop, functional testing noted in 3.3.3.1 is expected to verify can panel design criteria. Prototype static and dynamic load testing is underway to verify can panel structural adequacy for vibration, handling, operation, and seismic loads.

In the mechanical design of the spacer grids, particular attention is given to the ferrule-to-fuel-rod contact points. Sufficient load must be applied to position the fuel rods and to minimize fuel rod vibration, yet allow axial thermal differential expansion, and not produce fretting wear in the fuel rod cladding. Static load and functional testing of the prototype grids will demonstrate their adequacy to perform within the design requirements.

3.3.3.4 Control Rod Drive Tests and Inspection

3.3.3.4.1 Control Rod Drive Developmental Tests

The prototype roller nut drive is under test at the B&W Research Center, Alliance, Ohio.

Wear characteristics of critical components have indicated that material compatibility and structural design of these components will be adequate for the life of the mechanism.

The development program has been completed and the complete prototype control rod drive is being subjected to environmental testing under simulated reactor conditions (except radiation) in the Control Rod Drive Line (CRDL) Facility at Alliance. Environmental tests include:

Operational Tests

Operating speeds.

Temperature profiles.

Trip times for full and partially withdrawn control rod assemblies (CRA) for various flow-induced pressure drops across the CRA.

Life Tests

(With internals assembled to maximum misalignment permitted by drawing dimensions and tolerances.)

<u>No. of Partial Stroke Cycles</u>	<u>Stroke Length, in.</u>	<u>Span of Control Rod Stroke From "Full-In" Position, in.</u>
1,550	83	From 56 to 139
5,400	50	71 121
8,500	25	114 139
8,500	13	126 139
<u>No. of Trip Cycles</u>		
500	139	From 0 to 139

00000251

Misalignment Tests

100 full strokes and 100 full stroke trips with internal tolerances altered to 1.5 times maximum allowable misalignment.

Coupling Tests

Complete check of coupling operations after testing.

The cycles above meet the total test requirements of 5,000 full strokes and 500 trips. The assembly will be completely disassembled and inspected at various B&W facilities after completion of environmental tests.

3.3.3.4.2 Control Rod Drive Control System Developmental Tests

A control rod drive power supply unit has been built in group prototype form. Following the combined test of the power supply and mechanism, thermal, life, and simulated failure tests will be conducted. The simulated failure test will be designed to verify the safety analysis.

The control rod drive control system will be tested in conjunction with the control rod drive motor control to insure proper operation. Simulated failure testing will also be performed on the combined system to insure that protective requirements are being met.

The position indicator and limit switch subsystem has been built in prototype form and life-tested mechanically under expected environmental conditions. Further testing, both mechanical and electrical, will be done under expected environmental conditions at the B&W Research Center. Characteristics to be determined will include accuracy, repeatability, linearity, short term stability, and long term stability.

3.3.3.4.3 Production Tests

Production tests discussed in this section will be performed either on the drives installed, or on drives manufactured to the same specifications. The finished control rod drive will be proof-tested as a complete system, i.e., mechanism, motor control, and system control working as a system. This proof-testing will be above and beyond any developmental testing performed in the product development stages.

Mechanism production tests will include

a. Ambient Tests

Coupling tests.

Operating speeds.

00000252

Position indication.

Trip tests.

b. Operational Tests

Operating speeds.

Position indication.

Partial and full stroke cycles.

Partial and full stroke trip cycles.

Control system production tests will be performed as described in the following paragraphs.

The finished hardware will be systematically operated through all of its operating modes, checked over the full range of all set points, and checked for proper operation of all patch plugs. This will check completeness and proper functioning of wiring and components.

The operating modes to be checked will include such things as automatic operation, manual group operation, trim or single CRA operation, position indication of all CRA's, travel limit on all CRA's, trip circuit operations, IN command, OUT command, etc.

The trip circuit or circuits will be tested by repeated operation. The overall trip time will be measured.

The accuracy and repeatability of the position indication and limit switch systems will be tested.

Power supply tests will be performed to determine the upper and lower operating voltage and to prove immunity to switching transients.

Fault conditions will be simulated to prove that no unsafe action results from defective components, circuits, or wiring. Ability to detect unsafe fault conditions at the operating console will be determined. Typical of faults to be simulated are

- a. Defective limit switch or circuit.
- b. Improper CRA group patch.
- c. Defective patch plugs.
- d. Defective group sequencer.
- e. Defective clock.
- f. Defective automatic control signal.
- g. Defective command line.
- h. Defective fuses.
- i. Defective single CRA control circuit or switch.
- j. Defective power supply.
- k. Defective motor translator.
- l. Defective motor cable.
- m. Defective position transmitter.

00000253

The finished hardware will be visually inspected for quality of workmanship. This inspection will include an examination of the enclosure, cable entrances, dust-tightness, maintenance features, drawers and cable retractors, fasteners, stiffeners, module mounts, wire harnesses, and other similar details.

3.3.4 INTERNALS TESTS AND INSPECTIONS

The internals upper and lower plenum hydraulic design will be evaluated and guided by the results from the 1/6-scale model flow test which is described in detail in 3.3.2.1. These test results will indicate areas of gross flow maldistribution and allow verification of vessel flow-pressure drop computations. In addition, the test results will provide measured pressure pulses at specific locations to aid in assessing the vibration response characteristics of the internals components.

The effects of internals misalignment will be evaluated on the basis of the test results from the CRDL tests described in 3.3.3.4. These test results, when correlated with the internals guide tube final design, will insure that the CRA will have the capability for a reactor trip or fast insertion under all modes of reactor operation in the reactor coolant environment. These tests will not include the effects of neutron flux exposure.

After completion of shop fabrication, all internals components will be shop-fitted and assembled to final design requirements. The assembled internals components will be installed in a mockup of the as-built reactor vessel for final shop fitting and alignment of the internals for the mating fit with the reactor vessel. Dummy fuel and CRA's will be used to check out and insure that ample clearances exist between the fuel and internals structures guide tubes to allow free movement of the CRA throughout its full stroke length in various core locations. Fuel assembly mating fit will be checked at all core locations. The dummy fuel and CRA's will be identical to the production components except that they will be manufactured to the most adverse tolerance space envelope; even though the assembly weights will be representative of the production units, the dummy components will not contain fissionable or poison materials.

Internals shop fabrication quality control tests, inspection, procedures, and methods will be similar to the pressure vessel tests described in detail in 4.1.4.

With regard to the internals surveillance specimen holder tubes, the material irradiation surveillance program is described in 4.4.3.

All internal components can be removed from the reactor vessel to allow inspection of all vessel interior surfaces (see 4.4.1). Internals components surfaces can be inspected when the internals are removed to the canal storage location.

00000254

The internals vent valves will be designed to relieve the pressure generated by steaming in the core following the LOCA so that the core will remain sufficiently covered. The valves will be designed to withstand the forces resulting from rupture of either a reactor coolant inlet or outlet pipe. Testing of the valves will consist of the following:

- a. A full-size valve assembly (seat, locking mechanism, and socket) will be tested at steady-state conditions at the maximum pressure expected to result during the blowdown.
- b. Sufficient tests will be conducted at zero pressure to determine the frictional loads and clearances in the hinge assembly, the inertia of the valve cover, and the deflections resulting from impact of the cover so that the valve response to cyclic blowdown forces may be determined analytically.
- c. The valve assembly will be pressurized to determine what pressure differential is required to cause the valve to begin to open. A determination of the pressure differential required to open the valve to its maximum open position will be simulated by mechanical means.
- d. A valve assembly will be installed and removed remotely in a test stand to judge the adequacy of handling equipment.

Since the temperature differential existing across the valve assembly during normal operation in the reactor is only approximately 55 F, and since the same material is used for the valve seat, socket, and cover, there is no need to conduct tests at elevated temperatures.

The valves are located in a region of relatively low velocity and turbulence, and preliminary analysis indicates that there is insufficient energy in the coolant to cause vibrational problems. Therefore, no testing to prove the vibration adequacy of the valve is planned.

During refueling outages after the reactor vessel head and the internals plenum assembly have been removed, the vent valves will be accessible for visual and mechanical inspection. A remote inspection tool will be provided to engage with the previously mentioned valve disc hook or eye. With the aid of this tool, the valve disc can be manually exercised to evaluate the disc freedom. The hinge design will incorporate special features, as described in 3.2.4.1(f), to minimize the possibility of valve disc motion impairment during its service life.

Remote installation and removal of the vent valve assemblies will be performed with the aid of another tool which will include unlocking and operating features for the wedge ring. This handling tool design will be functionally developed and tested on a full-size mockup of the vent valve installation configuration prior to valve manufacture.

With the aid of the above described inspection tool, a visual inspection of the valve body and disc sealing faces can be performed for evaluation of observed surface irregularities.

The valve disc, hinge shaft, shaft journals (bushings), disc journal receptacles, and valve body journal receptacles will be designed to withstand without failure the internal and external differential pressure loadings resulting from a loss-of-coolant accident. These valve materials will be nondestructively tested and accepted in accordance with the ASME Code III requirements for Class A pressure vessels. | 1

The hinge materials will be selected on the basis of their corrosion resistance, surface hardness, antigalling characteristics, and compatibility with mating materials in the reactor coolant environment.

A remote inspection of hinge parts is not planned until such time as a valve assembly is removed because its free-disc motion has been impaired. In the unlikely event that a hinge part should fail during normal operation, the most significant indication of such a failure would be a change in the free-disc motion as a result of altered rotational clearances.

3.4 REFERENCES

- (1) Putnam, G. E., TOPIC - A Fortran Program for Calculating Transport of Particles in Cylinders, IDO-16968, April 1964.
- (2) Avery, A. F., The Prediction of Neutron Attenuation in Iron-Water Shields, AEEW-RL25, April 1962.
- (3) Bohl, H., Jr., et al., P3MGI, A One-Dimensional Multigroup P-3 Program for the Philco-2000 Computer, WAPD-TM-272.
- (4) Bohl, H., Jr. and Hemphill, A. P., MUFT-5, A Fast Neutron Spectrum Program for the Philco-2000, WAPD-TM-218.
- (5) Armster, H. J. and Callaghan, J. C., KATE-1, A Program for Calculating Wigner-Wilkins and Maxwellian-Averaged Thermal Constants on the Philco-2000, WAPD-TM-232.
- (6) Marlowe, O. J. and Suggs, M. C., WANDA-5, A One-Dimensional Neutron Diffusion Equation Program for the Philco-2000 Computer, WAPD-TM-241.
- (7) Honeck, H. C., THERMOS, A Thermalization Transport Theory Code for Reactor Lattices, BNL-5826.
- (8) Cadwell, W. R., Buerger, P. F., and Pfeifer, C. J., The PDQ-5 and PDQ-6 Programs for the Solution of the Two-Dimensional Neutron Diffusion-Depletion Problem, WAPD-TM-477.
- (9) Marlowe, O. J., Nuclear Reactor Depletion Programs for the Philco-2000 Computer, WAPD-TM-221.
- (10) Lathrop, K. P., DTF-IV, A FORTRAN-IV Program for Solving the Multigroup Transport Equation With Anisotropic Scattering, LA-3373.
- (11) Joanou, G. D. and Dudek, J. S., GAM-1: A Consistent P_1 Multigroup Code for the Calculation of Fast Neutron Spectra and Multigroup Constants, GA-1850.
- (12) Baldwin, M. N., Physics Verification Experiments, CORE I, ρ_{28} and Initial Conversion Ratio Measurements, BAW-TM-454.
- (13) Clark, R. H. and Pitts, T. G., Physics Verification Experiments, Core I, BAW-TM-455.
- (14) Clark, R. H. and Pitts, T. G., Physics Verification Experiments, Cores II and III, BAW-TM-458.
- (15) Spinks, N., "The Extrapolation Distance at the Surface of a Grey Cylindrical Control Rod", Nuclear Science and Engineering 22, pp 87-93, 1965.
- (16) Clark, R. H., Batch, M. L., and Pitts, T. G., Lumped Burnable Poison Program - Final Report, BAW-3492-1.
- (17) Neuhold, R. J., Xenon Oscillation, BAW-305, 1966.

- (18) Wilson, R. H. and Ferrell, J. K., Correlation of Critical Heat Flux for Boiling Water in Forced Circulation at Elevated Pressures, The Babcock & Wilcox Company, BAW-168, November 1961.
- (19) U.S.-Euratom Joint R&D Program, Burnout Flow Inside Round Tubes With Non-uniform Heat Fluxes, The Babcock & Wilcox Company, BAW-3238-9, May 1966.
- (20) Jens, W. H. and Lottes, P. A., Analysis of Heat Transfer Burnout, Pressure Drop, and Density Data for High Pressure Water, ANL-4627, May 1951.
- (21) Owen, D. B., Factors for One-Sided Tolerance Limits and for Variable Sampling Plans, SCR-607, March 1963.
- (22) DeBortoli, R. A., et al., Forced Convection Heat Transfer Burnout Studies for Water in Rectangular Channels and Round Tubes at Pressures Above 500 psia, WAPD-188, Bettis Plant, Pittsburgh, Pennsylvania, 1958.
- (23) USAEC Docket 50-244, Exhibit D-3, entitled "Rochester Gas and Electric Corporation, Brookwood Nuclear Station Unit No. 1", (Third Supplement to: Preliminary Facility Description and Safety Analysis Report, February 28, 1966).
- (24) Lee, D. H. and Obertelli, J. D., An Experimental Investigation of Forced Convection Burnout in High Pressure Water. Part 1, Round Tubes With Uniform Flux Distribution, AEEW-R-213, August 1963.
- (25) Matzner, B. and Griffel, J., Bimonthly Progress Report (MFR-XIII-11 and 12-63), Task XIII of Contract AT(30-3)-187, Basic Experimental Studies of Boiling Fluid Flow and Heat Transfer at Elevated Pressures, for November and December 1963, January 27, 1964.
- (26) Matzner, B. and Griffel, J., Monthly Progress Report (MFR-XIII-6-63), Task XIII of Contract AT(30-3)-187, Basic Experimental Studies of Boiling Fluid Flow and Heat Transfer at Elevated Pressures, for June 1963, June 28, 1963.
- (27) Matzner, B., Monthly Progress Report (MFR-XIII-5-63), Task XIII of Contract AT(30-3)-187, Basic Experimental Studies of Boiling Fluid Flow and Heat Transfer at Elevated Pressures, for May 1963, May 31, 1963.
- (28) Internal Memo, Weatherhead, R. J. to Lottes, P. A., Critical Heat Flux (Burnout) in Small Diameter Tubes at 2000 psia, December 29, 1958.
- (29) Swenson, H. W., Carver, J. R., and Kakarala, C. R., The Influence of Axial Heat Flux Distribution on the Departure From Nucleate Boiling in a Water Cooled Tube, ASME Paper 62-WA-297.
- (30) Nonuniform Heat Generation Experimental Program, Quarterly Progress Report No. 7, January - March 1965, BAW-3238-7, Joint U.S.-Euratom R&D Program, AEC Contract No. AT(30-1)-3238.
- (31) Hald, A., Statistical Theory With Engineering Applications, John Wiley & Sons, Inc., New York, 1955.

00000258

- (32) Worthing, A. G. and Geffner, J., Treatment of Experimental Data, John Wiley & Sons, Inc., New York, 1943.
- (33) Bowring, R. W., Physical Model, Based on Bubble Detachment, and Calculation of Steam Voidage in the Subcooled Region of a Heated Channel, HPR-10, OECD Halden Reaktor Project, December 1962.
- (34) Zuber, N. and Findlay, J. A., Average Volumetric Concentrations in Two Phase Flow Systems, Presented at the ASME Winter Meeting, 1964. To be published in the ASME Transactions.
- (35) Maurer, G. W., A Method of Predicting Steady-State Boiling Vapor Fractions in Reactor Coolant Channels, Bettis Technical Review, WAPD-BT-19.
- (36) Baker, O., Simultaneous Flow of Oil and Gas, Oil and Gas Journal, Vol. 53, pp 185-195, 1954.
- (37) Rose, S. C., Jr., and Griffith, P., Flow Properties of Eubbly Mixtures, ASME Paper No. 65-HT-38, 1965.
- (38) Haberstroh, R. D. and Griffith, P., The Transition From the Annular to the Slug Flow Regime in Two-Phase Flow, MIT TR 5003-28, Department of Mechanical Engineering, MIT, June 1964.
- (39) Bergles, A. E. and Suo, M., Investigation of Boiling Water Flow Regimes at High Pressure, NYO-3304-8, February 1, 1966.
- (40) Notley, N. J. F., The Thermal Conductivity of Columnar Grains in Irradiated UO_2 Fuel Elements, AECL-1822, July 1963.
- (41) Lyons, M. F., et al., UO_2 Fuel Rod Operation With Gross Central Melting, GEAP-4264, October 1963.
- (42) Notley, M. J. F., et al., Zircaloy-Sheathed UO_2 Fuel Elements Irradiated at Values of Integral kd_0 Between 30 and 83 w/cm. AECL-1676, December 1962.
- (43) Bain, A. S., Melting of UO_2 During Irradiations of Short Duration, AECL-2289, August 1965.
- (44) Notley, M. J. F., et al., The Longitudinal and Diametral Expansions of UO_2 Fuel Elements, AECL-2143, November 1964.
- (45) Duncan, R. N., Rabbit Capsule Irradiation of UO_2 , CVNA-142, June 1962.
- (46) Lyons, M. F., et al., UO_2 Pellet Thermal Conductivity From Irradiations With Central Melting, GEAP-4624, July 1964.
- (47) McGrath, R. G., Carolinas-Virginia Nuclear Power Associates, Inc., Research and Development Program, Quarterly Progress Report for the Period April - May - June 1965, CVNA-246.

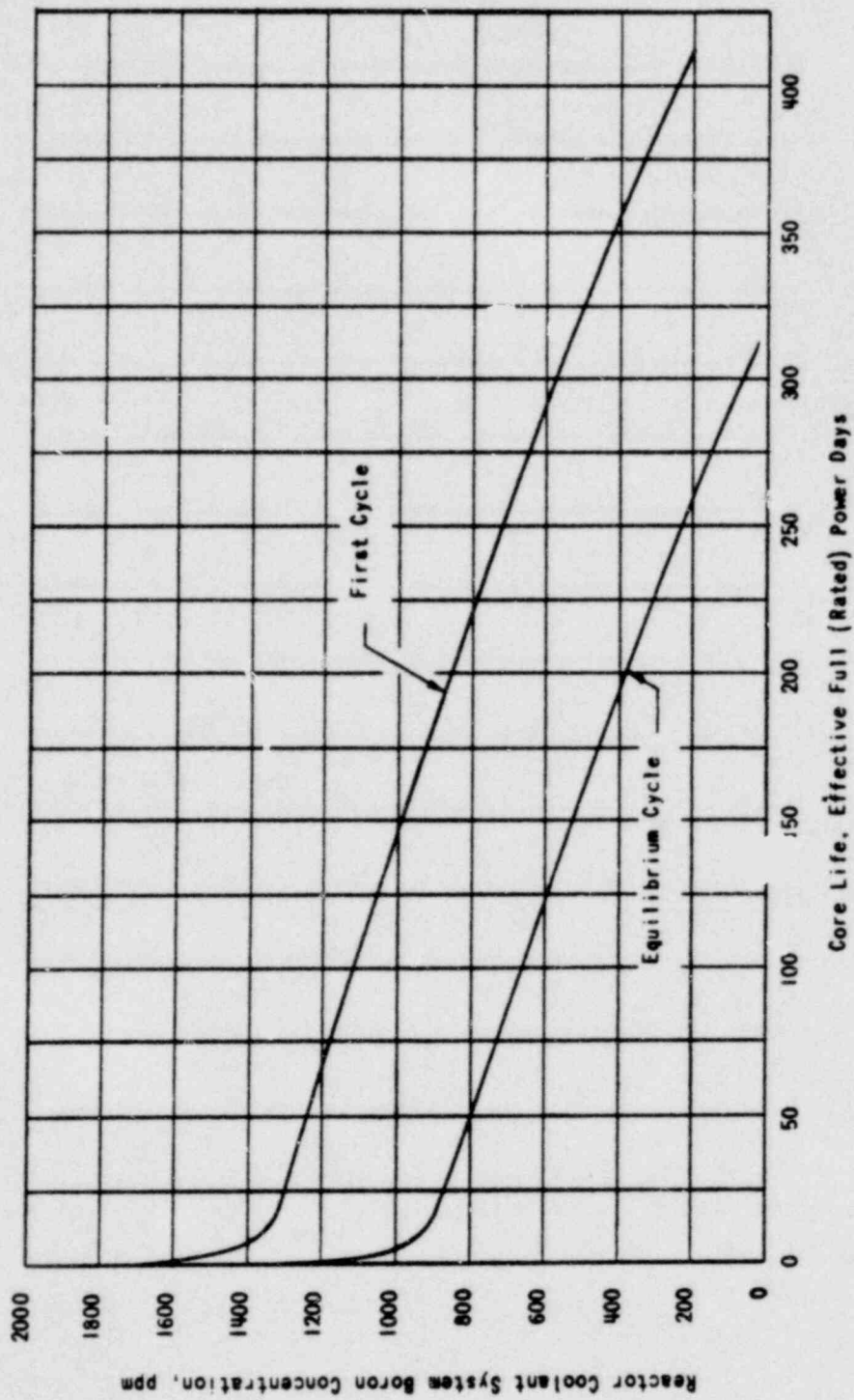
00000259

- (48) Ross, A. M. and Stoute, R. L., Heat Transfer Coefficients Between UO_2 and Zircaloy-2, AECL-1552, June 1962.
- (49) Hoffman, J. P. and Coplin, D. H., The Release of Fission Gases From Uranium Dioxide Pellet Fuel Operated at High Temperatures, GEAP-4596, September 1964.
- (50) Spolaris, C. N. and Megerth, F. H., Residual and Fission Gas Release From Uranium Dioxide, GEAP-4314, July 1963.
- (51) Robertson, J. A. L., et al., Behavior of Uranium Dioxide as a Reactor Fuel, AECL-603, 1958.
- (52) Parker, G. W., et al., Fission Product Release From UO_2 by High Temperature Diffusion and Melting in Helium and Air, CF-60-12-14, ORNL, February 1961.
- (53) Daniel, R. C., et al., Effects of High Burnup on Zircaloy-Clad, Bulk UO_2 , Plate Fuel Element Samples, WAPD-263, September 1962.
- (54) Blomeke, J. O. and Todd, Mary F., Uranium Fission Product Production as a Function of Thermal Neutron Flux, Irradiation Time, and Decay Time, ORNL-2127, Part 1, Vol. 1 and 2.
- (55) Duncan, R. N., CVTR Fuel Capsule Irradiations, CVNA-153, August 1962.
- (56) Frost, Bradbury, and Griffiths (AERE Harwell), Irradiation Effects in Fissile Oxides and Carbides at Low and High Burnup Levels, Proceedings of IAEA Symposium on Radiation Damage in Solids and Reactor Materials, Venice, Italy, May 1962.
- (57) Gerhart, J. M., The Post-Irradiation Examination of a PuO_2-UO_2 Fast Reactor Fuel, GEAP-3833.
- (58) Atomic Energy Clearing House, Vol. 12, No. 3, p 11.
- (59) Large Closed-Cycle Water Reactor Research and Development Program Progress Report for the Period, January 1 to March 31, 1964, Westinghouse Electric Corporation, Pittsburgh, Pa., 1964, WCAP-3269-2. Also WCAP-3269-3 for period from April 1 to June 30, 1964.
- (60) Physical and Mechanical Properties of Zircaloy-2 and -4, WCAP-3269-41, Figure 18.
- (61) Burgreen, D., Byrnes, J. J., and Benforado, D. M., "Vibration of Rods Induced by Water in Parallel Flow", Trans. ASME 80, p 991, 1958.
- (62) Large Closed-Cycle Water Reactor R&D Program, Progress Report for the Period January 1 to March 31, 1965, WCAP-3269-12.
- (63) Burnout for Flow Inside Round Tubes With Nonuniform Heat Fluxes, BAW-3238-9, May 1966.

00000260

- (64) Nonuniform Heat Generation Experimental Program, BAW-3233-13, July 1966.
- (65) Clark, R. H., Physics Verification Experiments, Cores IV and V, BAW-TM-178, September 1966.
- (66) Clark, R. H., Physics Verification Experiment, Core VI, BAW-TM-179, December 1966.
- (67) Clark, R. H., Physics Verification Experiment, Axial Power Mapping on Core IV, BAW-TM-255, December 1966.
- (68) Larsen, P. S., et al., DNB Measurements for Upwards Flow of Water in an Unheated Square Channel with a Single Uniformly Heated Rod at 1600-2300 psia, Proceedings of the Third International Heat Transfer Conference, August 1966.

00000261



00000262

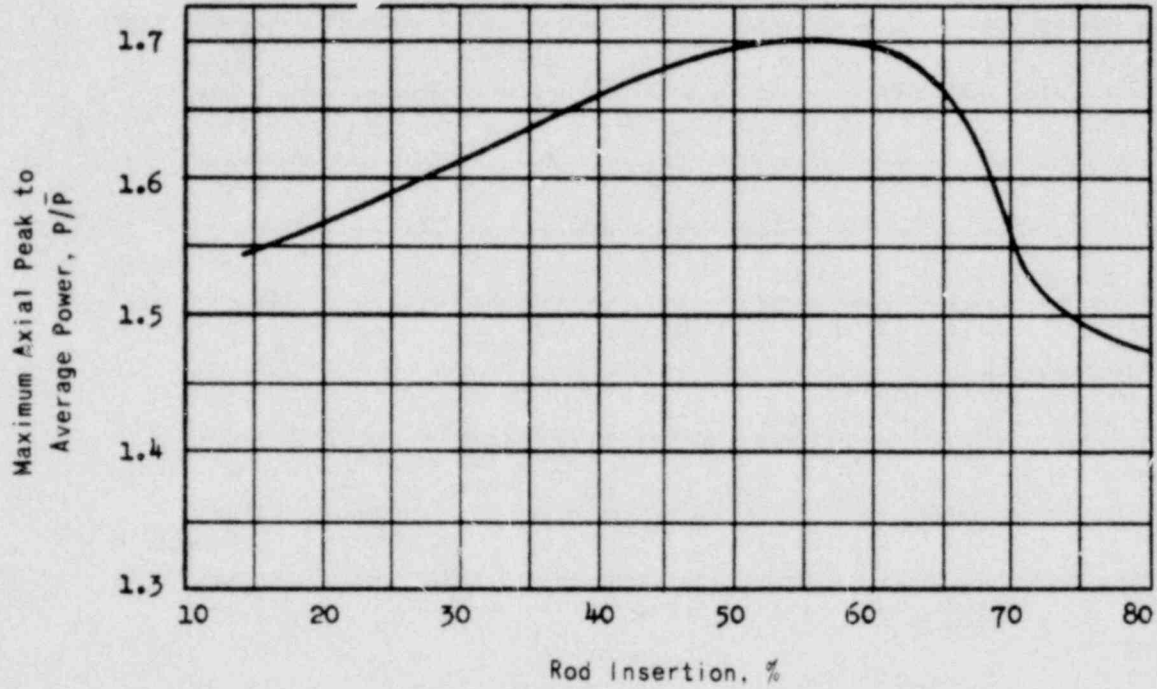
**BORON CONCENTRATION VERSUS CORE LIFE
CRYSTAL RIVER UNITS 3 & 4**



FIGURE 3-1

AMEND. 1 (1-15-68)

Axial Power Profile for
55% insertion is shown on
Figure 3-3.



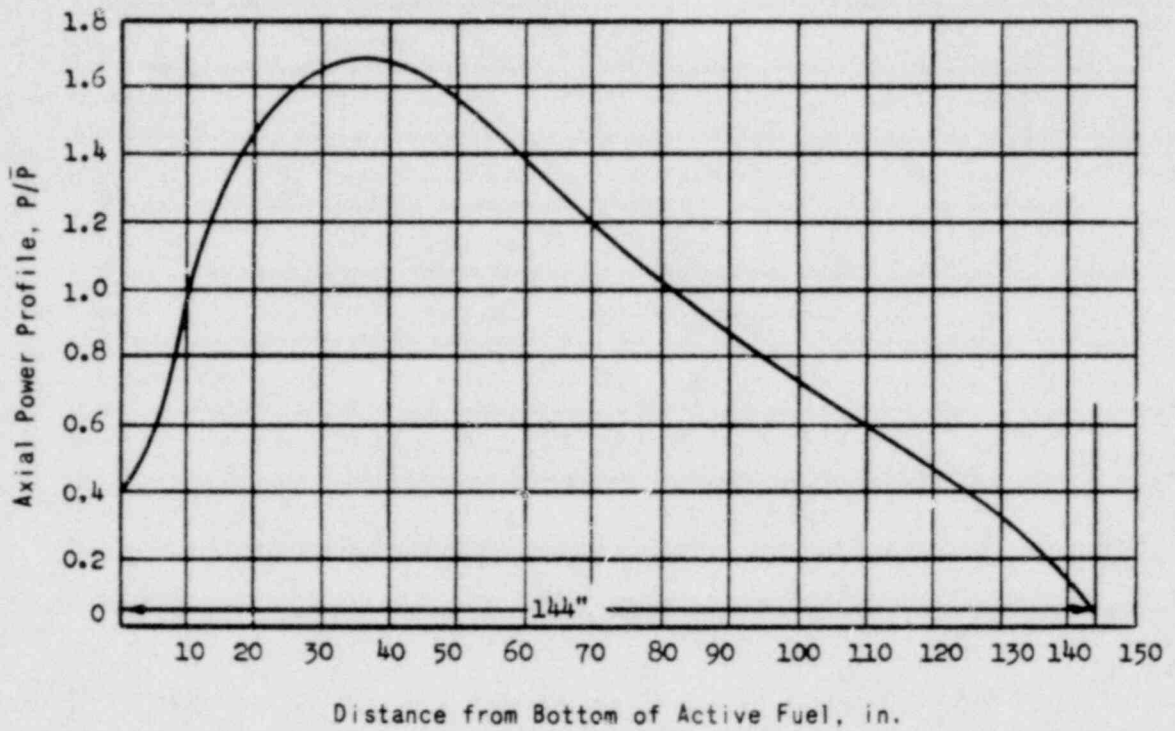
AXIAL PEAK TO AVERAGE POWER
VERSUS XENON OVERRIDE ROD INSERTION

CRYSTAL RIVER UNITS 3 & 4



FIGURE 3-2

00000263



05 0000

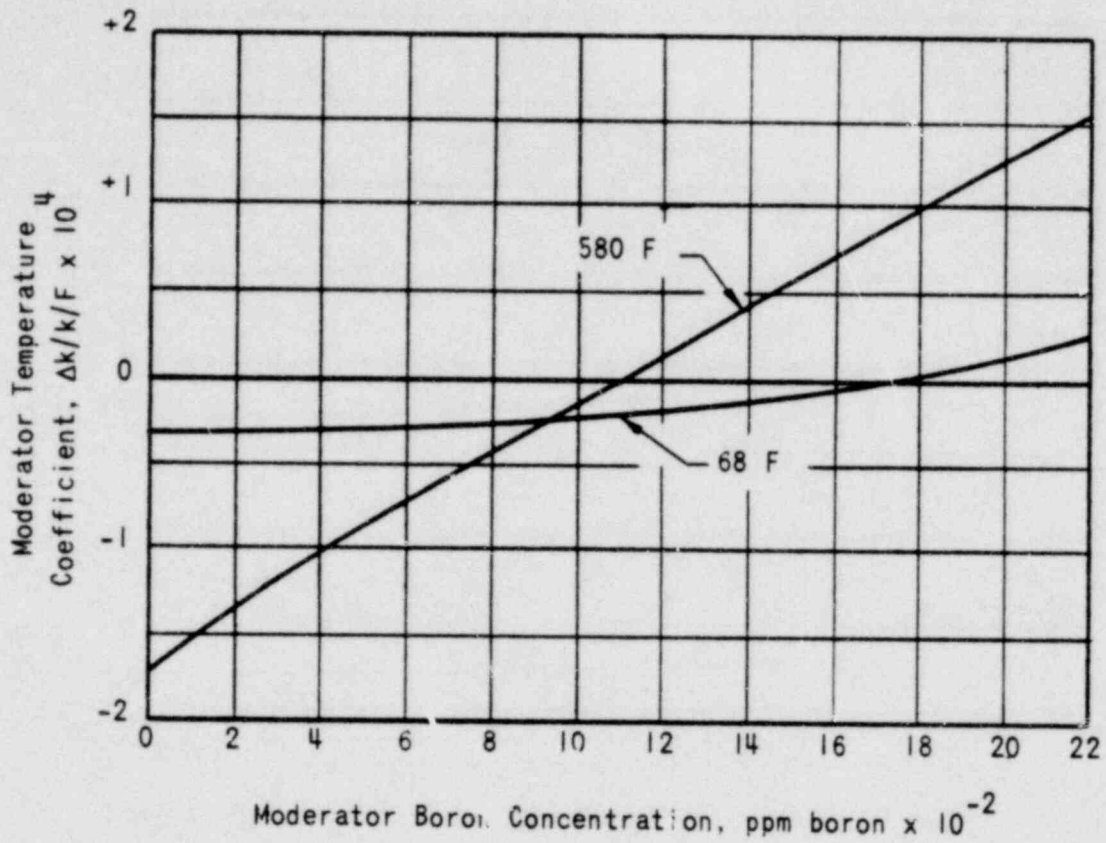
00000264

AXIAL POWER PROFILE, XENON OVERRIDE
RODS 55 PERCENT INSERTED

CRYSTAL RIVER UNITS 3 & 4



FIGURE 3-3

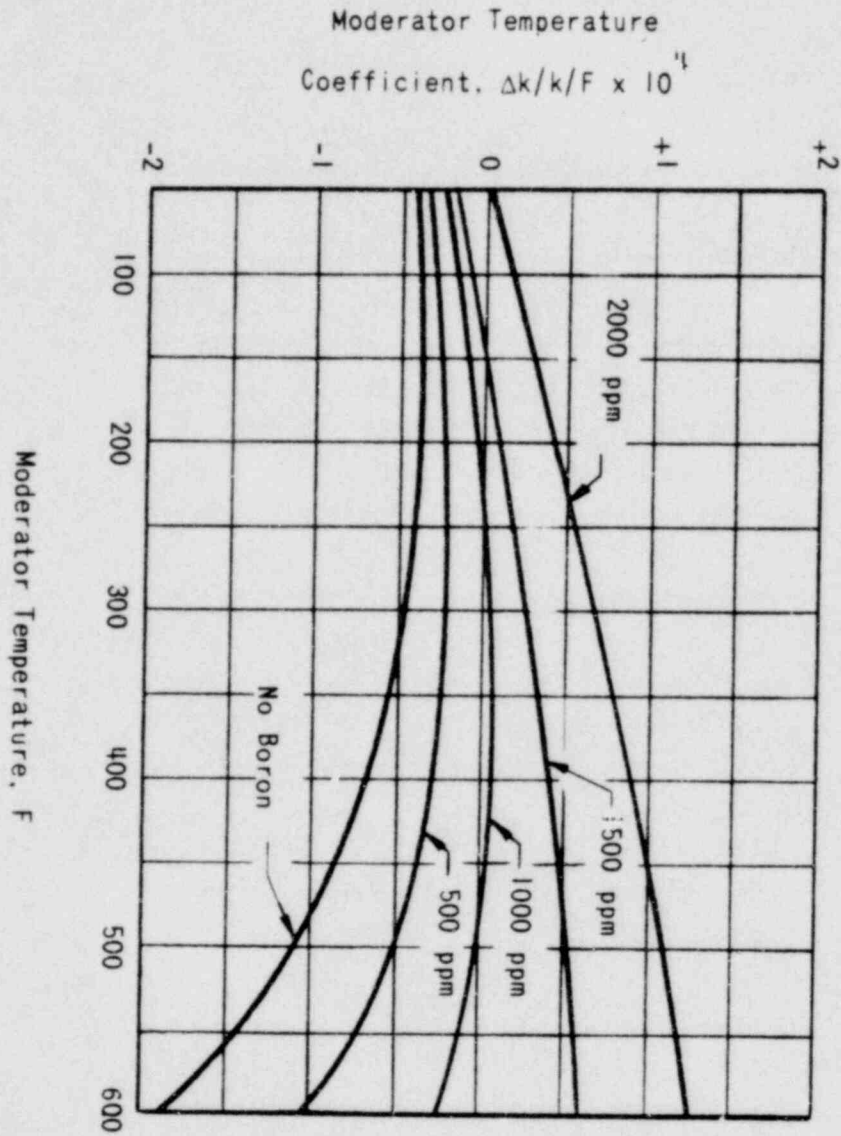


00000265

MODERATOR TEMPERATURE COEFFICIENTS
 VERSUS BORON CONCENTRATION
 CRYSTAL RIVER UNITS 3 & 4



FIGURE 3-4



00000266

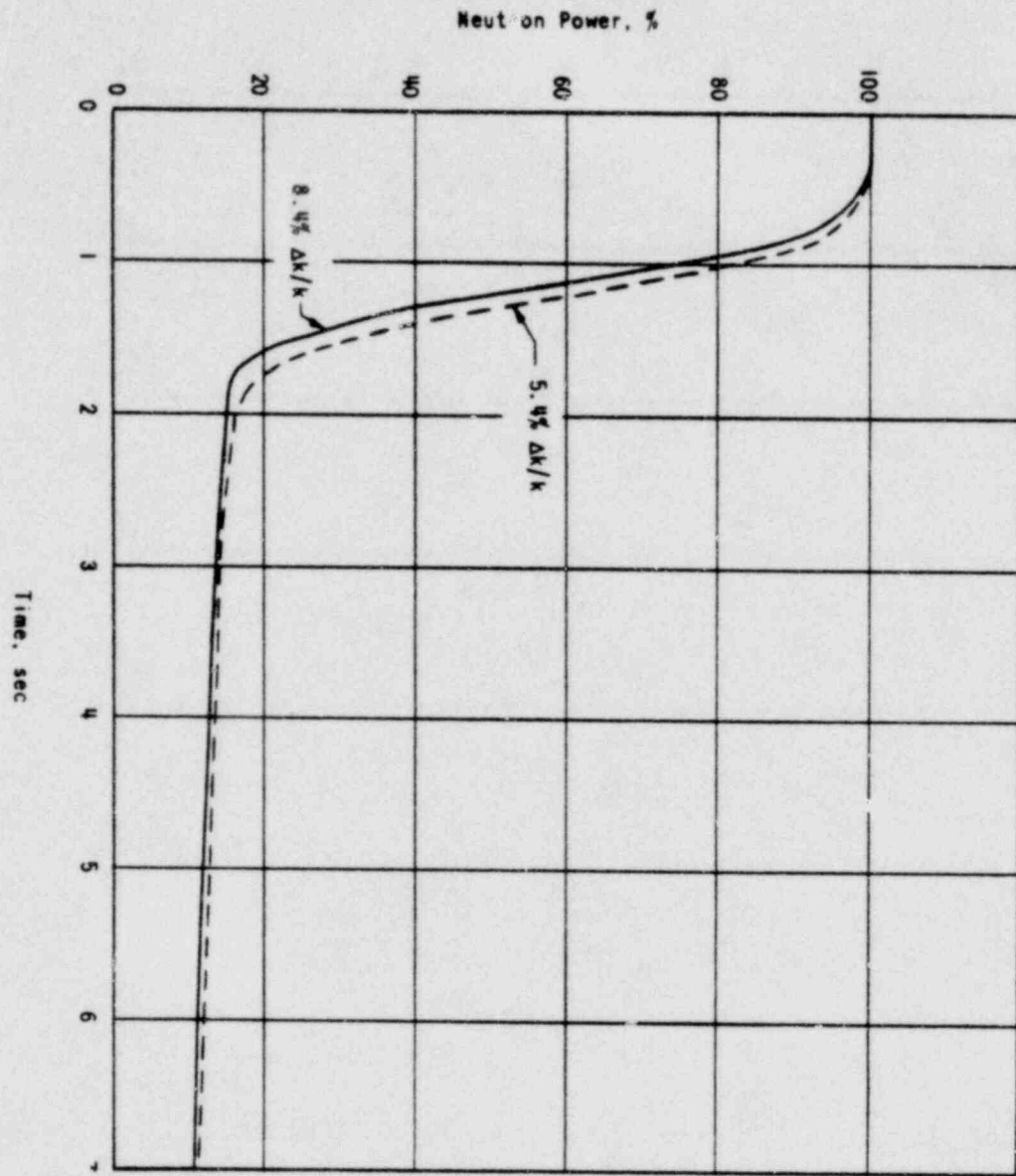
MODERATOR TEMPERATURE COEFFICIENTS VERSUS
MODERATOR TEMPERATURE & VARIOUS BORON LEVELS

CRYSTAL RIVER UNITS 3 & 4



FIGURE 3-5

AMEND. 1 (1-15-68)



PERCENT INITIAL POWER VERSUS TIME FOLLOWING TRIP

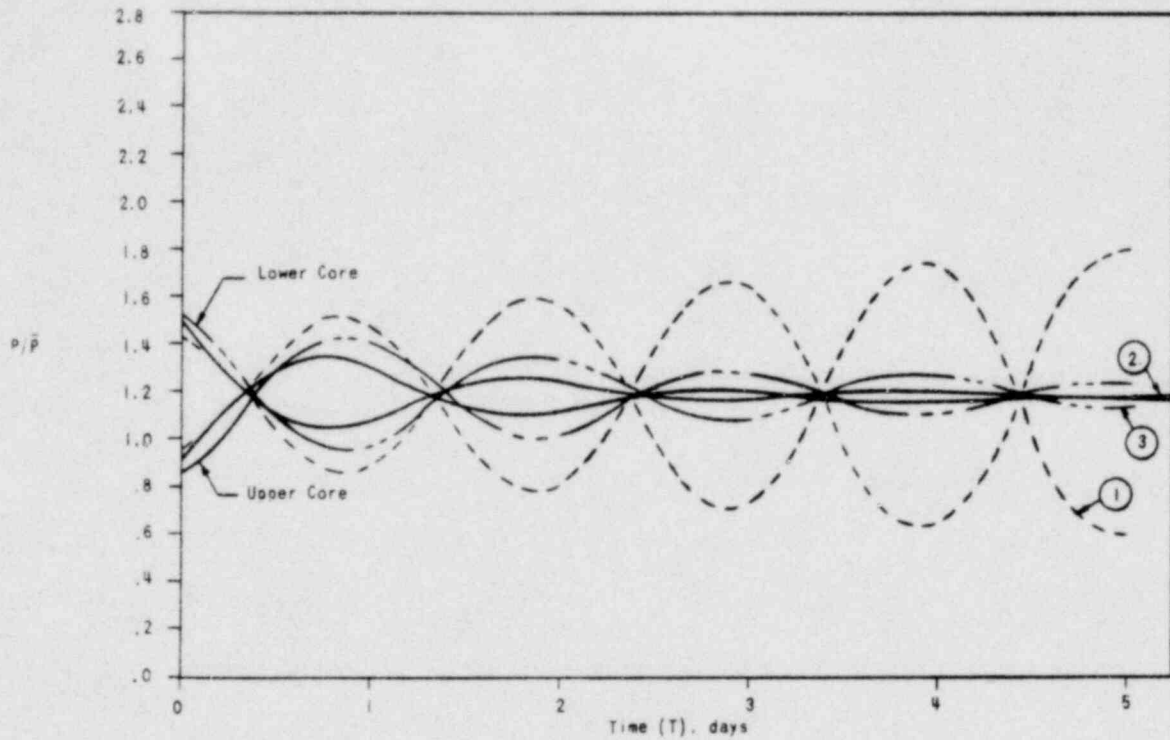
CRYSTAL RIVER UNITS 3 & 4



FIGURE 3-6

AMEND. 1 (1-15-68)

00000267



Notes:

1. Power Ratio taken 36 in. from top and bottom of active fuel.
 - Case 1 - No temperature iteration, $T_{fuel} = 1,400$ F.
 - Case 2 - Temperature iteration with $T_{fuel} = 1,400$ F.
 - Case 3 - Temperature iteration with $T_{fuel} = 900$ F.
2. Oscillation initiated at $T = 2$ days.

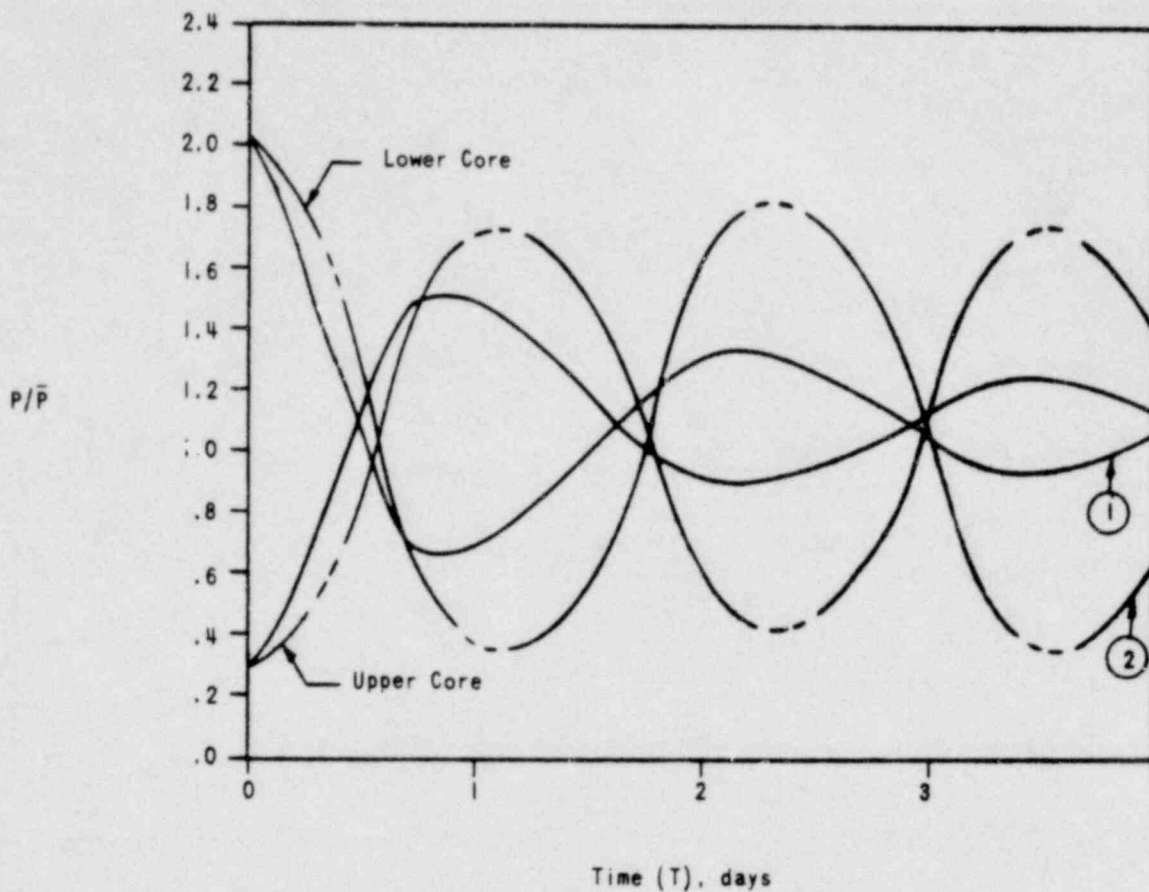
00000268

EFFECT OF FUEL TEMPERATURE (DOPPLER)
ON XENON OSCILLATIONS BEGINNING OF LIFE

CRYSTAL RIVER UNITS 3 & 4



FIGURE 3-7



Notes:

1. Power Ratio taken 36 in. from top and bottom of active fuel.
 Case 1 - Temperature Iteration with $\bar{T}_{fuel} = 1,400$ F.
 Case 2 - Temperature Iteration with $\bar{T}_{fuel} = 900$ F.
2. Oscillation initiated at $T = 300$ days.

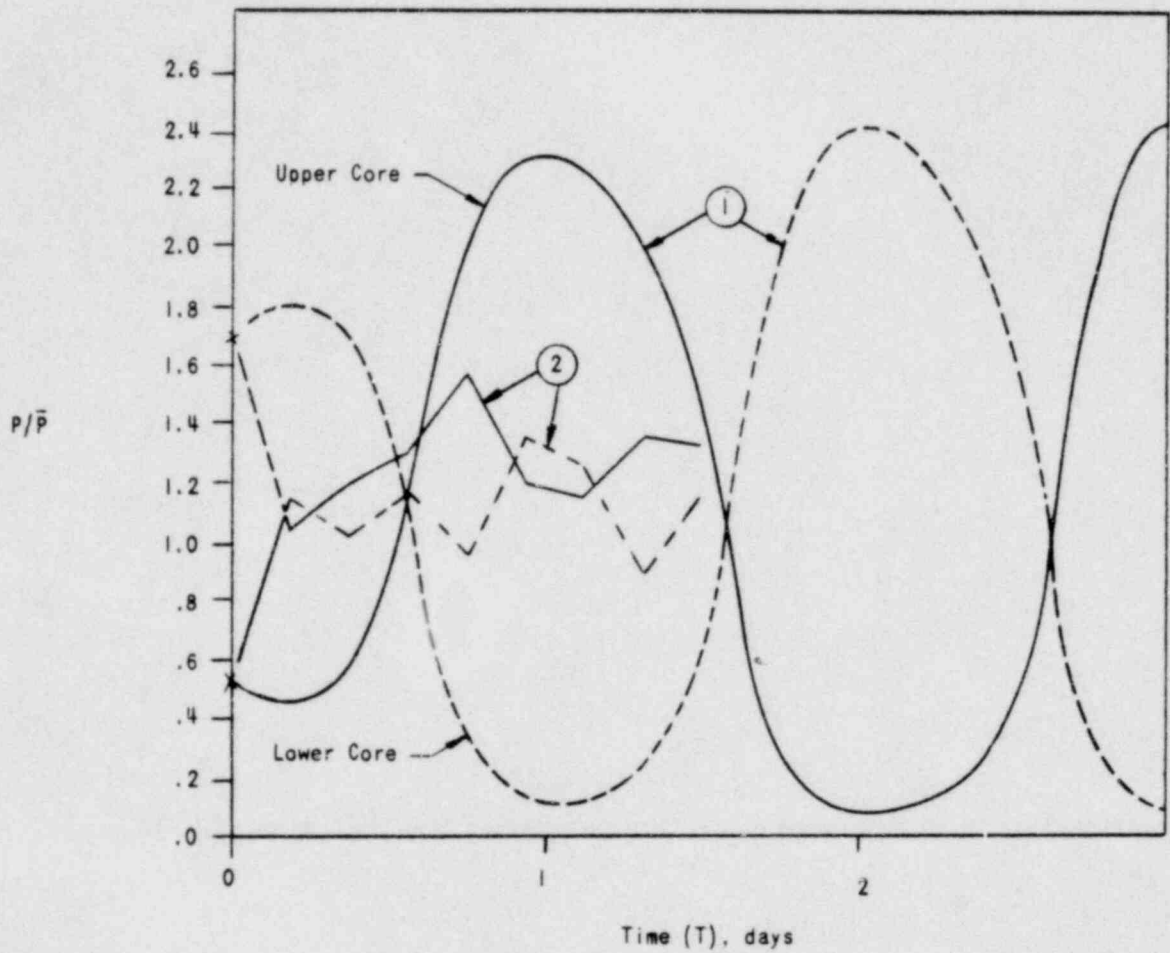
EFFECT OF FUEL TEMPERATURE (DOPPLER)
ON XENON OSCILLATIONS NEAR END OF LIFE

CRYSTAL RIVER UNITS 3 & 4



FIGURE 3-8

00000269



Notes:

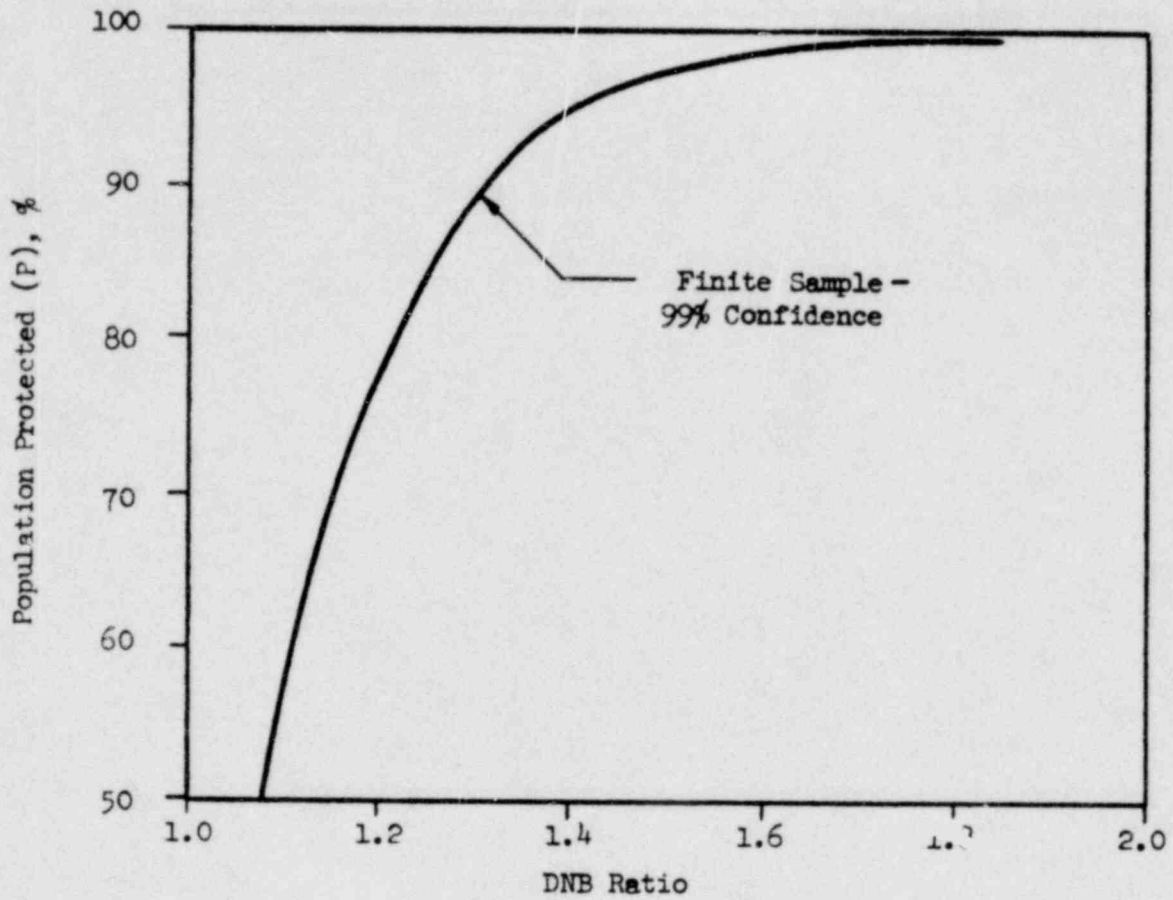
1. Case 1 - Divergent oscillation (without temperature iteration).
Case 2 - Power ratio variation with control (without temperature iteration).
2. Oscillation initiated at $T = 200$ days.

00000270

CONTROL OF AXIAL OSCILLATION WITH PARTIAL RODS
CRYSTAL RIVER UNITS 3 & 4



FIGURE 3-9



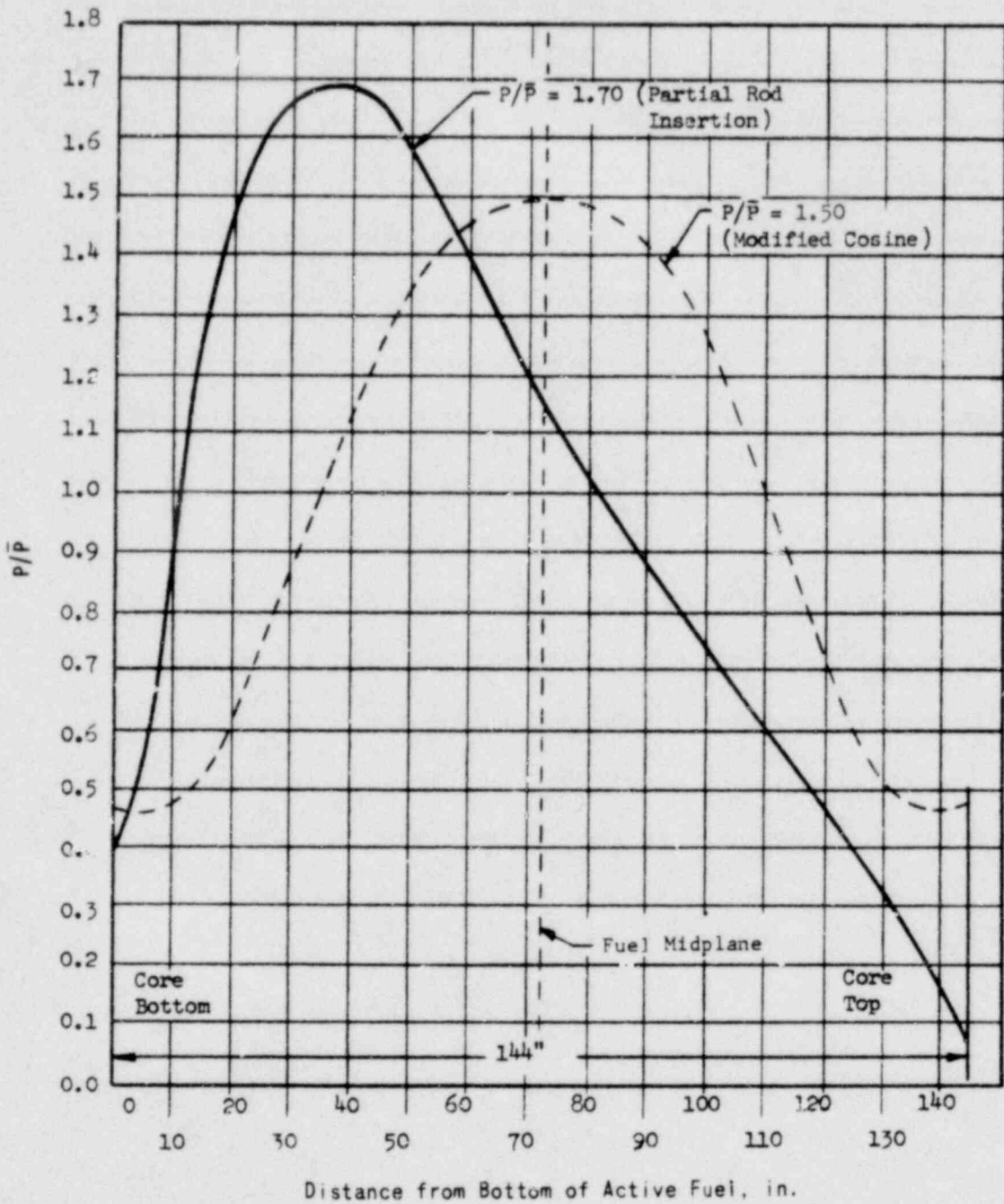
POPULATION INCLUDED IN THE STATISTICAL
STATEMENT VERSUS DNB RATIO

CRYSTAL RIVER UNITS 3 & 4



FIGURE 3-10

00000271



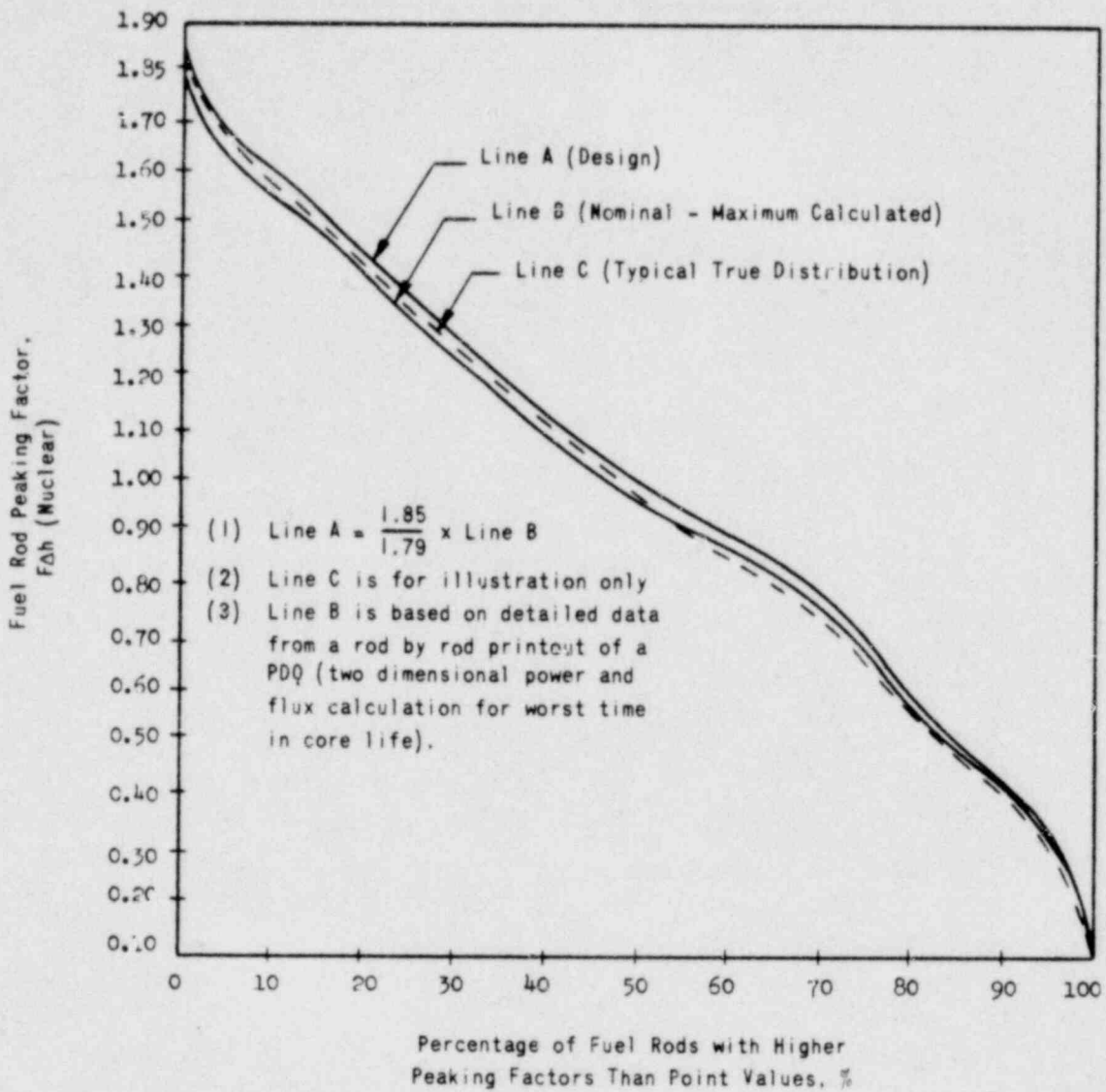
00000272

POWER SHAPE REFLECTING INCREASED AXIAL POWER PEAK FOR 144 INCH CORE

CRYSTAL RIVER UNITS 3 & 4



FIGURE 3-11



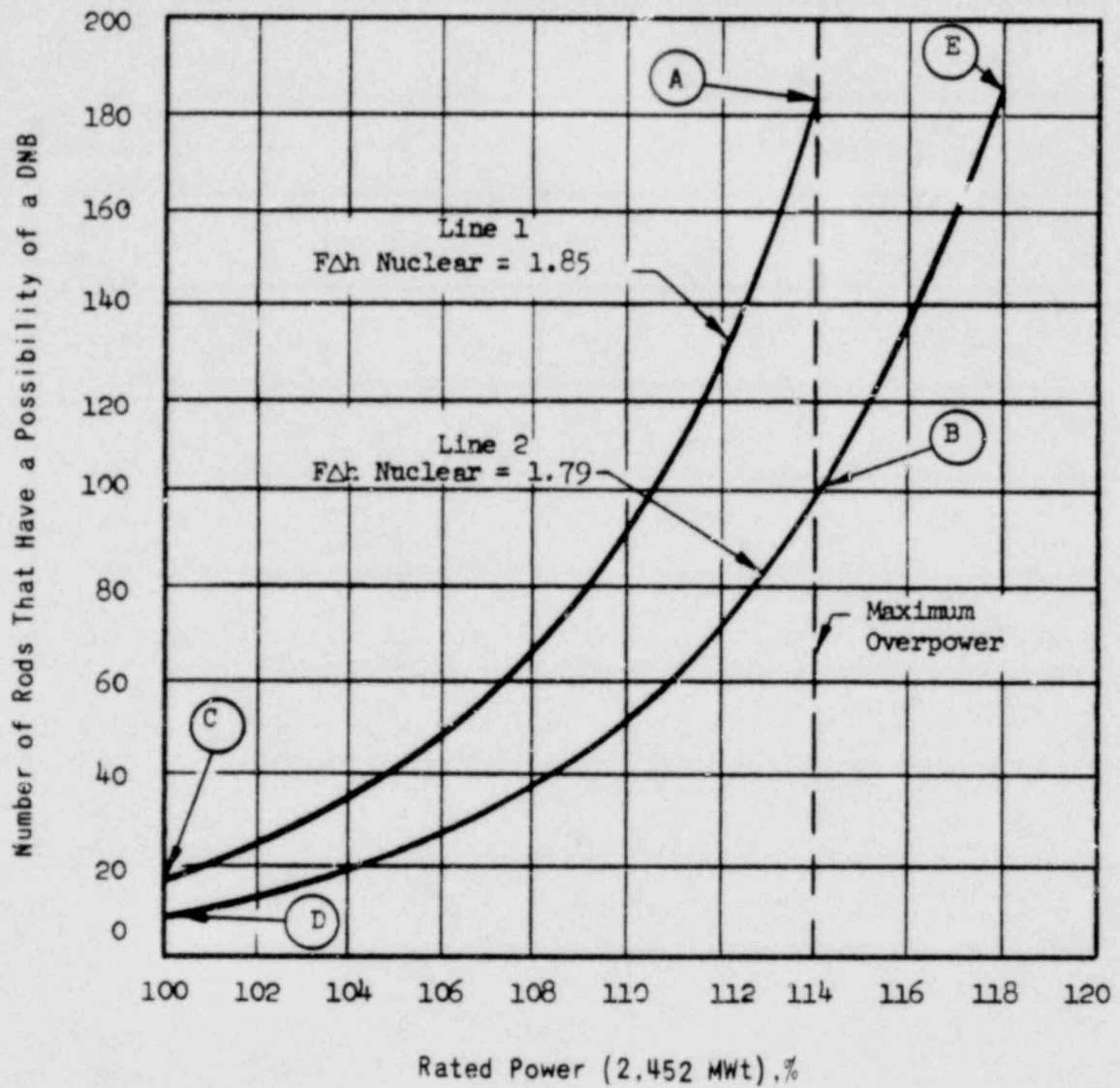
00000273

DISTRIBUTION OF FUEL ROD PEAKING

CRYSTAL RIVER UNITS 3 & 4



FIGURE 3-12



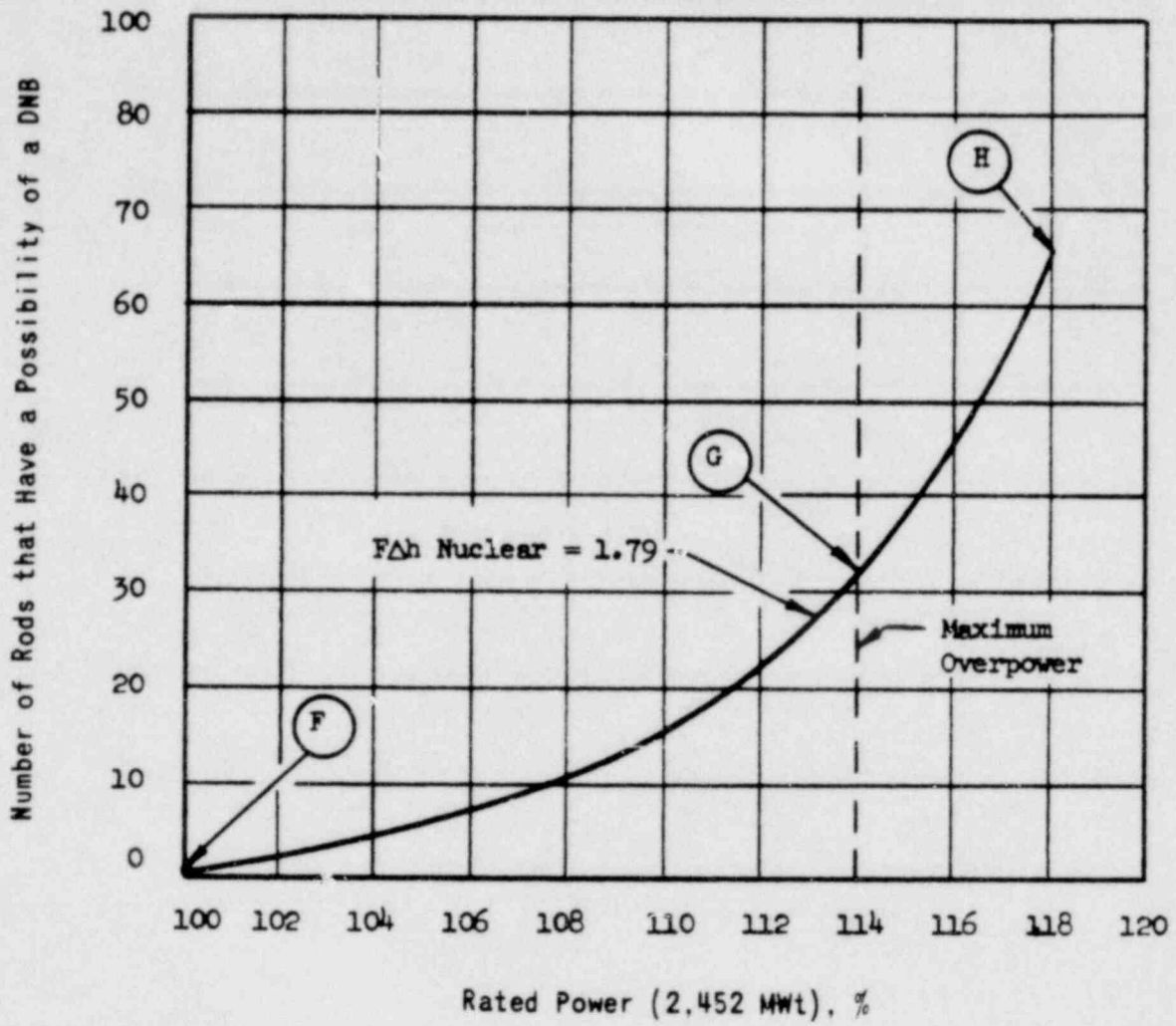
00000274

POSSIBLE FUEL ROD DNB's FOR MAXIMUM DESIGN CONDITIONS - 36,816 ROD CORE

CRYSTAL RIVER UNITS 3 & 4



FIGURE 3-13



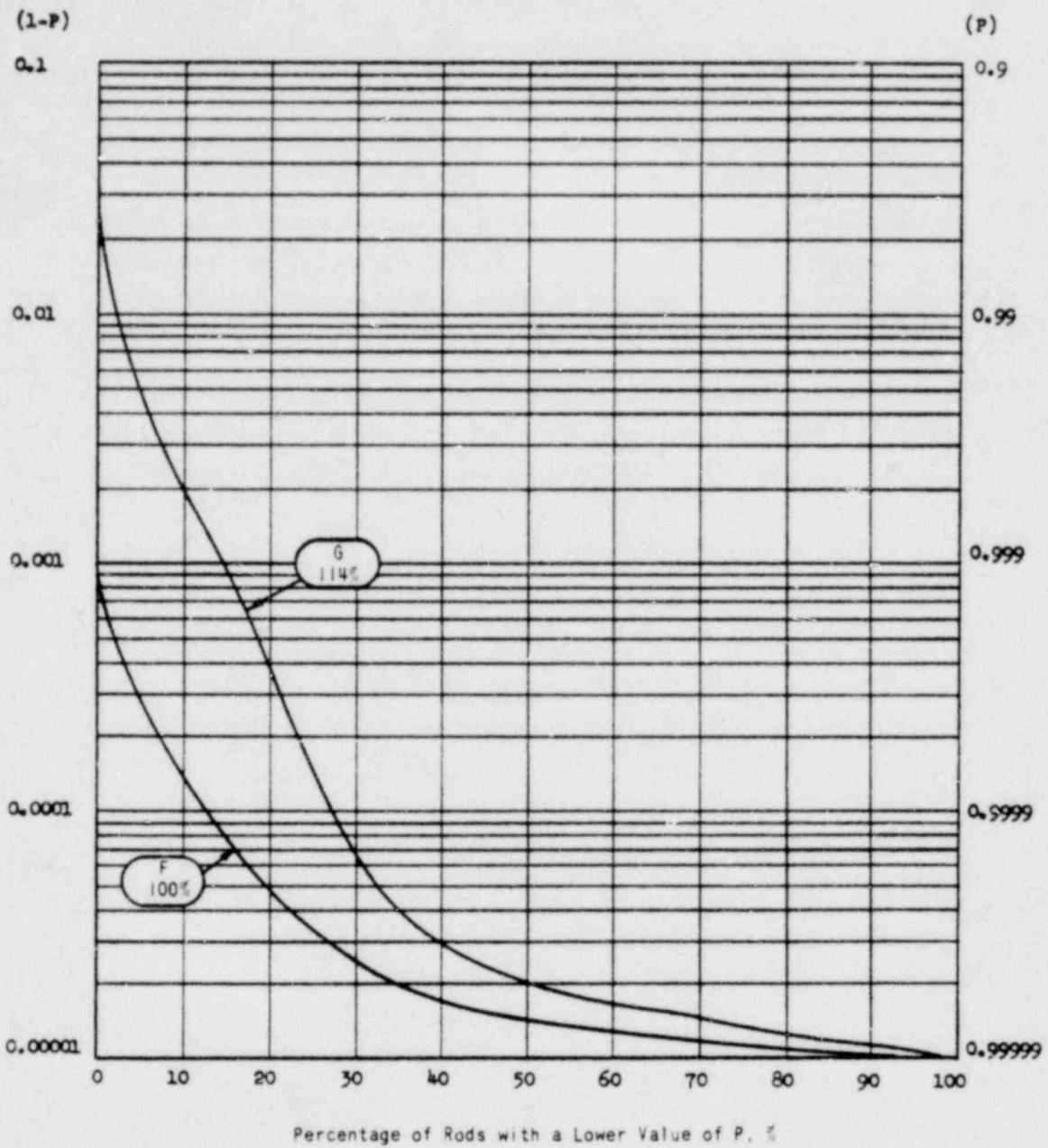
POSSIBLE FUEL ROD DNB's FOR MOST PROBABLE CONDITIONS - 36.816 ROD CORE

CRYSTAL RIVER UNITS 3 & 4



FIGURE 3-14

00000275



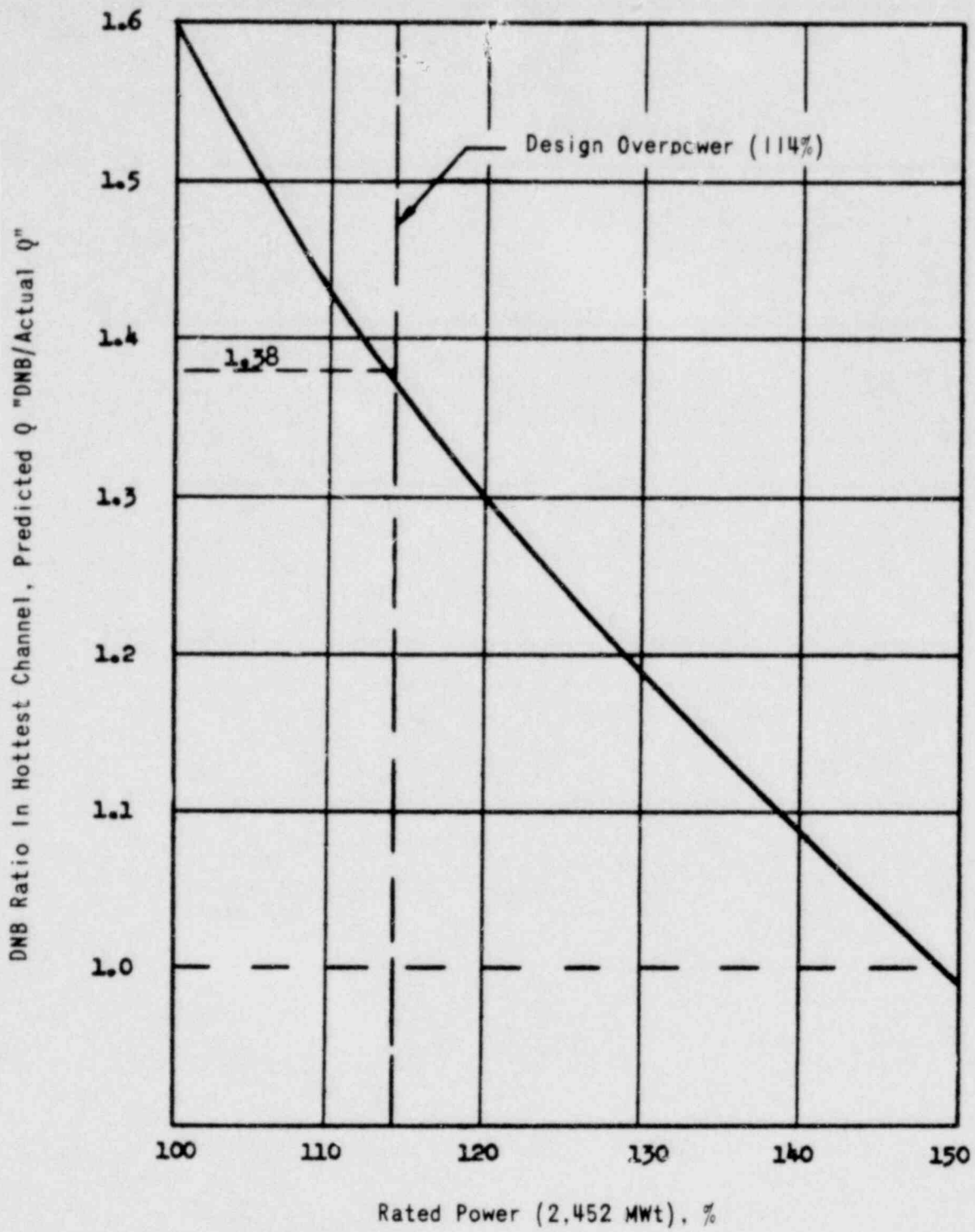
00000276

DISTRIBUTION OF POPULATION PROTECTED
 P, & 1-P VERSUS NUMBER RODS
 FOR MOST PROBABLE CONDITIONS

CRYSTAL RIVER UNITS 3 & 4



FIGURE 3-15



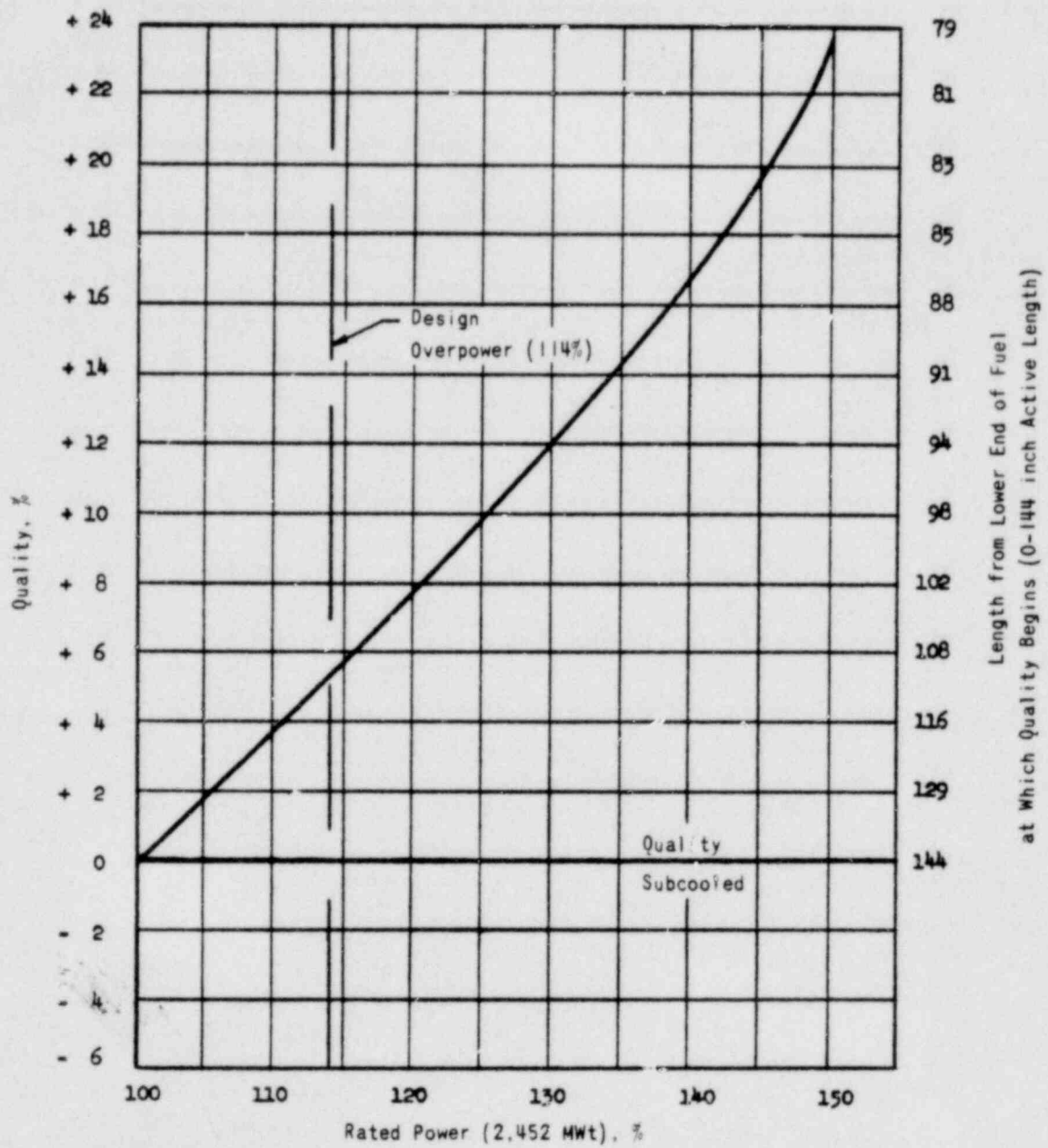
DNB RATIOS (BAW-168) VERSUS REACTOR POWER

CRYSTAL RIVER UNITS 3 & 4



FIGURE 3-16

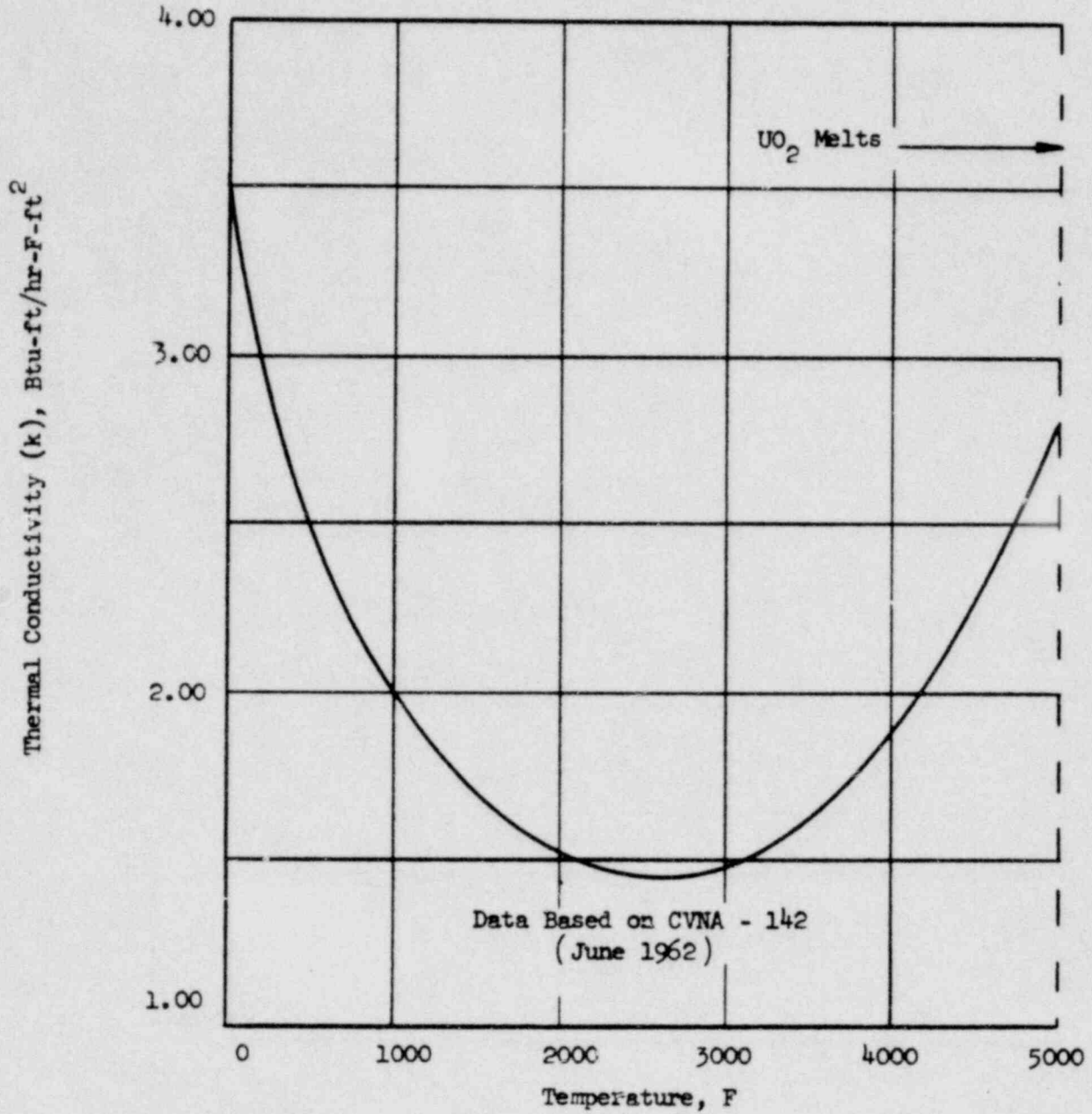
00000277



00000278

MAXIMUM HOT CHANNEL EXIT QUALITY
 VERSUS REACTOR OVERPOWER
 CRYSTAL RIVER UNITS 3 & 4



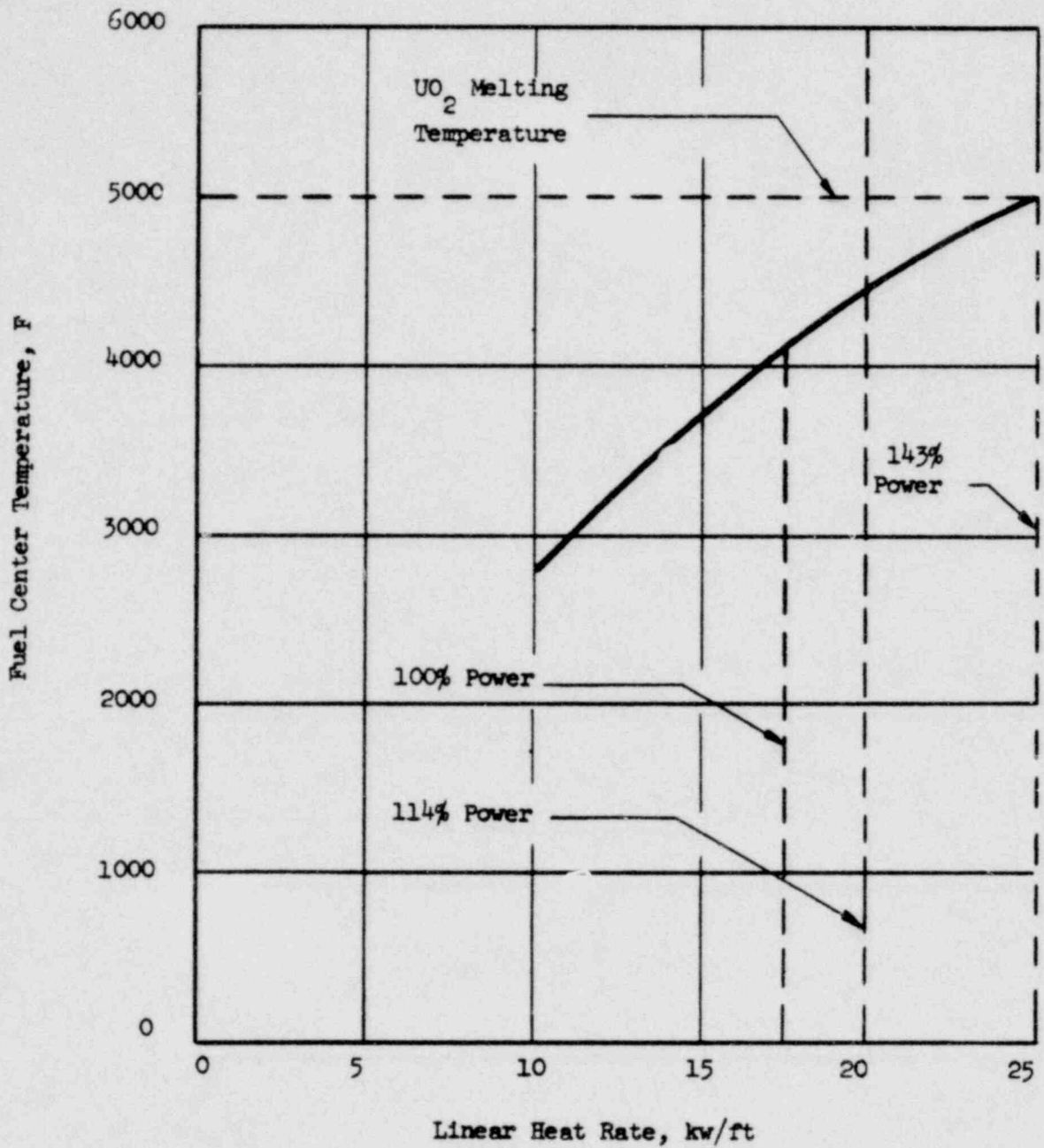


00000279

THERMAL CONDUCTIVITY OF UO₂
CRYSTAL RIVER UNITS 3 & 4



FIGURE 3-18



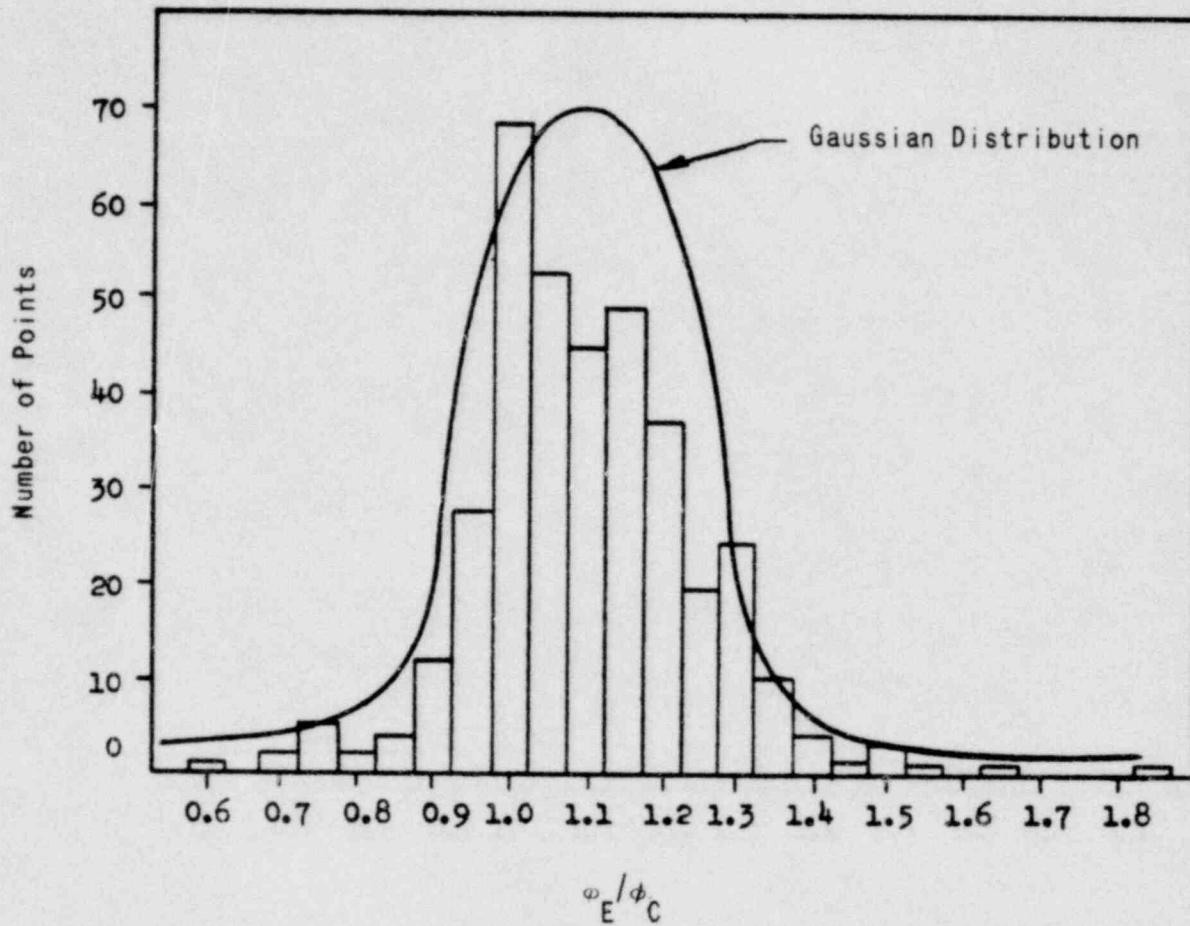
07000280

FUEL CENTER TEMPERATURE AT THE HOT SPOT
VERSUS LINEAR POWER

CRYSTAL RIVER UNITS 3 & 4



FIGURE 3-19



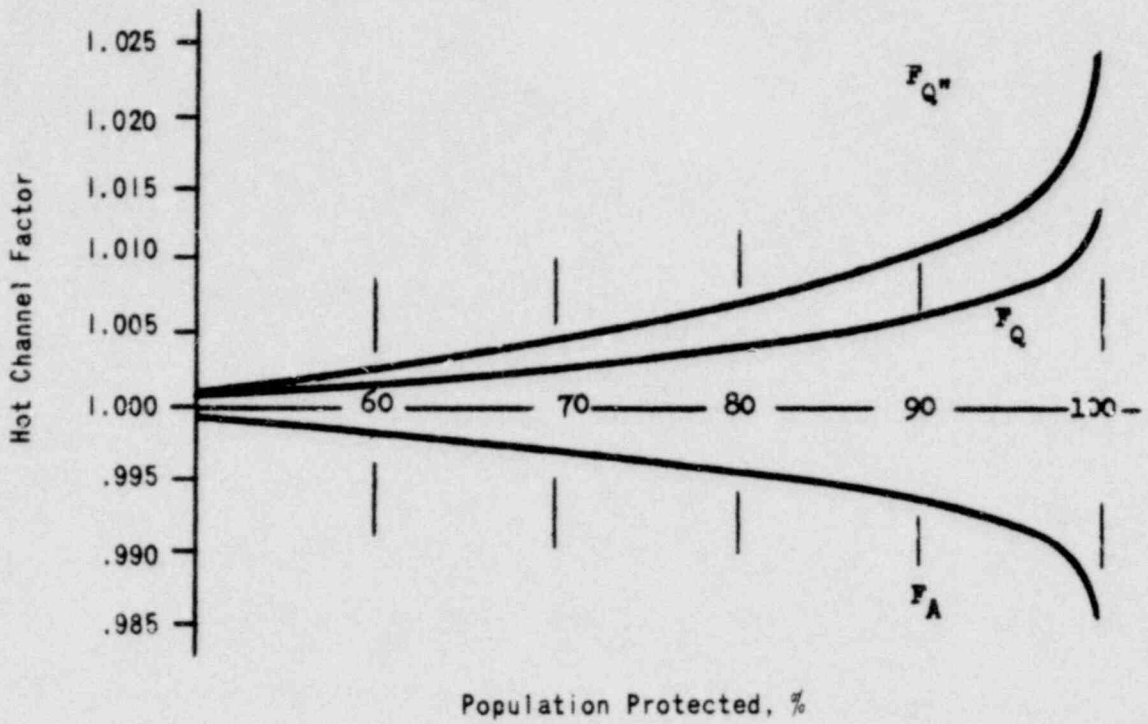
NUMBER OF DATA POINTS VERSUS ϕ_E/ϕ_C

CRYSTAL RIVER UNITS 3 & 4



FIGURE 3-20

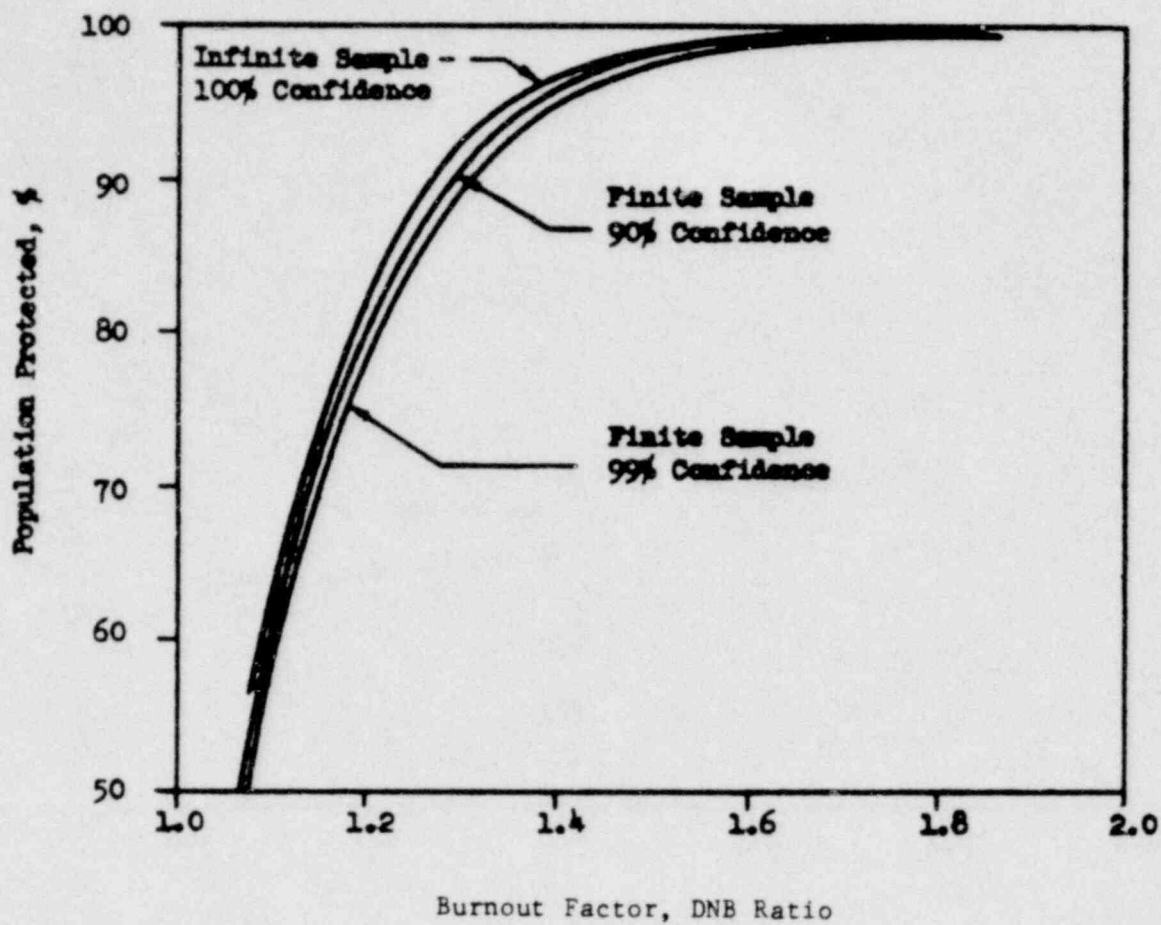
00000281



00000282

HOT CHANNEL FACTOR VERSUS
 PERCENT POPULATION PROTECTED
 CRYSTAL RIVER UNITS 3 & 4





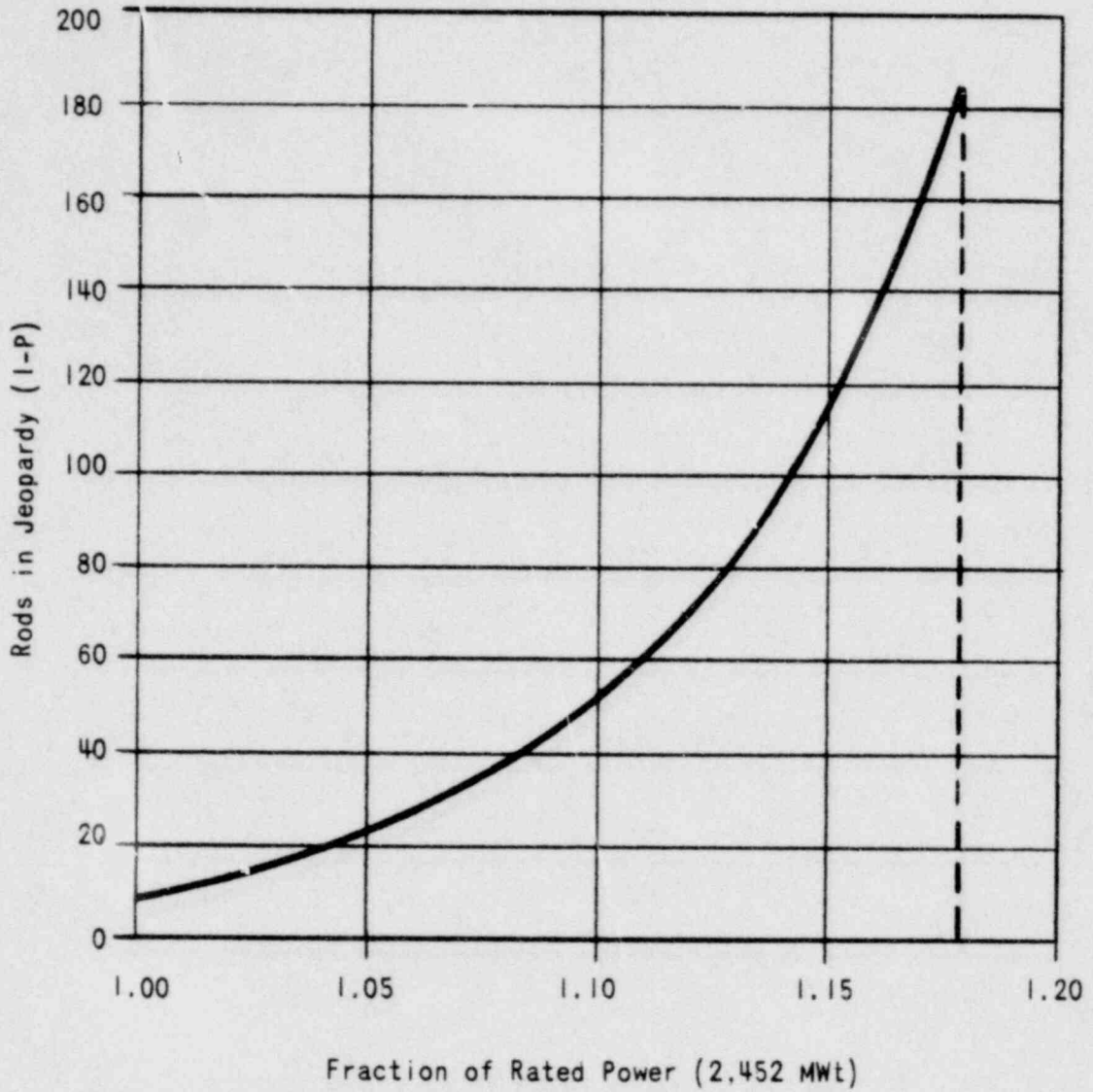
BURNOUT FACTOR VERSUS POPULATION
FOR VARIOUS CONFIDENCE LEVELS

CRYSTAL RIVER UNITS 3 & 4



FIGURE 3-22

00000283

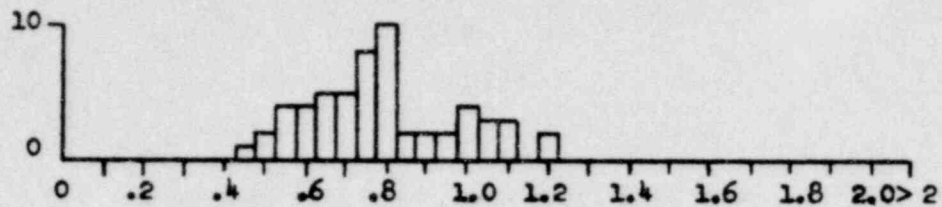


00000284

RODS IN JEOPARDY VERSUS POWER
CRYSTAL RIVER UNITS 3 & 4



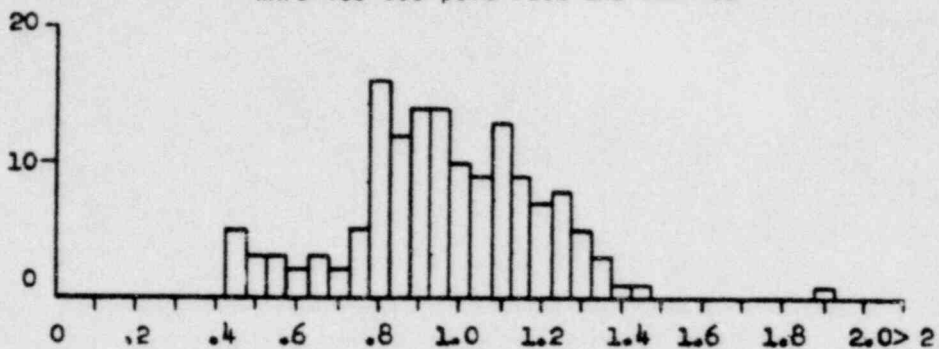
FIGURE 3-23



(1)

$$\phi_E/\phi_C$$

WAPD-188 500 psia Data and BAW-168

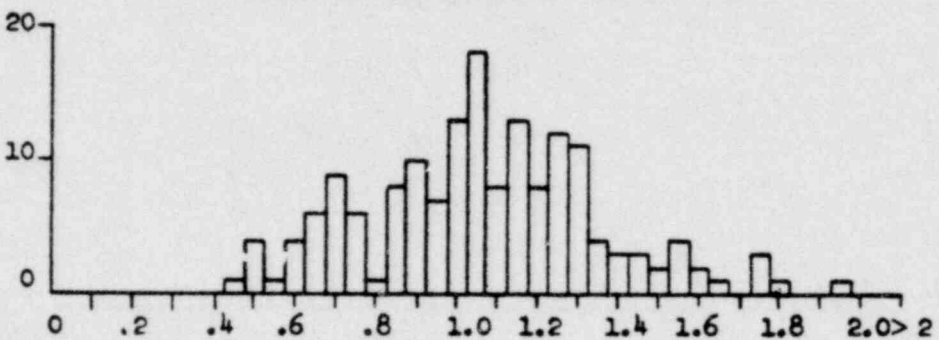


(2)

$$\phi_E/\phi_C$$

WAPD-188 600 psia Data and BAW-168

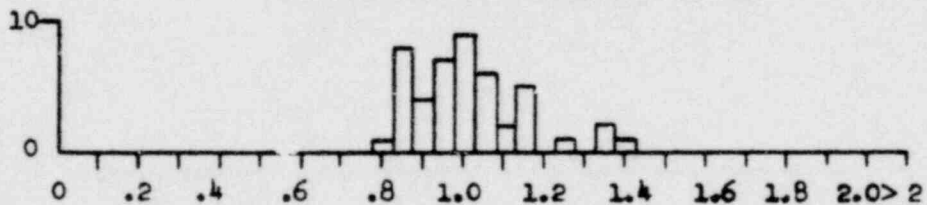
Number of Points



(3)

$$\phi_E/\phi_C$$

WAPD-188 1000 psia Data and BAW-168



(4)

$$\phi_E/\phi_C$$

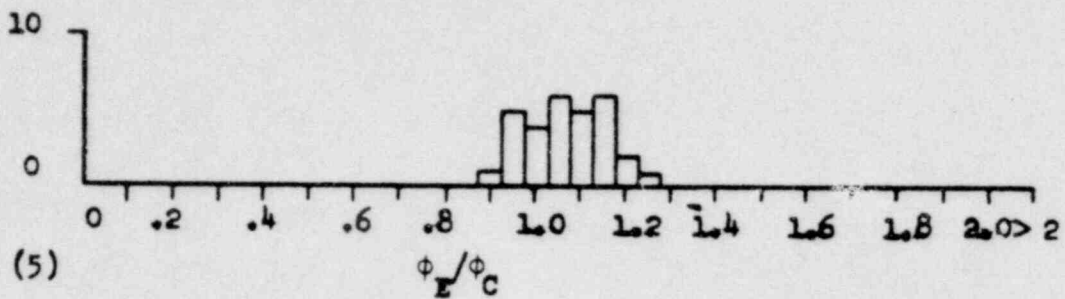
WAPD-188 1500 psia Data and BAW-168

RATIO OF EXPERIMENTAL TO
CALCULATED BURNOUT HEAT FLUX
CRYSTAL RIVER UNITS 3 & 4

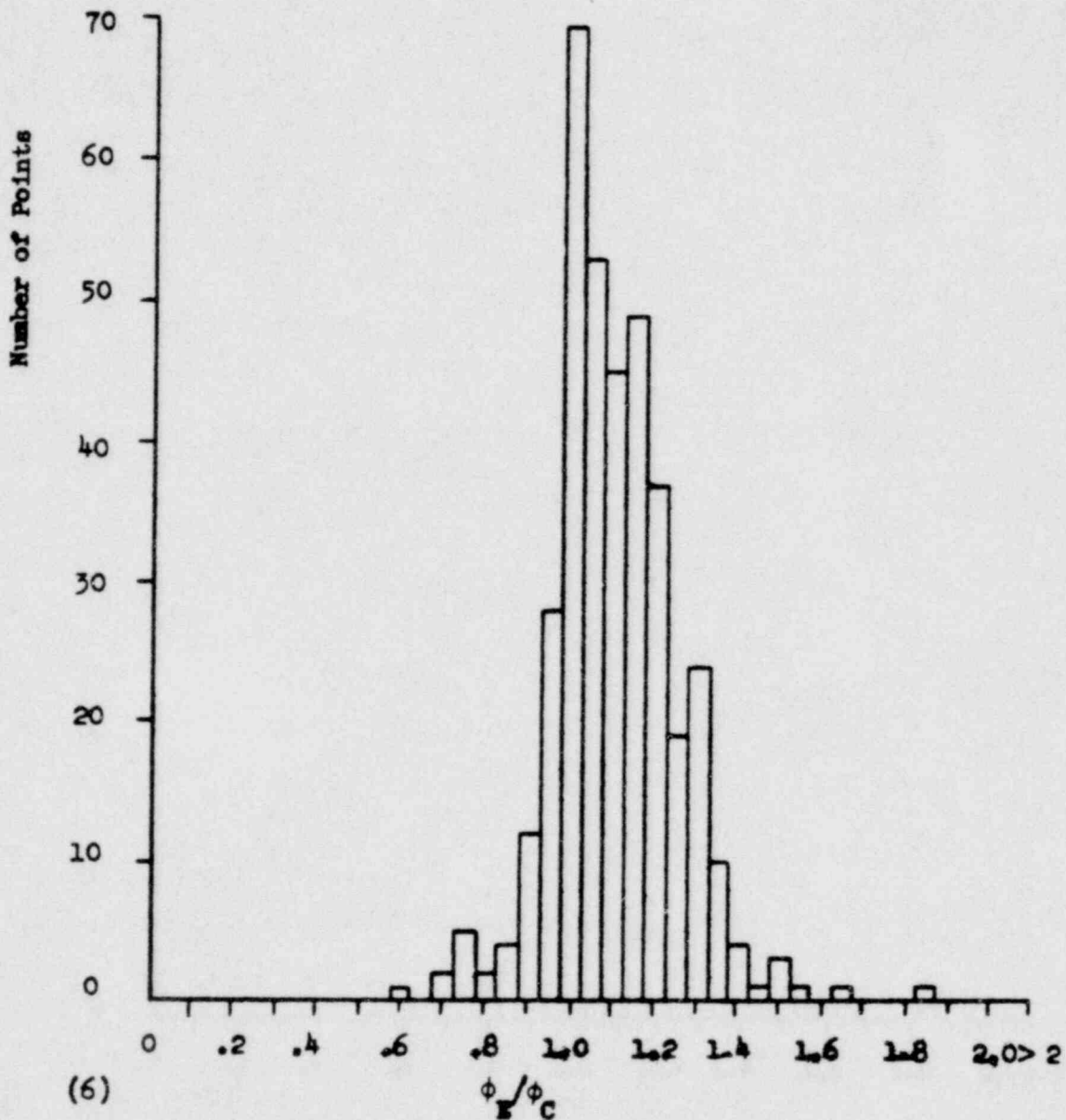
00000285



FIGURE 3-24



WAPD-188 1750 psia Data and BAW-168



WAPD-188 2000 psia Data and BAW-168

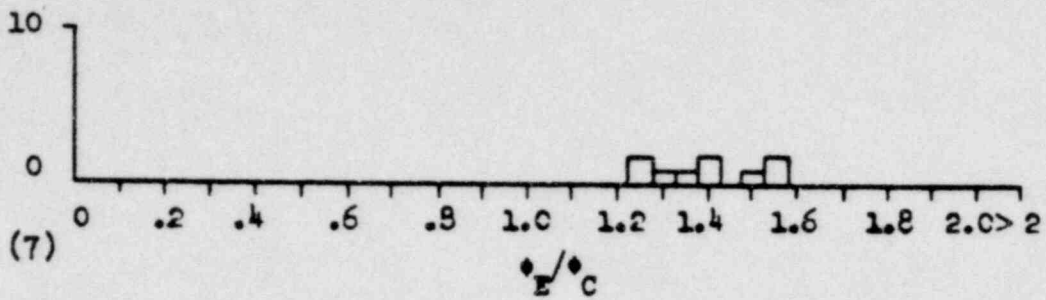
RATIO OF EXPERIMENTAL TO
CALCULATED BURNOUT HEAT FLUX

CRYSTAL RIVER UNITS 3 & 4

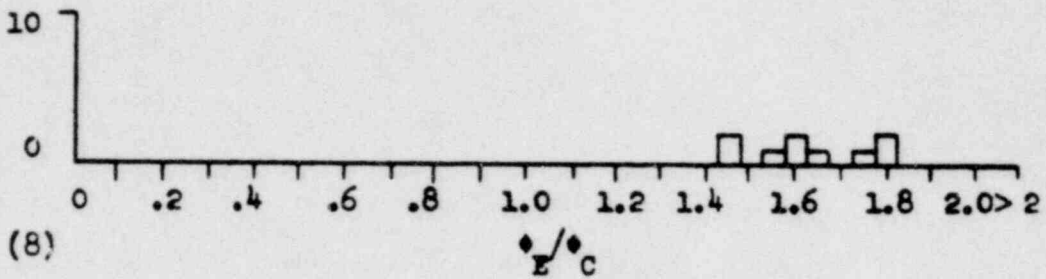
00000286



FIGURE 3-25

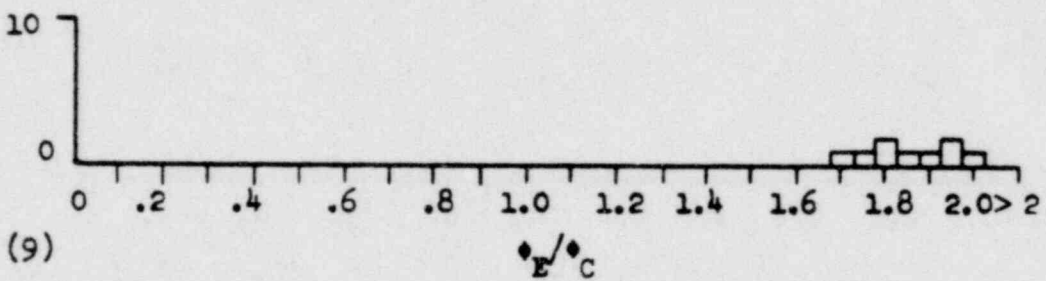


WAPD-188 2250 psia Data and BAW-168

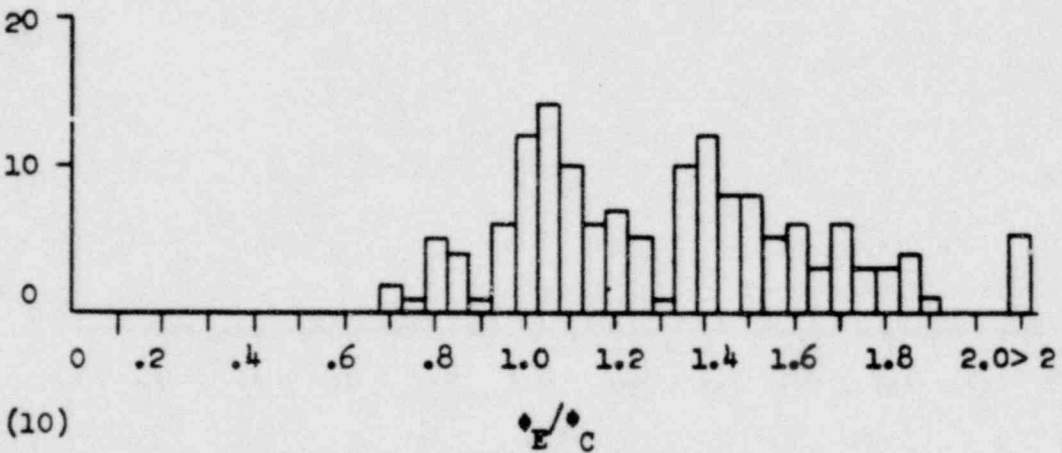


WAPD-188 2500 psia Data and BAW-168

Number of Points



WAPD-188 2750 psia Data and BAW-168

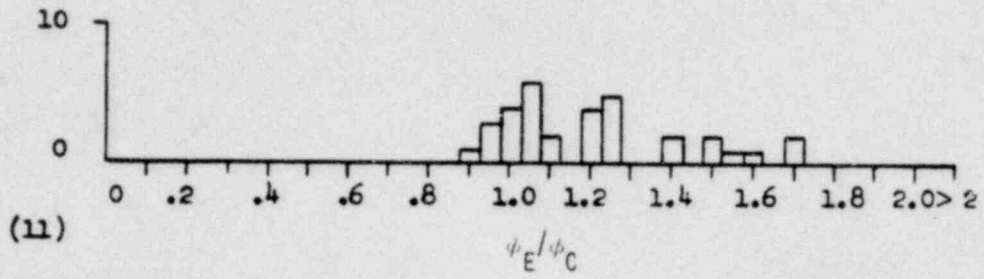


AEEW-R-213 560 psia Data and BAW-168

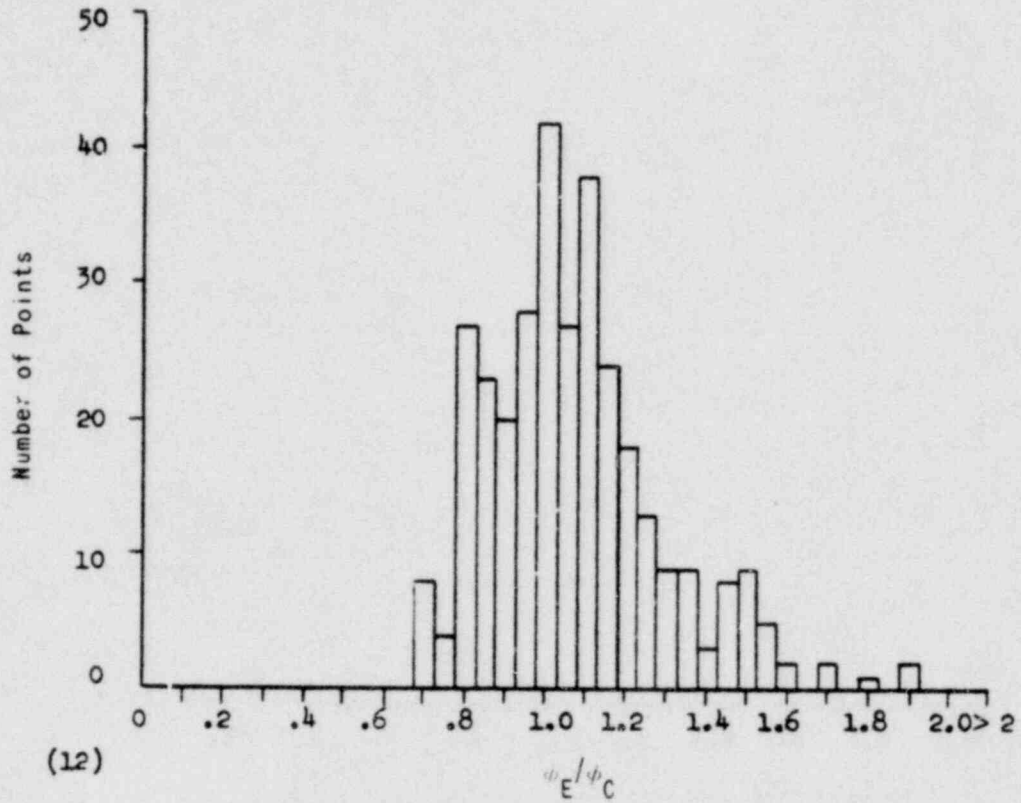
RATIO OF EXPERIMENTAL TO
CALCULATED BURNOUT HEAT FLUX
CRYSTAL RIVER UNITS 3 & 4

00000287

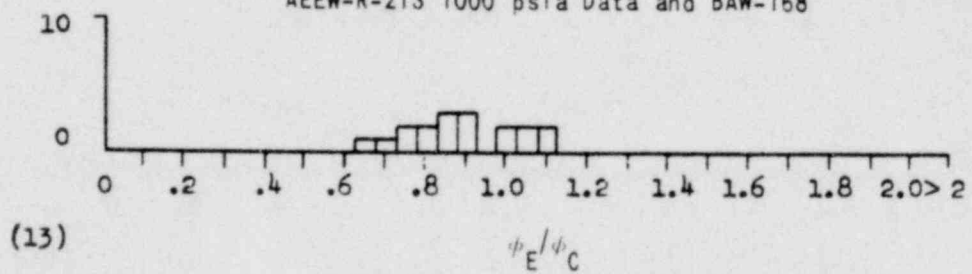




AEEW-R-213 720 psia Data and BAW-168



AEEW-R-213 1000 psia Data and BAW-168



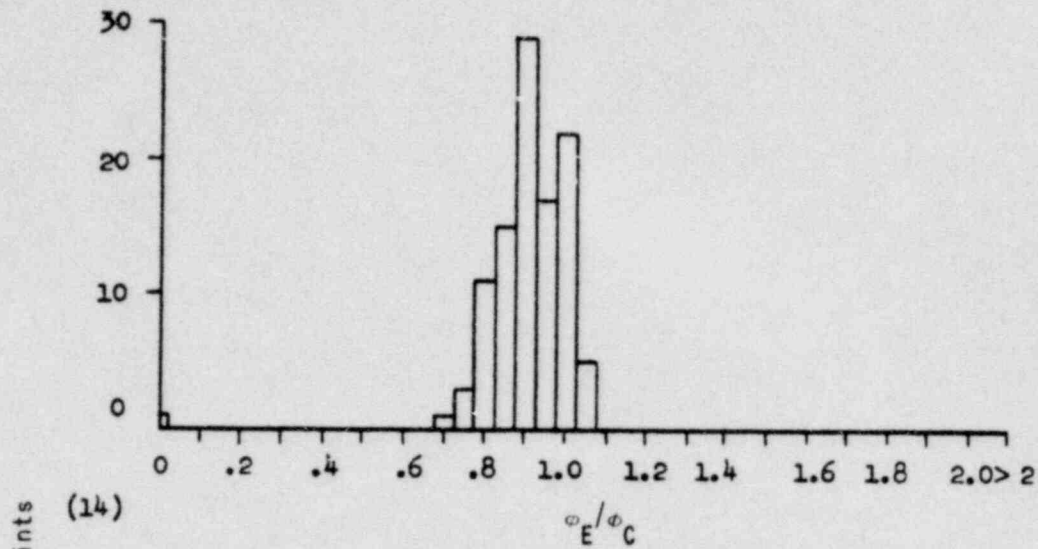
AEEW-R-213 1300 psia Data and BAW-168

00000288

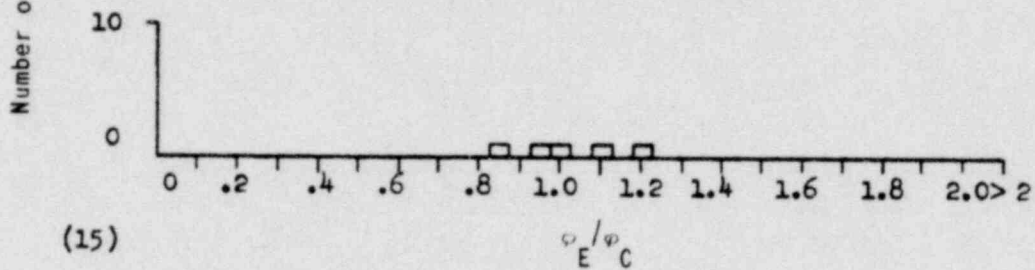
RATIO OF EXPERIMENTAL TO
CALCULATED BURNOUT HEAT FLUX
CRYSTAL RIVER UNITS 3 & 4



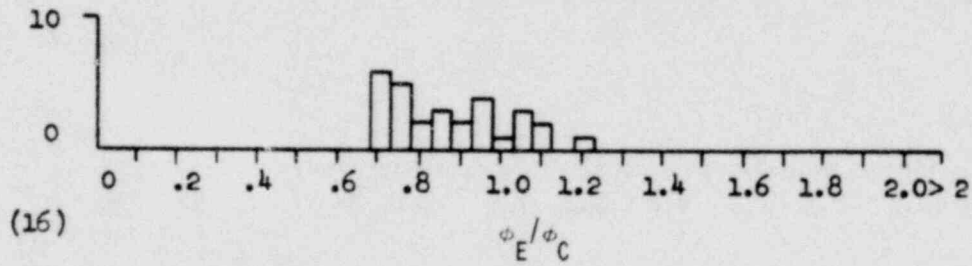
FIGURE 3-27



AEEW-R-213 1500 psia Data and BAW-168



Columbia 500 psia Data and BAW-168



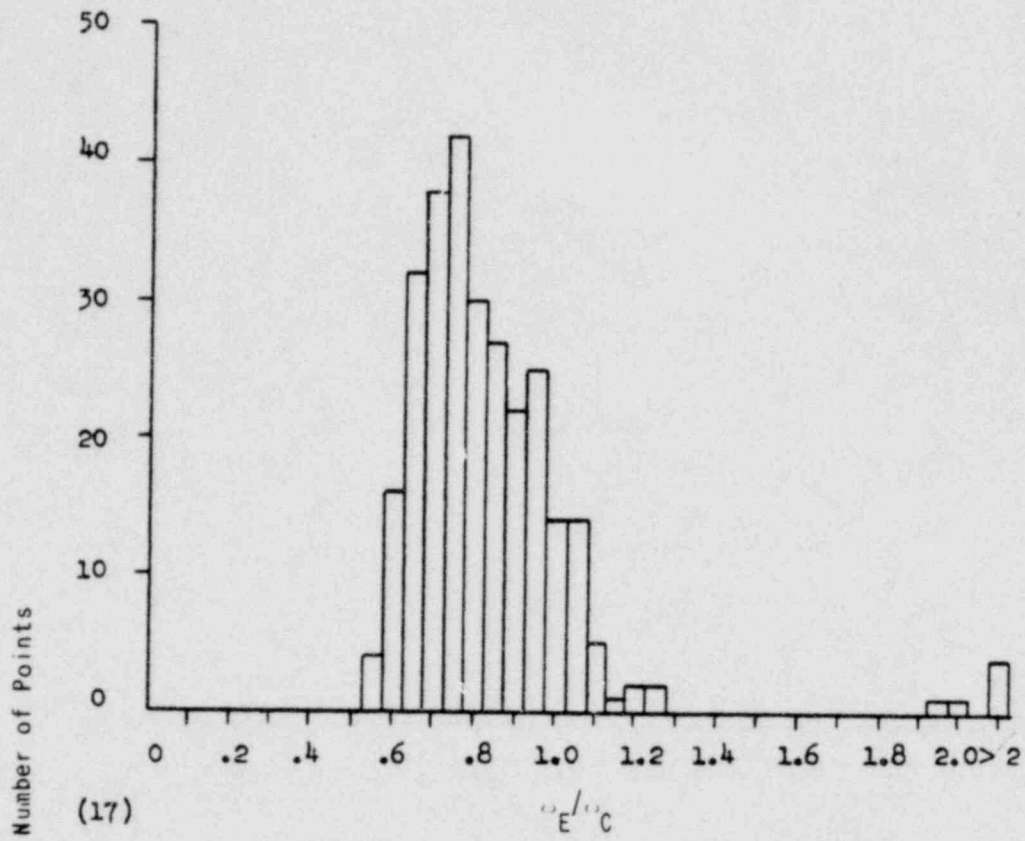
Columbia 720 psia Data and BAW-168

RATIO OF EXPERIMENTAL TO
CALCULATED BURNOUT HEAT FLUX
CRYSTAL RIVER UNITS 3 & 4

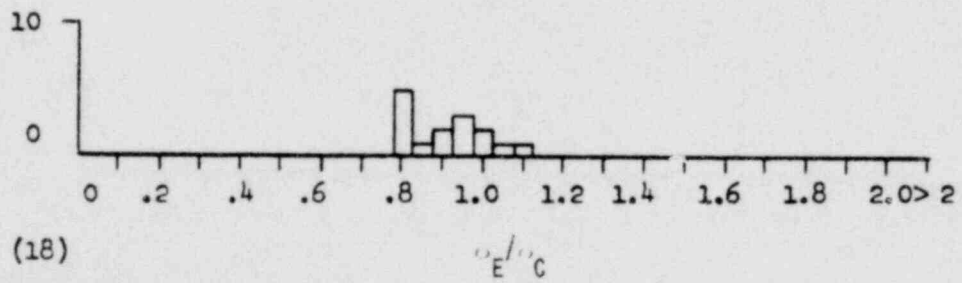


FIGURE 3-28

00000289



Columbia 1000 psia Data and BAW-168

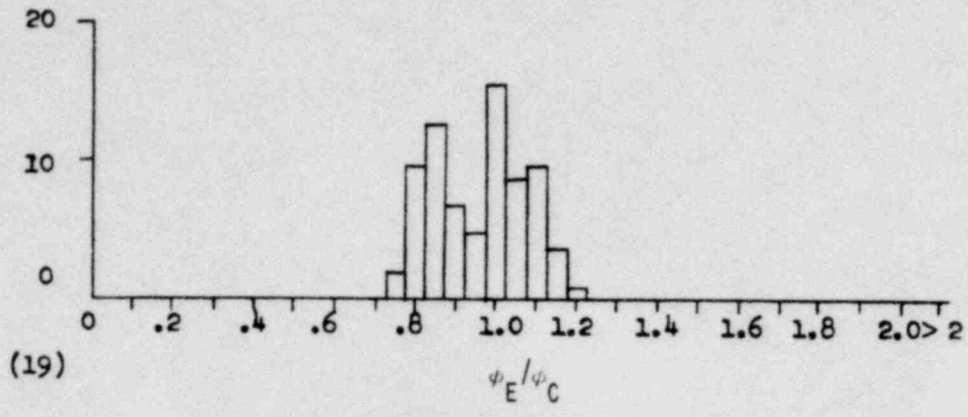


Columbia 1200 psia Data and BAW-168

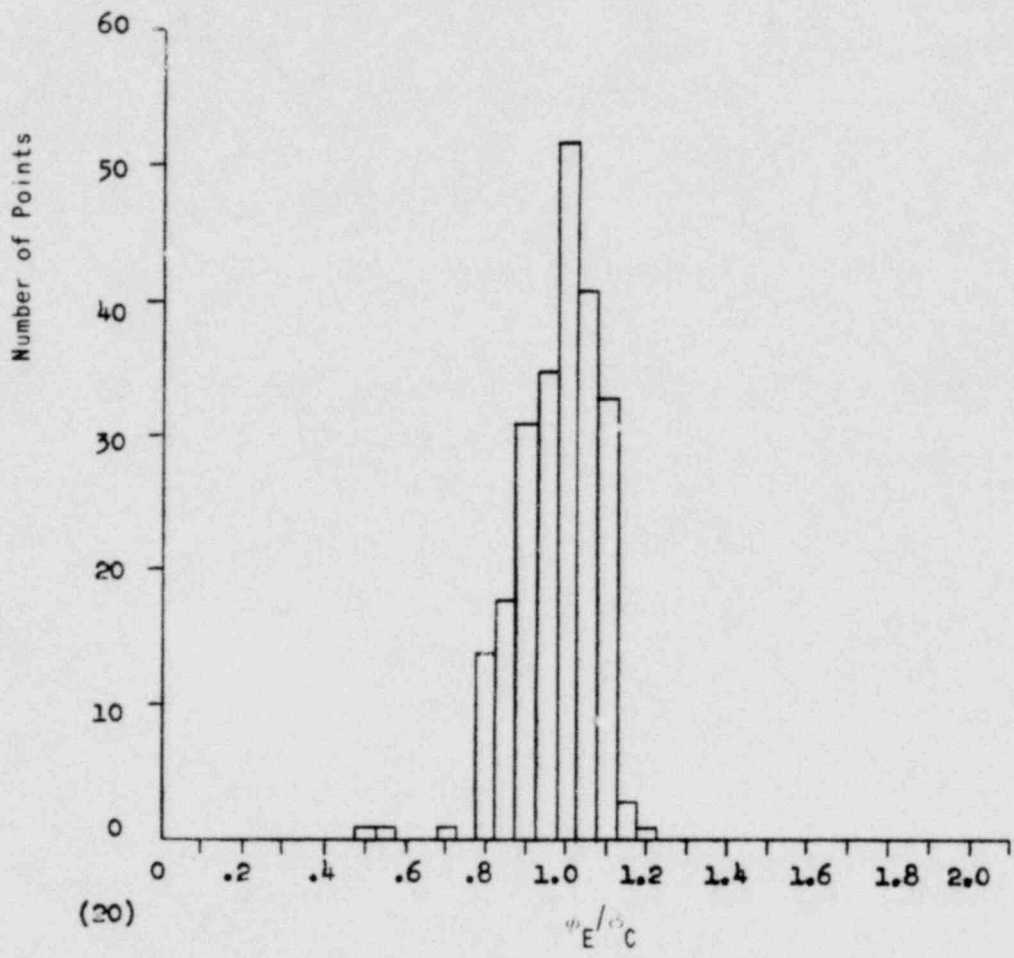
00000290

RATIO OF EXPERIMENTAL TO
CALCULATED BURNOUT HEAT FLUX
CRYSTAL RIVER UNITS 3 & 4





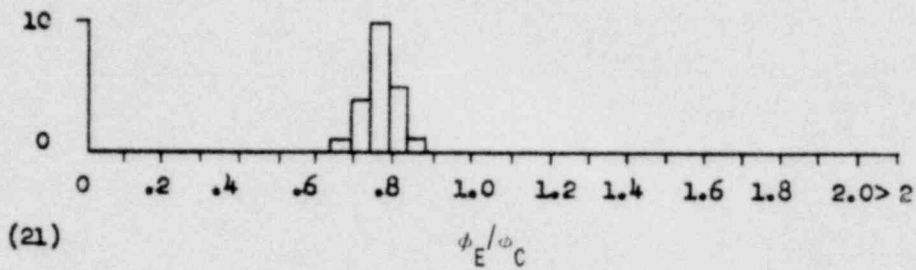
Columbia 1500 psia Data and BAW-168



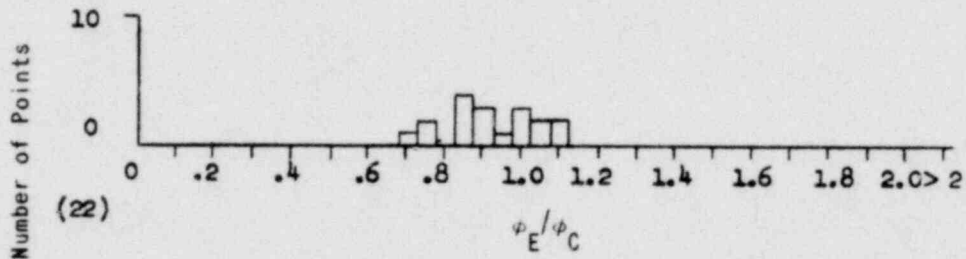
Argonne 2000 psia Data and BAW-168

RATIO OF EXPERIMENTAL TO
CALCULATED BURNOUT HEAT FLUX
CRYSTAL RIVER UNITS 3 & 4

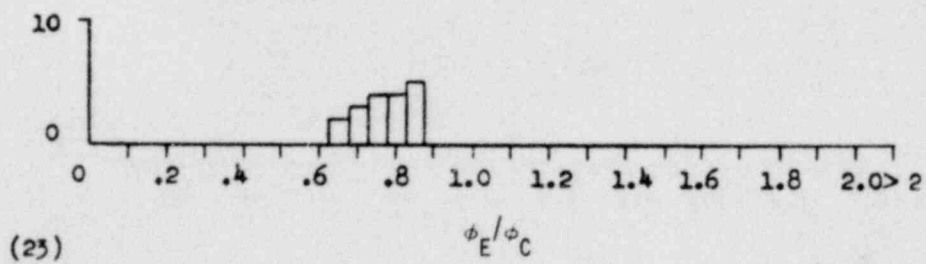




B&W 2000 psia Data and BAW-168



Euratom 1000 psia Data and BAW-168



Euratom 1500 psia Data and BAW-168

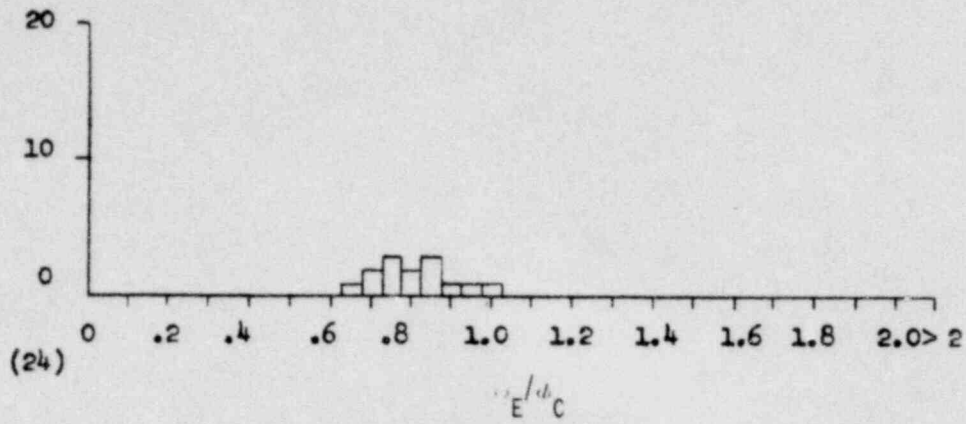
10000292

RATIO OF EXPERIMENTAL TO
CALCULATED BURNOUT HEAT FLUX

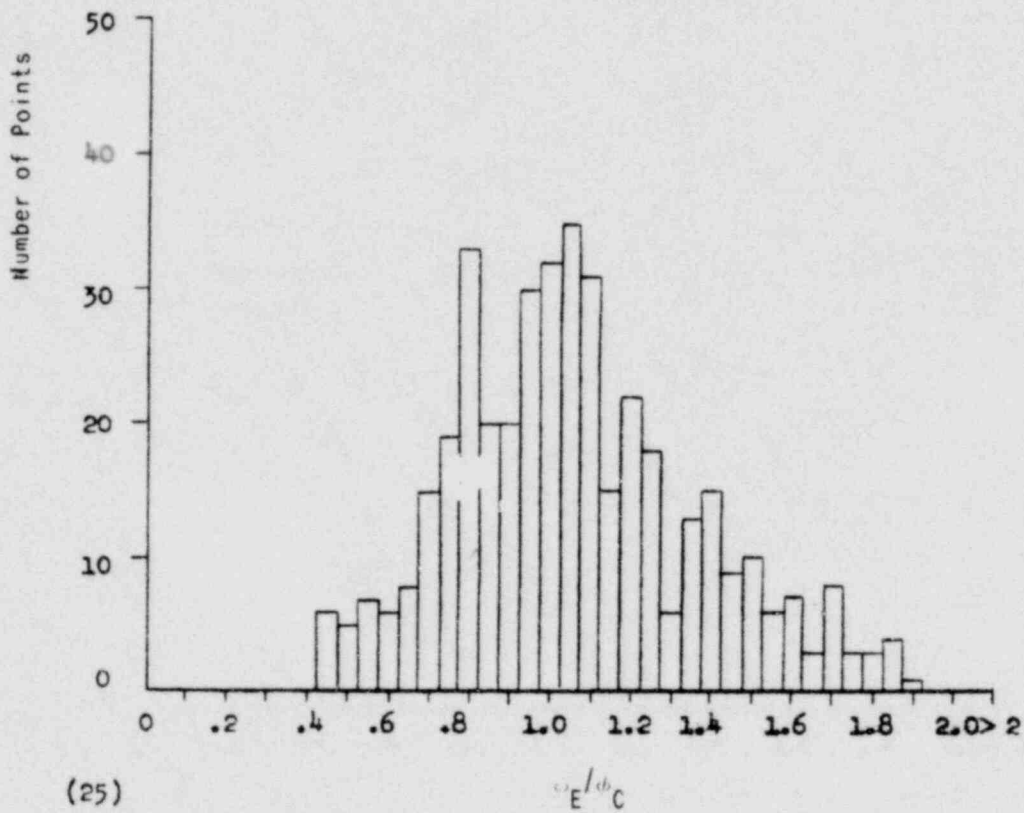
CRYSTAL RIVER UNITS 3 & 4



FIGURE 3-31



Euratom 2000 psia Data and BAW-168



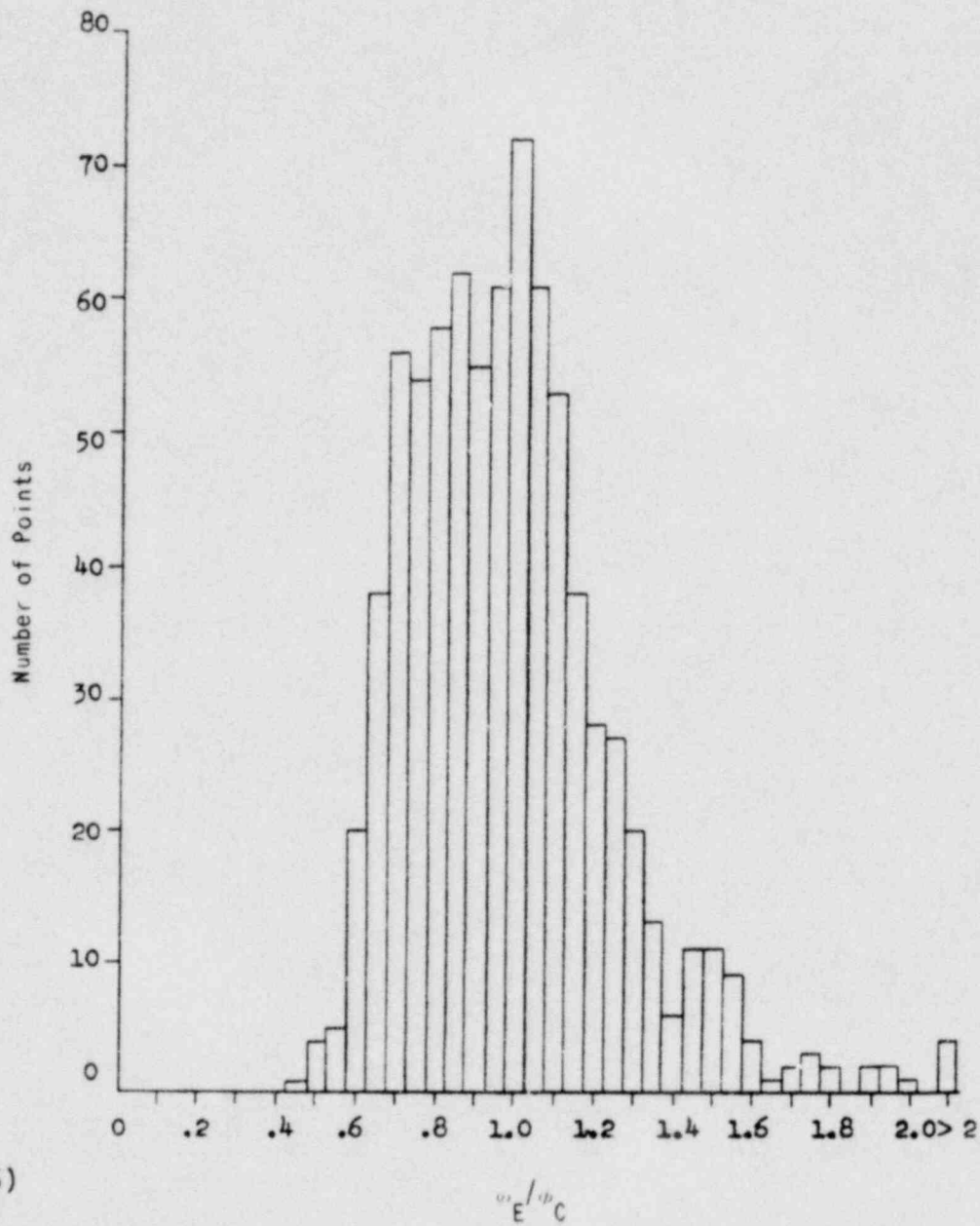
All 500-720 psia Data and BAW-168

RATIO OF EXPERIMENTAL TO
CALCULATED BURNOUT HEAT FLUX
CRYSTAL RIVER UNITS 3 & 4



FIGURE 3-32

00000293



All 1000 psia Data and BAW-168

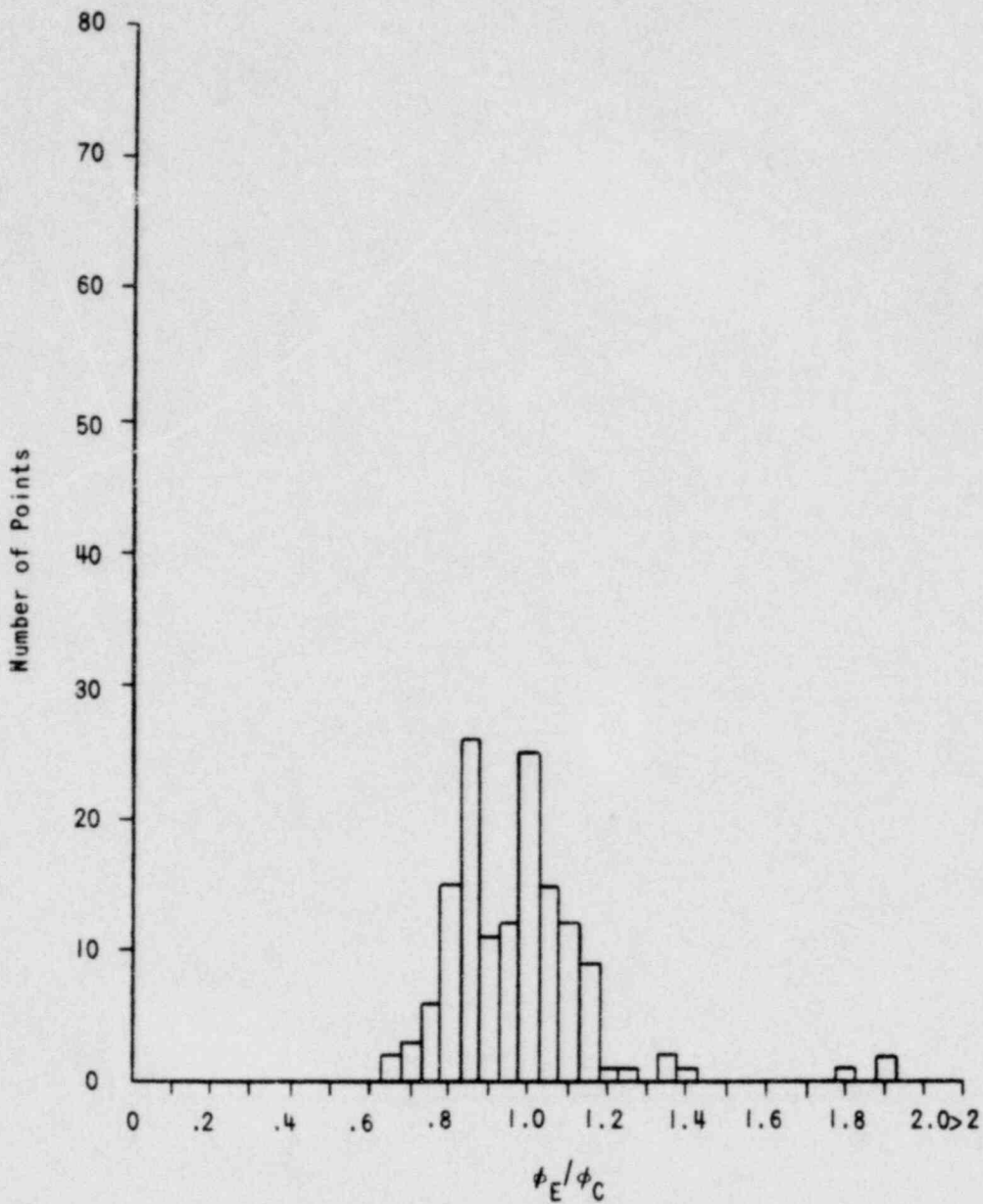
00000294

RATIO OF EXPERIMENTAL TO
CALCULATED BURNOUT HEAT FLUX

CRYSTAL RIVER UNITS 3 & 4



FIGURE 3-33



All 1500 psia Data and BAW-168

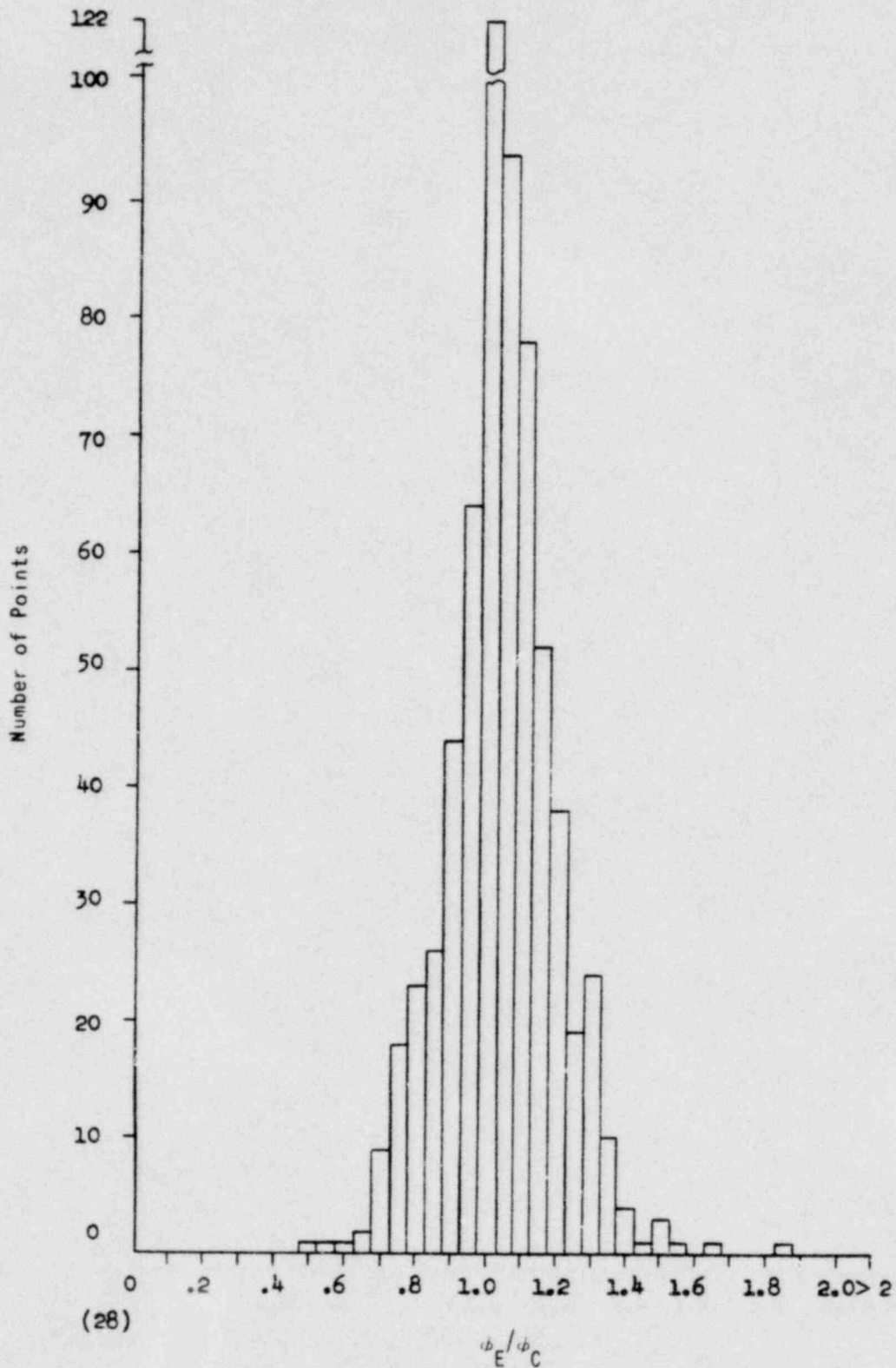
RATIO OF EXPERIMENTAL TO
CALCULATED BURNOUT HEAT FLUX

CRYSTAL RIVER UNITS 3 & 4



FIGURE 3-34

00000295



All 2000 osia Data and BAW-168

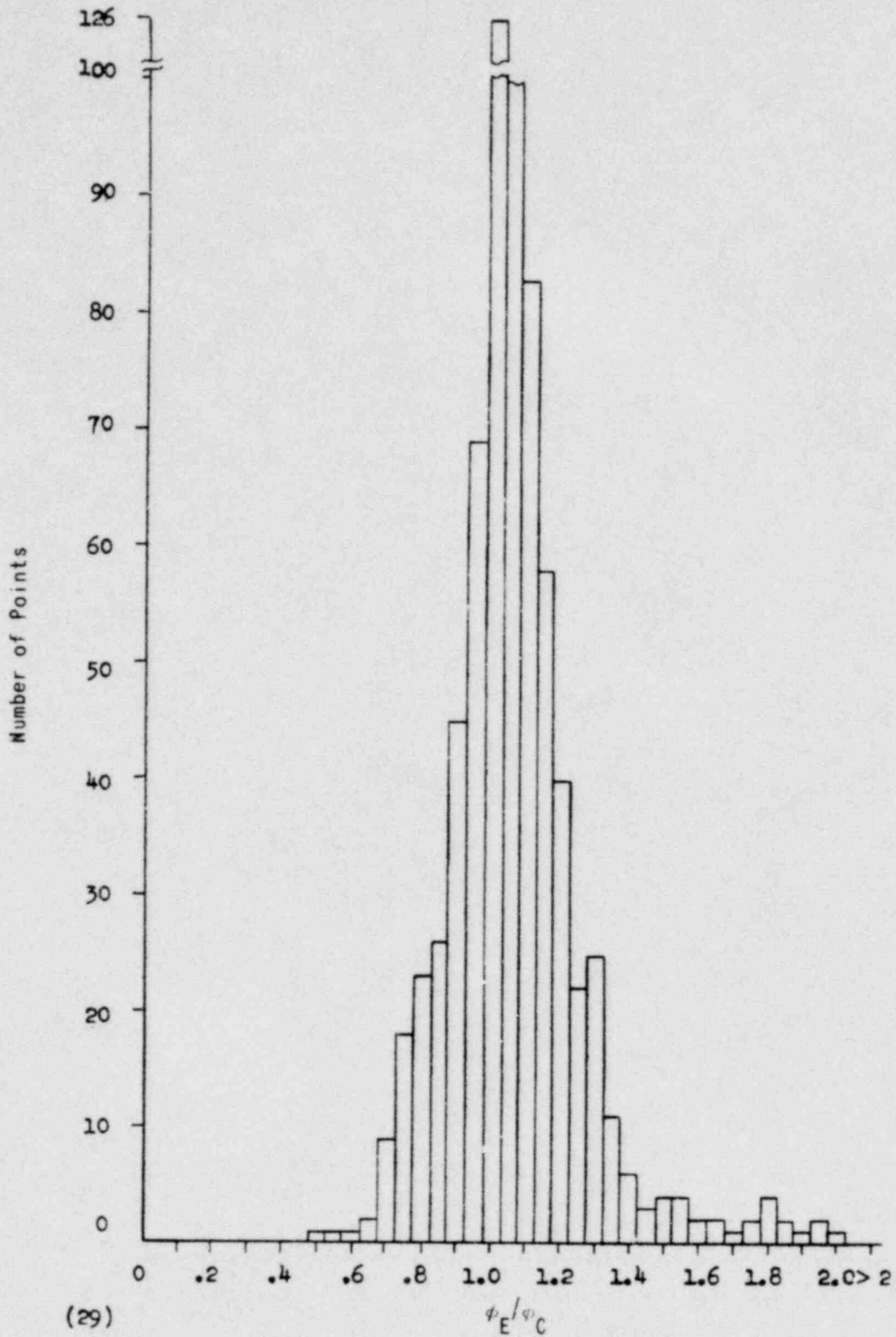
00000296

RATIO OF EXPERIMENTAL TO
CALCULATED BURNOUT HEAT FLUX

CRYSTAL RIVER UNITS 3 & 4



FIGURE 3-35



All 1750-2750 osia Data and BAW-168

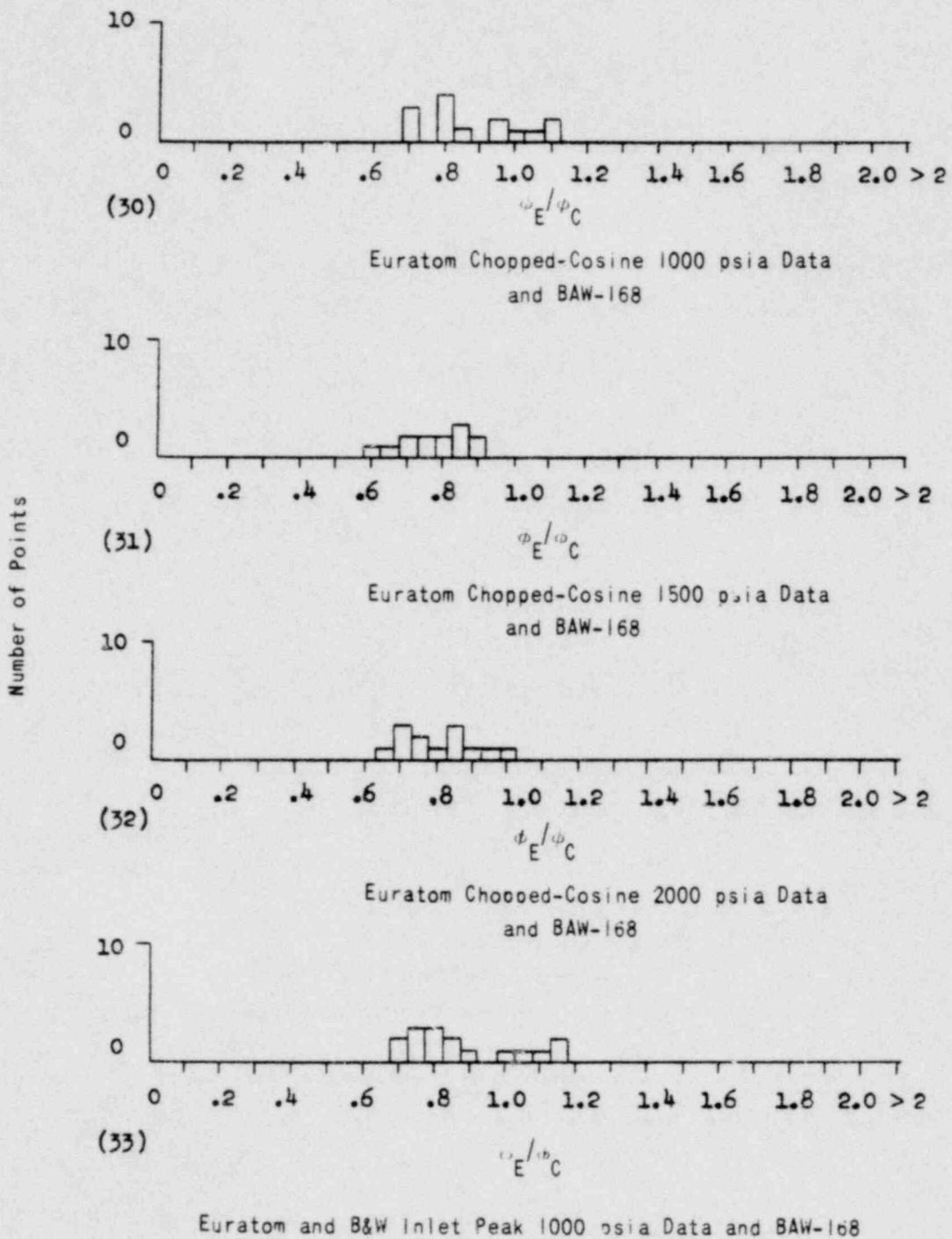
RATIO OF EXPERIMENTAL TO
CALCULATED BURNOUT HEAT FLUX

CRYSTAL RIVER UNITS 3 & 4



FIGURE 3-36

00000297

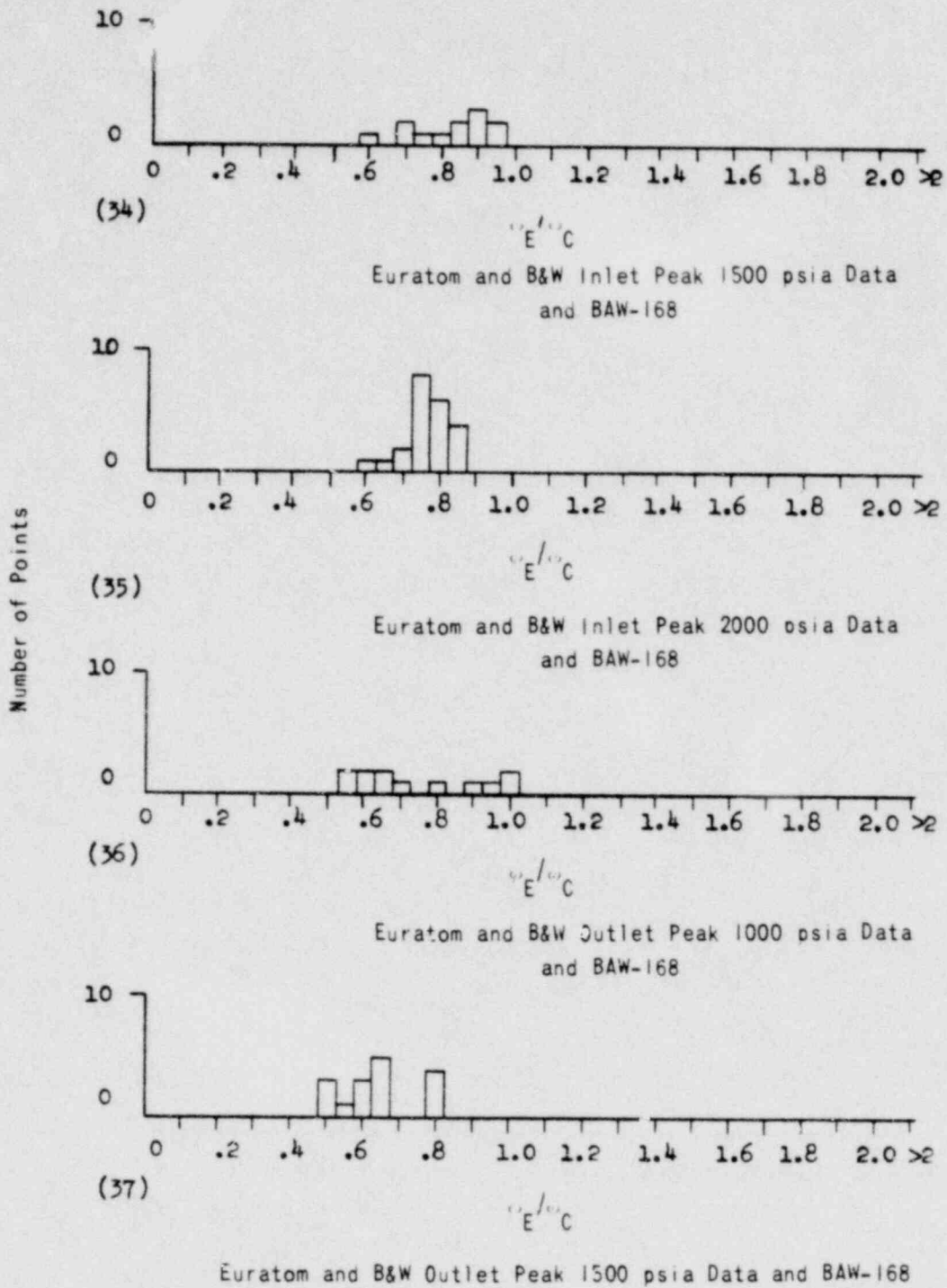


00000298

RATIO OF EXPERIMENTAL TO
CALCULATED BURNOUT HEAT FLUX
CRYSTAL RIVER UNITS 3 & 4



FIGURE 3-37



RATIO OF EXPERIMENTAL TO
CALCULATED BURNOUT HEAT FLUX

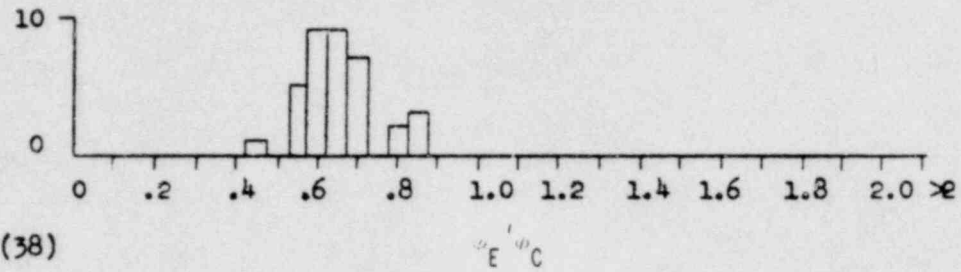
CRYSTAL RIVER UNITS 3 & 4



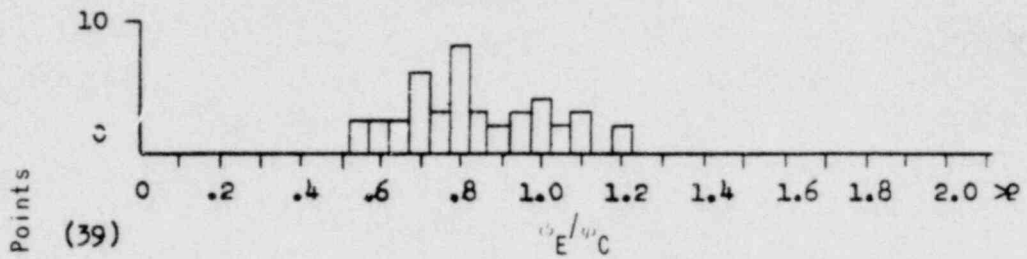
FIGURE 3-38

00000299

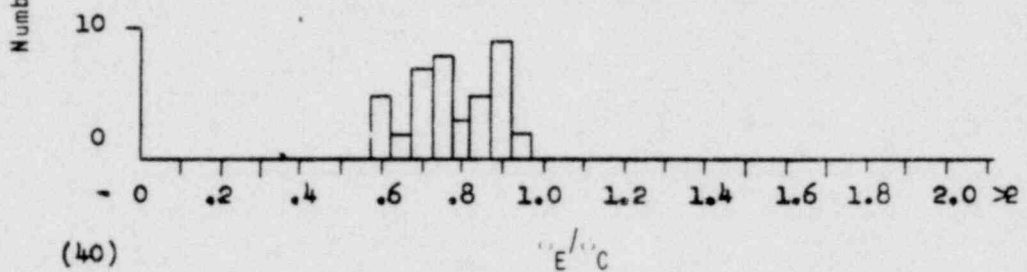
310



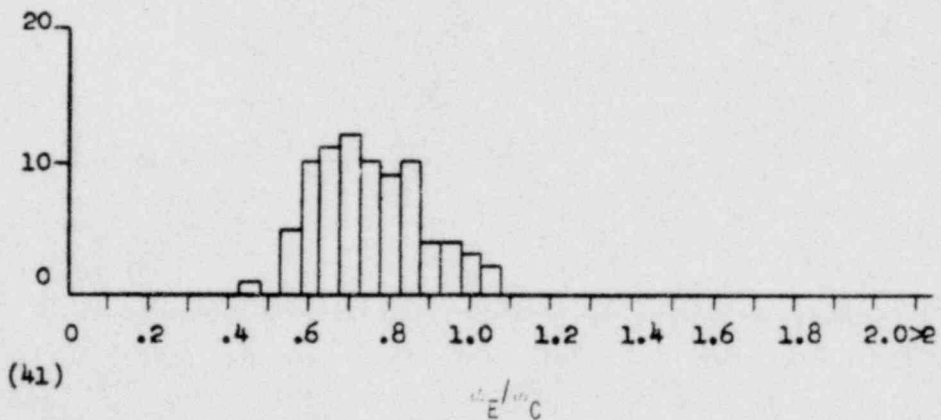
Euratom and B&W Outlet Peak 2000 psia
Data and BAW-168



All 1000 psia Non-Uniform Data and BAW-168



All 1500 psia Non-Uniform Data and BAW-168



All 2000 psia Non-Uniform Data and BAW-168

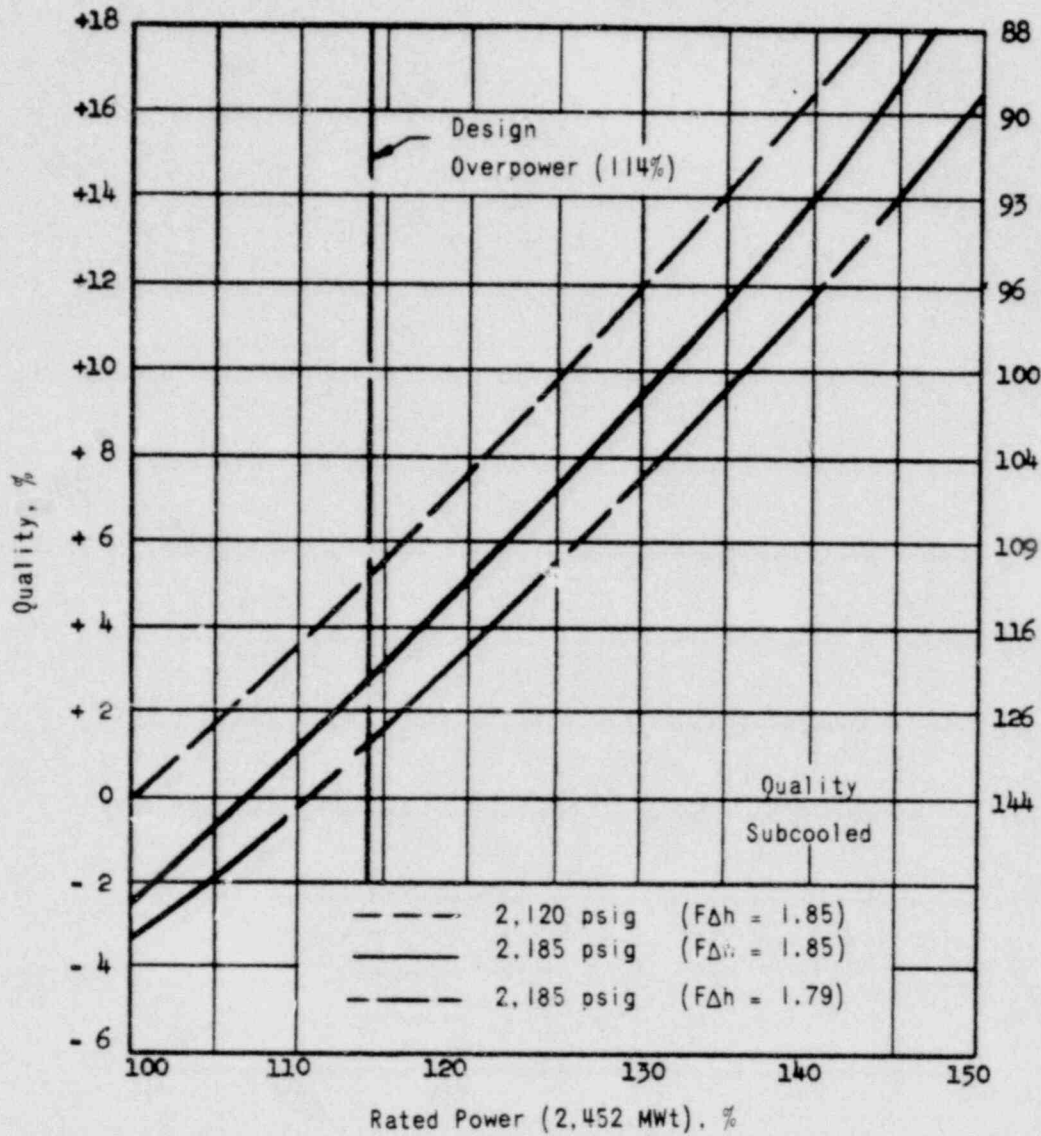
00000500

RATIO OF EXPERIMENTAL TO
CALCULATED BURNOUT HEAT FLUX
CRYSTAL RIVER UNITS 3 & 4



FIGURE 3-39

AMEND. 1 (1-15-68)



MAXIMUM HOT CHANNEL EXIT QUALITY
VERSUS REACTOR POWER

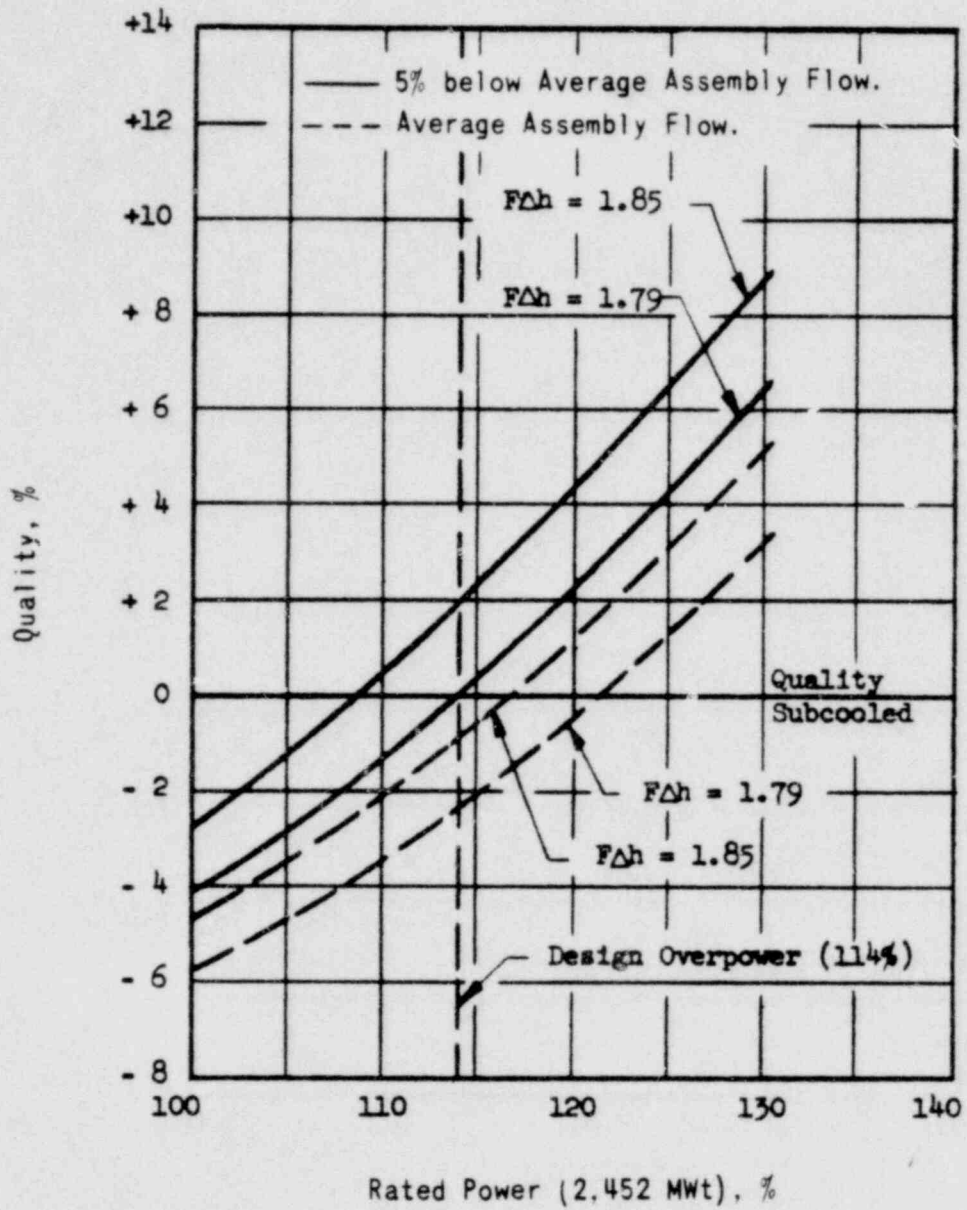
CRYSTAL RIVER UNITS 3 & 4



FIGURE 3-40

AMEND. 1 (1-15-68)

00000301



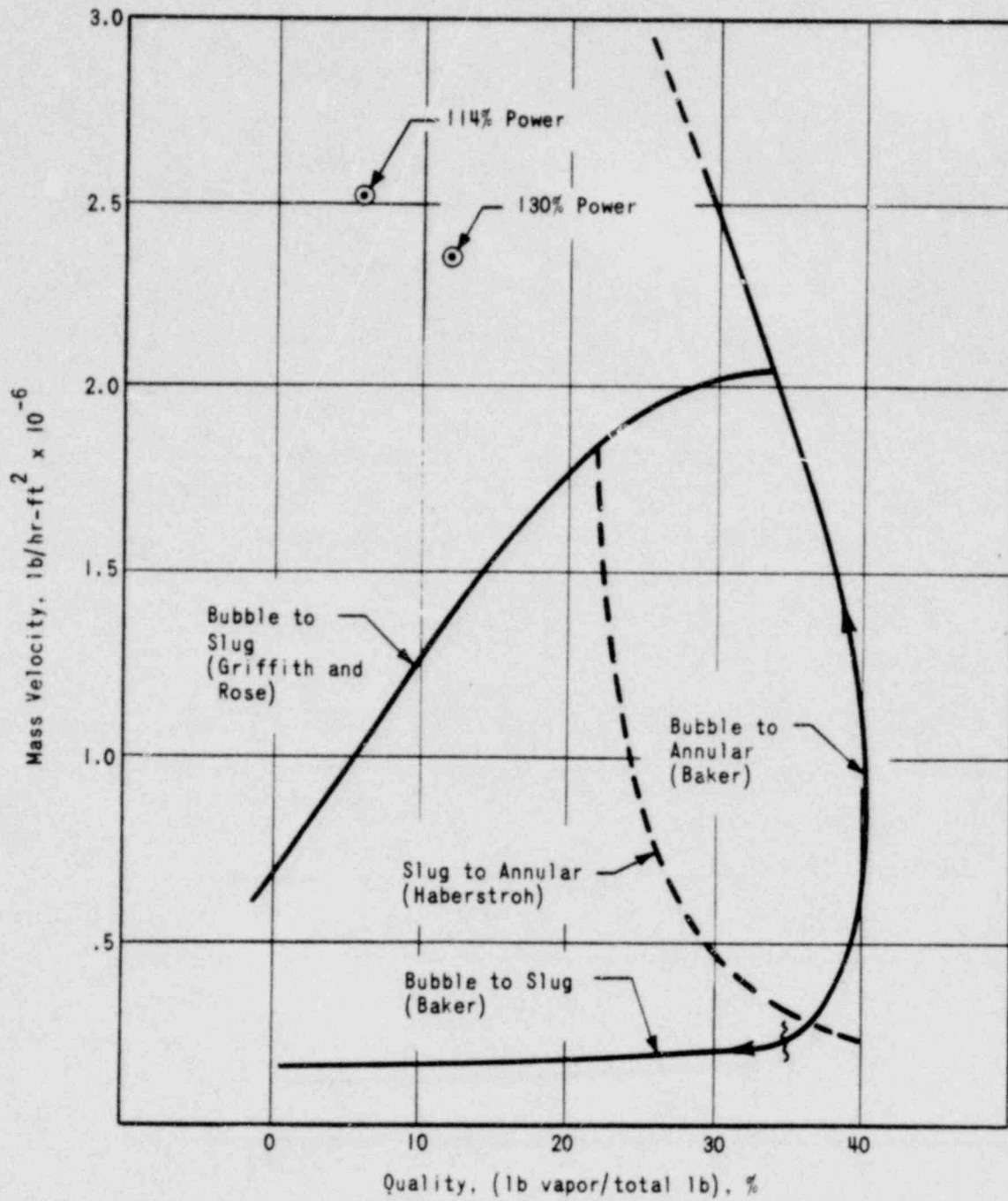
HOTTEST DESIGN & NOMINAL CHANNEL
EXIT QUALITY VERSUS REACTOR POWER
(WITHOUT ENGINEERING HOT CHANNEL FACTORS)

302

CRYSTAL RIVER UNITS 3 & 4



FIGURE 3-41



FLOW REGIME MAP FOR UNIT CELL CHANNEL
AT 2120 PSIG

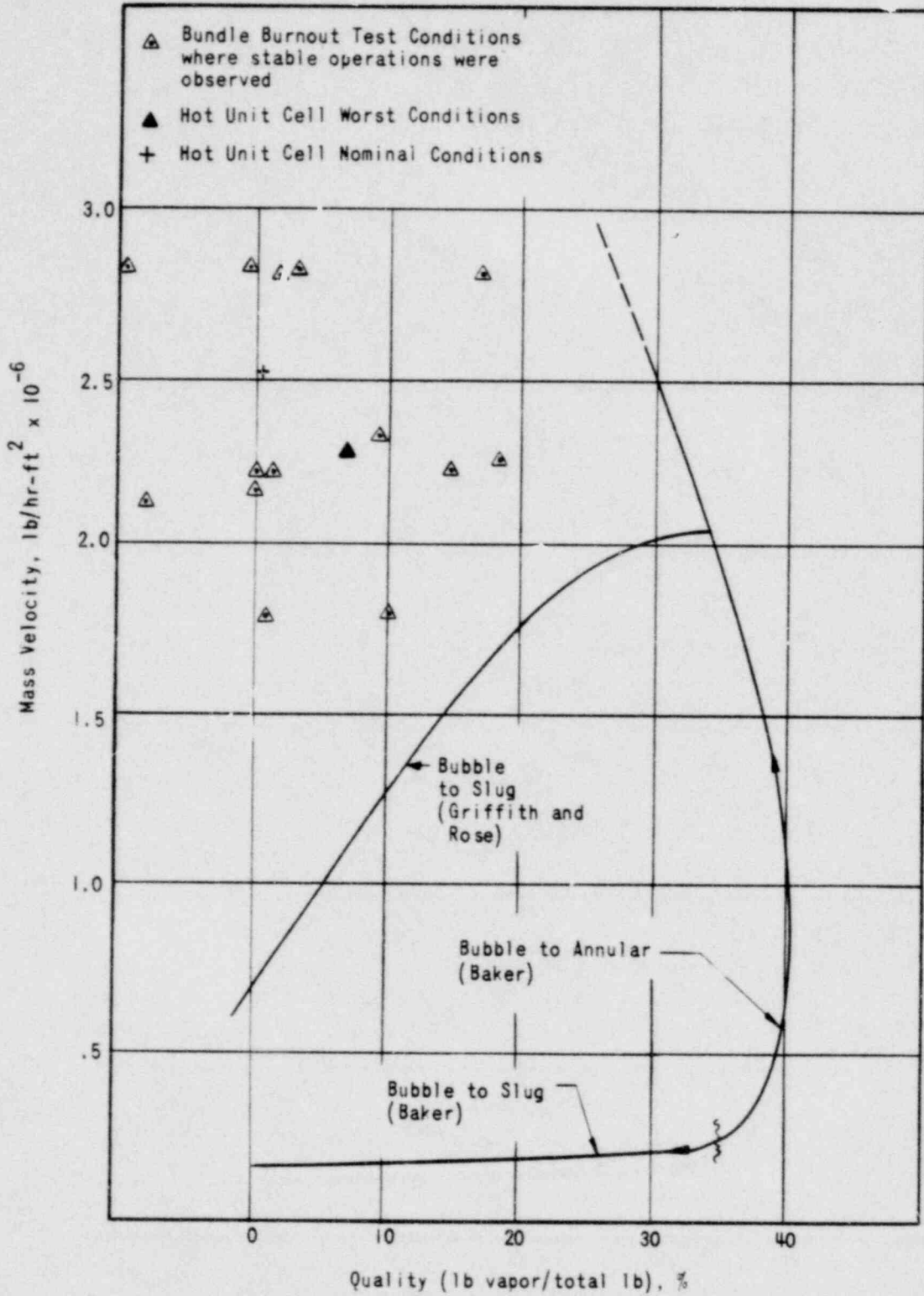
CRYSTAL RIVER UNITS 3 & 4



FIGURE 3-42

~~000000~~

00000303

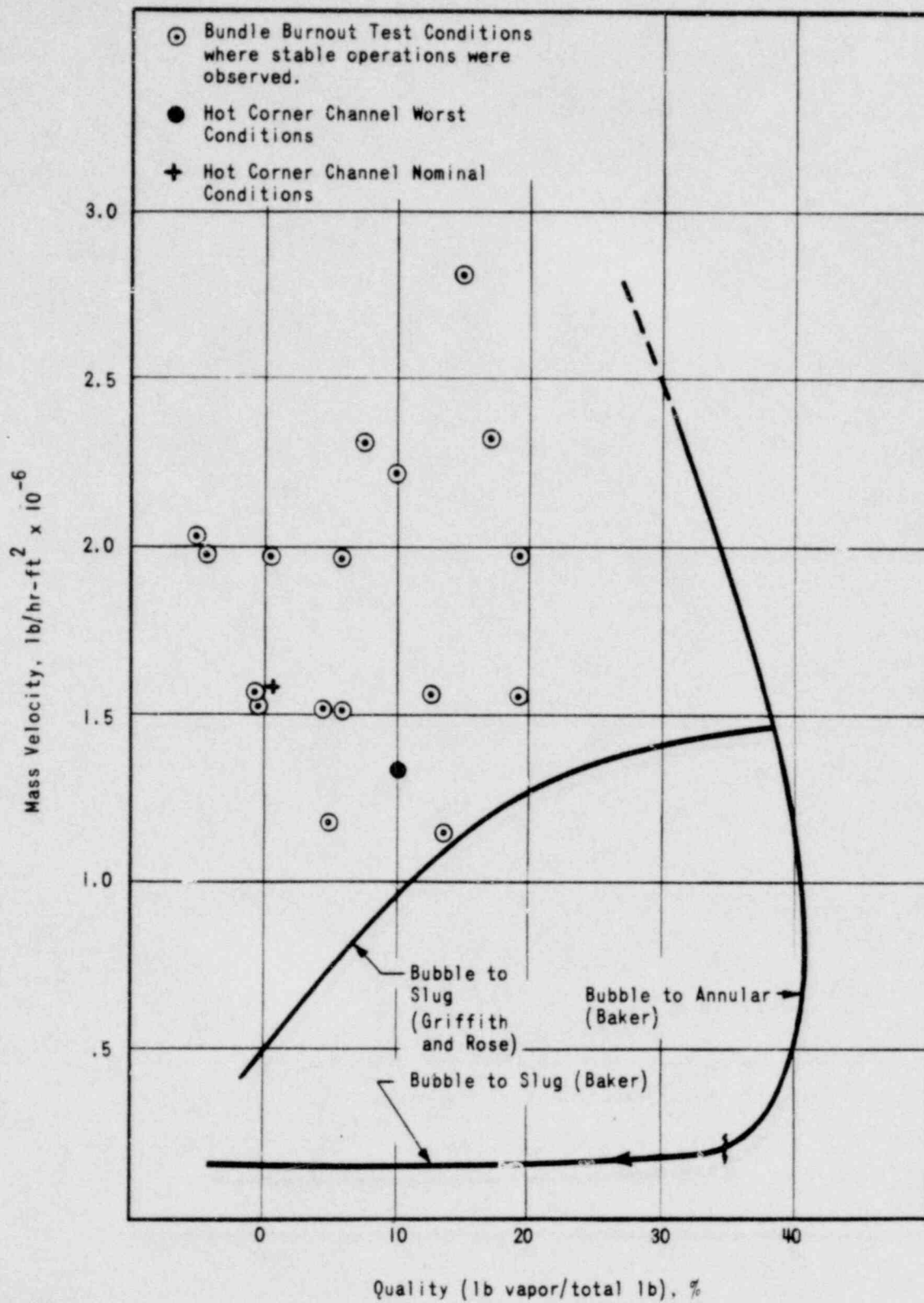


00000504

FLOW REGIME MAP FOR UNIT CELL CHANNEL
CRYSTAL RIVER UNITS 3 & 4



FIGURE 3-43



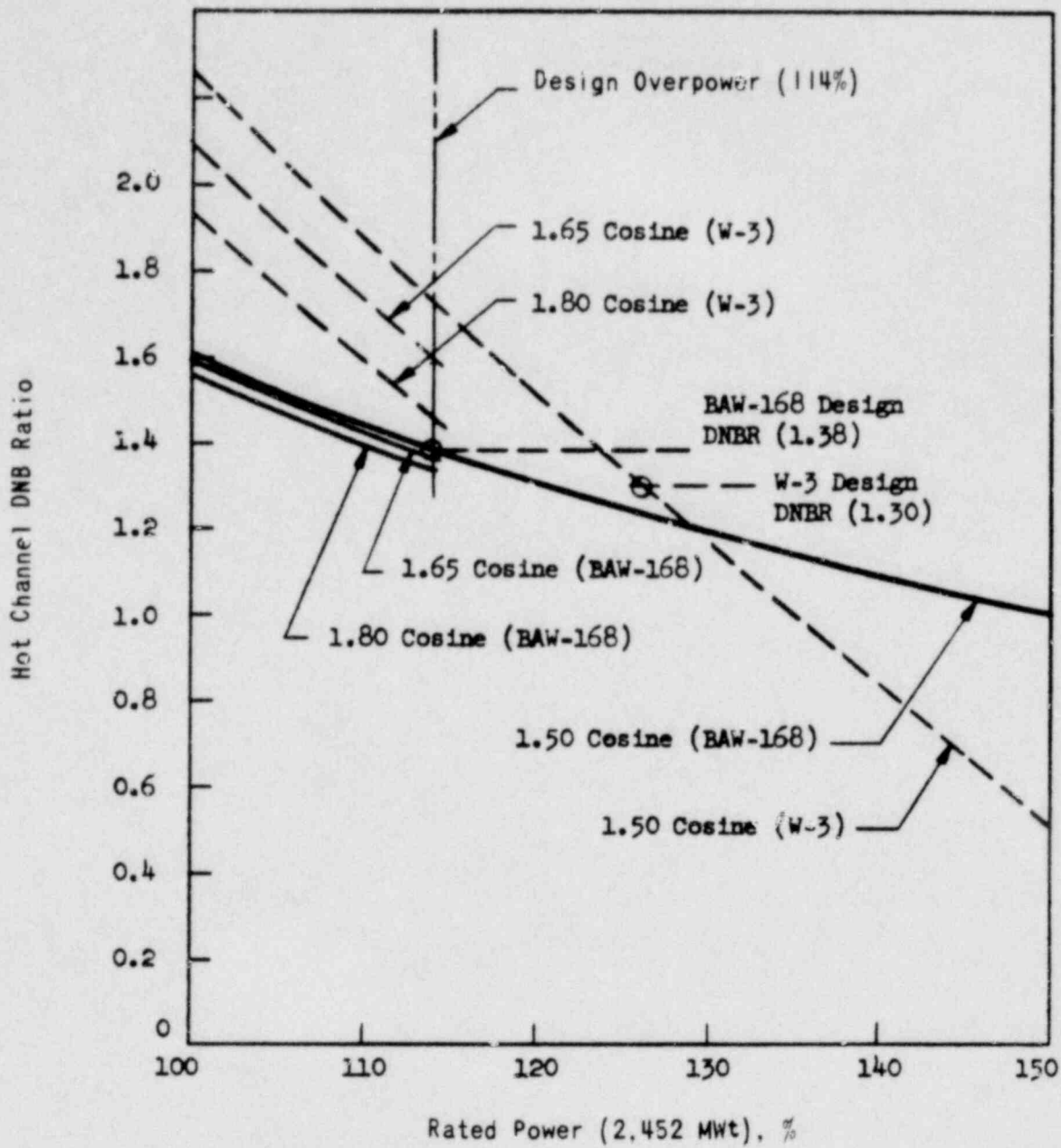
FLOW REGIME MAP FOR CORNER CHANNEL

CRYSTAL RIVER UNITS 3 & 4



FIGURE 3-44

00000505



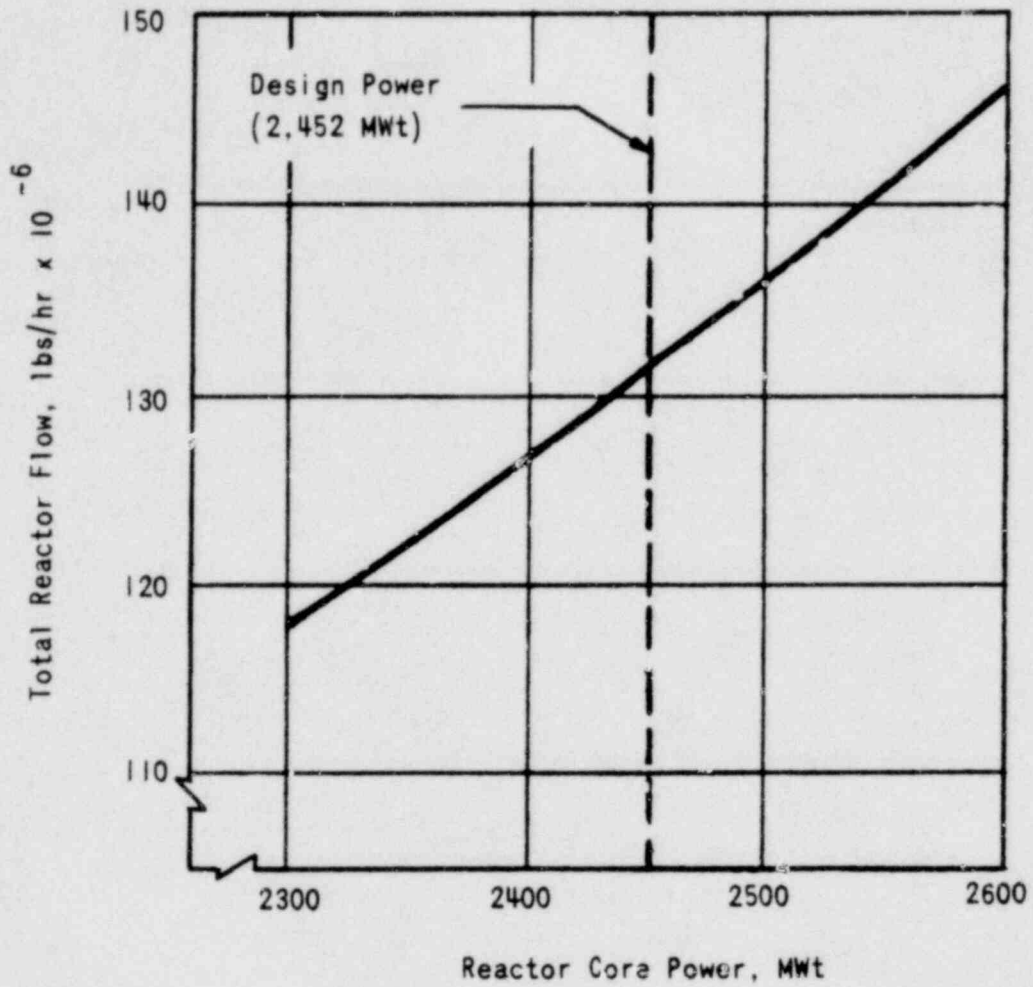
HOT CHANNEL DNB
RATIO COMPARISON

CRYSTAL RIVER UNITS 3 & 4

00000507



FIGURE 3-46



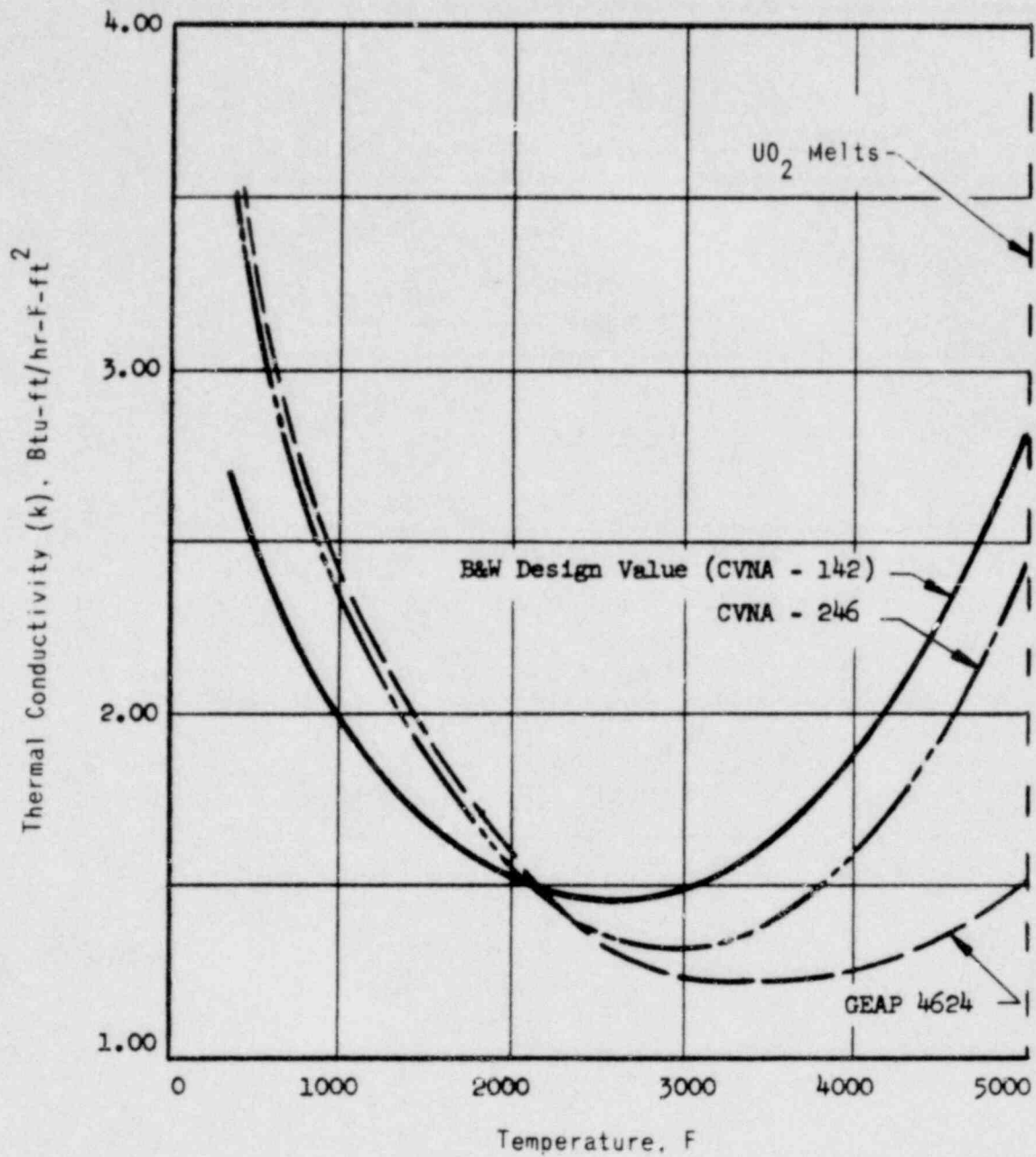
0000Q508

REACTOR COOLANT FLOW VERSUS POWER

CRYSTAL RIVER UNITS 3 & 4



FIGURE 3-47

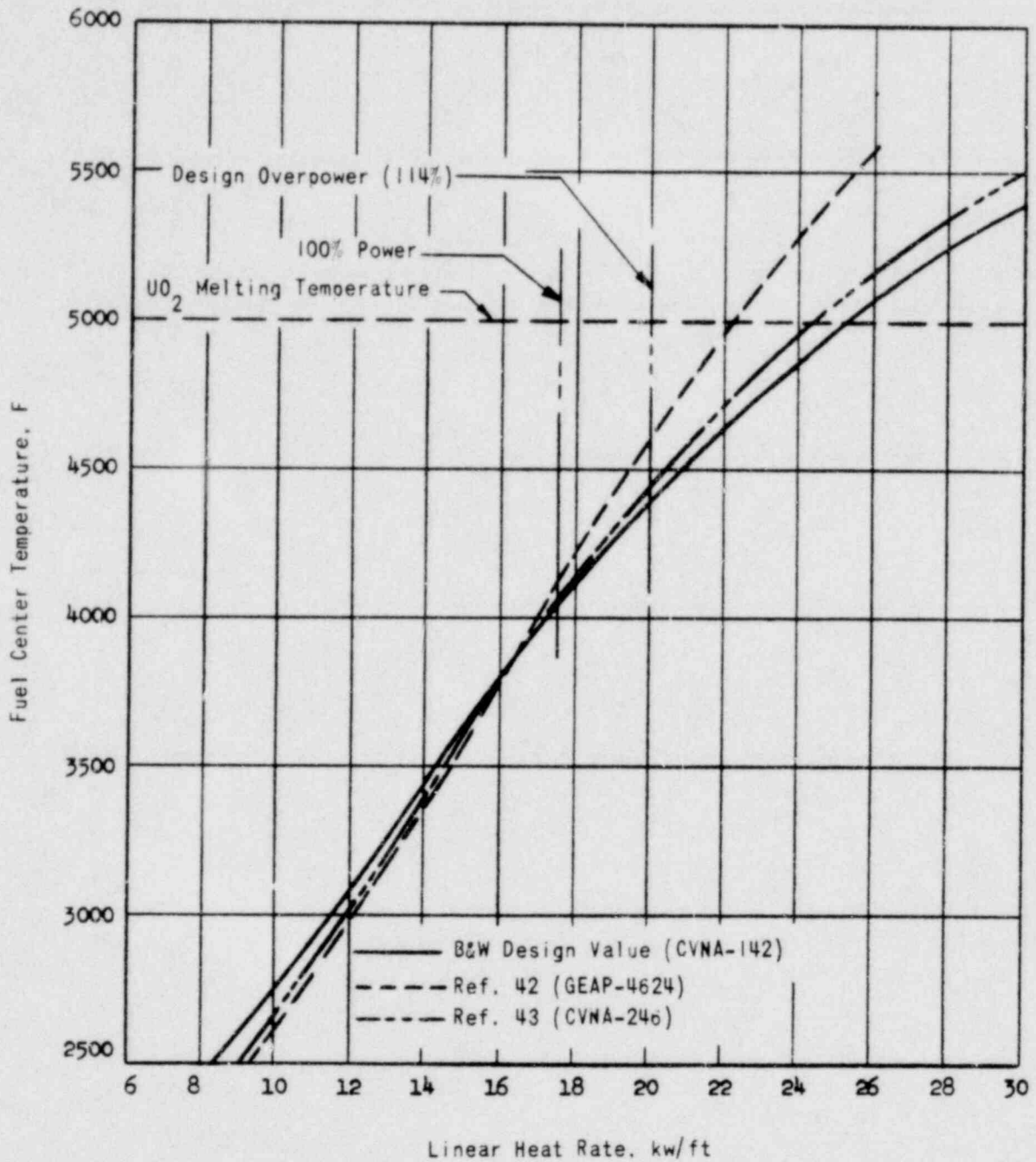


THERMAL CONDUCTIVITY OF 95%
DENSE SINTERED UO₂ PELLETS
CRYSTAL RIVER UNITS 3 & 4



FIGURE 3-48

00000309



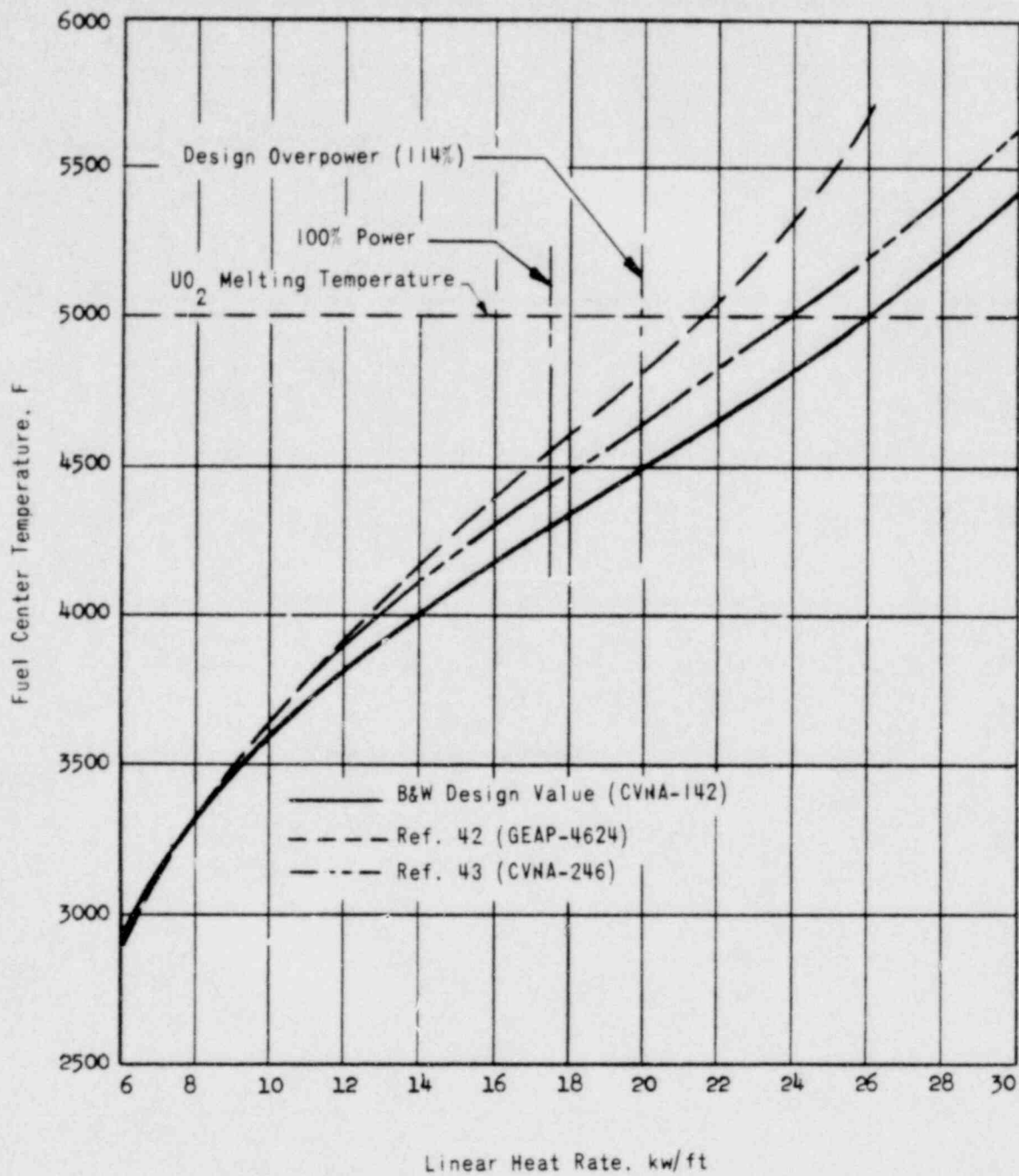
00000310

FUEL CENTER TEMPERATURE FOR
BEGINNING-OF-LIFE CONDITIONS

CRYSTAL RIVER UNITS 3 & 4



FIGURE 3-49



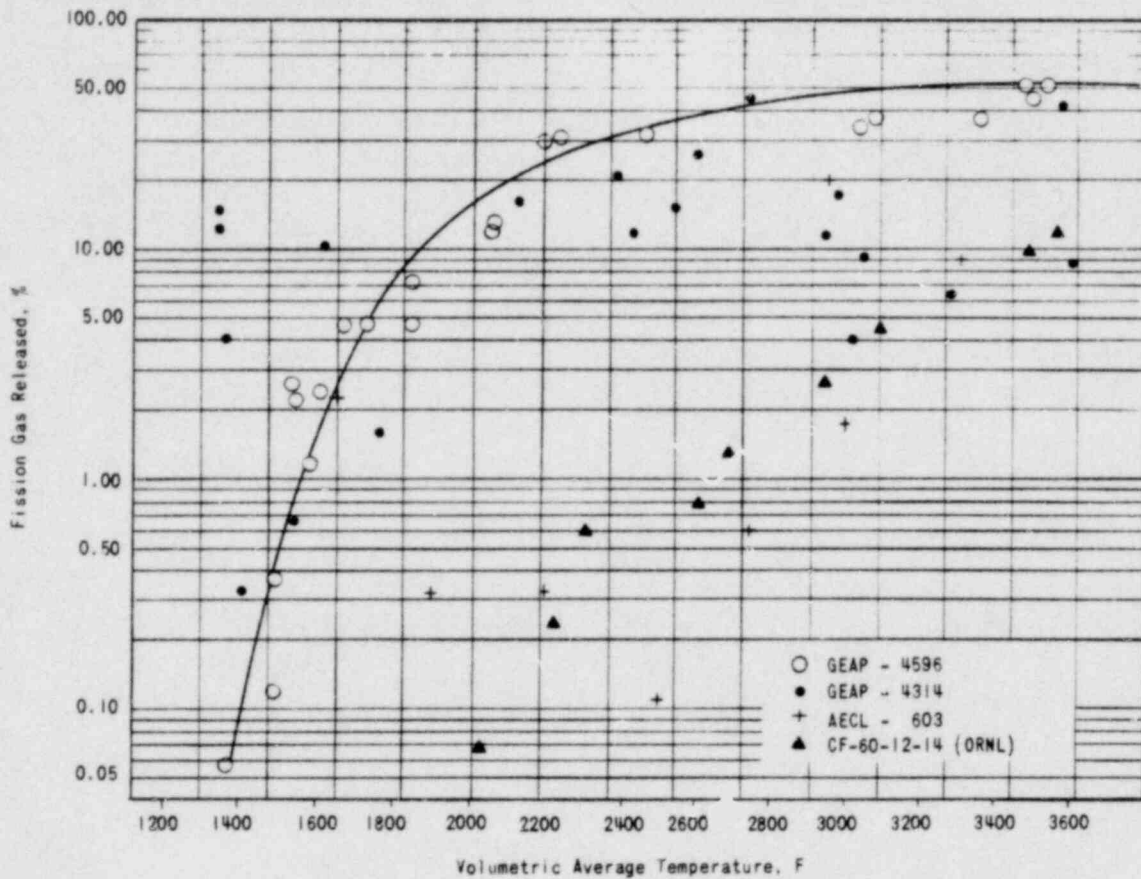
FUEL CENTER TEMPERATURE FOR
END-OF-LIFE CONDITIONS

CRYSTAL RIVER UNITS 3 & 4



FIGURE 3-50

00000311



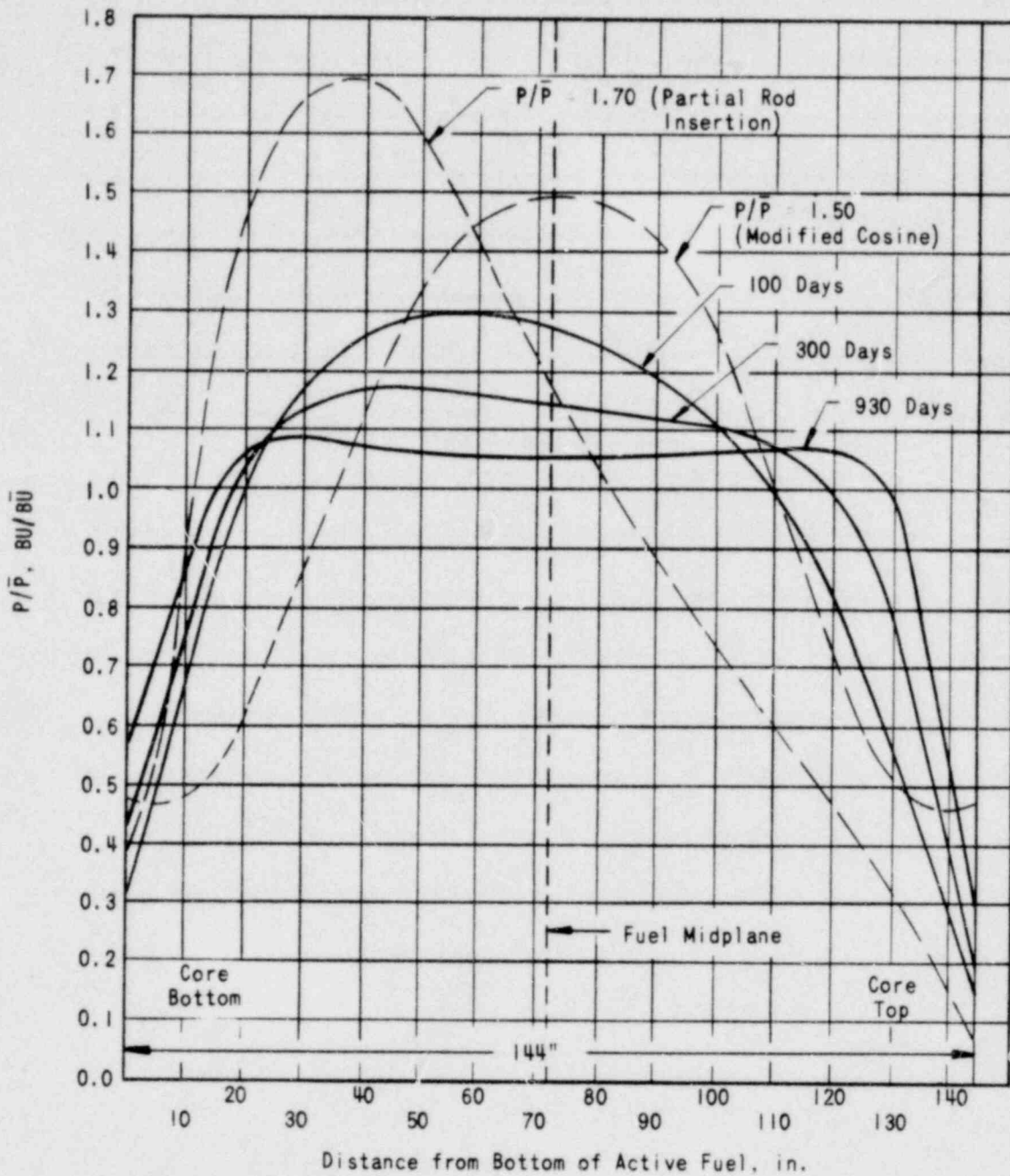
00000312

PERCENT FISSION GAS RELEASED AS A FUNCTION OF THE AVERAGE TEMPERATURE OF THE UO₂ FUEL

CRYSTAL RIVER UNITS 3 & 4



FIGURE 3-51



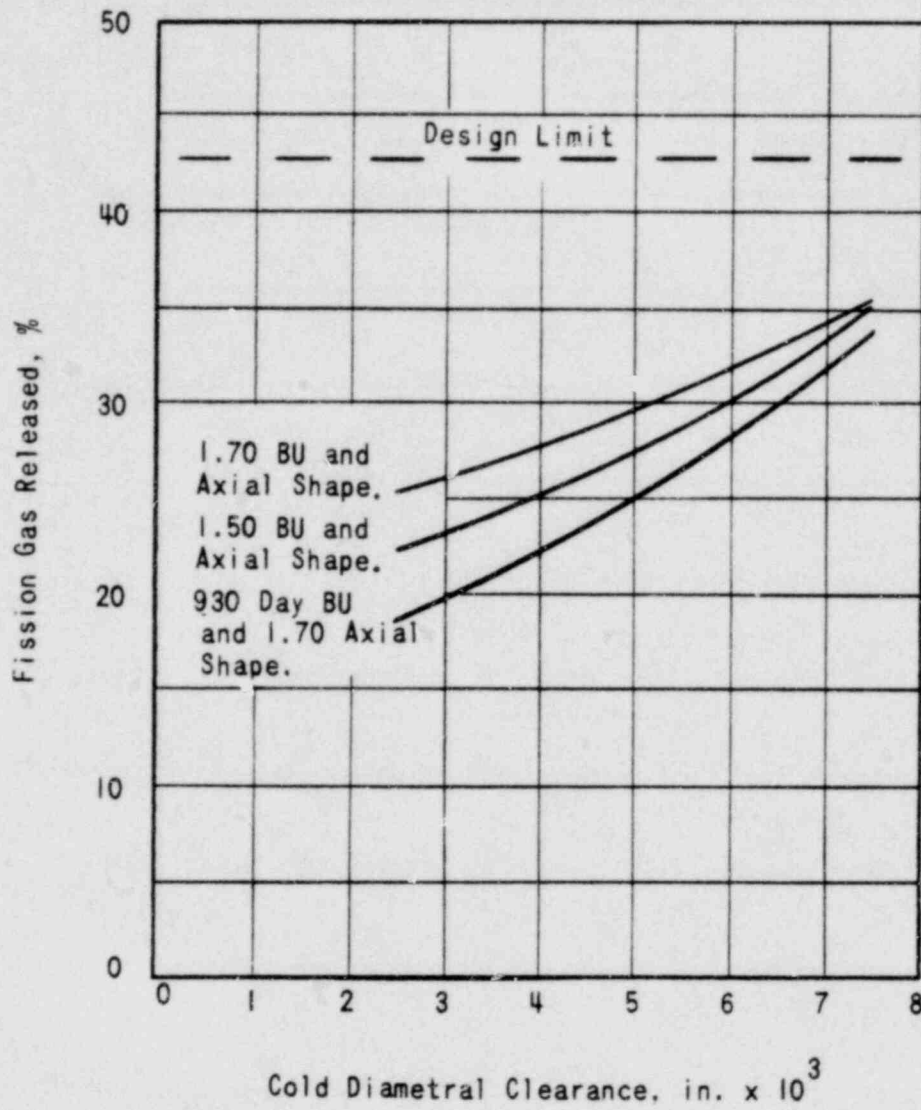
AXIAL LOCAL TO AVERAGE BURNUP AND INSTANTANEOUS POWER COMPARISONS

CRYSTAL RIVER UNITS 3 & 4



FIGURE 3-52

00000513



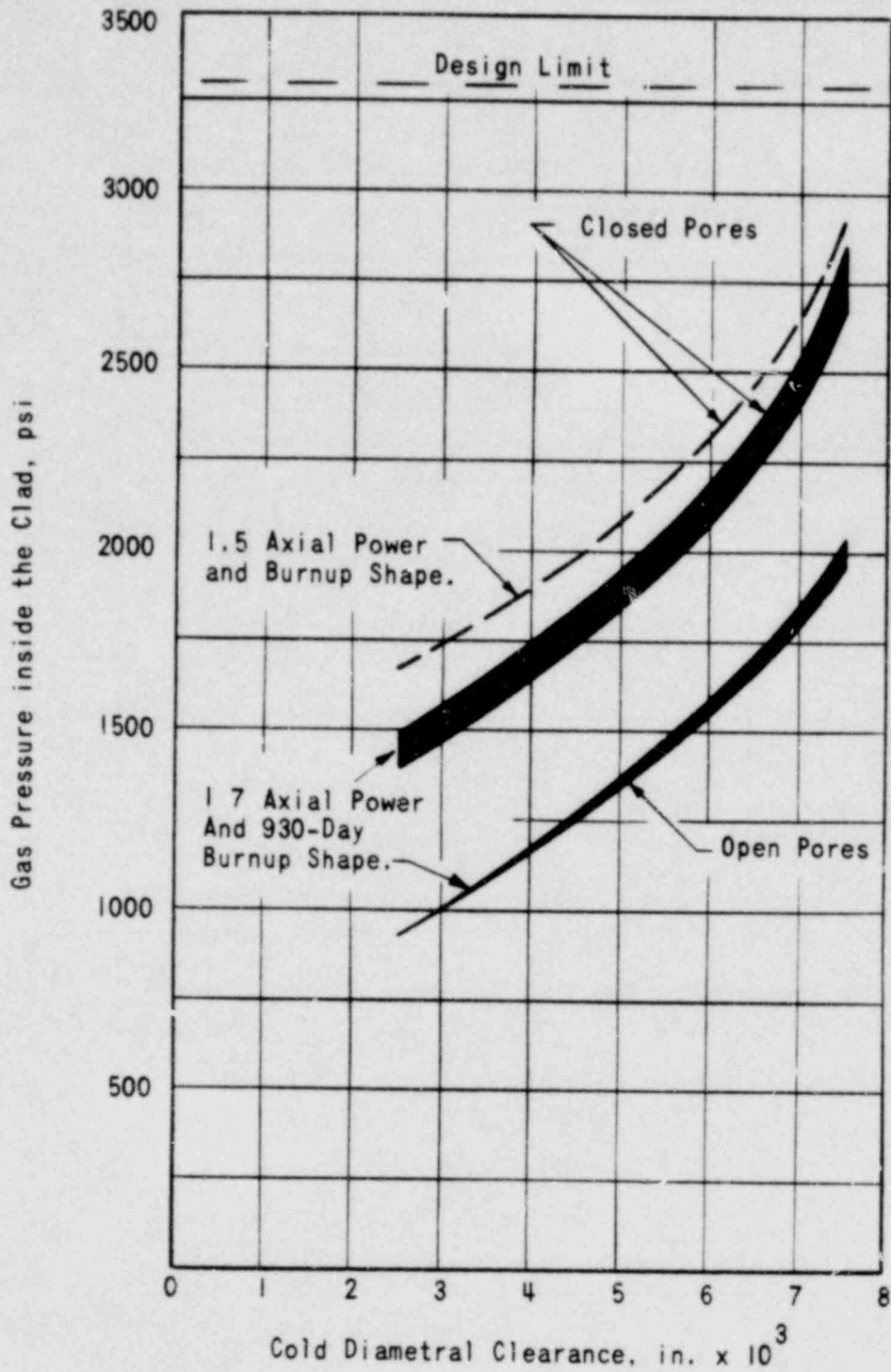
000003184

FISSION GAS RELEASE FOR 1.50 AND 1.70 MAX/AVG AXIAL POWER SHAPES

CRYSTAL RIVER UNITS 3 & 4



FIGURE 3-53



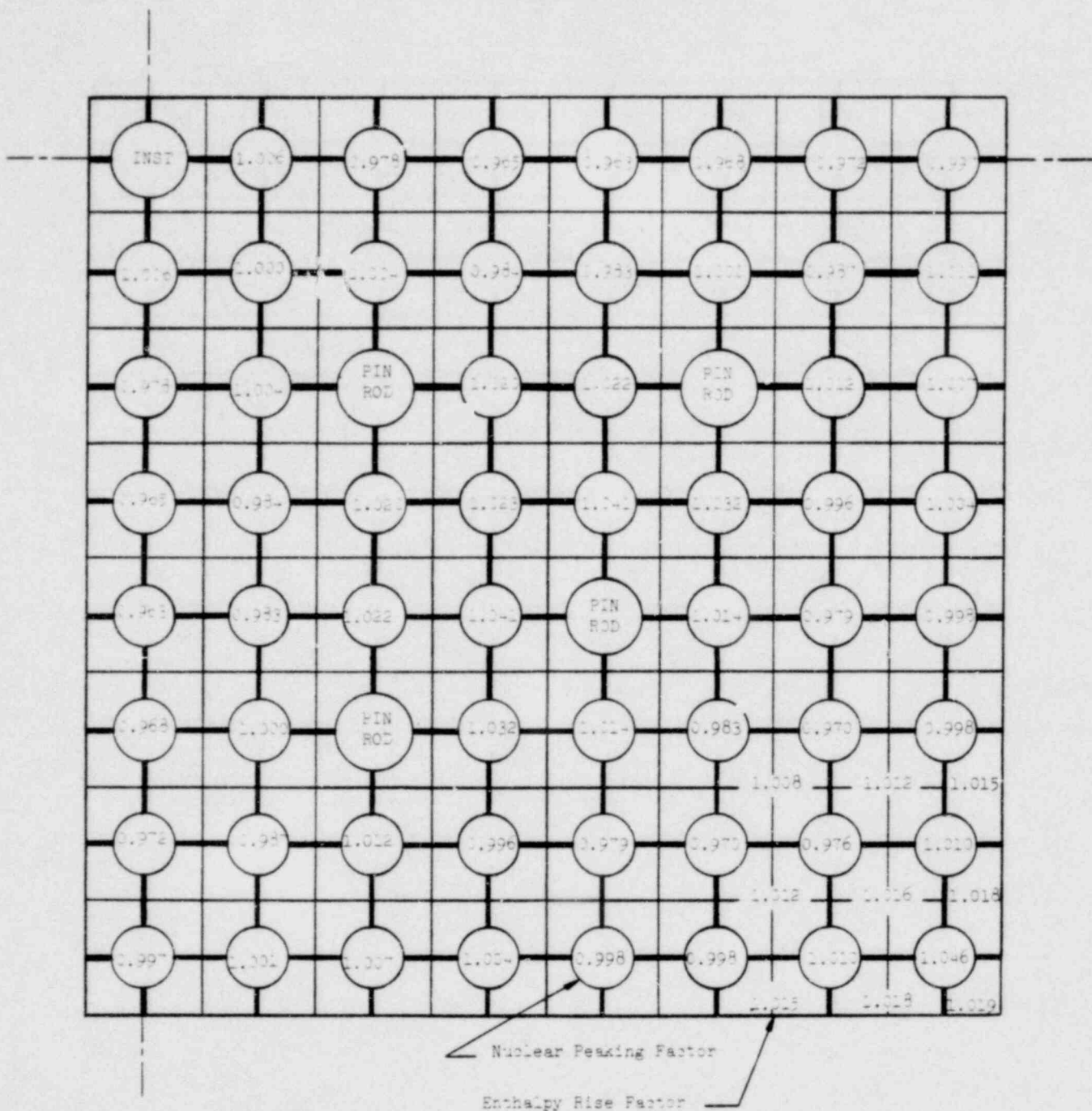
GAS PRESSURE INSIDE THE FUEL CLAD FOR VARIOUS AXIAL BURNUP AND POWER SHAPES

CRYSTAL RIVER UNITS 3 & 4



FIGURE 3-54

00000-15

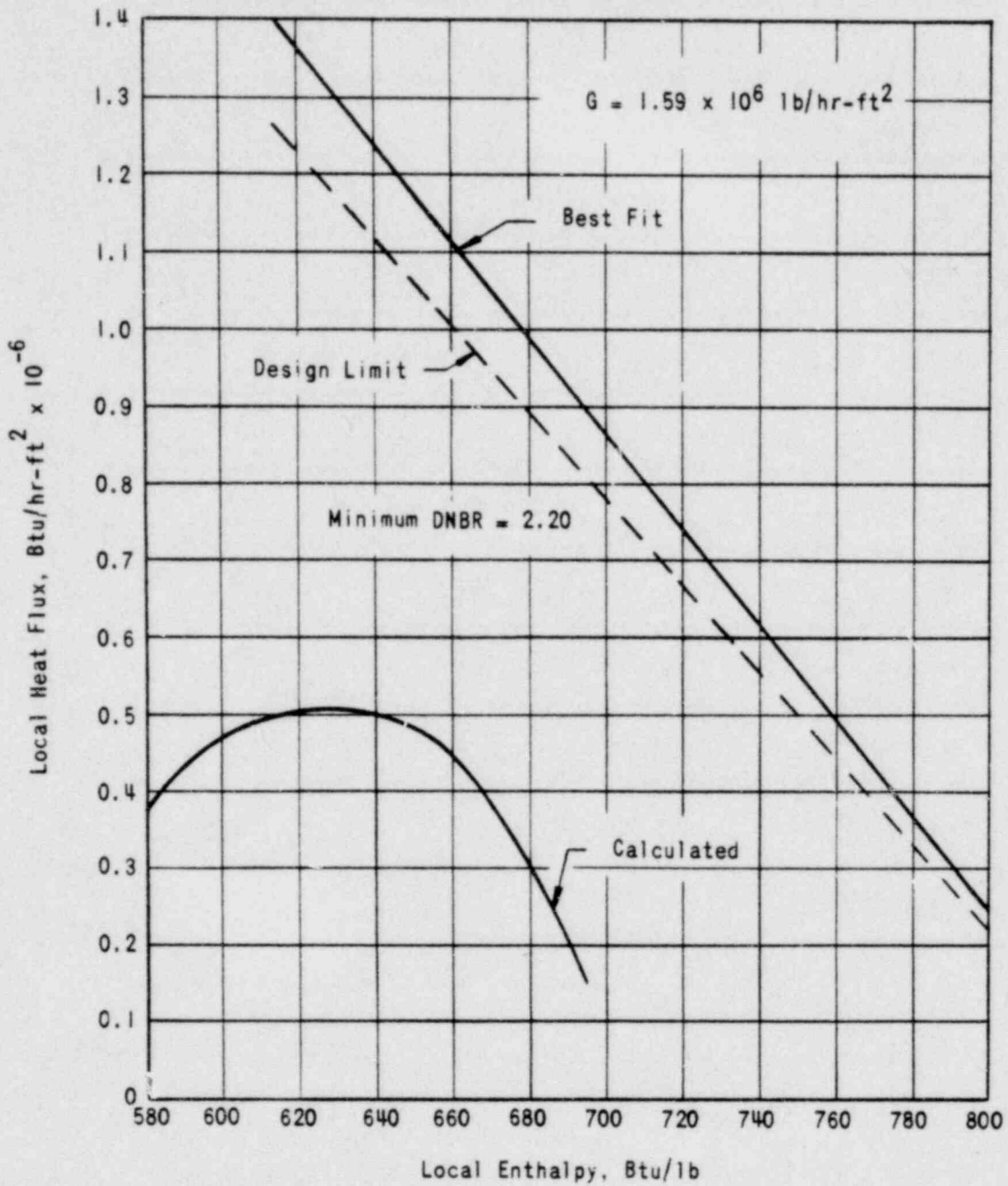


00000-16

NOMINAL FUEL ROD POWER PEAKS AND
CELL EXIT ENTHALPY RISE RATIOS
CRYSTAL RIVER UNITS 3 & 4



FIGURE 3-55



0000318

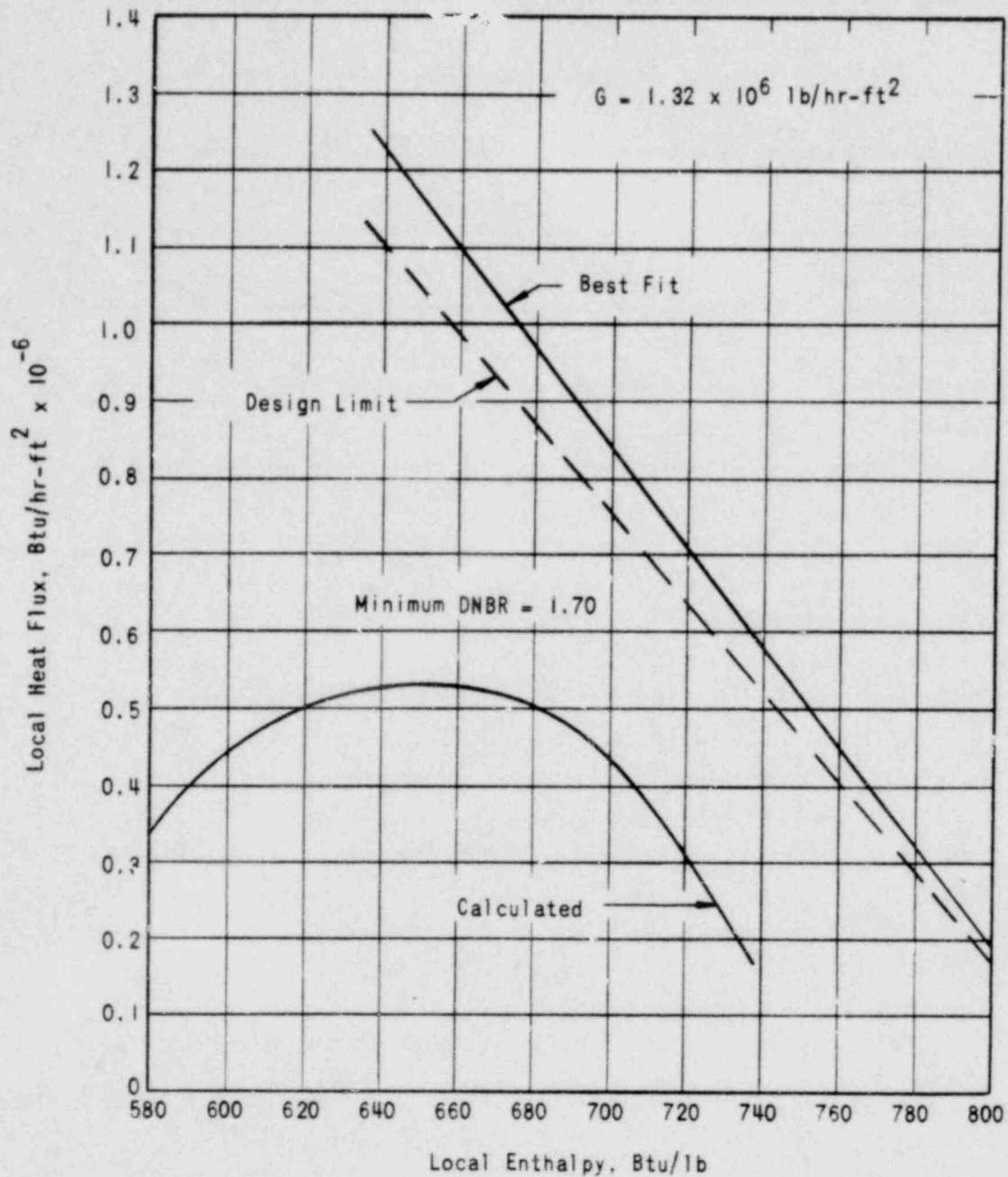
CALCULATED AND DESIGN LIMIT LOCAL HEAT FLUX VS ENTHALPY IN THE HOT CORNER CELL AT THE NOMINAL CONDITION

CRYSTAL RIVER UNITS 3 & 4



FIGURE 3-57

AMEND. 1 (1-15-68)



CALCULATED AND DESIGN LIMIT LOCAL HEAT FLUX VS ENTHALPY IN THE HOT CORNER CELL AT THE POSTULATED WORST CONDITION

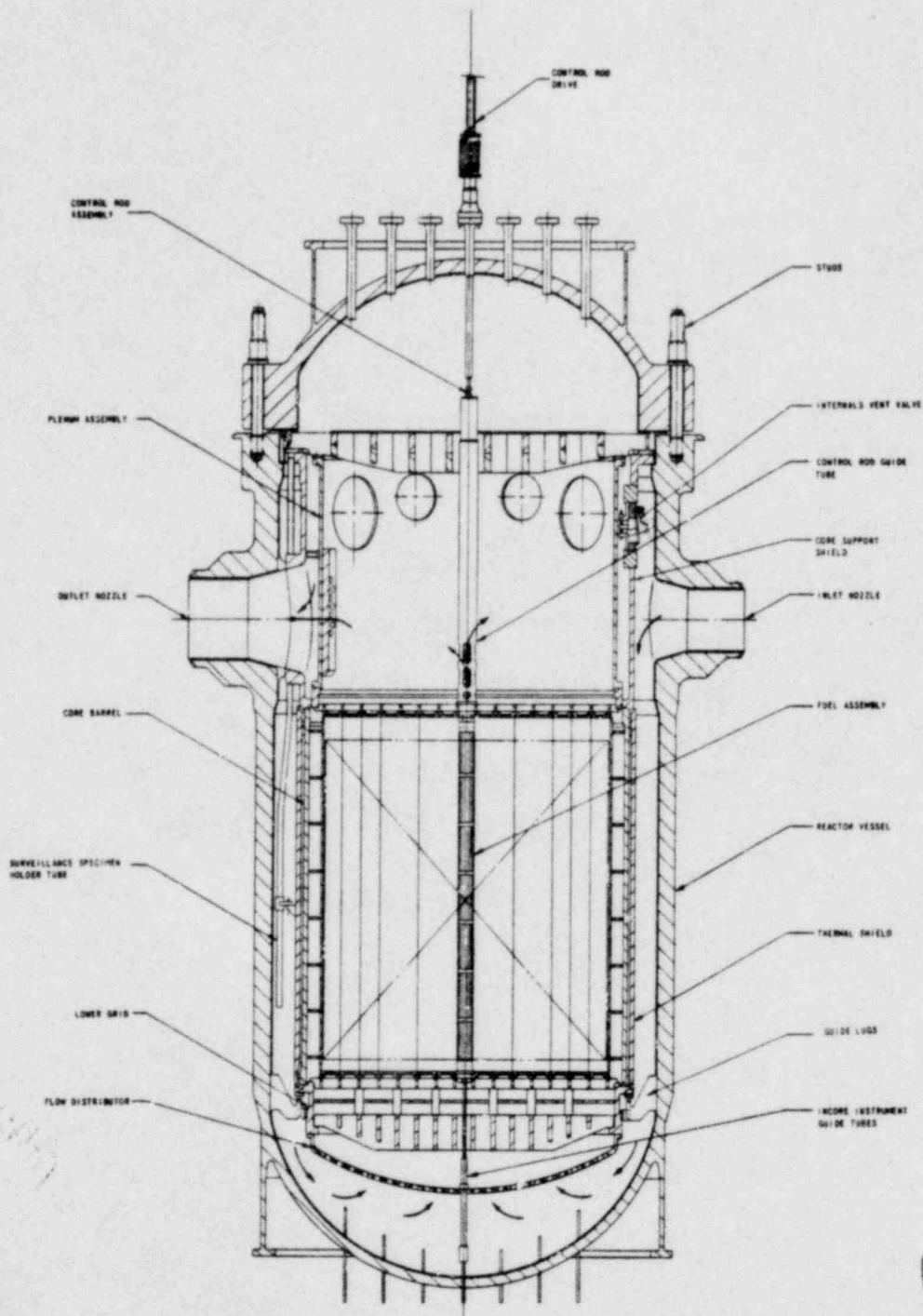
CRYSTAL RIVER UNITS 3 & 4



FIGURE 3-58

AMEND. 1 (1-15-68)

00000519



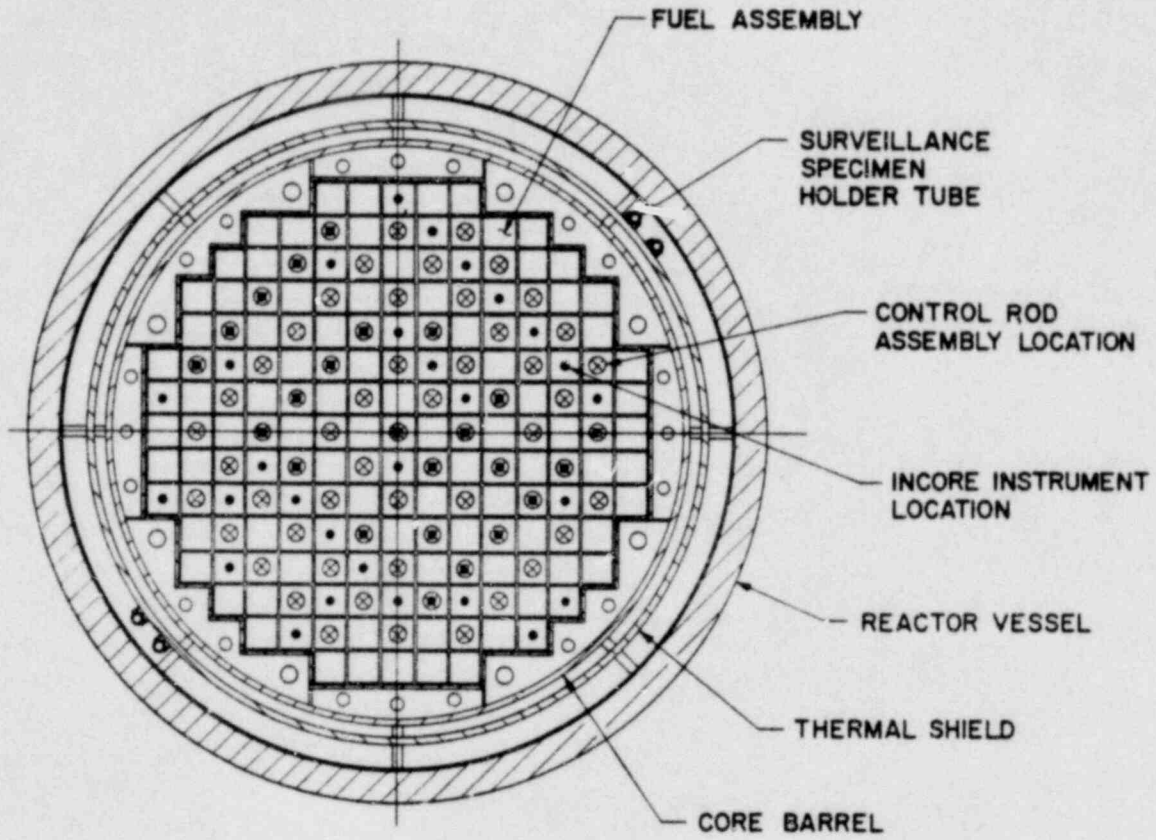
00000520

**REACTOR VESSEL AND INTERNALS
GENERAL ARRANGEMENT
CRYSTAL RIVER UNIT 3**



FIGURE 3-59

AMEND. 7 (7-15-69)



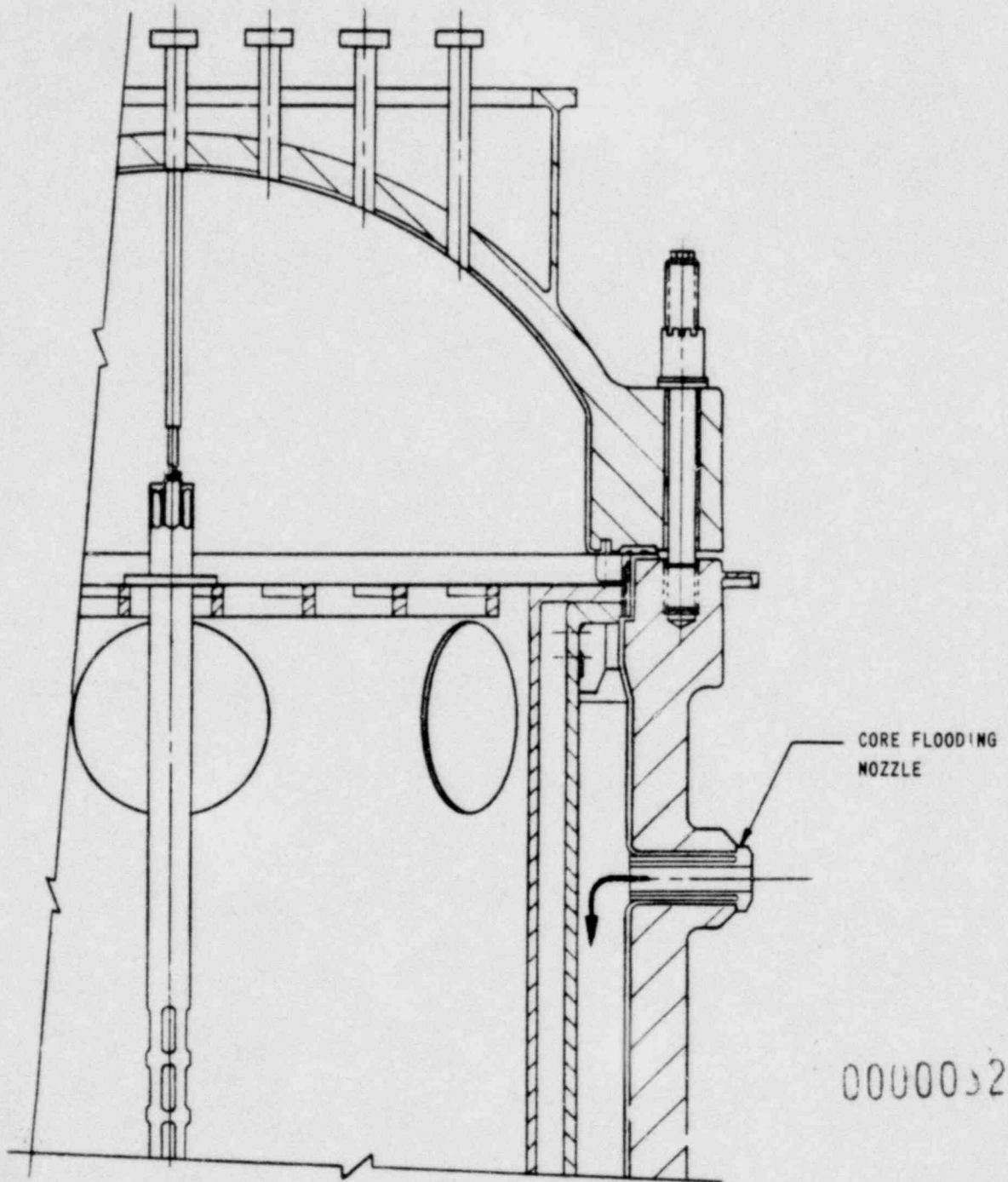
00000-21

**REACTOR VESSEL & INTERNALS
CROSS SECTION**

CRYSTAL RIVER UNITS 3 & 4



FIGURE 3-60



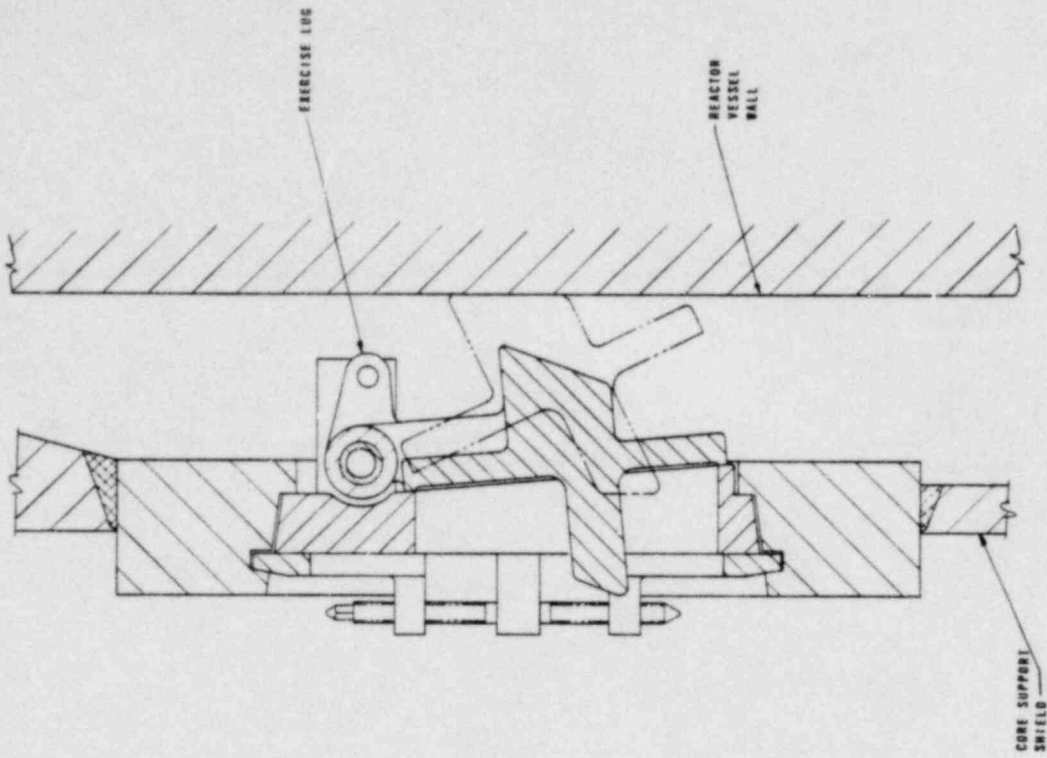
00000522

CORE FLOODING ARRANGEMENT
CRYSTAL RIVER UNITS 3 & 4

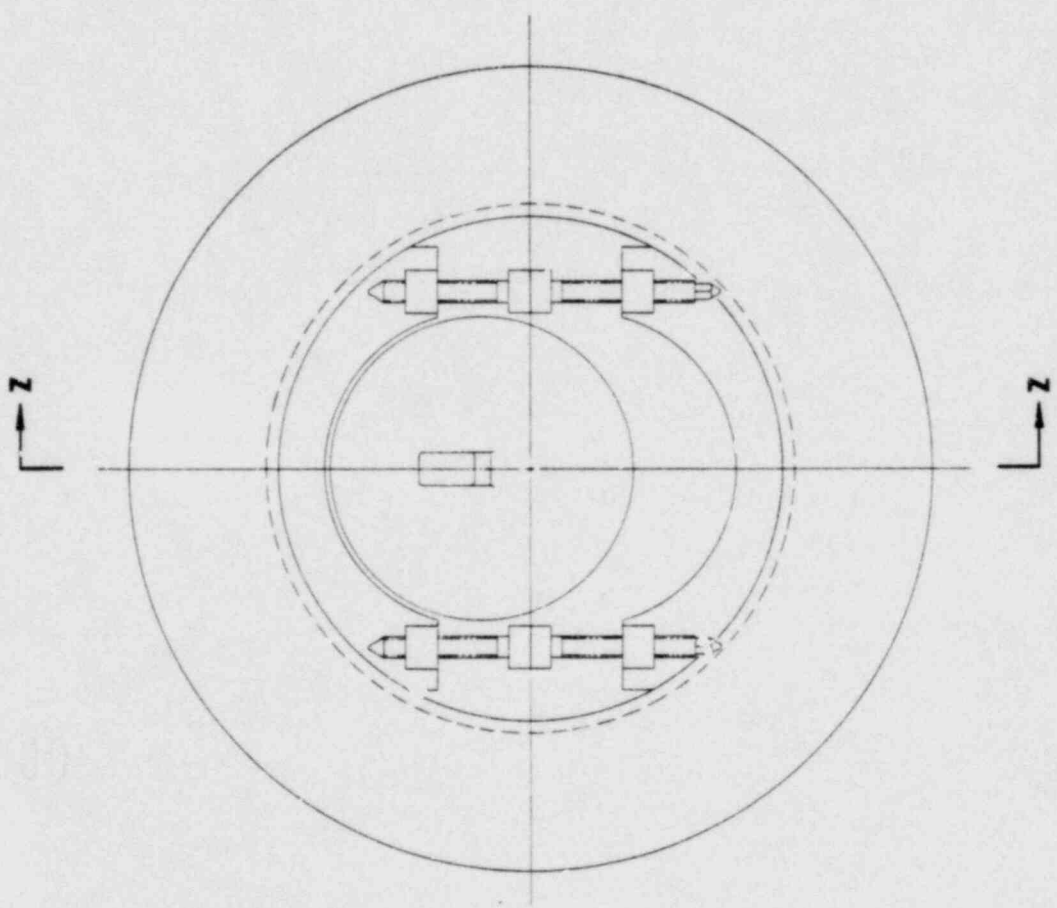


FIGURE 3-61


AMEND. 1 (1-15-68)



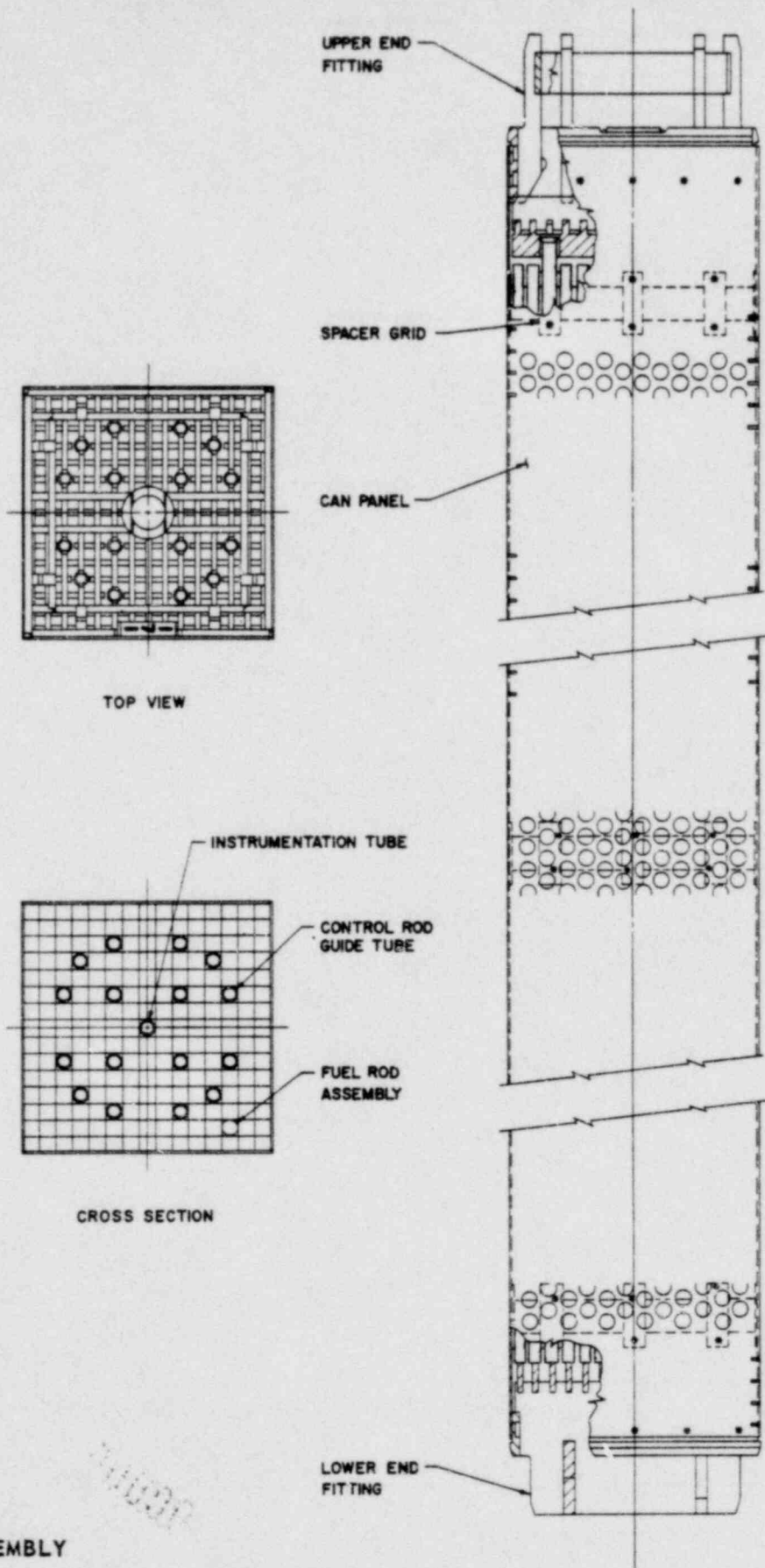
SECTION Z-Z



INTERNAL VENT VALVE
CRYSTAL RIVER UNITS 3 & 4

 FLORIDA POWER CORPORATION
FIGURE 3-61-a
AMEND. 1 (1-15-68)

000000 225



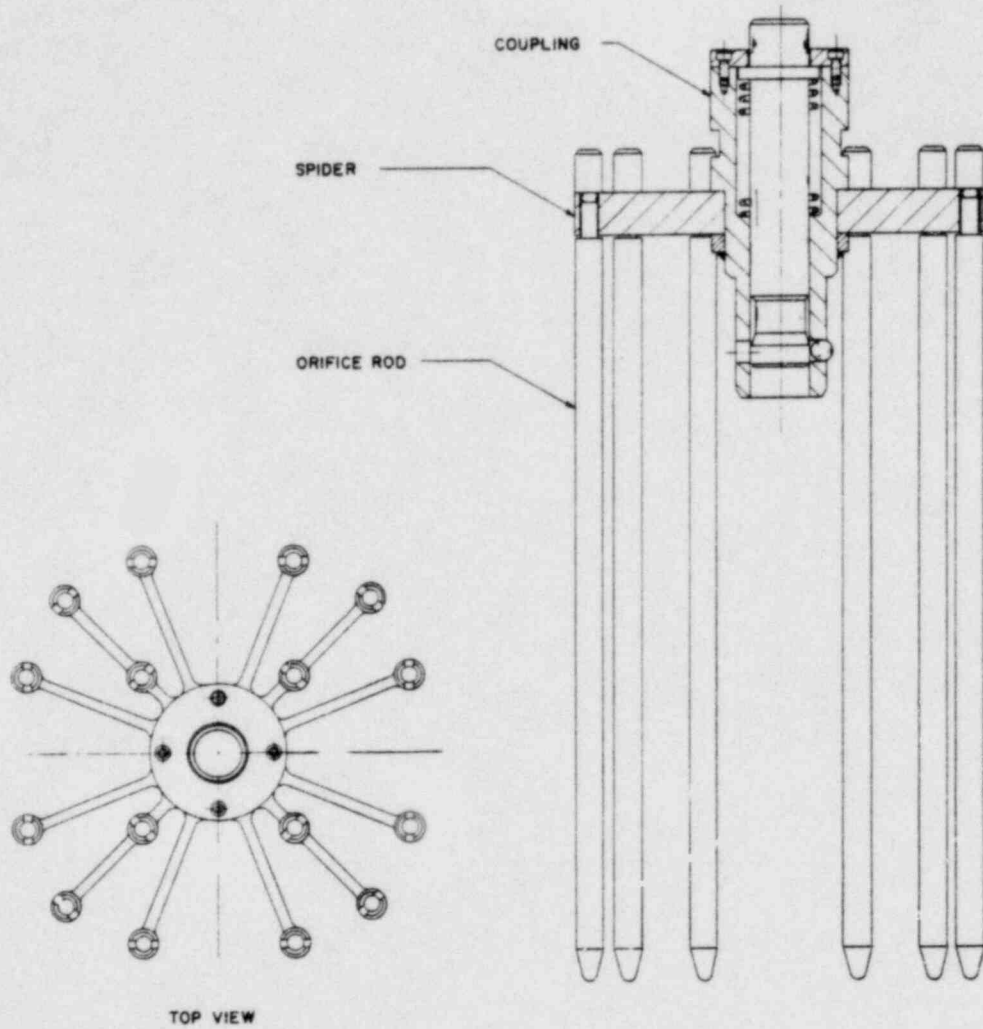
FUEL ASSEMBLY

CRYSTAL RIVER UNITS 3 & 4



FIGURE 3-62

00000524

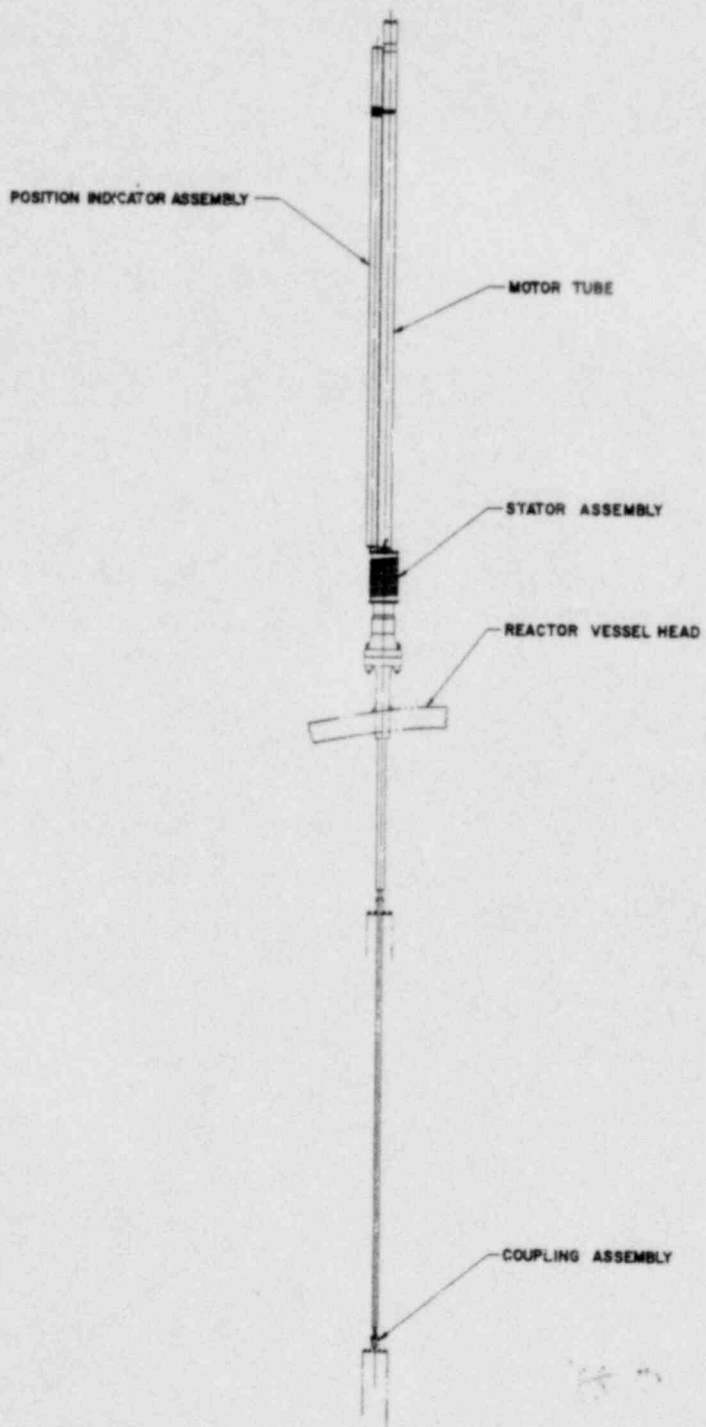


00000325

ORIFICE ROD ASSEMBLY
 CRYSTAL RIVER UNITS 3 & 4



FIGURE 3-63



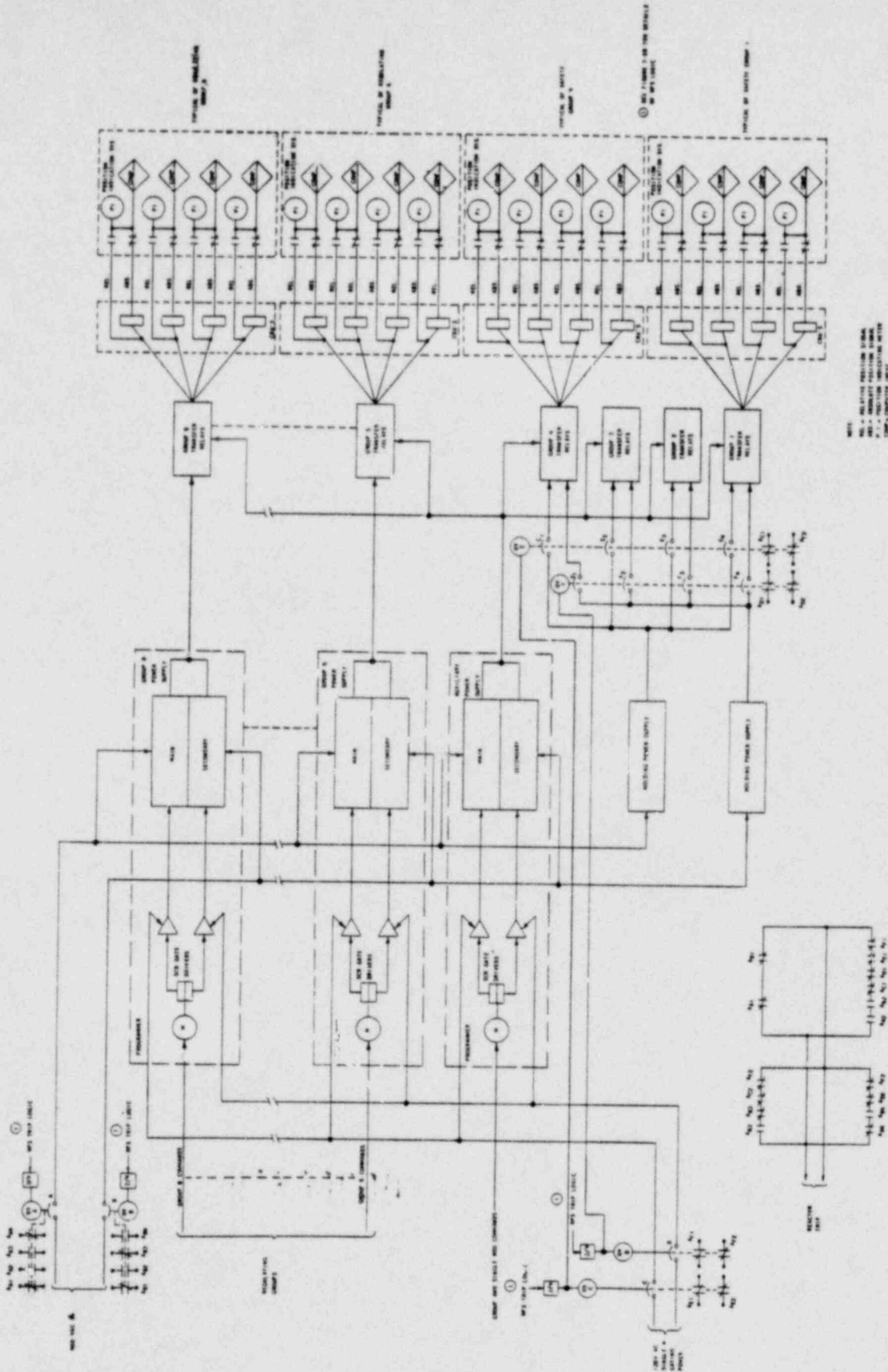
CONTROL ROD DRIVE
 GENERAL ARRANGEMENT
 CRYSTAL RIVER UNIT 3

00000426



FIGURE 3-64

AMEND. 7 (7-15-69)



TRIP COILS
 TRIP RELAYS
 TRIP COILS
 TRIP RELAYS

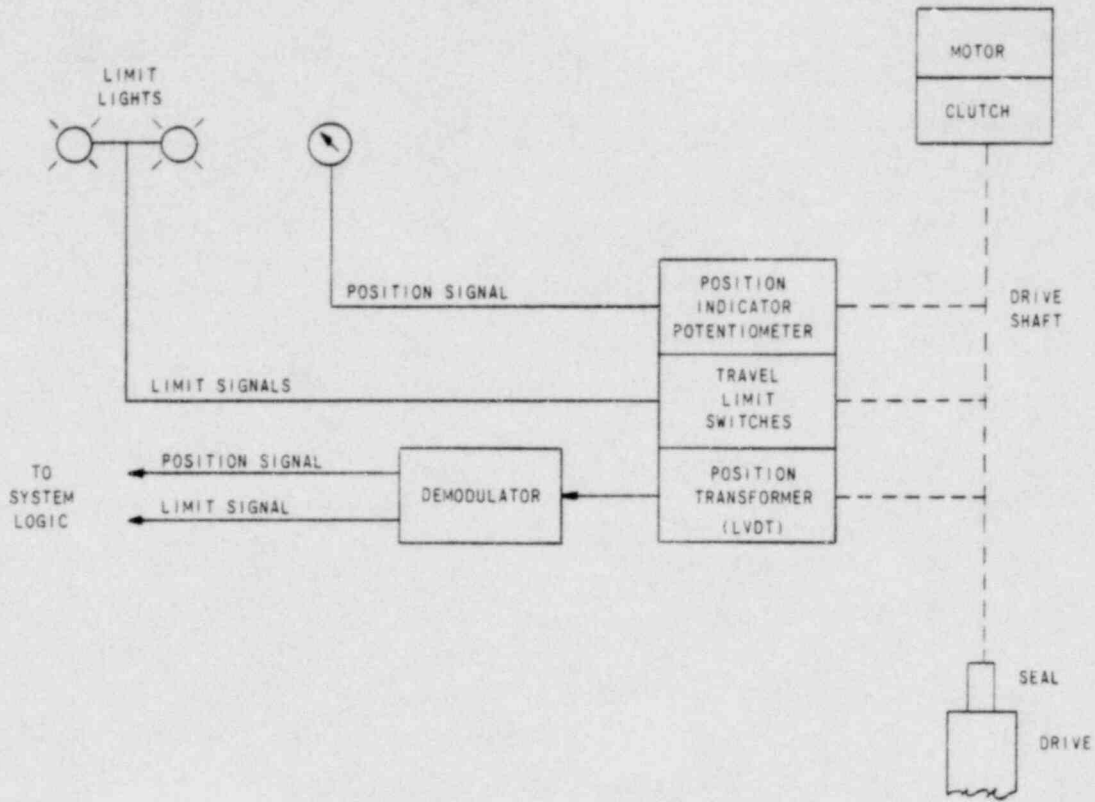
CONTROL ROD DRIVE SYSTEM
 AND TRIP BLOCK DIAGRAM
 CRYSTAL RIVER UNIT 3



FIGURE 3-66

AMEND. 7 (7-15-69)

00000528



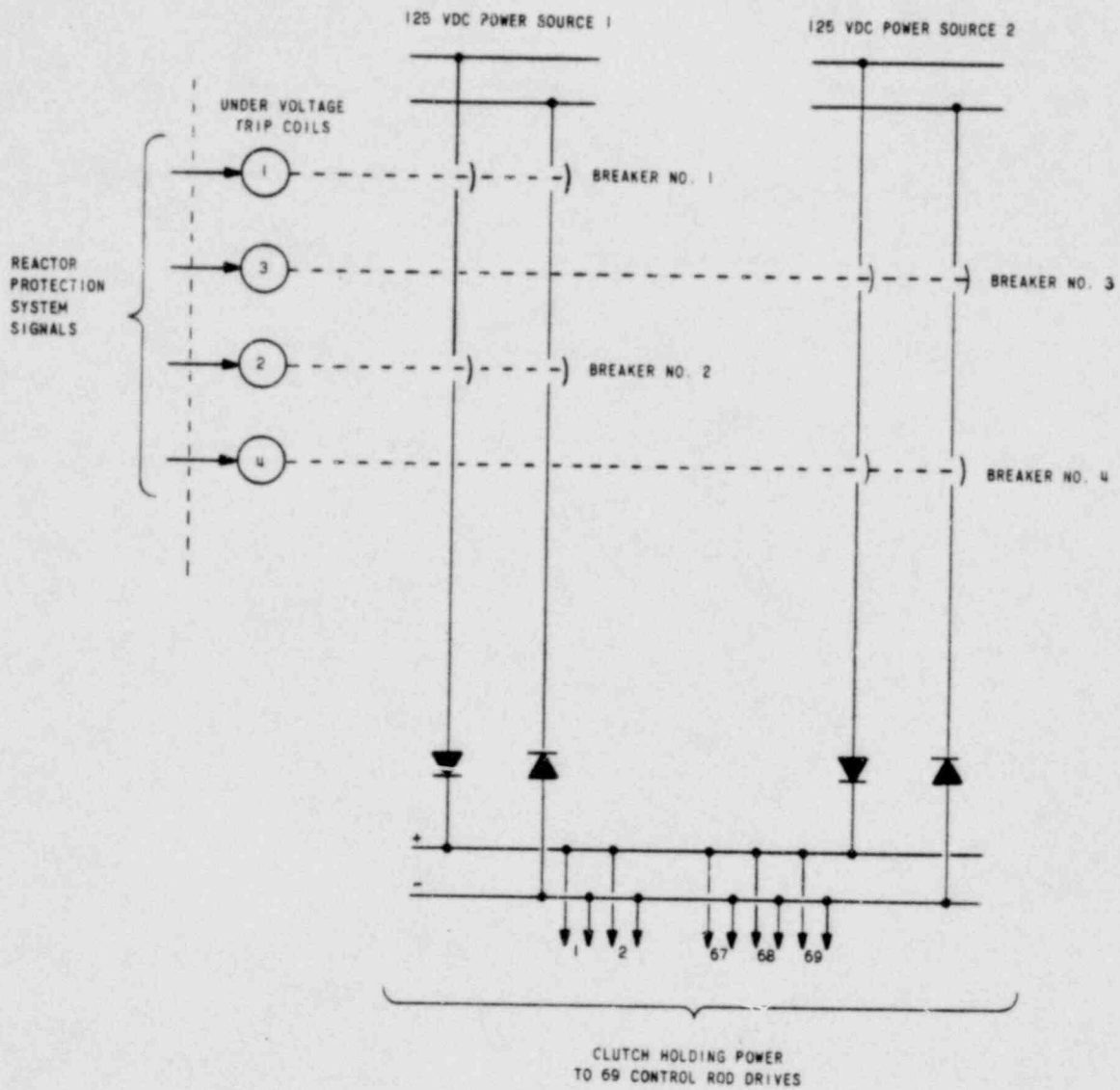
00000329

LIMIT SIGNAL AND POSITION INDICATION SYSTEM

CRYSTAL RIVER UNITS 3 & 4



FIGURE 3-67



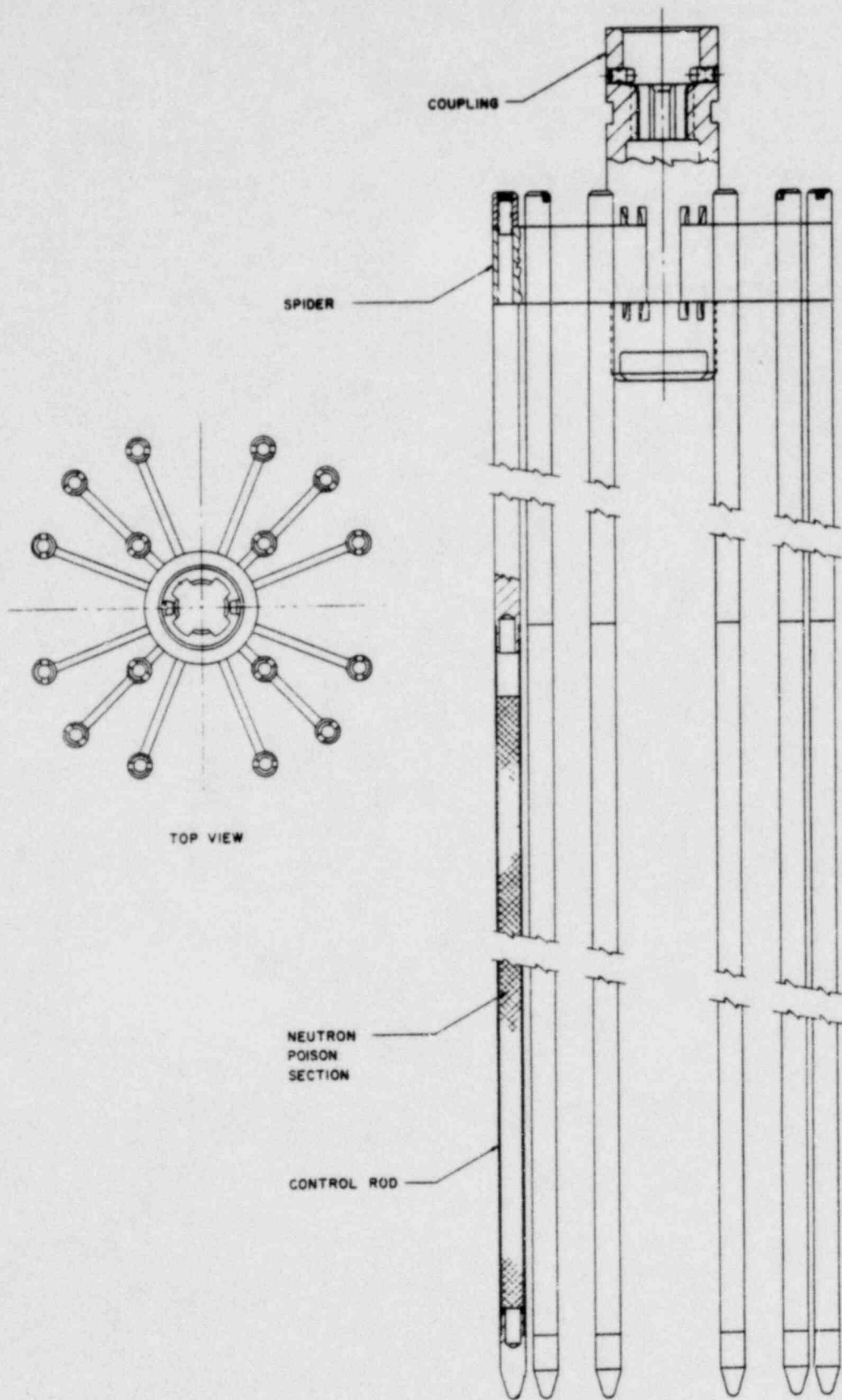
REACTOR TRIP CIRCUIT
CRYSTAL RIVER UNITS 3 & 4



FIGURE 3-68

AMEND. 1 (1-15-68)

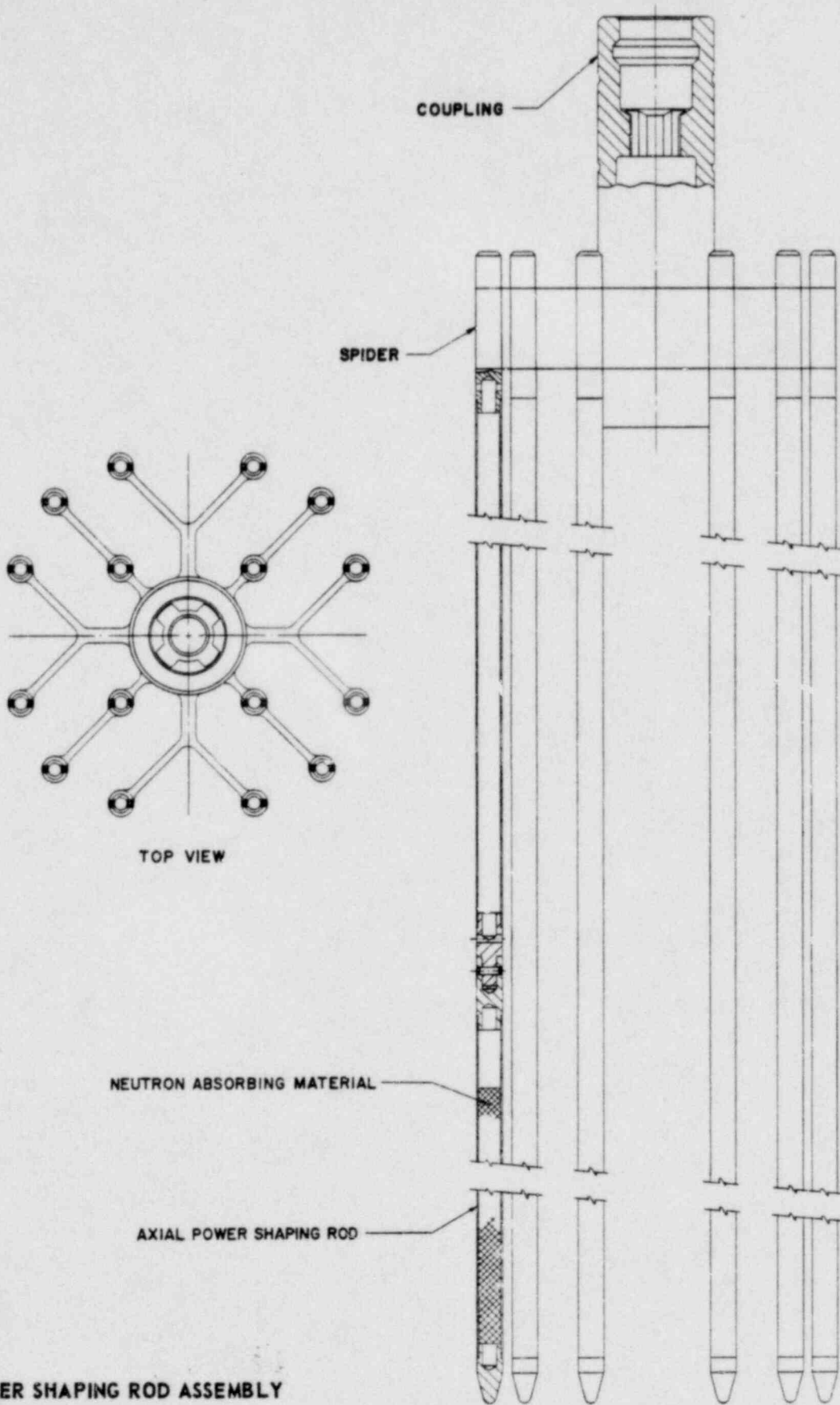
0000030



CONTROL ROD ASSEMBLY
CRYSTAL RIVER UNITS 3 & 4

00000331





AXIAL POWER SHAPING ROD ASSEMBLY
CRYSTAL RIVER UNIT 3



FIGURE 3-70

AMEND. 7 (7-15-69)

00000332